A Role for *Nanor* in Early Zebrafish Development and Validation of a Neurotoxic Zebrafish Model of Parkinson's Disease

By

Aileen Cronin

Supervisor: Dr. Maura Grealy

Co-supervisor: Dr. Lucy Byrnes

Pharmacology & Therapeutics

National University of Ireland, Galway

Doctor of Philosophy

January, 2018

Acknowledgements

First, I would like to thank my supervisor Dr. Maura Grealy. Thank you for your guidance throughout both my masters and PhD, I never imagined an 8 week research project would become over four years in the zebrafish lab. Thank you for your constant encouragement and support over the last number of years, especially during an extremely challenging final year.

To Dr. Howard Fearnhead, thank you for all the help and endless patience with my Co-IP experiments. I learned so much from you over a short number of weeks and you were always approachable and had valuable advice to offer throughout the PhD.

To my family and in particular my parents, for their constant love and encouragement, I couldn't have asked for a better support system. I appreciate everything ye have done for me more than I can put into words.

To past lab members Elaine O' Connor and Dr. Elke Rink for all your guidance and companionship during the first year of the PhD. Have a great time during your travels Elaine. I look forward to our next catch-up! Also thank you to Dr. Rebecca Ryan for collecting and sending samples from her research group in Paris.

To my lab partner Tracy Lynskey, for being a wonderful friend both inside and outside of the lab. We shared all the highs and lows together and you were always willing to help in any way you could. Best of luck in final year, I am sure you will get far more work done now that I'm not dragging you to the tea room for our tea breaks.

To all the friends I have made in Galway for making Galway feel like a second home and always being so supportive especially Conor, Kiah, Tena, Norma, Peggie, Tracy, Haz and Veronica. A special mention has to go to my roomie Norma. Norma you always were willing to lend an ear and always had valuable advice to offer. Thank you for being a great friend and housemate.

To the staff and students of the Biochemistry and Pharmacology departments, in particular Miriam, Danny, Ambrose, Toni, Vijai, John and Anne. Thank you!

Finally, to my boyfriend Steve, I know you are the second most relieved person to see the end of the PhD! Thank you for your support and encouragement and for asking for regular updates on how my lab work was going even though you didn't have a notion what I was on about.

List of commonly used abbreviations

6-OHDA	6-hydroxydopamine
ANOVA	Analysis of variance
BLAST	Basic local alignment search tool
BMP	Bone-morphogenetic protein
bp	base pair
BSA	bovine serum albumin
cDNA	Complementary DNA
CFC	Cripto, Formin related gene-1, Cryptic
Co-IP	Co-immunoprecipitation
DNA	Deoxyribonucleic acid
Dpf	Days post-fertilisation
EF1-α	Elongation factor 1 - alpha
EGF	Epidermal growth factor
FGF	Fibroblast growth factor
FSEW	Filter sterilised egg water
Hpf	Hours post fertilisation
HRMA	High resolution melt analysis
IFT	Intraflagellar transport
kD	Kilodalton
L-DOPA	Levodopa
Lrd	Left right dynein
MAO	Monoamine oxidase
MAPK	Mitogen activated protein kinase
miRNA	microRNA
mRNA	messenger Ribonucleic acid
µg	Microgram
µL	Microlitre
µM	Micromolar
mL	Millilitre

mM	Millimolar
MPTP	1-methyl-4-phenyl-1,2,3,6-tetrahydropyridine
Ndr1	Nodal-related-1
ng	Nanogram
Oct-4	Octamer-binding transcription factor 4
Oep	One-eyed pinhead
PAGE	Polyacrylamide gel electrophoresis
PBS	Phosphate buffered saline
PFA	paraformaldehyde
piRNA	piwi-interacting RNA
qPCR	Quantitative PCR
RISC	RNA induced silencing complex
RNA	Ribonucleic acid
ROCK	Rho-associated protein kinase
ROS	Reactive oxygen species
RT-PCR	Reverse transcription polymerase chain reaction
RVD	Repeat-variable di-residue
SDS	Sodium dodecyl sulphate
SEM	Standard error ± mean
siRNA	small interfering RNA
SNP	Single nucleotide polymorphism
Sox2	Sex determining region Y-box 2
Spaw	Southpaw
TALENS	Transcription activator-like effector nucleases
TNF	Tumour necrosis factor
TRAF3IP1	TNF receptor associated factor 3-interacting protein 1
Tween-20	Polyoxyethylenesorbitan monolaurate
UTR	Untranslated region
Xnr	Xenopus nodal-related

Contents

Abstract

Zebrafish are a versatile experimental model which have progressed the fields of many research areas through both genetic and pharmacological studies. In this thesis I studied a novel zygotic gene, *nanor,* in zebrafish and investigated expression, localisation and function of the gene during early development. I also investigated neuroprotective and neurorestorative properties of three novel Parkinson's disease drugs, calcium channel inhibitor - isradipine, tetracycline antibiotic - minocycline and monoamine oxidase inhibitor - rasagiline using a zebrafish model of Parkinson's disease.

The transition from maternal to zygotic control of embryo development occurs with activation of the zygotic genome and degradation of maternal transcripts. This stage is known as the mid-blastula transition in zebrafish. Following this, axis patterning begins with the anteroposterior axis, the dorsoventral axis and the left/right axes. Left/right axis formation is essential for asymmetric development and correct orientation of developing organs such as the heart, brain and gut. In zebrafish, asymmetric development begins with dorsal forerunner cell migration to form a transient organ, Kupffer's vesicle; the organ of asymmetry. Kupffer's vesicle sends signals to the lateral plate mesoderm during somitogenesis which will result in nodal-related gene expression and correct asymmetry development in the larvae.

A novel, first-wave zygotic gene in zebrafish, *nanor,* was discovered by our research group and has been linked to left/right asymmetry development. Nanor has 3 paralogues and 3 orthologues. The best hit following genomic sequence alignment is to a P2X7-like purinoreceptor in Austrofundulus limnaeus, a closely related genus of fish, with no known human ortholog. I investigated *nanor* expression by quantitative PCR and whole-mount in situ hybridisation and found highest expression at sphere and shield stage with ubiquitous expression which becomes restricted to anterior structure by 24 hours post fertilisation. A second paralogue, *nanor b,* then goes through a second wave of gene expression up to 120 hours post fertilisation.

Transcription activator-like effector nucleases (TALEN) technology was used to knockout *nanor* in order to identify downstream genes. High embryonic lethality was recorded in mutant embryos with severe defects such as underdeveloped or absent eyes, brain and heads with bent bodies and severe heart oedema and blood pooling. Knockout was found to be embryonic lethal in mutants.

Following this, Nanor protein-protein interactions were investigated using co-immunoprecipitation followed by mass spectrometry. Results identified over 1500

interacting proteins. However, on closer investigation the custom made anti-nanor antibody used for Nanor protein complex binding was found to be binding to an off-target protein, 14-3-3 β/α-B, with no detection of Nanor. Investigations could not be continued due to no alternative antibody available.

Calcium influx into cells and Fibroblast growth factor (FGF) signalling are known to be two of the earliest signalling events in establishing left/right asymmetry. This study has found *nanor* to be downstream of calcium and FGF signalling following inhibition of these events using calcium channel inhibitor (isradipine) and FGF signalling inhibitor (SU5402) which resulted in increased *nanor* expression at 24 hours post fertilisation. Nodal-related gene *southpaw*, co-receptor *one-eyed pinhead* and downstream *lefty1* showed no significant changes in relative gene expression. TRAF3IP1 (*elipsa)* and *plakoglobin* mutant lines with defective left/right asymmetry development were also investigated in this study. *Nanor* mRNA expression was increased in both mutant lines with no changes in *southpaw* or *one-eyed pinhead* and a slight decreased in *lefty1* in *elipsa* mutants. *Nanor* was concluded to be downstream of calcium signalling, FGF signalling, *elipsa* and *plakoglobin*.

Parkinson's disease is a common, debilitating, neurodegenerative disorder for which the current most popular treatment, levodopa (L-DOPA), is symptomatic but does not slow or halt disease progression. There is an urgent, unmet need for neuroprotective or, ideally, neurorestorative drugs. Neurotoxin 6-hydroxydopamine (6-OHDA) was used to induce neuronal loss and locomotor deficit in zebrafish larvae. Three drugs (isradipine, minocycline and rasagiline) were screened for neuroprotective effects by co-treatment with the drugs and 6-OHDA from 2 to 5 days post fertilisation. Isradipine showed no neuroprotective effect during behavioural testing or immunohistochemical staining of dopaminergic cell survival. In contrast, both minocycline and rasagiline improved locomotor deficit and were neuroprotective against dopaminergic cell loss. Neurorestorative potential of each drug was also assessed by exposure to 6-OHDA from 48 hours post fertilisation (hpf) – 80 hpf followed by drug treatment up to 120 hpf. Exposure to 6-OHDA during neuroprotective (3 days) or neurorestorative (32 hours) experiments induced similar, significant locomotor deficits and neuronal loss in 5-day-old larvae. Isradipine had no effect on 6-OHDA-induced locomotor deficit or neuronal loss. However, both minocycline and rasagiline improved locomotor deficit and dopaminergic cell loss following 6-OHDA exposure. This study has shown the versatility of zebrafish in the study of genes essential for early development through genetic manipulation as well as their use in pharmacological screening in neurodegenerative diseases.

Chapter 1: Introduction

The zebrafish is a versatile vertebrate model species for the study of human genetics, development and disease. Gene knockdown and knockout techniques such as morpholino, TALEN and CRISPR have been successfully applied in zebrafish, and larvae are also widely used in pre-clinical drug screens for the treatment of human diseases. Embryos develop rapidly and externally with hundreds of embryos produced from a single mating pair. Zebrafish also have a fully sequenced genome with approximately 70% gene orthologues to humans making them a popular model of human genetic diseases (Howe et al., 2013).

1.1 Maternal to zygotic transition

Vertebrate embryo development begins following fertilisation and egg activation. Subsequent cell divisions (cleavage) eventually leads to the onset of gastrulation where a single blastula layer develops into a tri-laminar embryo (Fig. 1.1).

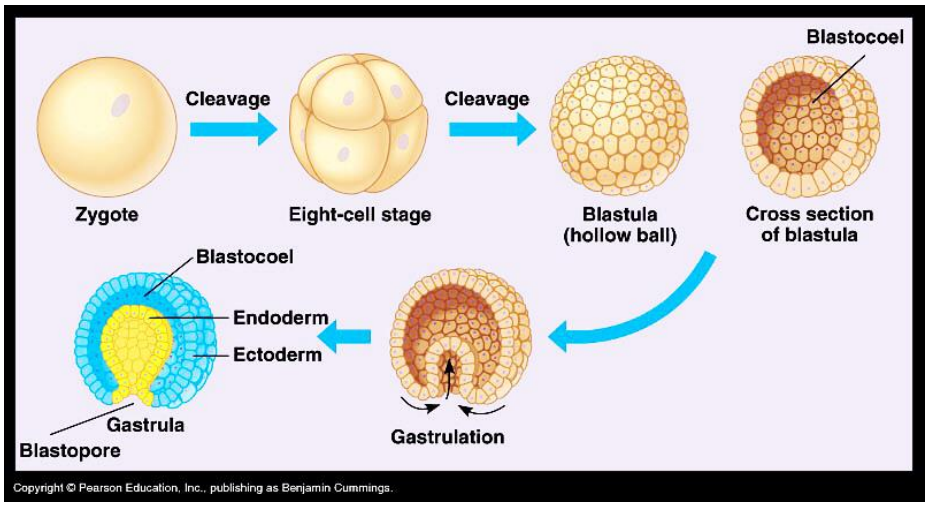

Fig. 1.1: Development of a one-cell embryo into a tri-laminar gastrula. Embryo development begins at the one-cell stage. Cleavage cycles eventually form a blastula. Following this gastrulation begins which forms the endoderm, mesoderm and ectoderm layers. (Lae, H. Gastrulation in Animals. Available https://hannahleaanimalkingdom.weebly.com/gastrulation.html. Last accessed 10th December 2017).

Across animal species, development begins with early cell cycles under maternal control; the transition from maternal to zygotic control of development (maternal to zygotic transition) spans the period from fertilisation to gastrulation (Fig. 1.2; Tadros and Lipshitz, 2009). During maternal control cell cycles are synchronous and lack gap phases; cycle length varies between species from 8 minutes in Drosophila, 15 minutes in zebrafish to 12 hours in mice. After a defined number of cleavage cycles, which is species dependent, maternal transcripts are depleted and there is a switch to zygotic transcription to control subsequent development. This point is known as the mid-blastula transition and in zebrafish occurs after 10 cleavage cycles. It is marked by changes in cell cycle and motility and precedes the onset of gastrulation in which ectoderm, mesoderm and endoderm are formed (Kane and Kimmel, 1993).

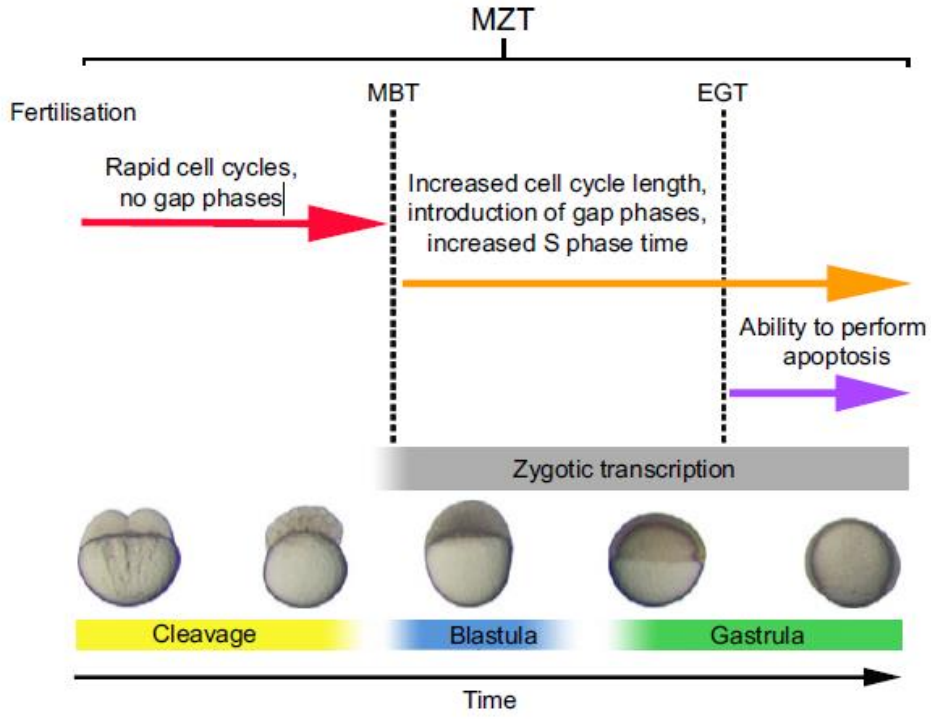

Fig. 1.2: The maternal to zygotic transition (MZT) in zebrafish. MZT spans from fertilisation to gastrulation where there is a switch from maternal to zygotic control of development. Cleavage is the first stage with rapid cell cycles and no gap phases. The mid-blastula transition (MBT) marks a specific point in the embryo which initiates transcription and sees cell cycles lengthen. Soon after this during the early gastrula transition (EGT) embryos acquire the ability to perform apoptosis (Image: Langley et al. (2014)).

Availability of next generation sequencing has greatly improved our understanding of genomic and epigenetic events prior to and subsequent to this transition. Up to the mid-blastula transition zygotic transcription has been silenced by four known mechanisms; cytoplasmic repressor, maternal clock, transcript arrest and chromatin mediated repression (Tadros and Lipshitz, 2009; Langley et al., 2014).

1.1.1 Mechanism of the zygotic genome activation

Embryonic cell cycle control by nucleo-cytoplasmic ratio has been extensively studied and was first described by Newport and Kirschner (1982). The mechanism of zygotic suppression is attributed to a repressor in the cytoplasm which is overcome by increased nuclei number as cells divide, relative to the cytoplasm, which has the effect of diluting out the repression of the zygotic genome (Dunican et al., 2008). Newport and Kirschner first stated this hypothesis by showing early genome activation in polyspermic Xenopus embryos. Stancheva and Meehan (2000) later linked DNA methyltransferase to this silencing event, independent of its methylation function.

Maternal clock is a second hypothesis on genome silencing and activation. Gene profiling in Drosophila found that activation was dependent on developmental stage rather than nucleo-cytoplasmic ratio (Lu et al., 2009). Also, in Xenopus the timing of Cyclin A and Cyclin E1 protein destruction was found to be independent of the nucleo-cytoplasmic ratio (Howe and Newport, 1996). Smaug, an RNA binding protein, is thought to be a key player in forming this clock. It functions in maternal RNA destabilisation and is thought to time zygotic genome activation (Benoit et al., 2009).

In Xenopus and Drosophila incomplete transcripts are abandoned by the DNA replication machinery during rapid early cleavage cycles and contribute to genome silencing (Shermoen and O'Farrell, 1991). Pharmacological inhibition of the cell cycle has been shown to result in extended interphase and early zygotic activation (Kimelman et al., 1987). The majority of early expressed maternal genes were found to encode for small proteins during these rapid cell cycles which further indicate short cycles may prevent

transcription of the zygotic genome and larger gene products (De Renzis et al., 2007).

The final proposed mechanism of zygotic genome silencing has been linked to histone modification in zygotic chromatin. During maternal control, chromatin structure renders zygotic genome incompetent for transcriptional activation. Aoki et al. (1997), showed pharmacological alteration of chromatin structure induced premature gene expression in mice.

Across vertebrates all four hypotheses of zygotic genome silencing have been validated and it is likely that a combination of these mechanisms aid in the silencing of the zygotic genome during initial cell divisions and later contributes to the activation of zygotic control of development (Tadros and Lipshitz, 2009).

1.1.2 mRNA degradation during the maternal to zygotic transition

Messenger RNA (mRNA) has a 5' cap and a poly-A tail which controls translation and stability of RNA. In the early oocyte, these mRNAs are unusually stable, however, as development proceeds maturation triggers mRNA instability leading to their destruction. Degradation by exonucleases is subsequent to deadenylation of the 3' poly-A tail by CCR4-NOT, a complex conserved across species, which regulates gene expression (Coller and Parker, 2004), and decapping of the 5' monomethyl guanosine by DCP2 and DCP1A resulting in totipotent identity of blastomeres through the loss of oocyte identity (Su et al., 2007). Inhibition of these complexes in mice has been shown to arrest mRNA degradation (Ma et al., 2013). Non-coding RNAs have also been linked to this degradation during early development.

The importance of microRNA (miRNA), small interfering RNA (siRNA) and piwi-interaction RNA (piRNA) during the maternal to zygotic transition has become clear in the last decade (Tam et al., 2008; Watanabe et al., 2008). They contribute to two events necessary for successful development of an embryo; stability and translation of maternal mRNA and transcriptional activation of zygotic genes (Svoboda and Flemr, 2010). Destabilisation of maternal RNA occurs through both zygotic and maternal degradation (Tadros and Lipshitz, 2009). In Drosophila, genome scale analysis has found

just over half of maternal transcripts are destabilised by maternal activity and zygotic activity destroys the remaining maternal transcripts (De Renzis et al., 2007).

1.1.3 The role of miRNA during the maternal to zygotic transition

miRNAs are approximately 22 nucleotides in length and bind the 3' untranslated region of target mRNAs to prevent translation and promote degradation (Giraldez et al., 2006). miRNAs are abundant on Argonaute proteins which control silencing of the zygotic genome as part of the RNA induced silencing complex and act as sequence specific guides for these complexes leading to repression of gene activation or mRNA degradation (Fig. 1.3; Chapman and Carrington, 2007; Svoboda and Flemr, 2010). Both maternal and zygotic miRNAs have important functions during early development and both contribute to clearance of transcripts with removal of either source resulting in developmental arrest due to transcript accumulation and interference prior to zygotic transition (Schier and Giraldez, 2006; Tang et al., 2007a).

A number of miRNAs are also zygotically transcribed and once zygotic transcription is activated, increased miRNAs provide enhanced efficiency of maternal mRNA degradation. miR-430 in zebrafish controls approximately 70% of vertebrate mRNAs and controls the rate of maternal mRNA decay and maintaining mRNA homeostasis (Giraldez et al., 2006). In Drosophila, miR-309 is analogous to miR-430 in zebrafish and is synthesised zygotically by *smaug* resulting in destabilisation of hundreds of maternal mRNAs (Benoit et al., 2009).

Nodal genes are common targets of miR-290 and miR-430 which contribute by clearance and gene silencing (Giraldez et al., 2006). The miR-290 family in Xenopus target mainly zygotic transcripts, however, miR-430 also controls a large amount of maternal mRNA in zebrafish (Svoboda and Flemr, 2010).

The most abundant zygotic miRNAs are the highly conserved let-7 family which are increased during the maternal-zygotic transition (Zeng and Schultz, 2005). In embryonic stem cells let-7 promotes differentiation and

clears and silences previously expressed transcripts, aiding embryonic progression to the next developmental stage (Bussing et al., 2008).

Although there is a wide variety of miRNA, a common theme emerges; levels of actively transcribed genes are modulated, and the clearance of transcripts is accelerated. Some miRNAs are ubiquitously expressed, however, the majority show restricted expression in tissues and organs (Giraldez, 2010).

1.1.4 The role of siRNA and piRNA during the maternal to zygotic transition

Endogenous siRNA in mice oocytes are derived from double stranded RNAs. The siRNA pathway is thought to act as a dominant RNA silencing mechanism controlling the maternal-zygotic transition through RNA induced silencing complex (Fig. 1.3). It guides the complex to the target mRNA, which is degraded by Argonaute protein cleavage (Giraldez, 2010).

piRNAs are a class of 24-30 nucleotide long RNAs produced by Argonaute proteins which play essential roles in RNA silencing processes and this class of non-coding RNAs also functions as part of the RNA induced silencing complex (Rouget et al., 2010). piRNAs control repression of transposable elements and act in cell maintenance and DNA integrity (Saito, 2013). Along with Smaug they activate maternal mRNA deadenylation and degradation in zebrafish and Drosophila embryos. In complex with Argonaute proteins Aub and Ago3, piRNAs recruit and stabilise the CCR4-NOT deadenylation complex together with Smaug to target *nanos* maternal mRNA. *Nanos* is responsible for posterior identity in Drosophila and has been found to be repressed in the first hours of embryogenesis by this complex (Fig. 1.3; Rouget et al., 2010).

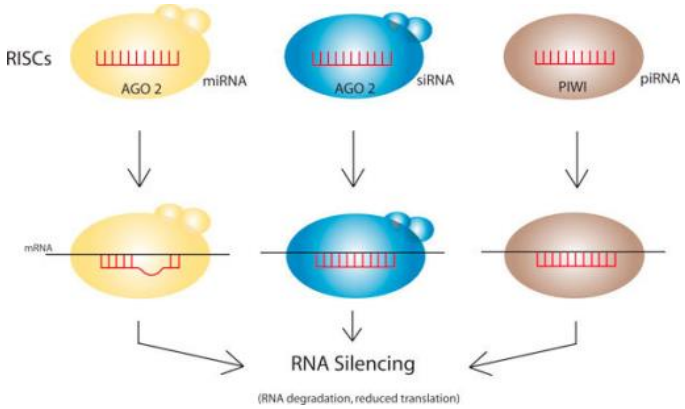

Fig. 1.3: Simplified image of miRNA, siRNA and piRNA induced silencing complexes along with argonaute proteins silence targeted mRNAs. Small miRNAs, siRNAs, or piRNAs serve as guide sequences within the RNA induced silencing complex (RISC) to capture target mRNA. The expression of the targeted mRNA is silenced either by RNA degradation or by inhibition of translation (Image Jeang (2012)).

1.1.5 The role of Smaug during the maternal to zygotic transition

Smaug is an RNA binding protein that coordinates aspects of the maternal to zygotic transition by repressing translation and triggering degradation of mRNA in the embryo. It acts through recruitment of the CCR4-NOT deadenylase complex to its target transcripts resulting in poly-A tail removal and transcript destruction (Semotok et al., 2005). Smaug expression is highest during upregulation of zygotic genome activation and replication checkpoint activation. The activity of Smaug prevents transcript build up during the mid-blastula transition (Benoit et al., 2009) and drives the molecular clock that controls the timing of this transition. Mutations in Smaug disrupt nuclear organisation during the syncytial blastoderm stage in Drosophila which shows that it also has an organisation role and results in a lack of cell cycle delays during the blastoderm stage with no DNA replication checkpoint activation during the maternal to zygotic transition (Dahanukar et al., 1999).

There are three types of zygotically transcribed genes; strictly zygotic genes, genes which are stable throughout the maternal to zygotic transition and increase in abundance following initiation of transcription, and genes which are degraded during the maternal to zygotic transition and later re-

expressed. Smaug is needed for the upregulation of 85-90% of strictly zygotic genes and genes stable throughout the maternal-zygotic transition; as well as having a role in down-regulation of 75% of the maternally provided zygotically transcribed genes (Tadros and Lipshitz, 2009).

1.1.6 Polyadenylation prior to gene activation

Harvey et al. (2013) successfully identified maternal and paternal mRNAs through RNA sequencing and nucleotide polymorphism and reported post-transcriptional regulation of maternal mRNA before onset of zygotic transcription. This led to the conclusion that maternal mRNAs which contribute to zygotic gene activation, are supressed in an inactive state through proteins bound to cytoplasmic polyadenylation elements in their 3' untranslated region (Mendez and Richter, 2001; Harvey et al., 2013). Upon requirement, these repressors are removed to activate mRNAs such as cyclin B1 to control cell cycle (Groisman et al., 2002). Lee et al., 2013 also found that some maternal mRNAs such as *nanog, pou5f1* and *sox19b* in zebrafish slowly become polyadenylated prior to their role in zygotic transcription.

1.1.7 The role of transcription factors during the maternal to zygotic transition

Zygotic genes that are maternally activated have been classed as first wave zygotic genes and are reliant on maternal factors for their transcription. In zebrafish 269 genes have been identified as first wave (Mathavan et al., 2005; Harvey et al., 2013; Lee et al., 2013). These first wave genes were shown by Lee et al. (2013) to be activated in the absence of zygotic gene function and primarily consist of genes that drive early embryo development.

Transcriptional activators are among the earliest mRNAs synthesised in an embryo and enhance the efficiency of zygotic transcription upon genome activation (Tadros and Lipshitz, 2009). *Oct4, Sox2* and *Nanog* are transcription factors in mice which control embryonic stem cell renewal and pluripotency (Boyer et al., 2005; Loh et al., 2006; Takahashi and Yamanaka, 2006). Reprogramming by these transcription factors can enable differentiated cells to adopt pluripotency and studies have shown that co-introduction of miRNA with *Oct4, Sox2* and *Nanog* will dramatically increase

reprogramming ten-fold when compared to introduction of these transcription factors alone. This is thought to be due to the ability of the miRNA to clear any unnecessary transcripts (Giraldez, 2010). In contrast to stem cell specific miRNA, some miRNAs such as let-7, prevent pluripotency once the cell has committed to a lineage, stabilising a cell's fate (Melton et al., 2010).

The three most highly translated transcription factors in zebrafish; *nanog, soxB1* and *pou5f1 (oct4)*, are involved in maintaining pluripotency in stem cells and contribute to widespread activation of zygotic genes during the maternal to zygotic transition as well as regulation miR-430 (Lee et al., 2013). *Pou5f1,* along with *soxB1* in zebrafish, regulates dorsal-ventral patterning and neuronal development (Okuda et al., 2010). However, *nanog* is crucial for regulation of *mxtx2* which results in endoderm formation (Xu et al., 2012).

A study by Lee et al. (2013) used a combination of morpholinos to study these transcription factors. By loss of function of *nanog, soxB1* and *pou5f1* they were able to prove that these genes regulate progression through gastrulation and early development. This study also demonstrated that combined loss of *nanog, soxB1* and *pou5f1* resulted in an 86% reduction in first-wave gene expression for strictly zygotic genes and failure in expression of 79% of maternal and zygotic genes when compared to wild-type embryos at 6 hours post fertilisation (hpf). At gastrulation stage, the affected genes included housekeeping genes, transcription factors and signalling factors in gastrulation, anterior-posterior and dorsal-ventral axis specification. These results proved that *nanog, soxb1* and *pou5f1* have a fundamental role in activating the first wave expression and this has a knock-on effect for subsequent waves of zygotic genome activation resulting in a complete block of gastrulation and developmental arrest. *Nanog* in zebrafish has been compared to *zelda* in Drosophila in activating a large number of downstream genes (Liang et al., 2008).

In zebrafish and Xenopus, Lee et al. (2013) have shown that miR-430 is regulated by *nanog, soxb1* and *pou5f1* with *nanog* appearing to be the main player in the control of miR-430 expression. Knockdown of *soxb1* and *pou5f1*

had no effect on miR-430 expression when compared to wild-types, however when combined with *nanog* knockdown, miR-430 expression was significantly reduced.

Nanor is a novel, zygotic gene discovered in our research group by Dr. Ronan Bree. He reported expression following the mid-blastula transition with no sequence similarity to any known gene or protein and found *nanor* to have a protein kinase C and 3 casein kinase II phosphorylation sites along with an N-myristoylation site and NFX-type zinc finger domain (Bree et al., 2005). It has been identified as one of the 269 first wave zygotic genes reported by Lee et al. (2013). These genes are responsible for the activation of second wave zygotic gene activation which in turn activates third wave gene expression (Hamatani et al., 2004). In general, first wave zygotic genes encode transcription factors and signalling pathway components in preparation for gastrulation but are also known to include housekeeping genes which carry out integral cell functions. In zebrafish, half of first wave genes have been classified as housekeeping genes and an equal proportion of genes encode transcription factors and signalling pathway components (Aanes et al., 2011).

Previous findings in the laboratory by Dr. Bree found negligible *nanor* expression at the 128-cell stage and high expression at sphere stage. During epiboly, he reported high expression in dorsal forerunner cells followed by solely anterior localisation at 24 hpf (Bree et al., 2005). Dr Shaun O' Boyle then went on to identify downstream genes from *nanor* through morphilino injection. He reported disruption to left/right asymmetry development and incorrect eye development and cardiac looping. In situ hybridisation also revealed disrupted Nodal signalling in the lateral plate mesoderm (O' Boyle, 2008). Melissa Walsh studied Nanor protein expression and found high expression following the mid-blastula transition with increasing protein expression up to 72 hours post fertilisation (hpf) (unpublished). No studies to date had further investigated mRNA and protein expression profiles as well as upstream and downstream genes and protein-interactions with Nanor.

Although zygotic activation is a complex process it can be summarised with three key events: genomic DNA must be activated through release of repressive forces (previously discussed repressive mechanisms of genome silencing), maternal mRNAs must be polyadenylated and translated leading to accumulation of transcription factors ready for zygotic transcription and the zygotic genome needs to be activated and transcribed (Smaug controlled timing of the mid-blastula transition) along with transcript clearance throughout the maternal to zygotic transition.

Our understanding of events during the maternal to zygotic transition has made significant advances in recent years. Despite this, we still have not fully elucidated the mechanisms of this transition. The maternal to zygotic transition is a complex event with many fundamental processes enabling development of the one-cell embryo into a multicellular organism. These events appear to be highly conserved across species and there is a clear co-dependence between maternal and zygotic transcripts in order for successful transition.

1.2 Gastrula period

Formation of the blastoderm layer in a zebrafish embryo occurs at 30% epiboly stage (4.5 hpf). Gastrulation period soon follows from 5.25-10 hpf where involuting cells and a thickening of cells at the blastoderm ring (germ ring) at 50% epiboly mark the beginning of gastrulation. This germ ring consists of two layers; the upper epiblast cells which migrate towards the margin and hypoblast cells which migrate in the opposite direction away from the margin (Warga and Kimmel, 1990) as shown in Fig. 1.4. Cells in the epiblast layer at the end of gastrulation will form the ectoderm and the hypoblast layer will become the mesoendoderm.

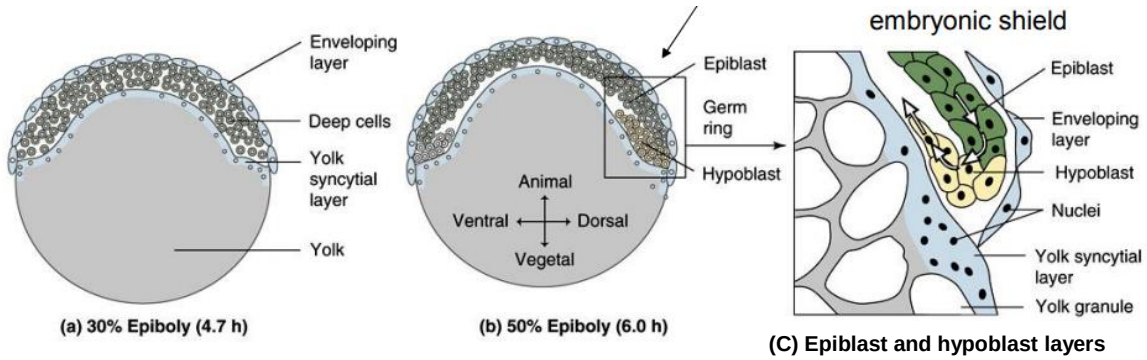

Fig. 1.4: Early development of a zebrafish embryo. (A) 30% epiboly. Developing cells are present on top of a yolk sac (B) 50% epiboly. Embryonic shield stage, cells migrate towards the germ layer and form the epiblast and hypoblast (C) moving in opposing directions. UMD. (2005). Gastrulation. Available: http://www.d.umn.edu/~pschoff/documents/Gastrulation-chickfishmammal.pdf. Last accessed 15thNov2017.

For an embryo to develop into a healthy adult, correct development of three axes are essential; the dorsoventral axis, anterioposterior axis and left-right axis. During gastrulation at shield stage (6 hpf) axis development and patterning is established in the embryo (Kimmel et al., 1995). The embryonic shield is the zebrafish equivalent of the Spemann-Mangold organiser in amphibians. Cells in the shield begin to involute and form the notochord which will pattern the body axis and establish dorsoventral polarity (Yamada et al., 1991). Cell migrations result in a thickening of the shield at the dorsal side of the embryo which is the first trace of the central nervous system known as the neural plate (Schmitz et al., 1993). At the end of shield stage, cells begin to elongate along the anterior-posterior axis where the embryo will develop a head and tail bud at the end of gastrulation (10 hpf) (Kimmel et al., 1995).

1.2.1 Primitive streak

During organisation and axis formation in avian, reptile and mammal embryos, undifferentiated cells migrate through the primitive streak (similar to shield in zebrafish) to generate the mesoderm and endoderm. Cells in the anterior primitive streak form the endoderm and anterior mesoderm. Cells in the middle region form the lateral plate mesoderm and cells in the posterior region form the hematopoietic cells. Embryonic patterning requires canonical Wnt/β-catenin, Activin/Nodal and bone morphogenic protein (BMP) signalling

pathways. During early embryo development, the Wnt/β-catenin pathway has important roles in forming the primitive streak, mesoderm and endoderm (Tam and Loebel, 2007). Activation of this pathway and the BMP signalling pathway are important for posterior primitive streak and mesoderm cells. Activin and Wnt/β-catenin synergistically function to induce cells to differentiate into endoderm progenitors. In zebrafish, formation of the head requires inhibition of Nodal, BMP and Wnt. Axis formation is due to Nodal signalling and inhibition of BMP and Wnt, with tail formation controlled by Nodal, BMP and Wnt signalling as shown in Fig. 1.5 (Sumi et al., 2008).

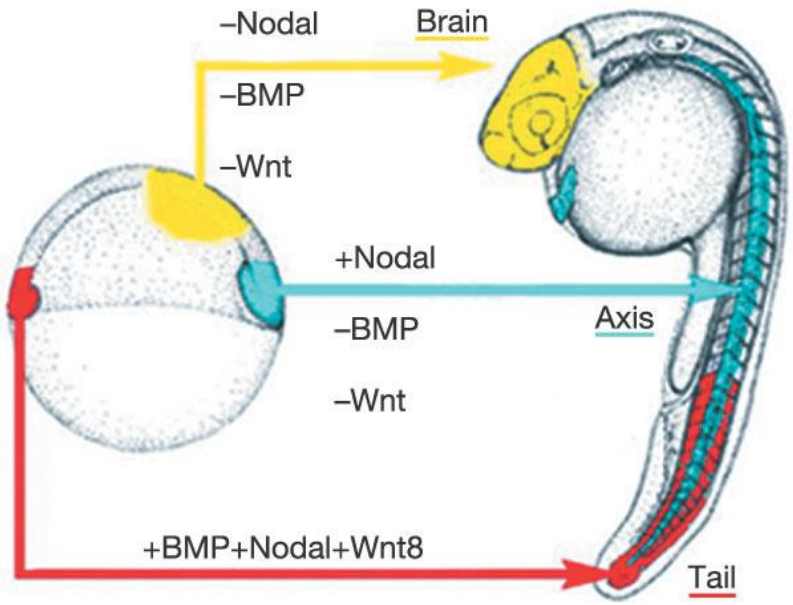

Fig. 1.5: Nodal, BMP and Wnt signalling in a zebrafish embryo. Nodal, BMP and Wnt signals contribute to patterning of the larva at early stages; - indicates inhibition of signalling and + indicates stimulation of signalling (Image: Agathon et al. (2003)).

1.3 Asymmetry development

A complex network of interactions occur to establish mesoderm and endoderm and control asymmetric patterning of developing organs in an embryo (Raya and Izpisua Belmonte, 2004). Nodals are the key players in inducing this patterning in mammals and first act prior to gastrulation to specify progenitors appropriate for their position (Feldman et al., 1998). Nodal is a secreted extracellular ligand of the TGFβ superfamily which binds

to Activin and extracellular growth factor (EGF)-CFC co-receptors and is highly conserved across species including mouse (*Nodal)*, zebrafish (*cyclops, squint and southpaw (spaw))* and Xenopus *(xnr1, xnr2, xnr4, xnr5 xnr6)* (Herpin et al., 2004).

To achieve this asymmetry, cilia must initiate calcium elevation on the left side of the left/right organiser, which is thought to be the earliest event leading to asymmetry development. Downstream of this calcium gradient, *Notch* is activated, which is responsible for *Nodal* activation. *Nodal* and downstream *Lefty* then display asymmetric patterns in the lateral plate mesoderm of chick, mice, frog and zebrafish (Yost, 1999; Amack et al., 2007).

1.3.1 Kupffer's vesicle; the organ of asymmetry

Left-right axis development in an embryo requires both symmetrical and asymmetric organ development. Kupffer's vesicle is a transient, fluid-filled cavity in a zebrafish embryo that is formed at approximately 12 hpf in the tail bud, responsible for establishing this asymmetric development and is formed from 5 steps that precede gene asymmetry (Fig. 1.6) (Essner et al., 2005).

1) Approximately twenty dorsal forerunner cells are induced during the blastula period by Casanova (Cas). Knockdown of this gene results in no endoderm development and forerunner cells with absent *left-right dynein (lrdr1), no tail (ntl)* and *spadetail (spt)* expression (Cooper and D'Amico, 1996; Alexander et al., 1999).
2) Following Cas, ciliary motor protein left-right dynein-1 (Lrdr1), is activated in dorsal forerunner cells. *Oep* is a Nodal signalling co-receptor and *sur* is a transcription factor linked to Nodal signalling that are essential for *lrdr1* expression along with *ntl*. In the absence of these three genes Lrdr1 is not expressed (Essner et al., 2005).
3) Dorsal forerunner cells ingress to form Kupffer's vesicle in the tailbud, with formation dependent on Nodal signalling and enhanced by *oep* as well as *ntl* and transcription factor *spt*.

4) Cilia then develop on cells in Kupffer's vesicle independent of Lrdr1 expression. As discussed later, these cilia are crucial for correct function of the vesicle.
5) For the final step, cilia motility and fluid flow are established with both processes requiring Lrdr1. These 5 steps are summarised in Fig. 1.6 (Essner et al., 2005).

Downstream of these events, the Nodal signalling cascade is activated which controls asymmetric development of organs.

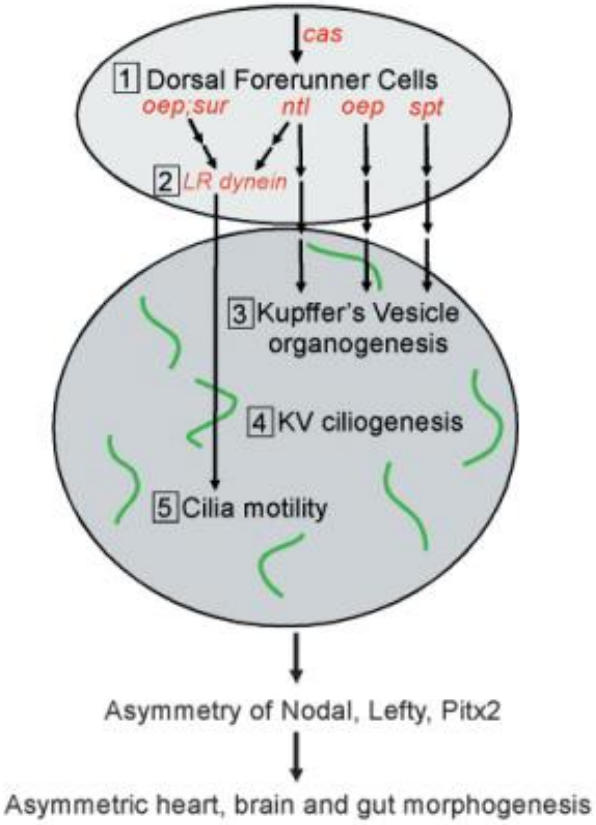

Fig. 1.6: Schematic diagram of the five milestones leading to correct Kupffer's vesicle formation (Essner et al. (2005)).

1.3.2 Cilia organisation in Kupffer's vesicle

The Kupffer's vesicle equivalent in mammals, the node, differs in structure with a flat, ciliated node floor with an overlying membrane known as Reichert's membrane. Cilia in the node also direct an asymmetric flow resulting in asymmetric gene expression (Nonaka et al., 1998). Kupffer's

vesicle in zebrafish consists of a ciliated dorsal roof and ventral floor with 80% of cilia on the dorsal surface and 20% on the ventral surface, with a higher concentration at the anterior end correlating with strong leftward flow in the anterior pole and weak rightward flow at the posterior end (Kreiling et al., 2008). This higher cilia concentration is known to establish asymmetry development and leftward fluid flow (Supatto et al., 2008). Remodelling of Kupffer's vesicle as development of the vesicle is near completion has been discovered, which creates a cell-cell tension gradient from anterior to posterior direction resulting in more cells concentrated at the anterior end with a higher cilia concentration mediated by Myosin II, as well as *rho-associated protein kinase (rock2b)* (Wang et al., 2011; Wang et al., 2012). *Dynein heavy chain 9* (*dnah9), intraflagellar transport 88 (ift88- polaris)* and *vang-like protein 2* (*vangl2)* have also been shown to have roles in the development, movement and positioning of cilia with silencing of these genes disrupting left/right asymmetry development (Olbrich et al., 2002; Haycraft et al., 2005; Borovina et al., 2010).

1.3.3 Nodal flow detection

Within the left/right organiser, three main hypotheses have been attributed to detection and functioning of Nodal flow;

1) Morphogen hypothesis claims a temporary enrichment of a molecule on the left side of the left/right organiser is detected and results in left/right asymmetric signal (Cartwright et al., 2004).

2) Nodal vesicular parcel hypothesis argues that morphogens are delivered in membrane bound vesicles to the left side of the left/right organiser establishing asymmetry development (Hirokawa et al., 2009).

3) The two-cilia hypothesis states motile cilia produce an asymmetric flow of extracellular fluids. Immotile sensory cilia then detect flow on the left but not right side of the left/right organiser and leads to a calcium signal in response and initiation of the Nodal cascade (Norris, 2012).

Although there is debate on the mechanism of Nodal flow, there is one consensus between all three hypotheses; they all result in a calcium

elevation on the left side of the vesicle. Calcium has also been attributed to communication to the lateral plate mesoderm and left/right asymmetry modulation at later developmental stages (McGrath and Brueckner, 2003; Praetorius et al., 2003; Sullivan-Brown et al., 2008).

1.3.3 The role of calcium channels in asymmetry development

Raya et al. (2004) found calcium to be a possible mediator between the asymmetric signal established in the node of mice and asymmetric activity of *Notch* to activate Nodal signals. Yuan et al. (2015) were first to show that cytoplasmic calcium is preceded by intra-ciliary calcium oscillations which are reliant on ciliary motility. They report beating motile cilia to be at the centre of the left/right organiser to establish the leftward flow. At the periphery of this field of motile cilia, immotile sensory cilia initiate the Nodal cascade in response and this leads to asymmetric organ development. They also found that this calcium initiation was dependent on polycystin 2; an intracellular calcium release channel found on cilia with a mechanosensory role. Loss of calcium asymmetry also resulted in loss of downstream Nodal activators in the embryo. Yuan et al. (2015) reported that calcium signals from the node travel as far as the lateral plate mesoderm which may provide a mechanism for asymmetric gene signalling from the node to the lateral plate. Connexin has been found by Beyer et al. (2012) to be responsible for sending signals from the left/right organiser to the left lateral plate mesoderm and Viotti et al. (2012) were able to show that gap-junction dependent calcium signals travelled from the node to the lateral plate mesoderm. In opposition to this a number of studies have found Nodal expression was self-regulating and sufficient for self-activation in the lateral plate mesoderm as reviewed by Hamada et al. (2002).

1.3.4 Polaris and Polycystin 2 during asymmetry development

Polaris has an important function in protein transport along cilia. Morphants have shortened cilia and as a result disrupt the retrograde flow in Kupffer's vesicle and inhibit intraflagellar transport (IFT) protein receptors needed for signalling (Barr et al., 2001). Defects in either polaris or polycystin 2 are known to result in polycystic kidney disease in mammals and left/right asymmetry defects (Moyer et al., 1994). Morpholino injection and knockdown

of these genes were shown to result in absent Nodal expression in the lateral plate mesoderm indicating that polaris and polycystin 2 are upstream of the Nodal signalling cascade. Expression has been found in dorsal forerunner cells activated by *no tail* and *spadetail* genes (Murcia et al., 2000; Bisgrove et al., 2005).

As well as controlling calcium flux in Kupffer's vesicle, calcium channels are localised to cilia and required for cell signalling and development. Cilia sense mechanical force in the surrounding environment through these channels (Jin et al., 2014). Defective cilia such as those found in ciliary mutants prevent signalling processes occurring and lead to asymmetry defects in the larvae (Praetorius et al., 2003; Sullivan-Brown et al., 2008).

1.3.5 TRAF3IP1 and *plakoglobin* function in ciliogenesis

Tumour necrosis factor (TNF) receptor-associated factor 3 interacting protein 1 (TRAF3IP1) (ENSDARG00000010300), also known as *elipsa* is an early marker of ciliogenesis. The protein binds to intraflagellar transport protein 20 (IFT20), a component of IFT particles which are an important part of correct cilia formation and function. Their role in Kupffer's vesicle establishes a leftward fluid flow and helps in the patterning of early gene expression. *Elipsa* mutant larvae have morphological defects characteristic of mutants with defective cilia such as curly body axis formation (Omori et al., 2008). mRNA localisation of Nodal and *lefty1* has previously been shown to be altered in left/right asymmetry mutant lines; organisation of asymmetry genes such as *lefty1* becomes bilaterally expressed instead of restricted left-sided expression in the lateral plate mesoderm (Kobayashi et al., 2010; Smith et al., 2011; Lee et al., 2015).

Junction Plakoglobin is also expressed in Kupffer's vesicle and has roles in cilia development. However, the gene is best known for its role in desmosome, adherens junction and gap junction formation in cardiac muscle and mutations have been linked to sudden adult death syndrome (Kaplan et al., 2004). Depletion of junction Plakoglobin has been reported in ciliated cells with disrupted formation and function (Laoukili et al., 2001). Gap junctions formed by *plakoglobin* have been linked as a possible

communication mechanism of cell signalling from Kupffer's vesicle to the lateral plate mesoderm, which allows correct development of asymmetric gene expression and left/right asymmetry development (Levin and Mercola, 1998).

1.3.6 Fibroblast growth factor (FGF) signalling during asymmetry development

FGF signalling is responsible for generating an anterior/posterior gradient which establishes caudal mesoderm with higher expression at the caudal end of an embryo (Dubrulle et al., 2001). Signalling has also been linked to transport and release of Nodal vesicular parcels in Kupffer's vesicle which carry sonic hedgehog and retinoic acid and are released on the left side of the left/right organiser to establish left-sided gene expression which is passed on to the lateral plate mesoderm (Tanaka et al., 2005). FGF receptors are now known to be localised to motile cilia and it was suggested that cilia have an FGF sensory function in the node. The FGF receptor inhibitor, SU5402, abolished calcium elevation on the left side of the node, inhibiting Nodal functioning and downstream gene expression leading to the conclusion that FGFs act as master genes to calcium elevation and Nodal activation. SU5402 also inhibited the transport of Nodal vesicular parcels to the left with a phenotypic rescue with retinoic acid and sonic hedgehog showing they are immediately downstream of FGF signalling (Tanaka et al., 2005).

Effects of FGF on Nodal and Lefty indicate that FGF has a function in transcriptional regulation. Early immediate response 2 (*ier2*) gene is an FGF target gene in the zebrafish embryo with FGF intercellular binding protein 1 (Fibp1) an interacting partner. Both targets are nuclear localised and knockdown results in severe left/right asymmetry defects in embryos with randomised *spaw* and *lefty1* expression. A defect in ciliogenesis was linked to this phenotype with a loss of *charon* also noted. These phenotypes were rescued with *Ier2* and *Fibp1* microinjection (Hong and Dawid, 2009).

During later developmental stages, FGF is necessary for correct development of the forebrain and left/right asymmetric patterning independent of asymmetry in the lateral plate mesoderm. A recent study has shown that *lefty1* is bilaterally expressed in the diencephalon following FGF inhibition with overexpression causing absent *lefty1* diencephalic expression (Neugebauer and Yost, 2014).

1.3.7 Activation of the Nodal signalling pathway

Nodal signalling is dependent on EGF-CFC co-receptors for signalling to occur. These EGF-CFCs are extracellular membrane anchored proteins which include Oep (zebrafish), CFC (chick) and Crypto (mouse) (Shen and Schier, 2000). In the absence of these co-receptors, Nodals are unable to form a complex with activin receptors resulting in a failure of the Nodal signalling cascade. Expression is found in the lateral plate mesoderm in regions where Nodals are present (Fig. 1.7) (Gritsman et al., 1999; Song et al., 1999; Bianco et al., 2002). Once bound, an intracellular complex is formed with phosphorylated Smad2, Smad4 and FoxH1 (Schier and Shen, 2000; Schier, 2003) which activates downstream *Lefty1, Lefty2* and *Pitx2* in the left lateral plate mesoderm (Ryan et al., 1998; Whitman and Mercola, 2001).

Downstream leftys are antagonists to Nodal signals and restrict *Nodal* expression in the lateral plate mesoderm. In Xenopus, *cerberus* is a closely related gene known to induce head formation in embryos (Bouwmeester et al., 1996). Structurally, it is related to antagonists of the TGFβ family and this protein functions as an antagonist of Nodal, BMP and Wnt proteins for correct patterning in an embryo (Piccolo et al., 1999).

Nodal proteins are translated as proproteins and reliant on convertases for activation. Spc1 and Spc4 are convertases implicated in Nodal maturation from a proprotein. Without convertases Nodal proteins would not be activated to enable downstream signalling (Beck et al., 2002). The Nodal signalling cascade is summarised in Fig. 1.7.

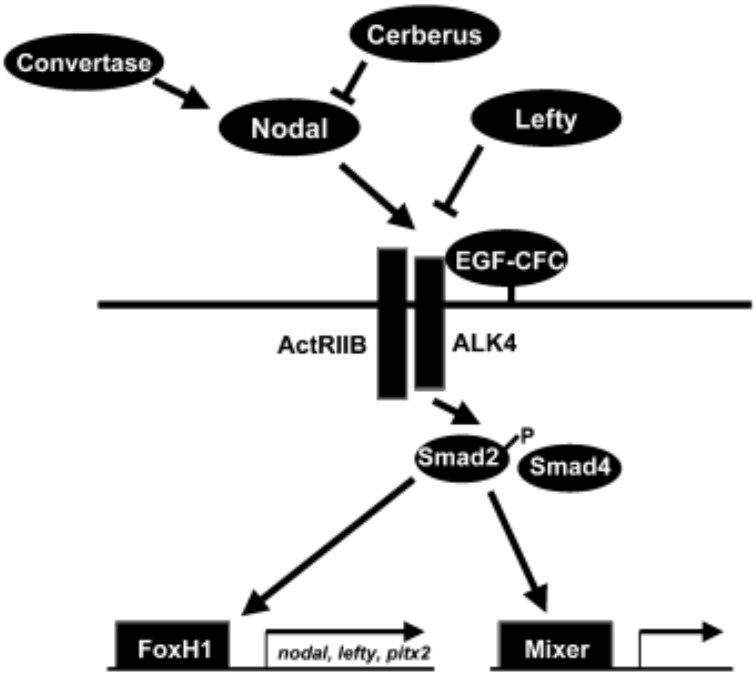

Fig. 1.7: Nodal signalling pathway. Nodal is activated by binding to activin receptors and EGF-CFC co-receptors and is inhibited extracellularly by lefty and Cerberus. Convertases process Nodal proproteins. Intracellularly Smad2 is phosphorylated and forms a complex with Smad4 and FoxH1 to activate downstream Nodal, Lefty and Pitx2. In Xenopus, the Mixer complex regulates expression of transcription factor Goosecoid (Schier, 2003).

1.3.8 Lefty expression and BMP signalling in the lateral plate mesoderm

The lateral plate mesoderm has three barriers which ensure gene expression is restricted and controlled. *Lefty1* expression forms a midline barrier which helps in restriction of Nodal signals to the left side. The posterior barrier is regulated by BMP signalling which oppresses *spaw* expression and the anterior barrier is controlled by *lefty2* expression. These barriers are thought to be highly conserved across all species (Lenhart et al., 2011). BMP signalling in the lateral plate mesoderm prevents ectopic Nodal expression by limiting Smad4 availability and is needed for *lefty1* activation in the midline (Furtado et al., 2008). Overexpression of BMP2a eliminates *spaw* in the lateral plate mesoderm with inhibition of BMP causing bilateral *spaw* expression (Chocron et al., 2007).

1.3.9 Cyclops and Squint Nodal-related genes

Cyclops and *squint* are Nodal related genes found in zebrafish also part of the TGFβ family which are essential for germ layer formation and capable of sending short or long range signals (Feldman et al., 1998) (Fig. 1.8). *Squint* is known to directly induce downstream genes in distant cells with *cyclops* acting only at short range in zebrafish embryos (Shen and Schier, 2000). *Cyclops* and *squint* are also known to induce most mesoderm and endoderm tissues with *cyclops* and *squint* double mutants failing to develop a head, trunk mesoderm and endoderm (Dougan et al., 2003). *Cyclops* mutants are found to have only minor defects in the prechordal plate with *squint* mutants having a mild defect in mesoderm and endoderm formation. Following these results, it was concluded that the mild developmental defects seen were due to a compensatory effect between the two genes. Cyclops and Squint proteins are expressed in cells close to the margin. Squint then has the ability to migrate away from the margin and exert its effects in distant cells. Contrary to this, Cyclops remains close to the margin and has effects at a close range (Fig. 1.8) (Dougan et al., 2003; Schier, 2003).

Downstream gene expression from Nodal signalling depends on concentration effects of Nodal signals. Squint has been found to induce *goosecoid* at short range signalling, responsible for pharyngeal endoderm and head mesoderm formation and *ntl* at long range signalling, which forms posterior structures. This has suggested that Nodal signalling and gene expression is dependent on a concentration gradient with strongest signalling at close range (Shen and Schier, 2000).

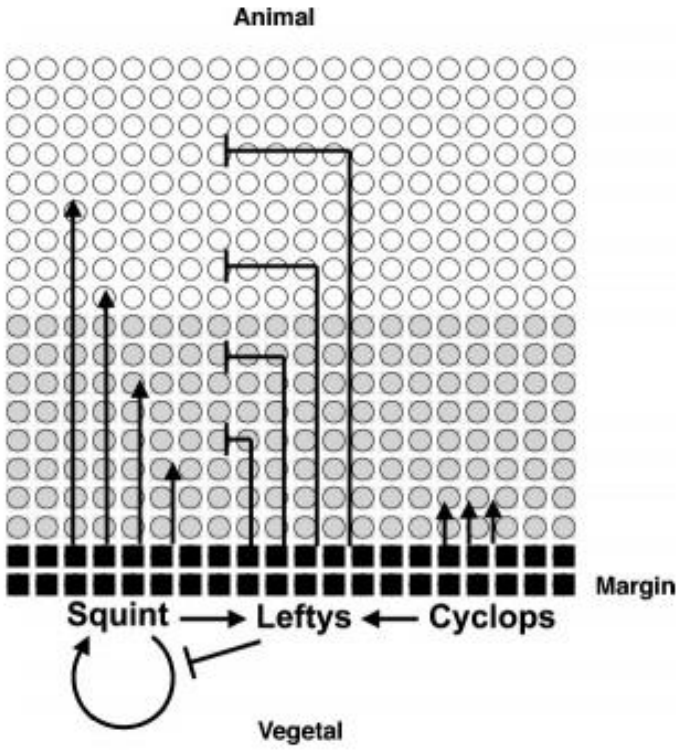

Fig. 1.8: Mesoendoderm induction in zebrafish. Cyclops and squint acting at short and long range are antagonised by leftys which determine the extent of mesoderm progenitors at the onset of gastrulation. Cross interactions control expression of all three genes (Schier, 2003).

Left/right asymmetry development is a complex process dependent on Nodal signalling which requires initiation by a number of factors; FGF signalling, calcium influx and dorsal forerunner migration, leading to successful development of the left/right organiser, are highly conserved processes across species activating downstream Nodal signals. Downstream of Nodal signalling organogenesis with correct laterality will result in an organism.

Calcium channel blockers, such as isradipine, are useful in the study of left/right asymmetry development and have also been proposed as a neuroprotective treatment for Parkinson's disease.

1.4 Parkinson's disease

Parkinson's disease is the second most common neurodegenerative disorder characterised by loss of dopaminergic neurons from the nigrostriatal pathway and the formation of α-synuclein protein aggregates known as Lewy bodies. Although incompletely understood, the disease is thought to be due to a

combination of environmental and genetic factors. Oxidative stress, mitochondrial dysfunction and neuro-inflammation have all been linked to disease progression (Dauer and Przedborski (2003) for review). Early diagnosis of Parkinson's disease is rare, as symptoms in patients only manifest after approximately 60% of nigral dopamine neurons have degenerated and 80% of striatal dopamine has been lost (Fearnley and Lees, 1991). In addition to the motor symptoms of tremor, rigidity and akinesia, many patients suffer from depression and sleep disorders along with slowed cognitive processes (Dauer and Przedborski, 2003) and can experience up to 84% decline in their cognitive function as the disease progresses (Jankovic, 1984). These non-motor symptoms are believed to be a result of dopamine deficiency in the non-motor portion of the striatum as well as pathological changes in the brainstem, thalamus and the cerebral cortex (Braak et al., 2003).

1.4.1 Basal ganglia function

The basal ganglia are a group of subcortical nuclei that have traditionally been associated with the control of motor function (Kemp and Powell, 1971). Major components of the basal ganglia include the dorsal striatum (caudate and putamen), ventral striatum (nucleus accumbens and olfactory tubercule), globus pallidus, ventral pallidum, substantia nigra and subthalamic nucleus (Fig. 1.9). The basal ganglia are now known to also have several functions in non-motor processes such as learning of complex behaviour, emotions, motivation and cognition. The circuitry forms a complex network that integrates associative, oculomotor, limbic and motor cerebral regions, basal ganglia nuclei, the thalamus and brainstem. Motor areas project to the putamen which sends signals to the globus pallidus *interna* and substantia nigra *pars reticula* and onto the anterior and ventrolateral thalamus. The thalamus is the final basal ganglia link back to the cortex (Haber and Calzavara, 2009 for review).

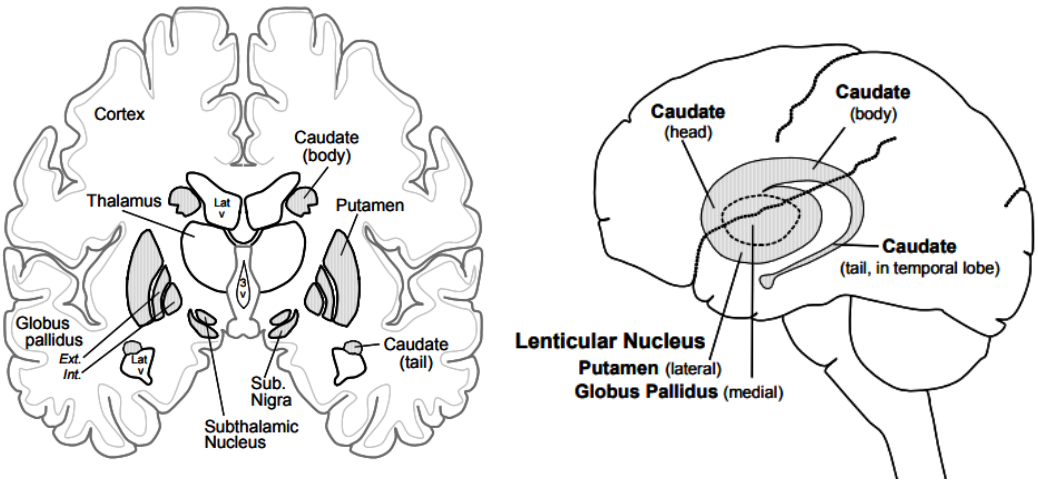

Fig. 1.9: Neuroanatomy of the basal ganglia in humans. The basal ganglia motor loop is located in the mid-brain and consists of the caudate, putamen, globus pallidus, substantia nigra and subthalamic nucleus and projects to the thalamus and frontal cortex. (Image: University of Wisconsin. (2006). Basal Ganglia. Available: https://www.wisc.edu/. Last accessed 20th Dec 2017).

1.4.2 Circuitry of the basal ganglia

Information sent from numerous cortical areas is processed in specific areas of the basal ganglia and returned to the frontal lobe via the thalamus. Regions of the frontal cortex form synaptic connections with defined regions of the basal ganglia. The anterior cingulate cortex and orbital frontal cortex involved in reward-based behaviour project to the ventral striatum which signals to the ventral pallidum and ventral tegmental area to the medial substantia nigra (Haber et al., 1995). Areas of the prefrontal cortex involved in planning and working memory project to the rostral and dorsal caudate nucleus, then signals the central part of the globus pallidum and substantia nigra (Selemon and Goldman-Rakic, 1990) and areas involved in planning action project to the dorsal and lateral caudate nucleus. This region signals the central and dorsal globus pallidus and ventral substantia nigra (Haber et al., 2000).

1.4.3 Direct and indirect pathways in the basal ganglia

Over 90% of the projection neurons within the striatum are made up of inhibitory GABAergic medium spiny neurons (Kemp and Powell, 1971).

Output from the basal ganglia is also inhibitory and pathways within the motor circuit lead to switching this inhibition on or off. Motor areas of the cortex project to the striatum through excitatory, glutamatergic synaptic connections. In the striatum, they form connections with medium spiny neurons and these connections are linked to globus pallidus interna and substantia nigra pars reticula by a monosynaptic, direct pathway which inhibits globus pallidus interna/substantia nigra pars reticula output or a polysynaptic indirect pathway which inhibits the globus pallidus externa, disinhibits the sub-thalamic nucleus and causes excitation of the globus pallidus interna/substantia nigra pars reticula (summarised in Fig. 1.10). Output from the globus pallidus interna and substantia nigra pars reticula are inhibitory GABAergic neurons and tonically inhibit thalamocortical neurons in the ventral anterior, ventrolateral and intralaminar nuclei of the thalamus and brainstem neurons (DeLong and Wichmann, 2007).

Increased output from the basal ganglia (via the indirect pathway) will result in less movement due to inhibition of thalamocortical projection neurons, conversely reduced basal ganglia output (via the direct pathway) translates into increased movement due to disinhibition of neurons. Combined action of direct and indirect pathways is thought to adjust movement. This balance is regulated by dopamine on striatal neurons in the substantia nigra *pars compacta*. D1 in the direct pathway with co-expressed peptides substance P and dynorphin and D2 in the indirect pathway and the peptide enkephalins both reduce globus pallidus interna and substantia nigra pars reticula output facilitating movement (Fig. 1.10) (Gerfen et al., 1990; Cepeda et al., 1993; Obeso et al., 2000; DeLong and Wichmann, 2007).

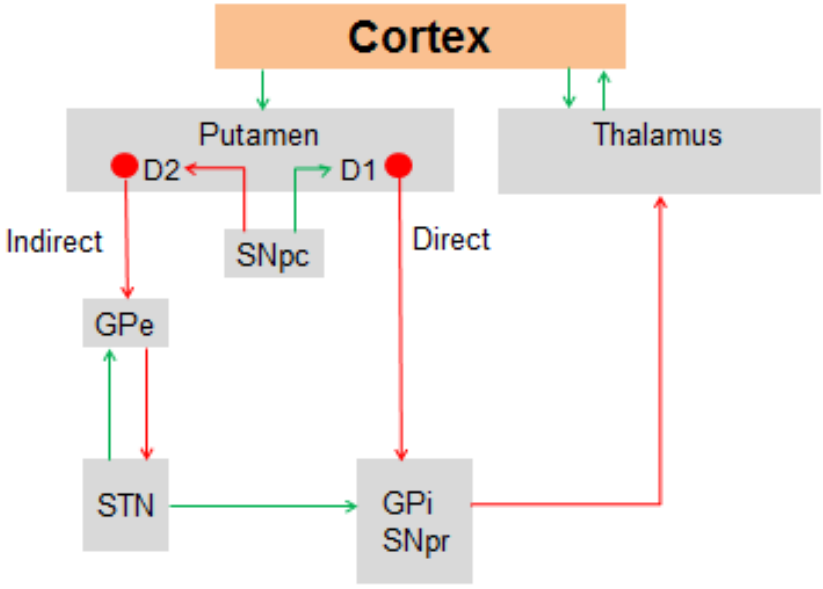

Fig. 1.10: Simplified representation of direct and indirect pathways of the basal ganglia motor circuit. Red connections represent inhibitory GABA signalling with green connections representing glutamatergic excitatory signalling. Signalling begins and terminates in the frontal cortex. (Image: DeLong and Wichmann (2007) with modification to give a more simplistic summary of direct and indirect pathways of the basal ganglia motor loop).

One of the main pathological hallmarks of Parkinson's disease is loss of dopaminergic neurons from this brain region leading to reduced function and motor impairment. In a healthy, aging person, gradual dopaminergic cell loss is seen in the dorsomedial substantia nigra pars compacta, however, Parkinson's disease patients have extensive cell loss in ventrolateral and caudal areas of the substantia nigra pars compacta. Significant nerve terminal loss in the striatum is also evident (Fearnley and Lees, 1991). In Parkinson's disease, increased neuronal activity in the globus pallidus interna/substantia nigra pars reticula output nuclei of the basal ganglia, leads to excessive inhibition of the thalamo-cortical and brainstem motor neurons. Reduced activation of dopamine receptors as a result of dopamine deficiency decreases inhibition of the indirect pathway with a reduced excitation of the direct pathway. Excessive activation of the basal ganglia output results, which inhibits glutamatergic signals from the thalamus and inhibits excitation of the motor cortex leading to motor effects of Parkinson's disease (DeLong and Wichmann, 2007).

1.4.4 Molecular pathology of Parkinson's disease

Oxidative stress, mitochondrial dysfunction, Lewy body formation and neuroinflammation have all been linked to Parkinson's disease progression.

Oxidative stress

Oxidative stress has been implicated in dopaminergic cell death in Parkinson's disease. Although all tissues can be damaged by oxidative stress, the brain is more susceptible due to its heavy oxygen demand. Within the brain, dopaminergic neurons are extremely vulnerable as they naturally produce a large quantity of reactive oxygen species (ROS) during dopamine metabolism. Dysfunction of mitochondria, excitotoxicity, nitric oxide toxicity and inflammation are all known to result in overproduction of ROS which leads to oxidative stress (Jenner and Olanow, 2006; Zhu and Chu, 2010). In a healthy cell, ROS play a role in respiration and have been implicated in cell signalling processes such as Mitogen Activated Protein Kinase (MAPK) pathways, which send signals from the cell surface to the nucleus, through ROS activation of extracellular signal-regulated kinases (ERKs), c-Jun N-terminal kinases (JNKs) and p38 MAPKs (Sun and Oberley, 1996). At low concentrations, they are a cell's defence against infectious agents and contribute to cell signalling systems. Overproduction of ROS inhibits normal function of a cell by damaging protein and DNA (Valko et al., 2007). The hydroxyl radical reacts with all elements of DNA damaging the purine and pyrimidine bases and the deoxyribose backbone (Halliwell and Gutteridge, 1986).

Mitochondrial dysfunction

Mitochondria consume the majority of molecular oxygen for use in adenosine triphosphate (ATP) production. Under normal conditions, the reduction of oxygen in the mitochondrial respiratory chain will lead to generation of ROS which are controlled by antioxidants such as superoxide dismutase and small molecules like vitamin C and E.

Dysfunction of mitochondria has been linked to progression of many neurodegenerative diseases such as Alzheimer's disease, Parkinson's disease, Amyotrophic Lateral Sclerosis (ALS) and Huntington's disease.

Disruption to homeostasis occurs though mitochondrial DNA mutations leading to damaging effects in Parkinson's disease through overproduction of ROS. Many genes linked to Parkinson's disease progression are also known to have interactions with mitochondria and mutations in these Parkinsonism genes will also disrupt normal mitochondrial function.

Damaging effects from mitochondria result from dysfunction of complex I of the respiration chain leading to the formation of toxic radicals through overproduction of ROS leaving neurons vulnerable to glutamate excitotoxicity (Sherer et al., 2002). Families with inherited Parkinson's disease have also been found with dysfunctional complex I activity and increased reactive oxygen species production (Swerdlow, 1998). Antioxidants such as superoxide dismutase appear to be overwhelmed by increased ROS production and are unable to prevent toxic accumulation (Halliwell, 2001).

Lewy body formation

A pathological hallmark of Parkinson's disease is accumulation and aggregation of α-synuclein in vulnerable dopaminergic neurons, known as Lewy bodies. Alpha-synuclein is a neuronal protein that is found predominately at presynaptic terminals and in a healthy brain is known to be degraded by both the proteasome and autophagy (Webb et al., 2003).

Two missense mutations found in the α-synuclein gene were the first Parkinson's disease mutations to be identified. They are now known to cause autosomal dominant early-onset Parkinson's disease (Dawson and Dawson, 2003). To date over 50 α-synuclein mutations have been identified.

Lewy bodies accumulate in surviving neurons in Parkinson's disease brains and are common to sporadic and genetic Parkinson's disease. Aggregated α-synuclein binds to the proteasome and inhibits ubiquitin-dependent proteasomal function (Snyder et al., 2003). Inhibition of the proteasome then leads to an inability to clear proteins targeted for degradation by the ubiquitin-proteasome system resulting in toxicity and the demise of dopaminergic neurons (Tanaka et al., 2001). These deficits in ubiquitin-dependent degradation of intracellular proteins have been linked to Lewy

body formation and disease progression (Ciechanover, 1998; Bennett et al., 1999).

Neuroinflammation

Inflammation results in oxidative stress and cytokine-dependent toxicity. Evidence for neuro-inflammation as a contributing factor to Parkinson's disease comes from findings of activated microglia, cytokine accumulation, nuclear factor kappa b (NFκB) pathway activation and oxidative damage to proteins in brains of patients (McGeer et al., 1988).

Microglia are type of macrophage present in the central nervous system and mediate the innate defence system as well as acting as scavenger cells in inflammation, infection and neurodegeneration (Beyer et al., 2000; Kim and de Vellis, 2005). These cells are highly sensitive to changes in homeostasis in the brain and activate in response to inflammation (Fig. 1.11) (Wojtera et al., 2005). Post-mortem analysis of Parkinson's disease patients revealed an elevated number of activated microglia in the substantia nigra (Hirsch et al., 1998).

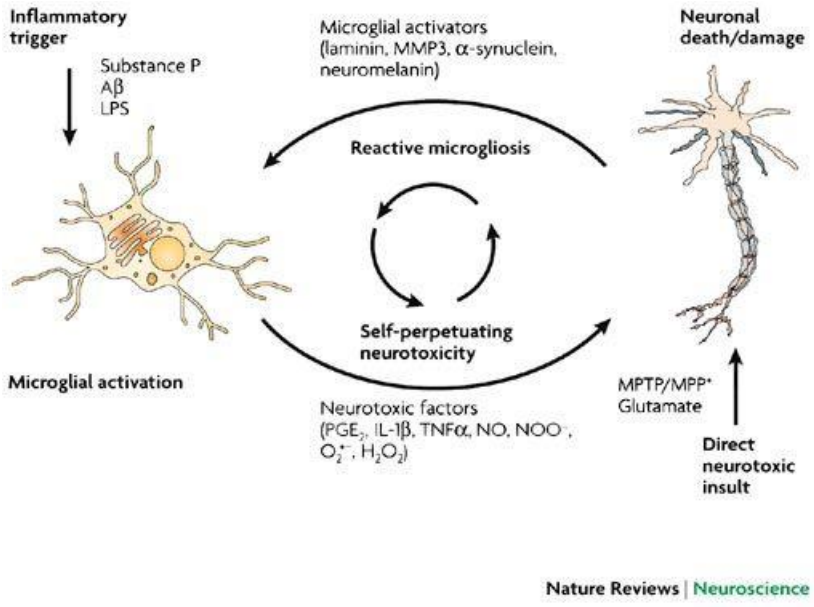

Fig. 1.11: Inflammation triggers microglial activation leading to neuronal death in Parkinson's disease. Inflammation triggers microglial activation which produce neurotrophic factors leading to neuronal death and damage. This neuronal death then results in further microglial activators which feeds back to inflammatory responses resulting in self-perpetuating neurotoxicity (Image: Block and Hong (2007)) .

Post-mortem analysis of Parkinson's disease brains has found inflammation in the basal ganglia, pons, striatum and frontal and temporal lobes (Gerhard et al., 2006). A combination of over-production of cytokines, microglial activation and ROS production contributes to inflammation and disease progression (Whitton, 2007). Midbrain dopaminergic neurons are in a region with a high density of microglia making them more vulnerable to degeneration as a result of inflammatory signalling than any other neuronal group (Lawson et al., 1990; Tansey and Goldberg, 2010). Chronic users of non-steroidal anti-inflammatory drugs which inhibit cyclo-oxygenase activity and scavenge ROS have a 46% lower incidence of Parkinson's disease than controls which further implicates inflammation in disease progression (Chen et al., 2003).

Inflammation in Parkinson's disease was also discovered through increased cytokine levels in the striatum and cerebrospinal fluid of patients. Pro-inflammatory cytokines such as TNFα, IL-1β and IL-6, T-cell activation (IL-2) and growth factors (EGF, TGF-α, bFGF, TGF-b1) are increased in Parkinson's disease striatum and substantia nigra pars compacta with a higher density of glial cells expressing these pro-inflammatory markers (Boka et al., 1994; Mogi et al., 1994a; Mogi et al., 1994b; Hunot and Hirsch, 2003). T-cell expression in these regions is thought to be a result of a modification in the blood-brain barrier permeability which under normal circumstances would not allow infiltration of T-cells from the circulatory system. Although little is known about changes to the blood-brain barrier in Parkinson's disease, changes in cerebral capillary walls and increased vasodilation has been reported in Parkinson's disease patients (Farkas et al., 2000).

Cytotoxicity by pro-inflammatory cytokines are a result of activation of inducible nitric oxide synthase (iNOS) responsible for mediating synthesis of high levels of nitric oxide (NO) which is toxic to neurons though ROS production and oxidative stress (Dawson et al., 1993). Glial cells with increased iNOS expression has been found in the substantia nigra of Parkinson's disease patients (Knott et al., 2000). Nitric oxide has been

shown to disrupt iron regulated proteins in mice resulting in higher iron concentration similar to findings in the substantia nigra of Parkinson's disease patients which may contribute to the generation of highly toxic hydroxyl radicals (Hirsch et al., 1998).

Both patient and animal studies have shown pro-inflammatory cytokines to be the most potent activators of iNOS in glial cells (Janabi et al., 1996; Hunot et al., 1999). Cytokine cell death of dopaminergic neurons may act through activation of cytokine receptors found on these neurons which initiates cell death pathways such as the TNF-α pathway and activates apoptotic caspases (Hengartner, 2000). NFκB has also been shown to be activated to induce dopaminergic cell death in patients (Hunot et al., 1997). Mechanism of disease pathology in Parkinson's disease is summarised in Fig. 1.12.

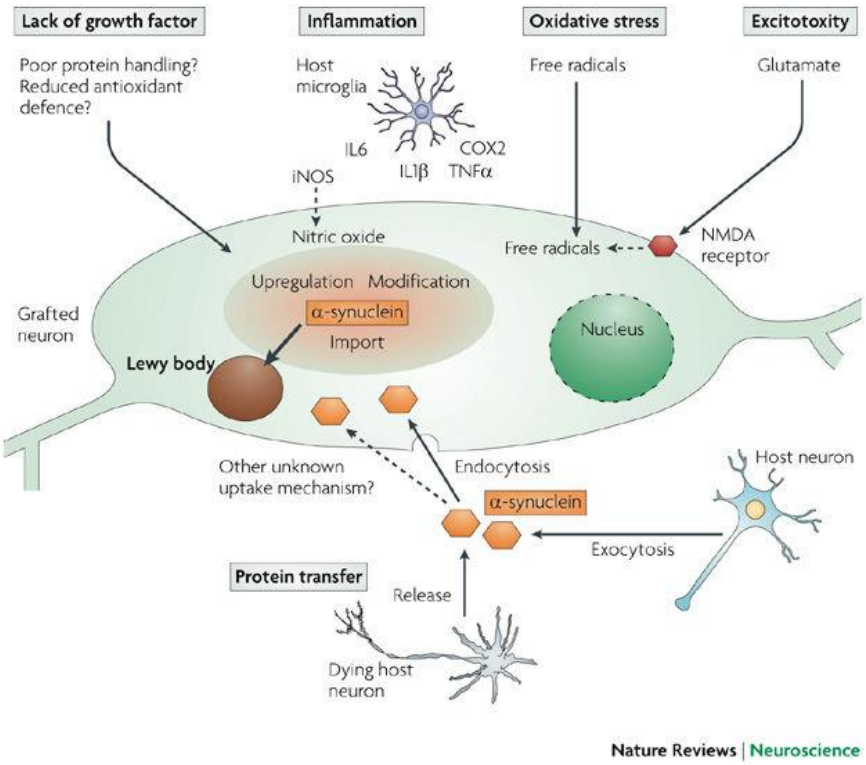

Fig. 1.12: Parkinson's disease pathology. Reduced antioxidant function, inflammation, oxidative stress and excitotoxicity have all been linked to disease progression leading to Lewy body formation, ROS production and dopaminergic cell death (Image: Brundin et al. (2008)).

1.4.5 Aetiology of Parkinson's disease

Age

Aging is the biggest risk factor in the development of Parkinson's disease. At the age of 60, 1% of the population suffer from Parkinson's disease with this figure rising to 5% of the population over the age of 85 (de Lau and Breteler, 2006). Approximately 5% of the patient population are under the age of 60 years with the majority of these patients showing genetic and non-sporadic causes of disease. Studies have found that dopaminergic cell populations are particularly vulnerable to loss with aging compared to many other cell populations. Substantia nigra pars compacta in a healthy aging brain has been shown to naturally have extensive loss of dopamine cells with 4.7% being lost every 10 years (Fearnley and Lees, 1991; Buchman et al., 2012).

In a healthy brain the dopamine transporter is protective against oxidative stress by transporting dopamine back to nerve terminals where it is repackaged into synaptic vesicles by vesicular monoamine transporter 2 (VMAT2). With increasing age, dopamine transporter expression is decreased in the dorsal portion of the substantia nigra which may account for the vulnerability of this area to neuronal loss in Parkinson's disease (Ma et al., 1999).

With increasing age, iron content in the substantia nigra is also increased resulting in over-production of ROS above the age of 40 in the substantia nigra pars compacta (Bilgic et al., 2012). Mitochondria also rely on iron for their function. Changes in concentration of iron in mitochondria could lead to mitochondrial dysfunction and subsequent ROS generation contributing to neuronal loss (Reeve et al., 2014).

Mitochondrial mutations have been found to occur naturally with positive correlation between the incidence of mutations and increasing age, and were also found to be higher in mitochondria of the substantia nigra than any other brain region (Soong et al., 1992). Mutations are likely to be a result of incorrect DNA repair from damage caused by double stranded breaks resulting from high oxidative stress in the substantia nigra due to dopamine metabolism (Reeve et al., 2014). Disruption of mitochondrial DNA in mice

was found to result in premature aging and extensive loss of dopaminergic neurons (Ekstrand et al., 2007). Aging is also known to increase microglial sensitivity which can cause a more severe inflammatory response and may account for an increased risk of disease development with age (Henry et al., 2009).

Two main pathways within neurons for removal of damaged proteins are the ubiquitin proteasome system and autophagy. Both are linked to mitochondria as they require ATP and both have been shown to decrease in function with age (Rubinsztein et al., 2011; Jana, 2012). In Parkinson's patients, further reductions in protease activity in the substantia nigra has been found which is also attributed to Lewy body formation as previously discussed (McNaught et al., 2003).

In the cellular environment, newly synthesised proteins are at risk of incorrect protein folding and loss of function which may also form toxic species. Therefore, cells have a family of chaperones which prevent protein aggregation and ensure correct protein folding. Efficiency of this family is known to decrease with increasing age and is associated with Alzheimer's and Parkinson's disease development (Hartl et al., 2011).

Environmental risk factors

Development of Parkinson's disease in most cases appears to be multi-factorial with the environment playing a significant role in disease susceptibility. Among the biggest risk factors is exposure to pesticides.

In 1983 several people developed Parkinsonism symptoms after intravenous injection of a drug which had been contaminated with 1-methyl-4-phenyl-1,2,3,6-tetrahydropyridine (MPTP). Further investigation followed and it was found that this compound was neurotoxic and selectively damaged dopaminergic cells in the substantia nigra (Langston and Ballard, 1983). Subsequently, this neurotoxin has been used in pre-clinical research for Parkinson's disease modelling. Exposure to this toxin or to herbicides such as paraquat and pesticides such as rotenone have been linked to increased risk of Parkinson's disease (Kanavouras et al., 2011). MPTP, paraquat and rotenone are mitochondrial complex I inhibitors and result in dopaminergic

cell death in the brain of animal models (Betarbet et al., 2000). Epidemiological studies in humans have reported an increased risk of disease development in populations living in rural areas and with a higher exposure to pesticides (Priyadarshi et al., 2001). These pesticides are now used in animals to model disease pathology seen in patients.

Exposure to heavy metals such as iron and zinc have also been found to increase risk of disease development by accumulation of metals in the substantia nigra and increased oxidative stress (Lai et al., 2002).

Some environmental agents are known to decrease risk of Parkinson's disease development such as cigarette smoking and caffeine consumption (Morens et al., 1995; Ross et al., 2000; Hernan et al., 2002). The most likely protective effect of cigarette smoking is due to stimulation of nicotinic receptors on dopaminergic neurons which may play an anti-oxidant role (Quik, 2004).

Genetic predisposition

Genome-wide association studies (GWAS) have enabled identification of genetic mutations which are risk factors for Parkinson's disease and have found 21 genes to date associated with familial or sporadic forms of the disease (Kalinderi et al., 2016). Familial Parkinson's disease has been classed into autosomal dominant or autosomal recessive forms and usually develops at an early age (before 50 years of age) with rapid progression (Fan et al., 2013). Table 1.1 represents the six genes with identified mutations within Parkinsonism families definitively associated with familial dominant or recessive Parkinson's disease.

Table 1.1: Some of the implicated genes in familial Parkinson's disease development.

Gene	Inheritance	Clinical features	Gene product	Function	Reference
SNCA (PARK1)	Autosomal dominant	Early onset, rapid degeneration	Alpha-synuclein	Synaptic plasticity	Burre et al., 2010
Parkin (PARK2)	Autosomal recessive	Early onset, slow progression	Ubiquitin ligase	Ubiquitin proteasome system component	Sauve et al., 2015
PINK1 (PARK6)	Autosomal recessive	Early onset	PTEN-induced kinase	Protect against mitochondrial dysfunction	Bonifati et al., 2005
DJ-1 (PARK7)	Autosomal recessive	Early onset	DJ-1	Protect against oxidative stress	Fitzgerald et al., 2008
LRRK2 (PARK8)	Autosomal dominant	Early onset	Dardarin	Bind 14-3-3 proteins to regulate protein interactions	Berge et al., 2005
VPS35 (PARK 17)	Autosomal dominant	Late onset	VPS35	Endosomal-lysosomal trafficking	Zimprich et al., 2011

Monogenic forms of Parkinson's disease are rare (<10% of all patients) and are a result of single inherited mutations in a gene. The majority of identified gene mutations are risk factors in sporadic forms of Parkinson's disease. Sporadic cases are attributed to an interaction between environmental and genetic risk factors (de Lau and Breteler, 2006; Kalinderi et al., 2016). Several of these 21 genes linked to both familial and sporadic Parkinson's disease affect protein metabolism or mitochondrial function (Gasser et al., 2011).

SNCA encoding for protein α-synuclein was the first gene identified to cause familial Parkinson's disease with a missense mutation found in families with early onset autosomal dominant Parkinson's disease with rapid progression (Polymeropoulos et al., 1997). The protein is known to have roles in synaptic plasticity and learning (Burre et al., 2010) and has also been shown to act as a molecular chaperone in the formation of the SNARE complex responsible for mediating vesicle fusion (Bonini and Giasson, 2005). Mutations in the gene are known to result in α-synuclein aggregates and Lewy body formation in the brain.

PARK2 (parkin) is the second largest gene in the human genome at 1.53 Mb in size. Mutations were identified to cause autosomal recessive juvenile Parkinson's disease (Kitada et al., 1998). More than 100 variable mutation types have been found to date. In most of these cases, Lewy bodies are not present in patients. Expression of cytosolic E3 ubiquitin ligase, parkin is found in the nervous system and has a role in proteasome degradation (Shimura et al., 2000). PINK1 accumulation triggers parkin recruitment and activation. Parkin then assembles ubiquitin chains on outer mitochondrial membrane proteins leading to their degradation (Narendra et al., 2010). Along with this function PINK1 and parkin also regulate mitochondrial turnover by promoting synthesis of new mitochondria (Vincow et al., 2013). Mutations cause a loss of function of this degradation, toxic build-up of proteins along with mitochondrial impairment (Palacino et al., 2004).

PARK 6 encodes PTEN-induced mitochondrial serine/threonine kinase (PINK1) and mutations cause recessive inherited Parkinson's disease. Multiple forms of mutations have been found (frameshift, missense etc.). The disease is early onset but progresses slowly (Bonifati et al., 2005). Pink1 is thought to interact as an upstream gene of parkin to activate and recruit parkin onto damaged mitochondria, resulting in their degradation and elimination along with regulation of mitochondrial synthesis (Clark et al., 2006).

DJ-1 protein (PARK 7) under normal conditions protects against oxidative stress and mitochondrial damage (Fitzgerald and Plun-Favreau, 2008). It recently has been found to regulate metabolism and cell proliferation through PINK1. Loss of function leads to oxidative stress and dopaminergic neurodegeneration in Parkinson's disease (Giaime et al., 2010).

Leucine-Rich Repeat Kinase 2 (LRRK2) mutations were found in families with autosomal dominant inheritance (Paisan-Ruiz et al., 2004). Over 80 mutations of the LRRK2 gene have now been found which account for 10% of familial disease cases and a significant amount of sporadic cases (Berg et al., 2005). Large variation is found in pathology of patients with LRRK2 mutations. The protein is known to interact with the 14-3-3 superfamily of proteins suggesting the gene has roles in many cellular processes and pathways which accounts for large variations seen in different mutations within the gene.

Mutations found in the vascular protein sorting 35 (VPS35) gene have been linked to familial and sporadic late-onset Parkinson's disease. The protein is responsible for mediating retrograde transport between endosomes and trans-golgi network which directs synthesised proteins to the correct cellular destination. Mutations in the gene are thought to prevent this transport of proteins (Zimprich et al., 2011).

1.4.6 Current symptomatic treatment of Parkinson's disease

Current treatment for the Parkinson's disease is only symptomatic but does not slow disease progression. Attempts to slow or stop disease progression have focussed on targeting α-synuclein aggregates, neuroprotection of

mitochondria, or reduction of microglial activation and consequent neuro-inflammation (Singleton et al., 2003; Sadeghian et al., 2016).

Dopamine agonists

Dopamine agonists are used to treat patients by replacing neurotransmitter dopamine in the brain and binding to dopamine receptors. Dopamine agonists symptomatically treat the disease by acting directly on intact postsynaptic receptors in the striatum but do not slow disease progression (Schwarz, 2003). These drugs are often used as an initial treatment prior to treatment with L-DOPA as they are less potent and results in fewer side-effects and later can also be used in conjunction with L-DOPA treatment as the disease progresses. Dopamine agonists are divided into ergoline and non-ergoline derived agonists. Ergoline classes such as bromocriptine, pergolide and cabergoline target D2 receptors but produce more side effects due to increased off-target interactions with D1, 5-HT and adrenergic receptors. Newer non-ergoline agonists (pramipexole, ropinirole and apomorphine) have less side effects due to high affinity binding, for this reason they are a far more popular class of dopamine agonist drugs and have several routes of administration (oral, transdermal, subcutaneous infusion) (Borovac, 2016).

Levodopa

The dopamine precursor, levodopa (L-DOPA) is still the best available treatment more than 50 years after it was first used in Parkinson's disease patients (Cotzias et al., 1969). The drug acts by increasing brain dopamine levels and decreasing motor symptoms. Due to problems associated with fluctuating levels of L-DOPA, several drugs are approved as add-ons to prolong its effects by inhibiting the L-DOPA-degrading enzyme, DOPA-decarboxylase, for example, carbidopa and opicapone, or by inhibiting the dopamine degrading enzyme, monoamine oxidase (MAO) B, for example selegiline, rasagiline and safinamide. In the absence of these inhibitors the majority of L-DOPA is metabolised before it can cross the blood-brain barrier to reach its target (reviewed by Oertel (2017)). Although it is the 'gold standard' treatment for patients, it is only symptomatic and fails to slow or halt progression of disease.

MAO/COMT inhibitors

Metabolism of dopamine is mediated by MAO and catechol-O-methyltransferase (COMT) and expression of COMT is found in the prefrontal cortex and limbic system (Schosser et al., 2012). COMT inhibitors such as entacapone are used in combination with L-DOPA to prolong drug half-life and subsequently increase delivery to the brain. In the absence of this inhibitor, it is estimated that only 10% of L-DOPA will reach the brain intact (Smith, 2003; Muller, 2015).

Monoamine oxidases (MAOs) are mitochondrial-bound enzymes which metabolise monoamine neurotransmitters (Carradori et al., 2014). In patients with Parkinson's disease, MAO-B activity is highly expressed in the substantia nigra, therefore, inhibitors are used for disease treatment to prevent degradation of dopamine. MAO inhibitors can provide mild, symptomatic relief in early Parkinson's disease and are approved for use along with L-DOPA co-treatment (Schapira, 2011). Rasagiline is an irreversible inhibitor of MAO B, and is thus used to prolong the effects of L-DOPA. However, it also has anti-apoptotic effects unrelated to its MAO-B inhibition and these effects are thought to underlie neuroprotective effects seen in cell culture and animal experiments (Akao et al., 2002; Blandini et al., 2004). In clinical trials, rasagiline has been reported to have beneficial effects on patient symptoms in early Parkinson's disease (Olanow et al., 2009; Hauser et al., 2016).

Other pharmacological treatments

The calcium channel blocker isradipine is currently in clinical trials for treatment of Parkinson's disease (NCT02168842 on-going), based on observations that treatment of hypertension with calcium channel antagonists resulted in diminished risk of developing the disease (Becker et al., 2008). The proposed mechanism is that the pacemaking activity of neurons in the substantia nigra, makes them vulnerable to excessive calcium influx, with increased risk with age, due to repetitive activation of calcium channels. This leads to increased calcium in the mitochondria and production of reactive oxygen species, ultimately causing neuronal death (reviewed by Zamponi (2016)). In mice, isradipine treatment restored juvenile pacemaking activity of

neurons and protected neurons from degeneration in vitro and in vivo (Chan et al., 2007).

The tetracycline antibiotic, minocycline, protected against the loss of dopaminergic neurons by inhibition of microglial activation in MPTP treated mice (Wu et al., 2002), and it reduced iNOS and caspase-1 expression (Du et al., 2001). In contrast, Yang et al. (2003) and Diguet et al. (2004) reported a deleterious effect of minocycline in MPTP-treated mice and primates. In clinical studies, minocycline has been found to block microglial activation but so far has not shown any clinical benefit in motor function (Ravina et al., 2006; Kieburtz et al., 2008; Olson and Gendelman, 2016).

1.4.7 Animal models of Parkinson's disease

Animal models of Parkinson's disease have proven to closely model many aspects of Parkinson's disease pathology in patients although none have been able to reproduce complete pathology of disease. The most popular species used to model the disease are rodents, however, zebrafish and Drosophila have also been used for both neurotoxic and genetic models of Parkinson's. A number of neurotoxins are commonly used in animals to model disease pathology.

6-OHDA induced neurodegeneration

6-OHDA is one of the most widely used neurotoxic models of Parkinson's disease in vitro and in vivo. Structurally it is analogous to catecholamines, dopamine and noradrenaline, and specifically targets catecholaminergic neurons making it a popular pre-clinical model of the disease (Simola et al., 2007 for review). Due to this structural similarity dopamine and noradrenaline transporters recognise and accumulate 6-OHDA (Sachs and Jonsson, 1975). The toxin is then oxidised by monoamine oxidase A (MAO A) which generates reactive oxygen species resulting in oxidative damage and also causes mitochondrial dysfunction (Drechsel and Patel, 2008).

MPTP induced neurodegeneration

MPTP is selective for dopaminergic neurons and causes oxidative stress, ROS inflammation but no Lewy body formation in neurons. MPTP can cross the blood brain barrier and once in the central nervous system enters

astrocytes, MAO-B then catalyses MPTP to toxic MPP+ (Schmidt et al., 1997; Gainetdinov et al., 1998). This active metabolite is transported by the dopamine transporter to dopaminergic neurons and can be taken up by VMAT2. Once in the neuron, complex I is inhibited which produces ROS and inhibition of mitochondrial function (Gainetdinov et al., 1998).

Rotenone induced neurodegeneration

Rotenone is an insecticide that can easily cross the blood-brain barrier (Alam and Schmidt, 2002). Exposure to the toxin inhibits the mitochondrial electron transport chain (Inden et al., 2007). Lewy body formation and oxidative stress with detrimental dopaminergic neuronal loss have been found in the brain of rodents following intravenous injection of the toxin (Cannon et al., 2009). However, the toxin has damaging effects on many neurological circuits and is not specific to the dopaminergic system also affecting serotonin, noradrenergic and cholinergic neurons (Hoglinger et al., 2003). Rotenone was also found to inadequately model disease pathology in various animal species such as mice and monkeys and results in high toxicity and mortality (Ferrante et al., 1997; Thiffault et al., 2000).

Paraquat & Maneb induced neurodegeneration

Paraquat is a herbicide with structural similarity to MPP+. The toxic effects of the drug are through oxidative stress leading to damage of lipids, proteins, DNA and RNA (Day et al., 1999). At high doses, the drug has been shown to behave much like MPP+ with transport by dopamine transporter and toxicity of dopaminergic neurons (Rappold et al., 2011). This model is less commonly used as it is reported to have more variable effects in animal models than the classic MPTP. The advantage of using this toxin to model Parkinson's disease is its ability to increase α-synuclein and induce Lewy body formation in dopamine neurons of the substantia nigra pars compacta (Manning-Bog et al., 2002). This herbicide is used in animal models to study properties of α-synuclein and Lewy bodies in Parkinson's disease for this reason.

The fungicide maneb, also closely resembles mechanisms of action of MPTP and paraquat and is known to cause locomotor deficit (Thiruchelvam et al.,

2000). It is often used in combination with paraquat which models Parkinson's disease more closely to the clinical situation (Berry et al., 2010).

Genetic models of Parkinson's disease

Identification of genes contributing to familial and sporadic forms of Parkinson's disease has led to disease modelling through gene editing techniques. Genetic forms of Parkinson's disease account for only 10% of all patient cases with the other 90% sporadic. Despite this, genetic models of disease have been valuable in implicating cellular cascades in Parkinson's disease progression and potential therapeutic targets, although none of these genetic models have proven to fully model Parkinson's disease pathogenesis as seen in patients. Autosomal dominant genes such as α-synuclein and LRRK2 can be modelled through overexpression and autosomal recessive genes such as Parkin, DJ-1 and PINK1 through knockdown or knockout gene technology such as morphilino and TALEN. Genetic models of disease have been successfully applied in rodents, Drosophila, C. elegans and zebrafish (Dawson et al., 2010).

1.4.8 Zebrafish as an animal model of Parkinson's disease

Zebrafish have several advantages in regards to screening of new drug compounds for the treatment of Parkinson's disease; it is a vertebrate, produces hundreds of embryos per mating, embryos and larvae are transparent allowing visualization of the developing larva, chemicals can be applied in the swimming medium, and their small size allows for high-throughput drug screening. Although there is no structure analogous to the mammalian substantia nigra in zebrafish, there is evidence that the corresponding dopamine neurons are those of the posterior tuberculum of the ventral diencephalon which have high D_1 receptor expression and receive direct ascending spinal projections. These neurons project to the subpallium which was found to be the teleostean equivalent of the mammalian striatum as shown in Fig. 1.13 (Rink and Wullimann, 2001; Rink and Wullimann, 2002a; Du et al., 2016).

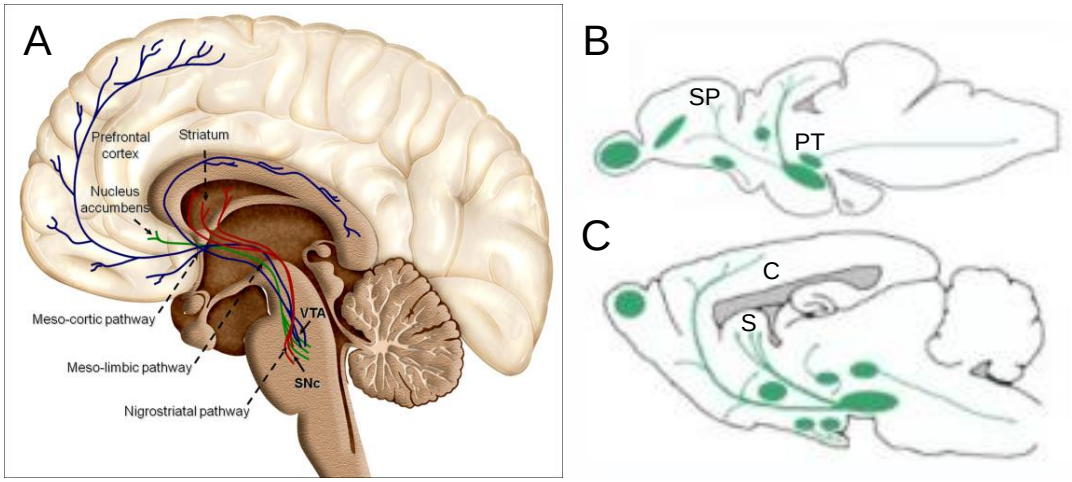

Fig. 1.13: Dopaminergic pathways in the human, zebrafish and rodent brain. (A) In the human brain, Dopamine neurons of the nigrostriatal pathway are found in midbrain structures substantia nigra (SNc) and the ventral tegmental area (VTA). Axons project to the striatum. (B, C) Schematic drawing illustrating the location of neural dopaminergic projections in adult zebrafish (B) (SP – subpallium, PT – posterior tuberculum) and rodents (C) (C – cortex, S – striatum) (Arias-Carrion et al., 2010) (Parker et al., 2013).

Development of the dopaminergic system in zebrafish begins at 15-18 hours post fertilization (hpf), and most of the cell clusters seen in the adult are present by 120 hpf (Rink and Wullimann, 2002b) making zebrafish larvae an ideal model for rapid, high-throughput drug screening in the treatment of Parkinson's disease. Several studies have successfully used zebrafish larvae in neuroprotective drug screens (Parng et al., 2006; Parng et al., 2007; Feng et al., 2014).

A number of neurotoxic and genetic models of Parkinson's disease have been successfully applied in zebrafish. Neurotoxins such as MPTP (McKinley et al., 2005), 6-OHDA (Feng et al., 2014), paraquat (Nellore and P, 2015) and rotenone have been used to induce dopamine neuronal cell loss and locomotor deficit, however high mortality was also recorded in rotenone exposed larvae (Melo et al., 2015).

In zebrafish, genetic knockdown/knockout models are also used in Parkinson's disease modelling with varied success. Overexpression of *parkin* protects against cellular stress with knockout resulting in moderate loss of dopaminergic neurons and mitochondrial dysfunction (Fett et al., 2010). DJ-1 knockout, similar to rodents, does not result in dopaminergic neuronal death

but is reported to increase susceptibility of these cells to neurotoxins (Bretaud et al., 2007). PINK1 knockdown also does not result in significant dopaminergic cell death but alters dopaminergic signalling and induces locomotor deficit (Xi et al., 2010). LRRK2 knockout is embryonic lethal with deletion of the WD40 domain of the protein resulting in dopaminergic loss and locomotor deficit in larvae (Sheng et al., 2010).

1.5 Aims of this study

The aims of this study were:

1) To validate zebrafish as a versatile research animal model through genetic and pharmacological studies. This was demonstrated in two studies:
    a. To investigate the function of the novel zygotic gene, *nanor* during early development.
    b. To validate a neurotoxic zebrafish model of Parkinson's disease suitable for drug screening.

Objectives of the thesis:

The main aim of the current study was to elucidate the function of *nanor* using wild-type larvae as well as generation of a mutant knockout line.

1) To investigate *nanor* mRNA and protein expression in wild-type embryos as well as to discover downstream genes of *nanor*.
2) To identify interacting proteins with Nanor.
3) To identify links between early asymmetry events such as FGF signalling and calcium flux before Kupffer's vesicle formation and during vesicle function on *nanor* expression.
4) To identify upstream and downstream genes of *nanor*.

To validate a neurotoxic zebrafish model of Parkinson's disease suitable for drug screening.

5) To validate a 6-OHDA model of Parkinson's disease in zebrafish larvae and induce locomotor deficit and dopaminergic neuronal loss in Parkinson's disease models during neuroprotective and neurorestorative screens.
6) To test neuroprotective and neurorestorative properties of three drugs: a calcium channel inhibitor (isradipine), monoamine oxidase inhibitor (rasagiline) and tetracycline antibiotic (minocycline) in a 6-OHDA Parkinson's disease model in zebrafish larvae up to 5 dpf.
    .

Chapter 2: Materials and Methods

2.1 Materials

2.1.1 Zebrafish maintenance

Unless otherwise stated, all solutions and protocols used in the care and maintenance of the zebrafish were taken from The Zebrafish Book (Westerfield, 2000). Adult zebrafish were housed at a stocking density of approximately 20 fish per 10 litre tank and fed twice daily. Morning feeds consisted of ZM small granular food (ZM systems), and in the afternoon a feed of live Artemia (ZM systems). Artemia cysts (3 g) were incubated with 54 g of Instant Ocean salt in a 1 litre hatchery for a minimum of 24 hours with strong aeration at a constant temperature of 28 °C. Fish were maintained at 28 °C on a 14:10 light: dark cycle and were spawned once a week in spawning trays (20 cm X 9 cm) by placing male fish in the tray with a female placed in a mesh insert above on the evening prior to spawning. Male and female fish were placed together in the upper insert after lights on the following morning. Embryos were collected from the bottom of the spawning trays and cultured in 90 mm petri dishes (approximately 50 embryos per dish). Embryos were incubated at 28 °C in filter-sterilised egg water (60 µg/ml stock salts in distilled water). Fish housing tanks were washed weekly while the fish were on to spawn. Filters were thoroughly rinsed with water and tanks were re-filled using dechlorinated tap water.

2.1.2 Chemicals and laboratory plastics

All chemicals were of standard analytical grade purchased from Sigma-Aldrich. All pipette tips and microcentrifuge tubes (Sarstedt) were autoclaved and bench surfaces wiped with 70% ethanol. Nuclease-free water was used in all molecular experiments. Glycerol stocks of all plasmids were made (50:50) and stored at -80 °C.

2.1.3 Enzymes and kits

Restriction enzymes (with buffers) were purchased from New England Biolabs. Enzymes were used according to the manufacturer's instructions with all digestions verified by gel electrophoresis. Proteinase K and

Superscript II Reverse Transcriptase were purchased from Invitrogen. Nucleobond® supplied plasmid preparation kits (midi and mini) and PCR purification and gel extraction kits were obtained from Qiagen. SP6/T7 mMESSAGE mMACHINE kit, MEGAclear kit and the DNase I enzyme and buffer were purchased from Ambion. pGEM-T Easy vector system I kit was purchased from Promega. High Resolution Melt Analysis kit (High Resolution Melting Master) and DIG - RNA probe labelling kits were manufactured by Roche and supplied by Sigma-Aldrich. Abcam supplied the antibody purification kit (AB138915) as well as the immunoprecipitation kit (AB206996).

2.1.4 Materials list

All materials that were used during experiments are listed in Table 2.1

Table 2.1: Materials list.

Chemical/Reagent	**Company**	**Catalogue number**
2-Methylbutane	Sigma-Aldrich	M32631
2-propanol	Sigma-Aldrich	I9516
5-bromo-4-chloro-3-indolyl-β-D-galactopyranoside (X-gal)	Thermo Scientific	R0941
6-hydroxydopamine hydrobromide	Sigma-Aldrich	162957
Acetic acid	Sigma-Aldrich	A6283
Acrylamide	Sigma-Aldrich	A3574
Adenosine triphosphate (ATP)	Sigma-Aldrich	A1852
Agarose	Invitrogen	16500-500
Ammonium acetate	Allied signal	32301
Ammonium persulphate	Sigma-Aldrich	A3678
Ammonium sulfate	Sigma-Aldrich	A4418

Anti-digoxigenin-AP Fab fragments	Roche	11093274910
BM purple AP substrate	Roche	11442074001
Bovine Serum Albumin (BSA)	New England Biolabs	B7004S
Bradford Reagent	Sigma-Aldrich	B6916
Bromophenol blue	Sigma-Aldrich	B5525
Calcium Chloride	Sigma-Aldrich	449709
Calf intestinal alkaline phosphatase	Fisher Scientific	18009019
Chloroform	Sigma-Aldrich	C2432
Coomassie stain	Sigma-Aldrich	B8522
Citric acid	Sigma-Aldrich	251275
Deoxynucleotide triphosphates	Promega	-
Diethylpyrocarbonate	Sigma-Aldrich	D5758
Dimethyl sulphoxide	Sigma-Aldrich	D5879
DMP	Sigma-Aldrich	
DTT	Roche	DTT-RO
Ethanol absolute	Sigma-Aldrich	E7023
Ethanolamine	Sigma-Aldrich	411000
Ethidium Bromide	Sigma-Aldrich	E2515
Ethylenediaminetetraacetic acid (EDTA)	Sigma-Aldrich	E6511
First strand buffer	Fisher Scientific	18080044
Formaldehyde	Sigma-Aldrich	F8775

Formamide	Sigma-Aldrich	F5786
Freon	Sigma-Aldrich	254991
Glycerol	Sigma-Aldrich	G6279
Glycine	Sigma-Aldrich	G8898
Heparin sodium salt	Sigma-Aldrich	84020
Hydrochloric acid	Fisher Scientific	AC12463-5001
Isopropyl β-D-1 thiogalactopyranoside (IPTG)	Sigma-Aldrich	I6758
LB Agar	Sigma-Aldrich	L2897
LB Broth	Sigma-Aldrich	L3022
Liquid nitrogen	Chemistry Dept., NUIG	-
Magnesium Chloride	Sigma-Aldrich	M8266
Mercaptoethanol	Sigma-Aldrich	M3148
Methanol	Sigma-Aldrich	322415
MOPS	Sigma-Aldrich	M1254
Mounting medium	VWR chemicals	361603E
Normal Goat Serum	Biosciences	G9023
Nuclease free water	Promega	BIO37080
Paraformaldehyde	Sigma-Aldrich	P6148
PBS tablets	Sigma-Aldrich	79382
Phenol	Sigma-Aldrich	P4557
Phenol red	Sigma-Aldrich	P3532
Phosphatase	NEB	M0289

Plasmid Safe DNase	My-Bio	-
Ponceau stain	Sigma-Aldrich	P3504
Potassium chloride	Sigma-Aldrich	31248
Protease inhibitor cocktail	Sigma-Aldrich	P2714
Radiance HRP substrate	Mason technology	AC2100
Random primers	Sigma-Aldrich	11034731001
Sheep Serum	Sigma-Aldrich	S3772
SOC medium	New England Biolabs	B9020S
Sodium acetate	Sigma-Aldrich	S7545
Sodium Borate	Sigma-Aldrich	S9640
Sodium chloride	Sigma-Aldrich	S7653
Sodium Citrate	Sigma-Aldrich	1613859
Sodium hydroxide	Sigma-Aldrich	S8045
Sodium Lauryl Sulfate	Sigma-Aldrich	1614363
Sodium phosphate	Sigma-Aldrich	S5136
Sucrose	Sigma-Aldrich	S7903
SYBR green	Biosciences	4385612
Tetramethylethylenediamine	Sigma-Aldrich	T9281
Tissue Tec	VWR	-
Torula RNA	Sigma-Aldrich	R6625
Tricaine methane sulphonate (MS222)		

Triethanolamine	Sigma-Aldrich	T58300
Triton X-100	Sigma-Aldrich	T9284
Trizma	Sigma-Aldrich	T1503
TRIzol®	Invitrogen	15596026
Tween-20	Sigma-Aldrich	P1379
Virkon	Fisher Scientific	12358667

Table 2.2: Molecular weight markers.

Ladder	**Fragment size**	**Supplier**
100 bp	1517, 1200, 1000, 900, 800, 700, 600, 500, 400, 300, 200, 100 bp	New England Biolabs
1 kb	10, 8, 6, 5, 4, 3, 2, 1.5, 1, 0.5 kb	New England Biolabs
Prestained protein marker	250, 150, 100, 75, 50, 37, 25, 20, 15, 10 kDa	Biorad

Table 2.3: Drug/antibiotic list.

Drug/Antibiotic/Primer	**Supplier**	**Catalogue number**
Ampicillin	Sigma-Aldrich	A9393
Random primers	Invitrogen	48190011
Spectinomycin	Sigma-Aldrich	S0692
Tetracycline hydrochloride	Sigma-Aldrich	T8032
Isradipine	Sigma-Aldrich	I6658

Levodopa	Sigma-Aldrich	L0400000
Rasagiline	Sigma-Aldrich	SML0124
SU5402	Sigma-Aldrich	SML0443
Minocycline	Sigma-Aldrich	M9511

Table 2.4: Primary and secondary antibodies.

Antigen	**Host Species**	**Supplier**	**Catalogue number**
Primary antibody			
Anti-Tyrosine hydroxylase	Mouse	Merck Millipore	MAB318
Anti-α-tubulin	Mouse	Sigma-Aldrich	T5168
Anti-Nanor	Rabbit	Sigma-Genosys	-custom made
Secondary antibody			
Peroxidase conjugated anti-rabbit	Goat	Sigma-Aldrich	AP132P
Alexa Fluor 546 anti-rabbit	Goat	Biosciences	A11010
Alexa Fluor 488 anti-mouse	Rabbit	Biosciences	A10667
Peroxidase conjugated anti-mouse	Rabbit	Sigma-Aldrich	AP124P

Table 2.5: Consumables.

Lab consumables	**Supplier**
20 µL microloader pipette tips	Eppendorf
96-well plates	Sarstedt
96-well plates square flat bottomed	Uniplate®
Centrifuge tubes	Sarstedt
Glass capillaries (injection needles)	Narishige Scientific Instrument Lab
Nitrocellulose membrane	Sigma-Aldrich
Grid cover slips	Millennium Sciences Inc
MicroAmp 96-well plate (RT-PCR)	Applied Biosystems
Microcentrifuge tubes	Applied Biosystems
Needles and syringes	BD
Petri dishes	Sarstedt
Pipette tips	Sarstedt
Transfer pipettes	Sarstedt

All oligonucleotides were supplied by Eurofins MWG Operon:

Table 2.6: PCR and sequencing oligonucleotides.

Gene	**Oligo name**	**Sequence (5' – 3')**
Elongation Factor 1 alpha (EF1-α)	EF1α F	GTG GTA TCA CCA TTG ACA TTGC
	EF1α R	TCA GCC TGA GAA GTA CCA GTG

Nanor	Nnr F1	TGG AAG GGG AGC TTC ATC AC
	Nnr F2	CGC AGA GAT GGA CAG CGA TT
	Nnr F10	CCA TGC CTG TGG ATG AAG GT
	Nnr UTRF1	ACT GTA AAG GGC CTC GAA CA
	Nnr R10	ACC CCG GGT GGT TTG TTA TG
	Nnr Ra	AAT ATT GGC CTC GTC TGG AGC
	Nnr Rb	GTC TGG AGC ATC TTC ACC TTC A
Nanor B	Nnrb F1	CCG TCC TGC AGC TGA CTA AT
	Nnrb R1	GAG CTG CGT TTC TCA TCT CC
Lefty 1	Lefty 1F	TGG ATC ATC GAG CCG TCC GGT
	Lefty 1R	CGG CAG CCG CCT TTA CAC CT
One-eyed pinhead (oep)	oepF	TCG AGT CAG GAT GTG AGG GGT CA
	oepR	TTG ACG TTG CGG CGT TTG CG
Southpaw (spaw)	spawF	AGA CCG GGT CAC GGC ACC A
	spawR	CGC TTC CAC TTC CAC TGC CCT G

Table 2.7: Oligonucleotides for TALEN experiments.

Primer	**Sequence (5’ – 3’)**
pCr8 F1	TTG ATG CCT GGC AGT TCC CT
pCr8 R1	CGA ACC GAA CAG GCT TAT GT
TAL F1	TTG GCG TCG GCA AAC AGT GG
TAL R1	GGC GAC GAG GTG GTC GTT GG
Nnr F1	ACT GTA AAG GGC CTC GAA CA

Nnr R1	ACC CCG GGT GGT TTG TTA TG

Table 2.8: Bacterial transformation cells.

Bacteria	**Company**	**Catalogue number**
DH5α competent cells	Invitrogen	18258012
Top10 competent cells	Thermofisher	12879416

Table 2.9: TALEN plasmid list.

Insert	**Plasmids**	**Supplier**	**Plasmid site map**
TALEN RVDs	RVDs pLR-HD pLR-NG pLR-NI pLR-NH pLR-NN	Addgene	Addgene website www.addgene.org
TALEN arms	pFUS A pFUS B1-10	Addgene	
Final forward TALEN	pCS2 TAL3 DD	Addgene	
Final reverse TALEN	pCS2 TAL3 RR	Addgene	

Table 2.10: RNA probes.

Probe	Enzyme	Polymerase	Reference
Nanor (sense)	NcoI	SP6	Bree *et al.* 2005
Nanor (anti-sense)	SalI	T7	Bree *et al*. 2005

2.1.5 Vector maps

The plasmids used for subcloning were pGEM-T Easy from Promega and pCS2+.

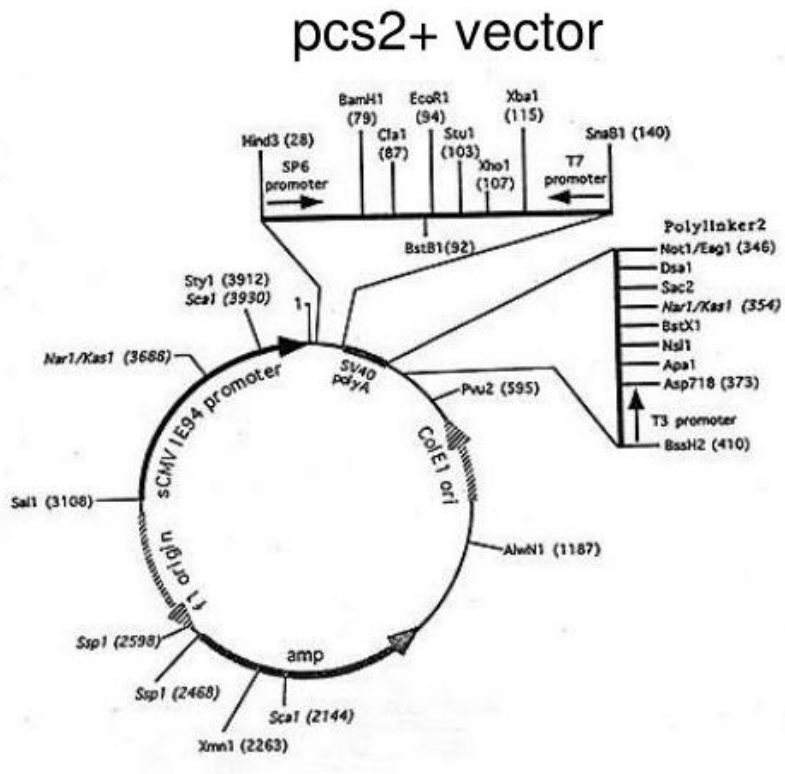

Fig. 2.1: pCS2+ vector (image from www.addgene.org)

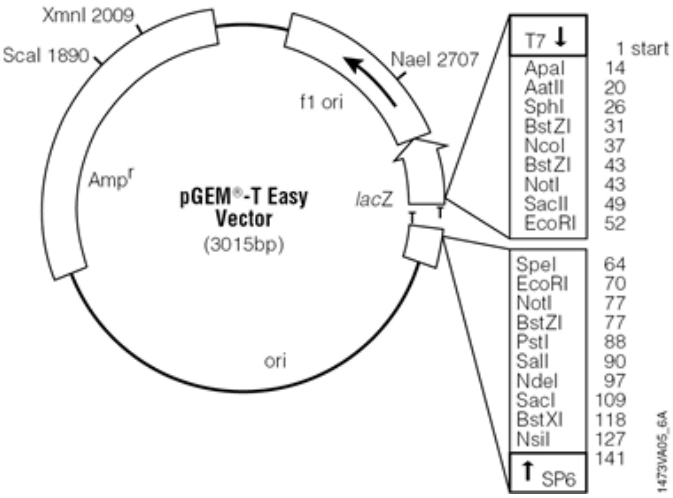

Fig. 2.2: pGEM-T Easy vector (image from www.addgene.org)

2.2 Methods

2.2.1 Pharmacological treatments in early stage embryos

To investigate a link between nanor expression and left-right asymmetry development L-type calcium channel blocker, isradipine (10 µM) and FGF signalling inhibitor, SU 5402 (12.5 µM), were used at various treatment time points in the early embryo. Initially, treatments were from 6 - 24 hpf or 24 - 48 hpf (Fig. 2.3 A). Following results from this experiment, treatment times were decreased and given before 24 hpf. Isradipine or SU5402 were given from 6 - 12 hpf or 12 – 24 hpf (Fig. 2.3 B). All drug treatments were made up in filter-sterilised egg water (FSEW) and drug stocks were stored in 1mM aliquots. All embryos were manually dechorionated prior to drug administration.

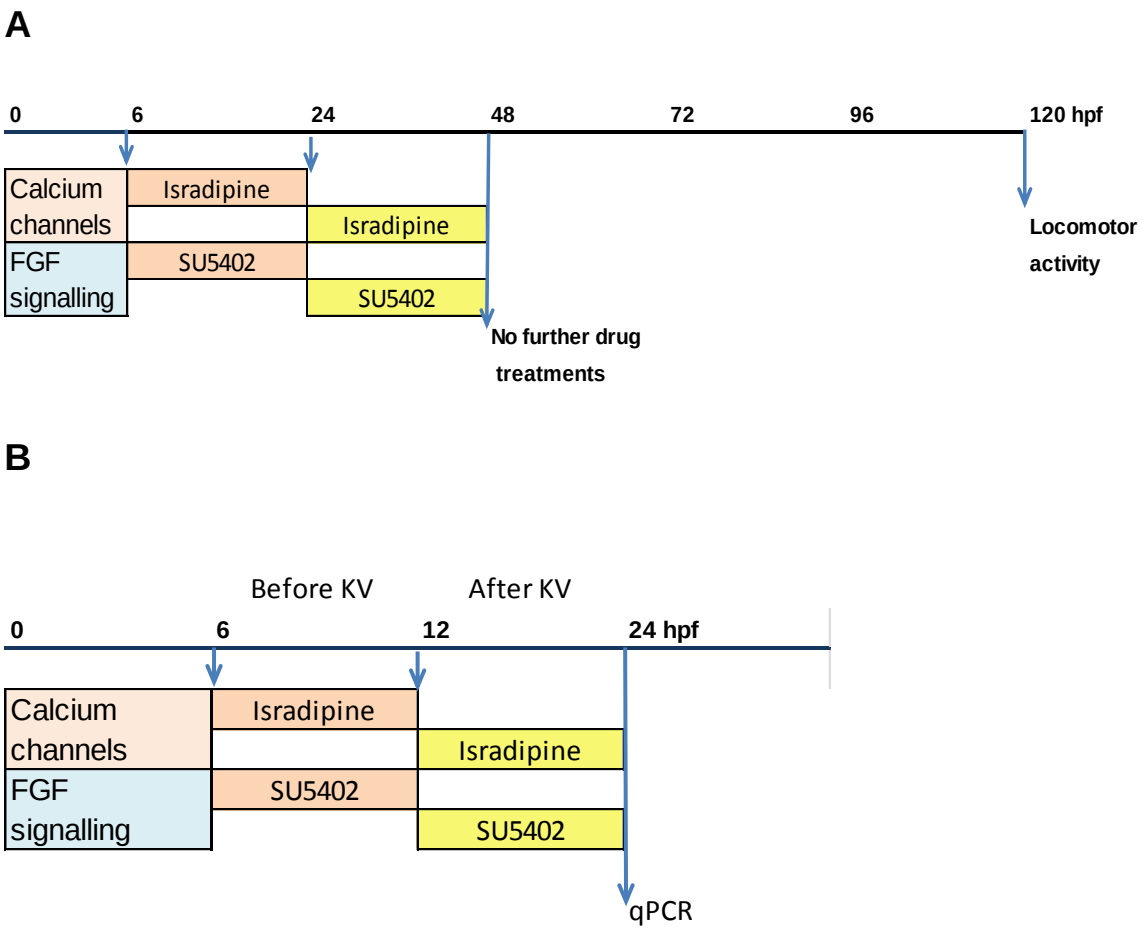

Fig. 2.3: Isradipine and SU 5402 treatment timelines during (A) locomotor activity (B) and qPCR assessment.

2.2.2 Pharmacological treatments in a 6-OHDA Parkinson's disease model

All embryos were manually dechorionated at 24 hpf and at 48 hpf exposed to 250 µM 6-hydroxydopamine (6-OHDA). When investigating neuroprotection, 6-OHDA exposure began at 48 hpf up to 120 hpf. Rescue effect groups were exposed to 6-OHDA from 48 hpf up to 80 hpf. All solutions were rinsed out and replaced with a fresh solution daily.

To test their neuroprotective potential, drugs were administered along with 6-OHDA beginning at 48hpf. Control embryos were in a 0.01% DMSO solution in filter sterilised egg water (FSEW). L-DOPA was used at a final concentration of 1 mM, minocycline at 10 µM, and isradipine and rasagiline at 1 µM . These concentrations were chosen following a dose response

analysis with morphology scoring and locomotor activity testing. All treatments lasted until 120 hpf when locomotor activity was recorded and embryos were stored for immunohistochemical analysis.

To test if drugs could rescue the effects of prior 6-OHDA treatment, 6-OHDA was administered at 48 hpf. At 80 hpf the 6-OHDA was removed by rinsing the wells three times with FSEW. Drugs were then added at the same concentrations chosen for the neuroprotection experiment. Control embryos were in a 0.01% DMSO solution in FSEW.

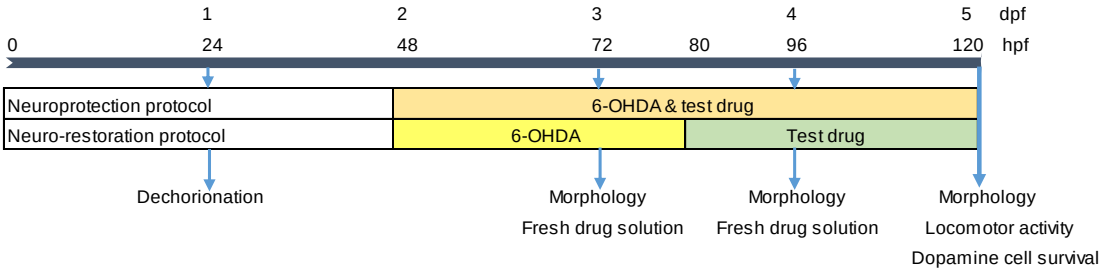

Fig. 2.4: Timeline of drug and toxin exposure and assessments for neuroprotection and neurorestoration protocols.

2.2.3 Imaging of zebrafish larvae

All embryos and larvae were photographed using a Nikon SMZ800 microscope and a DMX1200C camera.

2.2.4 Phenotypic analysis of zebrafish embryos

Embryo and larval morphology was scored using a modified scale from Brannen et al. (2010). Larvae were categorised into normal development, mild, moderate or severe defects. 11 structures/systems were scored as shown in appendices and included the heart (size, oedema, pooling, bloodflow), body (tail, somites), brain (oedema, structure), eyes and yolk (sac, extension). Scores assigned for each individual organ/system were 4 for normal development, 3 for mild defects, 2 for moderate defects, 1 for severe defects and 0 if the organ was absent at time of scoring. A normal developing embryo with no abnormalities was given a maximum score of 44. Any embryo that was given an overall score between 40 and 44 was deemed to have normal development. An overall score of 25-40 was said to have mild

abnormalities, 13-24 had moderate abnormalities, 1-12 had severe abnormalities and if an embryo was dead at the time of scoring it was given a score of 0.

2.2.5 Locomotor activity tracking

Daniovision® was used as a tracking system to record individual locomotor activity over a 50 minute time period with alternating 10 minute dark: 10 minute light phases during pharmacological experiments at 5 dpf. Larvae were transferred to 96 square well plates (Uniplate®) with one embryo per well on the evening before testing in a total volume of 250 µL. Test larvae were allocated to inner wells, as larvae in the outer wells have increased locomotor activity. Larvae in the outer wells were excluded from analysis. Water at 28 °C was circulated around the 96-well plate in the Daniovision chamber. Larvae were acclimatised to the chamber for 30 minutes prior to the test. Live tracking was set up and locomotion was measured at 30 frames a second. Data were exported to Excel, and graphed using GraphPad Prism.

2.2.6 Fixing of larvae

Larvae at the desired stage were manually dechorionated and fixed in 4% paraformaldehyde (PFA) and kept at 4 °C overnight. Following fixation, tissue was dehydrated in 70% ethanol (50% for 5 minutes, 70% for 5 minutes) for storage and later rehydrated by washing for 10 min in 50% ethanol, followed by three washes in phosphate buffered saline (PBS) (3 x 5 minutes) and 20 minutes in 10% sucrose with at least 3 hours in 30% sucrose solution in PBS.

Larval tissue to be sectioned was embedded in Tissue-Tek® (Sakura® Finetek, VWR) and rapidly frozen in iso-pentane, which had been cooled by liquid nitrogen. Tissues were cryosectioned in a rostral to caudal direction at 20 µm thickness on positively charged glass slides.

2.2.7 Whole tissue immunostaining

Tissue was rinsed in PBS (2 x 1 hour) and incubated at room temperature for 2 days in nanor anti-serum (1:300) diluted in normal goat serum with 5% BSA. On the third day tissue was washed in PBS (5 x 1 hour) and incubated

in secondary antibody (Alexa Fluor 546 anti-rabbit 1:500) at room temperature overnight. The following day embryos were washed in PBS (5 x 1 hour) and stored at 4°C in 70% glycerol stocks.

2.2.8 Immunohistochemistry (sectioned tissue)

Tissue sections were washed three times for 5, 10 and 15 minutes in PBS and blocked in 3% Bovine Serum Albumin (BSA) for 30 minutes followed by 3% normal goat serum (NGS) for 30 minutes at room temperature. For Parkinson's disease studies sections were incubated with primary antibody (mouse anti-tyrosine hydroxylase-MAB318, Merck Millipore) at a 1:300 dilution with 0.3% Triton X-100 overnight at 4°C. Sections were then washed three times (3 x 5 minutes) in PBS and incubated with secondary Alexa Fluor 488 Goat anti-mouse antibody (Biosciences) at a 1:200 dilution with 0.3% Triton X-100 for 1 hour at room temperature before 3 final wash steps in PBS for 5, 10 and 15 minutes and slides were cover slipped. Images were examined by fluorescence microscopy (Nikon Eclipse E600 Epi-fluorescence microscope, 200 x magnification captured using Cellsens™ software). Dopaminergic cell numbers were quantified using Image J.

For Nanor staining, a standard protocol for immunostaining of sectioned tissue was followed. Tissue sections were incubated in 1:1000 dilution of primary nanor antiserum and 1:1000 secondary antibody (Alexa fluor 546 anti-rabbit). Images were captured by confocal microscopy (Andor Revolution Confocal Microscope-Spinning disk confocal-Yokagawa CSU22). All immunohistochemistry was carried out with minus primary (rabbit serum) and minus secondary controls.

2.2.9 RNA extraction and cDNA synthesis

Isolation of total RNA

Embryos were harvested at the desired development stage in batches of 20-80. TRIzol® reagent was used to extract RNA from the whole tissue with 100 µL of TRIzol® being added per 20 embryos in a 1.5 mL microcentrifuge tube. A sterile 1 mL syringe and needle (21 G) were used to shear the tissue which was then incubated for five minutes at room temperature. Chloroform (200 µL per 1 mL TRIzol®) was added and samples were vortexed immediately

and incubated at room temperature for three minutes. Samples were centrifuged at 4 °C for 15 minutes at 12,000 g.

The supernatant was transferred to 1.5 mL microcentrifuge tube and isopropanol added (500 µL per 1 mL TRIzol®). The samples were incubated at room temperature for 10 minutes. Tubes were centrifuged at 4 °C and 16,000 g for a further 10 minutes. The supernatant was removed and the pellet was washed with 100 µL of 70% ethanol (pre-chilled on ice). Tubes were centrifuged at 16,000 g for 10 minutes at 4 °C. The ethanol supernatant was then removed and the pellet was left to air-dry for 5-10 minutes. The RNA pellet was resuspended in 88 µL of nuclease-free water and incubated at 55 °C for 10 minutes.

The RNA solution was DNase treated by adding 10 µL of DNase buffer and 2 µL of DNase enzyme, samples were incubated at 37 °C for ten minutes. 200 µL of phenol and 20 µL of 3 M sodium acetate were added to samples which were then thoroughly mixed and centrifuged at 16,000 g speed at 4 °C for five minutes. The supernatant was then transferred to a new microcentrifuge tube to which 200 µL of chloroform:isoamyl alcohol was added and tubes were vortexed. This chloroform:isoamyl alcohol step was repeated, and the resulting supernatant was once again transferred to a fresh tube. Isopropanol (200 µL) was added to the supernatant, and the samples were then incubated at -80°C for twenty minutes. Tubes were centrifuged at max speed for 30 minutes at 4 °C. The supernatant was discarded and the RNA pellet was washed with 200 µL of a pre-chilled 70% ethanol solution. Tubes were centrifuged for 5 minutes at max speed at 4 °C. The ethanol supernatant was removed and the pellet was left to air dry for 5-10 minutes before re-suspension in 10 µL of nuclease-free water and stored at -80 °C. The total RNA concentration and quality were determined by spectrophotometry.

cDNA synthesis

Total RNA was reverse transcribed using random hexamers. The reaction mixture contained 1 µg of total RNA, 0.5 µM random hexamers, 4 µL of Superscript II first strand buffer (50 mM Tris-HCl, 75 mM KCl, 3 mM $MgCl_2$), 2 µL of 0.1 M DTT, 10 µL nuclease-free water, 1 µL of 10 mM dNTP mix and

1 µL of the reverse transcription polymerase. The reaction was incubated for 1 hour at 42 °C and then 15 minutes at 70°C to heat inactivate the enzyme. cDNA was stored at -20 °C.

2.2.10 Polymerase chain reaction (PCR)

PCR was run to amplify fragments of DNA during primer validation and TALEN design and screening. A standard PCR reaction (25 µL) contained reaction buffer (50mM KCl, 10mM Tris-HCl, pH 9.0 and 0.1% Triton X-100), 200 µM of dATP, dCTP, dGTP, dTTP, 1.5 – 4 mM $MgCl_2$, 15 pmoles of F primer and 15 pmoles of R primer and 1.25 units of *Taq* DNA polymerase. Standard PCR conditions are outlined below. Optimal annealing temperature was selected based on the melting temperature of the primers and after optimisation using a PCR temperature gradient (table 2.11).

General PCR

Table 2.11: Standard PCR conditions in the thermal cycler.

Stage	**PCR conditions**	**Temperature °C**	**Time**	**Repeats**
1	Denaturation (initial)	95	5 min	1
2	Denaturation (cycle)	94	30 sec	30 cycles
3	Annealing (primers)	55-60 (Tm)	30 sec	30 cycles
4	Elongation	72	1 min/kb	30 cycles
5	Final extension	72	10 min	1

Quantitative RT-PCR

Quantitative reverse transcription PCR was performed using a protocol adapted from 'High Throughput Real-Time Quantitative Reverse Transcription PCR' from current protocols in molecular biology (Bookout et al., 2006). SYBR green and the $\Delta\Delta C_T$ method were used for all assays.

Primer Design and Validation

Primers were designed to meet the specific requirements for quantitative RT-PCR, with a 40-60% GC content and melting temperatures of approximately

60 °C. Oligonucleotides containing runs of the same nucleotide, repetitive sequences, or more than two G/C bases at the 3' end were deemed unsuitable. Amplicon length was short and never exceeded 150 bases. Validation of primers consisted of standard cDNA dilution series (1:5) from which linear regression curves were plotted. Primer pairs with a slope of -3.3 ± 0.1 were deemed valid for use in qPCR experiments and had an efficiency of 92-100%.

Template cDNA was diluted to give a range of concentrations from 50 – 0.08 ng/µL. A 5 µL aliquot of each cDNA concentration was added to a microcentrifuge tube on ice in a total 35 µL of reaction mixture with 20 µL SYBR green, 4.8 µL primer mix (150 nM of F and R primer solution) and 10.2 µL NFW. Each sample was plated in triplicate (10 µL) on a 96-well optical plate. No template controls (NTC) were also prepared in which nuclease-free water was substituted for the cDNA solution. If amplification occurred in NTC's the plate was void.

Gene expression assays

Housekeeping gene Elongation Factor 1-alpha (EF1-α) was chosen as the reference gene for all experiments as I found it to be most stable across different development stages when quantifying *nanor* gene expression. It has also been well documented as a suitable reference gene for qPCR in several studies (Nicot et al., 2005; Ingerslev et al., 2006; Tang et al., 2007b). For data analysis embryos treated with control (0.01% DMSO) in drug treatment experiments were used as calibrator samples. The calibrated value or ΔΔCt, for each sample was then calculated (ΔΔCt=ΔCtsample -ΔCtcalibrator). The fold-change for each sample relative to the calibrator was then calculated (fold-change=$2^{(-\Delta\Delta Ct)}$). Fold-change was then efficiency corrected using the Pfaffel method, i.e. by adjusting the efficiency value (E) of the reaction from the standard value of 2 (assuming perfect doubling of the PCR template) to a value obtained from the standard curve validation assay. Efficiency of a primer pair was calculated using the formula $10^{\wedge(-1/slope)}$.

DNA electrophoresis

Samples were electrophoresed alongside a standard base pair marker to determine DNA fragment size. 1-2% agarose gels were cast with TAE buffer pH 8.0 (Tris, acetic acid and EDTA) and with 3 µL of ethidium bromide per 60 mL of agarose. The running buffer used in the gel rig was 1 x TAE, pH 8.0. Gels were electrophoresed according to the protocol of Sambrook and Russell (2001). DNA fragments were visualised by UV transilluminator.

2.2.11 Sequencing of DNA samples

Nucleic acids were sequenced by Eurofins genomics and sent at the desired concentration and volume diluted in NFW. ApE software was used to analyse sequences.

2.2.12 Transcription Activator-Like Effector Nucleases (TALENs)

TALEN design

TALENs were targeted towards the beginning of a gene to induce a premature translational stop mutation (Dahlem et al., 2012). TALENs were designed to meet the required criteria adapted from Cermak et al. (2011); have a thymine base upstream of TALEN start site, forward and reverse TALEN should be 15-20 RVDs in length, 15-24 bases in spacer region, using NH RVD for guanine binding. In addition, the nucleotide composition of target sites should be: 31 ± 16% A, 37 ± 13% C, 9 ± 8% G and 22 ± 10% T. To avoid off target effects, the TALENs chosen had a maximum of one non-specific hit in one of the arms only. The workflow for TALEN generation was as follows;

1) Assembly of TALEN using Golden Gate cloning method
2) Linearisation of vector RNA transcription
3) RNA microinjections
4) Genomic DNA extraction 24 or 48 hpf
5) HRMA and sequencing to verify TALEN induced mutation

TALEN library set up

The Golden Gate TALEN kit consisted of 86 plasmid glycerol stocks purchased from Addgene. All TALEN plasmids were plated on appropriate antibiotic LB plates (ampicillin, tetracycline, spectinomycin). Colonies were picked and grown in LB broth overnight. Plasmids were prepared using mini and midiprep kits and all plasmids were sequenced prior to storage and throughout TALEN assembly.

Manufacture of TALENs

TALENs were manufactured using the Golden Gate protocol adapted from Cermak et al. (2011).

Precautions were taken to ensure TAL-effector nucleases were not designed to target regions that contained single nucleotide polymorphisms (SNPs); six healthy wild-type AB fish (3 males and 3 females) were fin-clipped for genotyping. Genomic DNA was isolated from the harvested tail material, and used to sequence the region of interest to ensure good fidelity between the proposed target region and the sequence available in the Ensembl zebrafish database (www.ensembl.org/Danio_rerio/index.html). These sequenced tank families were then used as parent fish for all subsequent experiments.

Design Guidelines

Construct synthesis using the Golden Gate cloning method

Custom TALEN assembly involves a two-step process, (1) assembly of a series of repeat modules (RVDs) into intermediary arrays of 1-10 repeats, and (2) the joining of these repeats into a “backbone” destination vector to complete the final construct.

RVD plasmids from the TALEN plasmid library (Addgene) for the selected TALEN sequence were chosen and assembled using the Golden Gate cloning method as follows:

For TALENs 12-21 RVDs in length

- Plasmids for RVDs 1-10 (e.g. pHD1, pNG2, pNN3, etc.) and destination vector pFUS_A were selected (set A)

- Plasmids for RVDs 11- (N-1) and destination vector pFUS_B (N-1) were selected (set B)

A Golden Gate Reaction (comprising of 150 ng of each module vector, 1 µL of restriction enzyme BsaI, 1 µL of T4 DNA ligase, 2 µL of 10X T4 DNA ligase buffer and nuclease-free water to a final volume of 20 µL) was mixed separately for each set of vectors. These reactions were then run in a PCR machine for 10 x (37 °C/5 min +16 °C/10 min) + 50 °C/5 min + 80 °C/5 min. 1 µL of 10 mM ATP and 1 µL of Plasmid-Safe Nuclease was then added to each Golden Gate Reaction #1 and tubes were incubated at 37 °C for 1 hour. A 5 µL aliquot of each reaction was transformed into 45 µL of chemically competent DH5-α cells. Cells were incubated at 37 °C for 1-2 hours following transformation to allow recovery after heat-shock. The recovered cells were spread on spectinomysin plates with IPTG and X-gal, and plates were incubated overnight at 37 °C.

Following overnight incubation 1-3 white colonies were selected from each plate and checked by colony PCR using primers pCR8_F1 and pCR8_R1. Correct clones were then cultured overnight at 37 °C in spectinomysin LB broth. Plasmid DNA was extracted and purified, and sequenced using colony PCR primers as above.

Clones, confirmed by sequence analysis, were then used for Golden Gate Reaction #2 (150 ng of vector set A + B / vector set A1 + A2 + B, 150 ng of the respective pLR vector containing the last RVD, 75 ng of destination vector pCSTAL3DD or pCSTAL3RR, 1 µL of restriction enzyme Esp3I, 1 µL T4 DNA ligase, 2 µL 10X T4 DNA ligase buffer and nuclease-free water to a final concentration of 20 µL). A PCR cycle of 37°C/10 min + 16°C/15 min +37°C/15 min+ 80°C/5 min was used to provide suitable reaction conditions. A 5 µL aliquot of this reaction was then transformed; recovered cells were spread on ampicillin agar plates treated with X-Gal and IPTG, and cultured overnight at 37 °C as before.

Following overnight incubation, 1-3 white colonies were selected from each plate and correct clones were identified by colony PCR using primers TAL_F1 and TAL_R2. Correct clones were identified by a “smear-and-

ladder" effect visible after gel electrophoresis, and these clones were cultured overnight in ampicillin LB broth. Overnight cultures were plasmid-extracted and purified, and these final constructs were sent for sequencing.

Completed TALEN constructs were sequenced and analysed using the TAL plasmids sequence assembly tool, available online courtesy of the Bao lab at http://baolab.bme.gatech.edu/Research/BioinformaticTools/assembleTALSequences.html. TALEN constructs confirmed by sequence analysis were then linearized with restriction enzyme Not I and these linearized plasmids were used as template for *in vitro* mRNA transcription using the SP6 mMessage mMachine Kit. Following mRNA transcription sample concentration was determined using a spectrophotometer and samples were normalised to a standard concentration of 100 ng /µL. Injection aliquots were prepared by mixing equal amounts of left and right TALEN mRNA, and all mRNA were then stored at -80 °C.

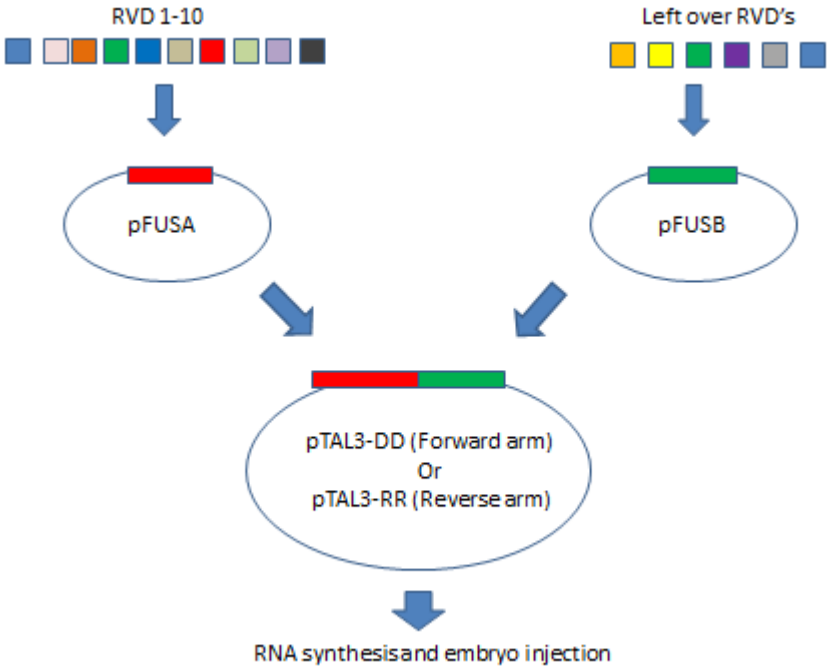

Fig.2.5: Simplified overview of TALEN assembly.

Synthesis of RNA for microinjections

10ug of each plasmid was incubated at 37 °C overnight along with 5 µL of the appropriate restriction enzyme and 5 µL of the restriction buffer with 0.5 µL BSA if required up to a final volume of 50 µL NFW. The following morning the enzyme was inactivated at 65 °C for 20 minutes. 1 µL of calf-intestinal alkaline phosphatase (CIAP) was added for Phosphatase treatment to dephosphorylate the 5' end and incubated for 15 minutes at 37 °C. Both plasmids were run on a gel to ensure the plasmid had been linearised. Ambion mMessage Machine kit was used for mRNA synthesis; conditions were set up according to the manufacturer's instructions. The yield was measured and the mRNA stored in aliquots in the -80 °C until needed for microinjection.

2.2.13 Microinjection protocol

Microinjection needles were made from pulled glass capillaries using Flaming Brown pipette puller and settings of 500 units of heat, 70 units of pulled force and velocity of 75 m/s.

mRNA was diluted to 100 pg of the forward TALEN arm and 100 pg of the reverse TALEN arm for injection in NFW and 0.05% phenol red stock solution (1.4 mM phenol red, 0.2 M KCl). Solutions were heated for 10 minutes at 65°C before being loaded into the needle using a microloader pipette tip. The needle was placed in the microinjector apparatus and calibrated by holding the pressure at 40psi and adjusting the injection time until a volume of 1 nL was being injected estimated by drop diameter on a gridded cell UV slide.

Petri dishes with 2% agarose solution and moulds were used to hold embryos for injection where all embryos were injected at the one-cell stage with 1 nL of solution using Narishige IM-300 microinjector. Control embryos were injected with 0.05% phenol red stock solution. Following injection the embryos were incubated at 28°C and after six hours, unfertilised embryos were removed from the dish. Embryos were monitored on a daily basis and the morphology scored accordingly.

2.2.14 Fin-clipping of adult zebrafish

Adult fish were anaesthetised in 1% MS222 in housing water for approximately 1 minute; a small amount of the tail fin was clipped using a sterile blade and forceps to transfer the tissue sample into a 0.5 mL microcentrifuge tube. Fish were placed into a small tray for 5 minutes for recovery and observation before being put into individual small tanks until genotyping results had been analysed.

2.2.15 Genomic DNA extraction

Genomic DNA samples were extracted from embryos and adult finclips using the following protocol established by Meeker et al. (2007); 100 µL of 50 mM NaOH was added and the sample was heated to 98°C for 13 minutes. Samples were quickly vortexed and put back on the heat block for a further 2 minutes. Samples were cooled at room temperature for 15 minutes and then incubated at 4 °C for a further 10 minutes. 10 µL of 1M Tris-HCl pH 8.0 was added and the sample was centrifuged at 8,000 g for 10 minutes. Genomic DNA was stored at – 20 °C.

2.2.16 Screening of F_0 founders

A random selection of control and TALEN injected embryos (10-20 per group) were selected for mutant screening. Embryos at 24 - 48 hpf were collected in 500 µL tubes and genomic DNA was extracted using the NaOH extraction protocol as previously described in Section 2.2.14. Samples were PCR amplified using primers flanking the targeted exon (exon 1) and PCR products were purified and sent for sequencing to Eurofins genomics. Morphology was scored up to 2 dpf as described in Section 2.2.3 on all injected embryos. When successful TALEN mutation had been confirmed by sequencing all larvae were raised to adulthood.

2.2.17 Cloning PCR products

In cases of ambiguous sequencing results during TALEN screening due to mosaic patterns in the genotype, products were cloned into pGEM-T Easy vectors and each ligation was cloned into an E.coli host (Top10-IBA lifesciences) prior to colony selection and mini-prep where each clone selected was sent for sequencing. Ligation reactions were set up according

to manufacturer's instructions and cloning procedure was followed according to host strain. Promega pGEM-T Easy Vector System I was used for PCR product cloning.

2.2.18 Identification of germline mutations

Injected embryos were raised to adulthood. These "donor" or F_0 fish were outcrossed with wild-type AB fish and embryos were screened for germline mutations. Embryos were assessed both phenotypically and genotypically. For genotypic analysis, ten randomly selected F_1 embryos per clutch were harvested from individual F_0 crosses and genomic DNA was isolated from these individual embryos at 24 hpf as previously described in Section 2.2.14. High resolution melt analysis (HRMA) was then used for initial screening and mutant sequences were PCR amplified, purified and sent for sequencing. The A plasmid Editor (ApE) program (http://biologylabs.utah.edu/jorgensen/wayned/ape/) was used to align all sequencing results to a nanor wild-type reference sequence. Following identification of mutant families, siblings were incrossed to give homozygous F_2 mutant embryos as described in Fig. 2.6.

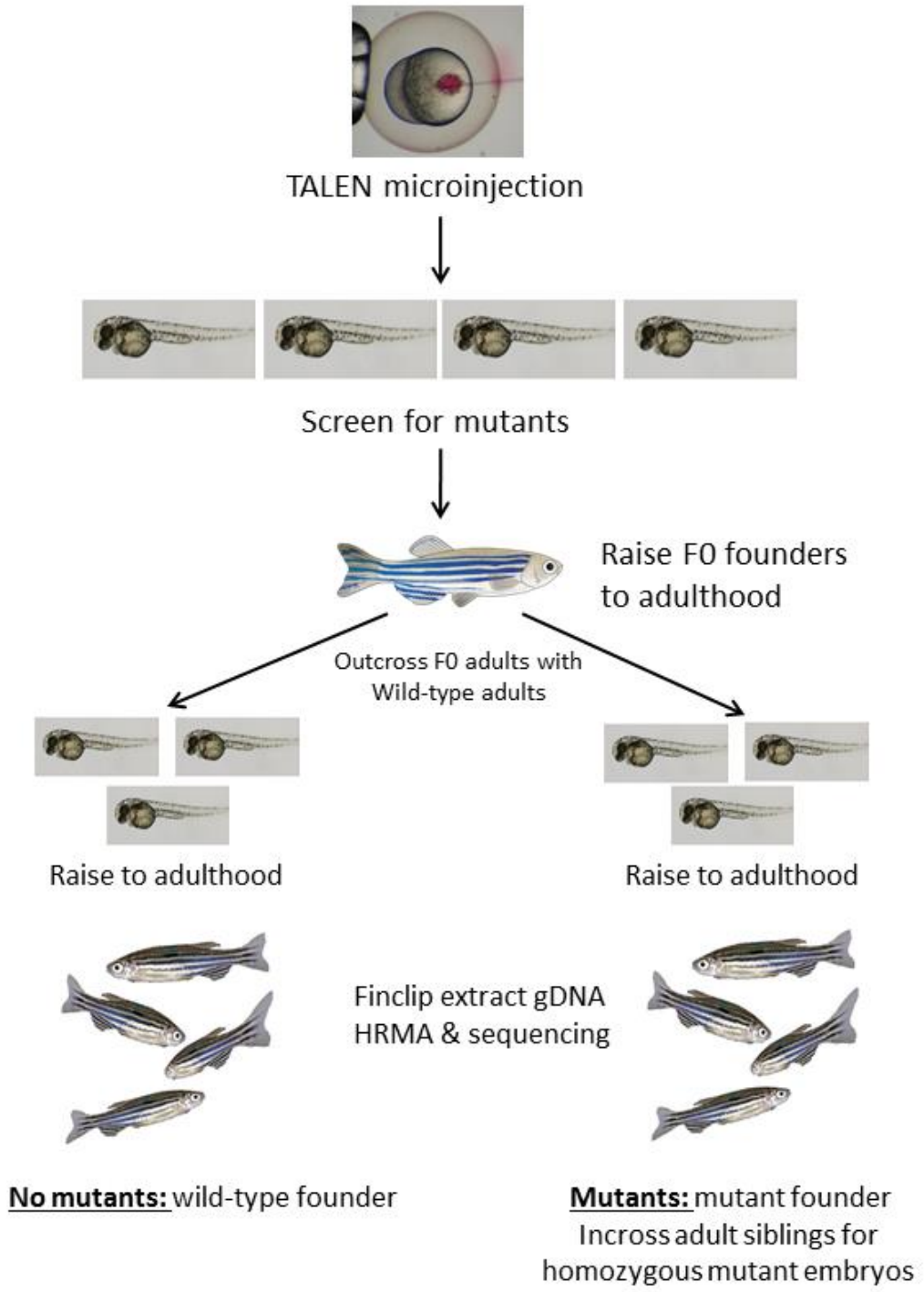

Fig. 2.6: Summary of TALEN screening process and TALEN F_0, F_1 and F_2 generation.

2.2.19 Genotyping by High Resolution Melt Analysis (HRMA)

HRMA was used to verify TALEN induced mutations in a subset of F_1 embryos (F_0 adult outcross) harvested for genomic DNA extraction. PCR reactions with high-resolution melt-curves were performed using the Roche

Lightcycler 480. PCR primers were designed to flank the region of interest and amplify a product of less than 100 base-pairs. Primers were diluted to a concentration of 100 pmol and then forward and reverse primers were mixed in a 1:1 ratio. Final concentration of primer mix used in a reaction was 5 pmol. Roche High Resolution Melt Master was used to detect changes in the melting temperature of the amplicon due to induced mutations in the sequence. Standard reaction set up was followed according to manufacturer's instructions with 20 ng of genomic DNA in each 20 µL reaction. 40 cycles of a PCR reaction preceded the high resolution melt curve. A random selection of 10 wild-type and 10 TALEN embryos from each F_0 outcross showing a diverging melt-curve in comparison to wild-type controls demonstrated successful TALEN induced mutations. Any genomic DNA samples that were flagged as mutants were sent for sequencing. Mutant families were kept and raised to adulthood. At approximately 5 months fin-clips were taken from adult F_1 fish to screen mutant from wild-type sequences. Wild-type adults were humanely euthanised and mutants were kept for F_1 incrossing to generate a stable F_2 homozygous generation.

2.2.20 Zebrafish *elipsa* mutant line

Elipsa mutant samples from sphere stage to 72 hpf were collected and sent to our lab by Dr. Rebecca Ryan (Imagine institute, Paris, France) with the permission of Dr. Malicki who produced this left/right asymmetry mutant line.

2.2.21 SDS page and Western blot

Zebrafish lysate preparation

All embryos up to 3 dpf were manually dechorionated and transferred to microcentrifuge tubes and 1 mL of deyolking buffer (55 mM NaCl, 1.8 mM KCl, 1.25 mM $NaHCO_3$, 10% protease inhibitor cocktail [0.2 mM 4-(2-aminoethyl) benzenesulfonyl fluoride (AEBSF), 1 mM EDTA, 130 µM bestatin, 14 µM E-64, 1 µM leupeptin and 0.3 µM aprotinin]) was added. A 200 µL pipette tip was used to disrupt the yolk sac and remove yolk proteins from the lysate. Microcentrifuge tubes were shaken for 5 minutes followed by centrifugation at 268 g for 30 seconds. The supernatant was removed and 1 mL of wash buffer (110 mM NaCl, 3.5 mM KCl, 2.7 mM $CaCl_2$, 10 mM Tris

pH 8.5) was added to the pellet. Tubes were shaken again for one minute and centrifuged for 30 seconds at 268 g. Supernatant was removed and the wash step was repeated. Pellets were stored at -80°C or were freon treated. Larvae older than 3 dpf were collected and stored at -80°C until ready for sonication in lysis buffer followed by a 12,000 g spin for 10 minutes at 4°C. Supernatant was collected and stored in -20°C ready for protein quantification by Bradford assay (Bradford, 1976).

Freon treatment

Pellets were thawed on ice and 50 µL of lysis buffer (1% Triton X-100, 10 mM Tris-HCl, pH 7.5, 140 mMNaCl, 5 mM EDTA, 2 mM EGTA, 1 mM PMSF) was added per 100 embryos. Pellets were sonicated for one second. 150 µL of freon was added to pellets which were vortexed for 30 seconds and left on ice for 2 minutes. Lysates were centrifuged at 4°C for 30 minutes at maximum speed. The supernatant was removed and stored at -20°C. Total protein concentration was estimated using the Bradford method.

Sodium Dodecyl Sulphate-Polyacrylamide Gel Electrophoresis (SDS-PAGE)

SDS-PAGE was used to separate proteins using an Atto minigel system. Stock solutions for the gel were prepared including 1.5M Tris pH 8.8, 1 M Tris pH 6.8, 10% SDS, 10% Ammonium persulphate (APS), 5x sample buffer (250 mM Tris pH 6.8, 10% SDS, 0.5% bromophenol blue, 500 mM DTT) and 10x running buffer (2.5 M Glycine, 0.035 M SDS, 0.25 M Tris, pH 8.3). To achieve reducing conditions samples were also heated to 95°C for 5 minutes prior to gel loading. 25 µg of protein was resolved on a reducing 10-15% separating gel, run at a 0.04 A for 90 minutes.

Western blotting

The nitrocellulose membrane was soaked in distilled water for 10 minutes prior to transfer of proteins. The membrane along with the filter paper and SDS-PAGE gel was then soaked in transfer buffer (24 mM Tris, 192 mM glycine, 20% methanol, 1.3 mM SDS, pH 8.3) for a further 10 minutes. The gel and membrane were sandwiched between 5 sheets of filter paper and a semi-dry transfer system was used to transfer proteins from the gel to the nitrocellulose membrane at a 0.15 A constant current for 90 minutes.

Following transfer, membranes were blocked in 5% milk/PBS for one hour at room temperature with agitation. Primary antibodies were diluted in the blocking solution and incubated overnight at 4°C with agitation. Primary antibody dilutions were as follows; anti-nanor 1:300 and anti-α-tubulin 1:2000. The following day membranes were washed six times with PBS for 5 minutes and incubated with secondary antibody diluted in blocking solution for 1 hour at room temperature with agitation. Peroxidase conjugated anti-rabbit antibody (1:20,000) was used to detect anti-nanor primary antibody. Peroxidase conjugated anti-mouse antibody (1:8,000) was used to detect anti α-tubulin primary antibody. Membranes were then washed six times in PBS for 5 minutes with agitation and were developed using Azure biosystems Radiance chemiluminescent substrate (2 ml) for three minutes. Azure C300 imaging system was used for signal detection.

Coomassie staining

Stock solution of Coomassie stain was made up prior to use; 120 g of citric acid, 80 g of ammonium sulphate and 4 g of Coomassie Brilliant Blue G-250 were dissolved in a total volume of 800 ml of distilled water. The solution was mixed for several hours and stored at room temperature. Directly before use 10 mL of methanol was added to 40 mL of staining solution. The gel was placed into staining solution for 3-5 hours with agitation. Following incubation, gels were destained in 1% acetic acid with several water changes until the background was clear.

2.2.22 In situ hybridisation

Purification of plasmids

LB broth with 0.25 mg of ampicillin was inoculated with a glycerol stock of the plasmid of interest and cultured overnight at 37°C. These cultures were then centrifuged at 5,000 g for five minutes and plasmid DNA was isolated and purified using a Nucleobond® mini-prep kit in accordance with the manufacturer's instructions. The concentration and quality of the isolated plasmid DNA was then assessed using a Nanodrop spectrophotometer, with an A260/280 ratio of approximately 1.8 indicating good quality pure DNA.

Restriction digestions

Purified plasmid DNA was digested using restriction enzymes in conditions recommended by manufacturers NEB. Restriction digestion was monitored by gel electrophoresis, with a single band indicating complete digestion. DNA was then purified by phenol-chloroform extraction as performed for RNA isolation

Preparation of digoxigenin-labelled RNA probes

RNA probes for whole mount in situ hybridisation were prepared using the Digoxigenin (DIG) RNA-labelling kit from Roche, according to the manufacturer's instructions as follows: 1 µg of linearised plasmid was added to the reaction mixture: DIG-labelling RNA mix, transcription buffer, nuclease-free water, RNA polymerase (SP6/T7) and RNase inhibitor. The reaction was incubated at 37 °C for 2 hours. Samples were treated with DNase for 15 minutes at 37 °C and probes were purified by ammonium acetate precipitation before being resuspended in 20 µL of nuclease-free water.

In situ hybridisation

When collecting embryos for ISH they were rinsed with PBST, dehydrated through a methanol series (25%, 50%, 75%, 100%) and stored at -20°C.

When ready to be used embryos were re-hydrated through a methanol series (100%, 75%, 50%, 25%), rinsed with PBST and if older than 24 hpf, treated with proteinase K (10 µg/ml in PBST) to facilitate penetration of the probes. Batches of 30-50 embryos were used for in situ hybridisations according to Hauptmann & Gerster (1994). Embryos were pre-hybridised in HYB solution (50% formamide, 5X Sodium Chloride Sodium Citrate (SSC) [0.15 M NaCl, 0.015M sodium citrate, pH 7], 50 µg/ml Heparin, 0.1% Tween 20, 0.5% Torula RNA) for 2-4 hours at 70°C. DIG-labelled RNA probe was thawed on ice and 2 µL of probe was added to 100 µL of pre-hybridisation buffer. The probe and pre-hybridisation buffer were heated at 100°C for five minutes and cooled in a water bath to 70 °C before hybridising with embryos overnight at 70 °C. Following incubation, embryos were washed twice for 30 minutes with 50% formamide/50% 2 X SSC/0.1% Tween 20, once for 15 minutes with 2 X

SSC/0.1% Tween 20 and twice for 30 minutes with 0.2X SSC/0.1% Tween 20. Embryos were blocked for three hours at room temperature with blocking solution (5% heat-inactivated sheep serum in PBS, 0.1% Tween [PBST]). Anti-digoxigenin-AP Fab fragments were diluted in blocking solution (1:5000) and incubated with embryos overnight at 4°C. Embryos were washed three times in PBST for five minutes each and then three times in PBST for 20 minutes each. Embryos were washed twice in staining buffer (100 mM NaCl, 50 mM MgCl2, 100 mM Tris HCl, 0.1 % Tween 20 pH 7.2) and transferred to four-well plates. BM-Purple AP-Substrate (1 ml) was added to each well and embryos were incubated in the dark until colour developed. Staining was stopped by washing three times in PBST (3 x 5 minutes). 70% glycerol was used when photographing embryo and larvae In situ hybridisation staining.

2.2.23 Antibody purification

Nanor antiserum was purified using the Ambion EpiMAX Affinity Purification Kit. Protocol was followed according to manufacturer's instructions. In order to purify the antibody from serum a nanor peptide was needed for the resin to successful capture the nanor antibody. The 13 amino acid peptide was synthesised by Biomatik with the sequence CRMRQKLPEGNEN at a molecular weight of 1.58 kDa. This is the peptide sequence that was used as the epitope to produce the anti-nanor antibody. A cysteine amino acid was added into the sequence to allow coupling to the residue. In total three purifications of nanor serum were completed with concentrations ranging from approximately 10 µg/ml to 50 µg/ml.

2.2.24 Co-Immunoprecipitation

In order to identify protein-protein interactions with nanor a Co-IP kit was used (Abcam, 206996). Protein was collected and sheared using sterile needles and quantified by the Bradford method. Total protein used during Co-IP was approximately 300 µg with non-denaturing conditions to avoid breakdown of protein complexes. To achieve these non-reducing conditions, where protein complexes would not be broken down, standard western blot protocol was altered; the samples were not heated to 95 °C prior to gel loading and DTT was not added to the sample. Before use protein A/G beads were washed thrice in 1 mL PBS. Purified nanor antibody was bound

to protein A/G beads which then bound to nanor protein complexes; 100 µL of antibody was added to 30 µL of protein A/G beads for 1 hour at 4 °C with agitation. Beads with antibody bound were then washed three times with 1 mL PBS. 200 µL of protein was added to the beads incubated at 4 °C overnight with agitation. Unbound supernatant was collected the following morning following centrifugation (2,000 g x 30 seconds). Beads were washed three times with 1 mL of PBS. Protein was eluted off the beads using a peptide; 80 µL (130 µg) incubated with beads for 1 hour (later changed to 30 minutes) on ice or using a low pH glycine elution; room temperature for 10 minutes with agitation. All elution steps were repeated twice. Attempts to elute nanor off the beads using a nanor peptide proved unsuccessful due to the peptide also taking nanor antibody off in the eluate. Samples sent for mass spectrometry were eluted in a low pH glycine buffer neutralised using 1M Tris-HCl in a total volume of 44 µL. A small amount of each sample was checked by western blot and Coomassie staining of the gel before sending for analysis to ensure nanor could be detected as well as unknown bands of interest. Samples were sent on dry ice to European Molecular Biology Laboratory (EMBL), Proteomics Core Facility in Heidelberg, Germany for mass spectrometry analysis. When sending a gel to the facility a maximum amount of eluate was loaded on the gel under reducing conditions and Coomassie stained gel (Section 2.2.20) was sent to EMBL for band excision and mass spectrometry analysis. Gels were vacuum packed and sealed with a few drops of distilled water added to prevent the gel from drying out during transport.

2.2.25 Mass spectrometry analysis

Samples were subjected to an in-solution tryptic digest (modified SP3 protocol) and peptides purified by a reverse phase cleaning step (OASIS) followed by analysis on Q-Exactive. Acquired data was processed using MaxQuant 1.6. iBAQ values were used for the label free quantification. Contaminants and hits from the reverse database were filtered. Unique peptides were also filtered to display only hits with a minimum of 2 unique peptides. iBAQ values were copied and zeros in the control samples were replaced by 100 to calculate the iBAQ ratio.

Results Chapter 3: Nanor mRNA Expression and Homozygous Mutant Generation

In zebrafish, left/right asymmetry development begins following FGF signalling and calcium signalling in migrating dorsal forerunner cells. Approximately two-dozen of these cells migrate to form a transient organ known as Kupffer's vesicle equivalent to the node in rodents (Nonaka et al., 1998). Beating cilia in Kupffer's vesicle then result in leftward fluid flow and asymmetric calcium elevation on the left side, which signals to the lateral plate mesoderm resulting in left-sided expression of nodal-related genes such as *spaw, cyclops* and *squint.* Downstream signalling results in left/right asymmetry development in the zebrafish embryo and larvae (Amack et al., 2007). Previous findings had linked *nanor* to asymmetry developed in zebrafish (O' Boyle, 2008).

3.1 Findings of previous *nanor* studies, hypothesis and aims

Nanor was discovered in our research group by Dr. Ronan Bree through suppression subtractive hybridisation studies at the mid-blastula transition and was confirmed to be zygotically expressed with undetectable expression in the maternal transcript in a pattern similar to *vox/vega1*. Whole mount in situ hybridisation up to 24 hpf confirmed the absence of *nanor* prior to the mid-blastula transition followed by rapid upregulation following the maternal-zygotic transition. *Nanor* was found in dorsal forerunner cells and Kupffer's vesicle with highest expression in ventral brain cells by 24 hpf (Bree et al., 2005). Dr. O' Boyle went on to successfully knock down *nanor* expression by morpholino injection and observed disruption of gene expression in the lateral plate mesoderm and disrupted left/right signalling. Defective eye and brain formation as well as incorrect cardiac looping were seen during later developmental stages. The earliest recorded developmental defect was found at shield stage where expression and signalling were disrupted in morphants (O'Boyle, 2008) leading to my hypothesis that *nanor* is most important during early development and upstream of Nodal signalling and organisation of left/right patterning. A previous research student in the lab

(Melissa Walsh) then investigated the expression pattern of Nanor protein by western blot and detected expression following the mid-blastula transition with high expression up to 72 hpf (unpublished).

Disadvantages of morpholinos are due to variable effects of morpholino injection between individual embryos along with transient effects and the risk of damage from mechanical stress contributing to the phenotypes observed. Therefore TALENs were designed in order to generate a *nanor* knockout mutant line. TALENs have been successfully used in a variety of experimental models such as cell lines, rodents, drosophila and zebrafish and more recently are being investigated for use in the treatment of human diseases such as sickle cell disease (Sun et al., 2012).

This chapter discusses investigations on *nanor* mRNA expression in wild-type embryos and larvae. Attempts were then made to generate a mutant line using TALEN technology, to investigate loss of function and identify downstream genes.

3.2 Nanor genomic sequence and protein structure

Nanor is located on chromosome 15 and consists of four exons, 626 base pairs in length (Table 3.1) (Bree et al., 2005). Nanor orthologues from online database ensembl.org gave three species hits; Ciona intestinalis (sea squirt), Latimeria chalumnae (coelacanth-closely related to lungfish) and Xenopus tropicalis (western clawed frog). Transcript identification of these orthologues has shown all three hits are uncharacterised proteins in their respective species, with no definitive information on protein function or localisation.

A similar gene located on chromosome 22, (*nanor b*), was identified as a paralogue of *nanor* that is 748 base pairs long predicted to encode a 197 amino acid protein. This protein has five casein kinase II phosphorylation sites, two N-glycosylation sites and an N-myristoylation site. N-glycosylation is necessary for protein folding and responsible for the addition of saccharides. A summary of *nanor* paralogues, Ensembl identification numbers and basic gene information is provided in Table 3.1. *Nanor b* was ‘retired’ and archived in Ensembl 45 (released June 2007) and is currently listed under the gene identification zgc:195170, with the new identification

ENSDARG00000076264. Alignment of both these sequences gives 100% sequence identity with no base mismatches or gaps. NCBI currently list both gene identifications, which are shown in Table 3.1; *nanor b* (NCBI Reference Sequence: NP_001124110.1) and zgc:195170 (NCBI GenBank: AAI63199.1). For simplicity, I will refer to this *nanor* paralogue as *nanor b* throughout the thesis.

A third *nanor* paralogue has also been identified in zebrafish on chromosome 4. This paralogue shows 41% genomic sequence identity to *nanor* and 78% sequence identity to *nanor b.* All three *nanor* paralogues have been listed as plasma membrane localised in Uniprot (Table 3.1).

Table 3.1. *Nanor* accession numbers and bioinformation

Gene	***Nanor***	***CR387997.2***	***Nanor b***	***ZGC:195170***
Gene ID	ENSDARG00000058917	ENSDARG00000101488	ENSDARG00000052108	ENSDARG00000076264
Location	Chromosome 15: 1,624,904 reverse strand	Chromosome 4: 29,023,751-29,024,527	Chromosome 22: 4,413,132 reverse strand	Chromosome 22: 4,413,132-4,414,505
Sequence homology	100% (*nanor*) 53% (*nanor b*)	41% (*nanor*) 78% (*nanor b*)	53% (*nanor*) 100% (*nanor b*)	53% (*nanor*) 100% (*nanor b*)
Transcript ID	ENSDART00000081875	ENSDART00000170534.1	ENSDART00000073891	ENSDART00000114465.6
Protein ID	ENSDARP00000076314	ENSDARP00000135199.1	ENSDARP00000068381	ENSDARP00000103963.4
Exon number	4	3	2	2
Base pair length	626	453	748	796
Paralogues	3			
Orthologues	3 (Ciona intestinalis, Latimeria chalumnae, Xenopus tropicalis)			
Domains	P2X purinoreceptor			
Subcellular localisation	Plasma membrane			
Information sources (last accessed)	Ensembl (11th December 2017) NCBI (11th December 2017) Uniprot (11th December 2017)			

Although the gene was first discovered over a decade ago, little is known about the expression or function of *nanor*. Rapid upregulation following the mid-blastula transition suggested that it was an important gene during early development but there were many unanswered questions regarding gene function and protein interactions.

When investigating sequence homology between species using blast alignment, the closest hit was 47% sequence identity to P2X7-like purinoreceptor in Astrofundulus limnaeus (genus of fish), with similar

matches to P2X7-like proteins in other lower species (Fig. 3.1 A). However, there is no significant sequence homology to the human P2X7 purinoreceptor or any other mammals, and when Nanor and human P2X7 protein sequences were aligned, only 27% sequence identity was found (Fig. 3.1 B). A P2X7-like protein in zebrafish has previously been discovered with 42% sequence identity to the human ortholog. When aligning this known P2X7-like protein to Nanor protein sequence only 30% identity is found between sequences.

The human P2X7 purinoceptor is made up of a number of domains: cytoplasmic domain (amino acid 1–25), followed by a transmembrane helical domain (amino acid 26–46) the majority of the protein is then extracellularly localised (amino acid 47–334) followed by another helical transmembrane domain (amino acid 335–355) with the remaining amino acids (356–595) localised in the cytoplasm. Alignments of P2X7–like protein in zebrafish and *nanor* to the human P2X7 protein shows sequence homology in both occurring at the end of the P2X7 protein, in the cytoplasmic domain.

P2X7 purinoreceptor is a member of an ATP gated cation channel family as listed in the British Pharmacological Society (BPS) and the International Union of Basic and Clinical Pharmacology (IUPHAR) guidetopharmacology.org which is a definitive authority on all receptors. These receptors modulate synaptic transmission and have also been shown to regulate ATP-evoked calcium signalling in rodent glial tissue (James and Butt, 2001), and contribute to activation of interleukin-1 processing and release (Ferrari et al., 2006). C-terminal domain in human P2X7 has been shown by several studies to be critical for signalling (Hu et al., 1998; Gu et al., 2001; Costa-Junior et al., 2011). P2X7 C-terminal region is also essential for formation of cytolytic pores in the plasma membrane (Surprenant et al., 1996). A number of accessory proteins have been linked to function of P2X7 such as heat shock proteins (HSP-70, HSP-90), Pannexin, Laminin α-3 and Supervillin (Adinolfi et al., 2003), however, none of these display any significant sequence similarity to *nanor*.

A

Description	Max score	Total score	Query cover	E value	Ident
PREDICTED: P2X purinoceptor 7-like [Austrofundulus limnaeus]	128	128	80%	1e-34	47%
PREDICTED: P2X purinoceptor 7-like isoform X1 [Nothobranchius furzeri]	117	117	92%	5e-30	41%
PREDICTED: P2X purinoceptor 7-like [Nothobranchius furzeri]	114	114	92%	1e-28	41%
uncharacterized protein LOC111136026 isoform X2 [Crassostrea virginica]	93.2	93.2	70%	5e-21	37%
uncharacterized protein LOC110983474 [Acanthaster planci]	93.2	93.2	92%	4e-20	34%
P2X purinoceptor 7-like isoform X1 [Crassostrea virginica]	91.7	91.7	80%	9e-20	34%
P2X purinoceptor 7-like [Crassostrea virginica]	90.1	90.1	92%	4e-19	30%
PREDICTED: P2X purinoceptor 7-like [Amphimedon queenslandica]	89.0	89.0	63%	4e-19	39%
P2X purinoceptor 7-like [Mizuhopecten yessoensis]	86.3	86.3	67%	3e-18	35%
PREDICTED: uncharacterized protein LOC102801802 [Saccoglossus kowalevskii]	86.7	86.7	81%	5e-18	34%
PREDICTED: P2X purinoceptor 7-like [Sinocyclocheilus anshuiensis]	87.8	87.8	83%	7e-18	35%
PREDICTED: uncharacterized protein LOC107725790 isoform X3 [Sinocyclocheilus rhinocerous]	87.8	87.8	83%	8e-18	35%
P2X purinoceptor 7-like [Crassostrea virginica]	86.3	86.3	92%	8e-18	30%
PREDICTED: P2X purinoceptor 7-like [Lingula anatina]	86.3	86.3	72%	1e-17	34%

PREDICTED: P2X purinoceptor 7-like [Austrofundulus limnaeus]

Sequence ID: XP_013881450.1 **Length:** 146 **Number of Matches:** 1

Range 1: 1 to 142 GenPept Graphics ▼ Next Match ▲ Previous Match

Score	Expect	Method	Identities	Positives	Gaps
128 bits(321)	1e-34	Compositional matrix adjust.	68/144(47%)	91/144(63%)	6/144(4%)

```
Query  33   MPVDEGEDAPDEANIKVSQRCSCGNCR-LTPEENVCCRDIPQVKHKCGQVNV-CCITNHP  90
            MP     +  ++    VS+ C+CG+C  L+P ENVCCR+ P+V ++C QV V  CIT+HP
Sbjct  1    MPEAAAAETMEDRMAPVSEWCTCGHCSSLSPVENVCCRETPKVMNRCEQVGVYTCITDHP  60

Query  91   GFELVTLNPDVLQVSYCRYQDVYGKTLPD--LNSRNRHLACINFIFMCWSDAGQQTRAVI  148
            GF+LV LNP VLQ  Y  Y  ++G+ +P+  LNSR RHLA  N +  CW   GQ  R VI
Sbjct  61   GFQLVALNPYVLQAVYGTYVQLFGE-MPETMLNSRYRHLAYRNVVRWCWGYLGQHIRVVI  119

Query  149  PSCVAGRMRQKLPEGNENYNGLFP  172
            PSC+  R+RQ+ PE +  Y G  P
Sbjct  120  PSCIVTRIRQEFPE-DGLYRGFLP  142
```

B

Sequence ID: Query_160235 **Length:** 595 **Number of Matches:** 4

Range 1: 477 to 591 Graphics ▼ Next Match ▲ Previous Match

Score	Expect	Method	Identities	Positives	Gaps
43.9 bits(102)	8e-10	Compositional matrix adjust.	34/125(27%)	51/125(40%)	17/125(13%)

```
Query  53   CSCGNCRLT--PE-----ENVCCRDIPQVKHKCGQVNVCCITNHPGFELVTLNPDVLQVS  105
            C CG+C   +  PE     E +CCR  P            CIT    F  + L+  VLQ
Sbjct  477  CQCGSCLPSQLPESHRCLEELCCRKKPGA----------CITTSELFRKLVLSRHVLQFL  526

Query  106  YCRYQDVYGKTLPDLNSRNRHLACLNFIFLCWSDVGQQTRAVIPSCVAGRMRQKLPEGNE  165
             + +    +   NSR RH A   +    +        A++PSC   R+R++ P+
Sbjct  527  LLYQEPLLALDVDSTNSRLRHCAYRCYATWRFGSQDMADFAILPSCCRWRIRKEFPKSEG  586

Query  166  NYNGL  170
              Y+G
Sbjct  587  QYSGF  591
```

Fig. 3.1: Blast alignment results summary of nanor. (A) Results show highest sequence similarity to P2X7-like purinoreceptor across many species. In humans there are currently seven P2X receptors. The closest sequence match was to the P2X7-like purinoreceptor in Austrofundulus limnaeus (a genus of fish native to South America). Sequence similarity corresponds to the C-terminal domain of human P2X7 purinoreceptor. (B) When nanor was aligned to the human P2X7 receptor only 27% sequence identity was found, again matches were to the C-terminal domain of the purinoreceptor.

Predictprotein.org was then used to investigate the properties of Nanor protein. However, the databases did not contain any protein with significant sequence similarity to Nanor, making 3D structure difficult to predict. Predicted secondary structure was classified as 36.14 % helix, 4.46 % strand and 59.41 % Loop. Predictions made based on protein structure conclude it is not likely to be nuclear or transmembrane localised. Protein motif searches on expasy.org found a protein kinase C phosphorylation site, three casein kinase II phosphorylation sites, an NFX-type zinc finger domain, indicating a possible role in transcriptional regulation and a N-myristoylation site from amino acid 12-17. Myristoylation functions at the N-terminal of a protein and adds a myristoyl group known to promote protein-membrane, protein-protein interactions and signal transduction pathways.

3.3 Nanor mRNA expression in wild-type zebrafish

Semi-quantitative PCR was previously used to quantify mRNA expression before and after the mid-blastula transition. Dr. Bree found undetectable expression at the 128-cell stage and high expression at sphere stage (Bree et al., 2005). To further progress mRNA studies, quantitative PCR (qPCR) was used to quantify expression with a higher degree of accuracy than previously used semi-quantitative methods for both *nanor* and *nanor b* paralogues.

mRNA was quantified at nine stages; 128 cell, sphere (4 hpf), shield (6 hpf), 6-somite stage (12 hpf), 24 hpf, 48 hpf, 72 hpf, 96 hpf and 120 hpf using primers that achieved 92-100% efficiency during primer validation as described in Section 2.2.9.

While *nanor* mRNA expression is negligible at the 128-cell stage (cycle threshold 35 of 40 cycles), there is a large increase in *nanor* expression levels (10,000 fold) at sphere and shield stage which is rapidly down-regulated at 24 hpf and further decreased at 72 hpf back to pre-mid-blastula transition levels (Fig. 3.2 A; One-way ANOVA $F_{(6,\ 20)} = 82.25$, $P < 0.0001$; Dunnett's post hoc test $P < 0.001$ sphere, shield, 12 hpf vs. control (128 cell

stage)). *Nanor b* goes through a similar peak in gene expression at sphere and shield stage (1,000 fold) followed by rapid down-regulation (Fig. 3.2 B; One-way ANOVA $F_{(8, 20)} = 27.51$, $P < 0.0001$; Dunnett's post hoc test $P < 0.001$ sphere, shield, 24 hpf, 48 hpf, 72 hpf vs. control (128 cell stage)). However, this paralog goes through a second wave of expression and is upregulated at 24 hpf up to 120 hpf (Fig. 3.2 B). Expression levels of both *nanor* and *nanor b* were found to be highest during sphere and shield stages which are soon after the mid-blastula transition and the onset of zygotic control of cell divisions and subsequent development.

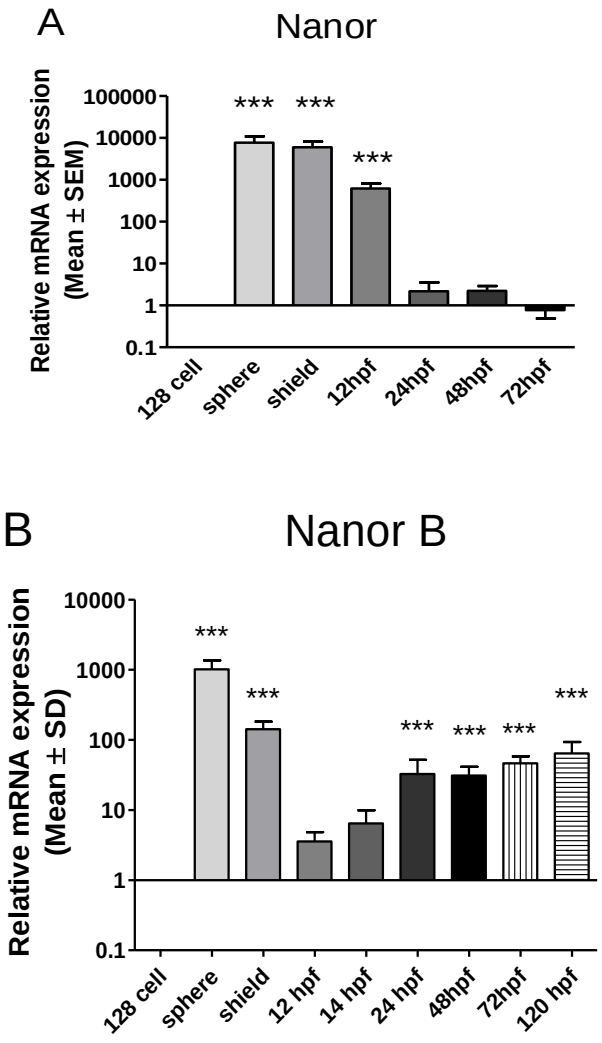

Fig. 3.2: mRNA expression of *nanor* in wild-type embryos. *Nanor* (A) and *nanor b* (B) mRNA expression at 128 cell stage up to 120 hpf; n≥3 with 50-80 embryos or larvae per biological replicate. Both paralogues show huge upregulation following the mid-blastula transition quickly followed by down-regulation at approximately 24 hpf. *Nanor b* goes through a second wave of gene expression up to 120 hpf ($P < 0.001$ vs. control (128-cell stage)). Data shown are mean ± SEM.

The expression pattern of *nanor* mRNA by whole mount in situ hybridisation was then studied. Previous work in the lab had only investigated up to 24 hpf, later developmental stages of the larvae up to 72 hpf were investigated in this study. Expression was ubiquitous during early embryogenesis at sphere and shield stage (Fig. 3.3 A – F). By 24 hpf *nanor* mRNA was restricted to anterior structures in all embryos and staining can clearly be seen in the brain with commissures separating the left/right and midbrain/hindbrain boundaries clearly visible with no staining in the tail (Fig. 3.3 G). At 48 hpf and 72 hpf *nanor* expression is restricted to neural and anterior structures with expression gradually decreasing as larvae develop. Following 72 hpf *nanor* expression was no longer detected in larvae. This is in agreement with qPCR studies in which negligible traces of *nanor* mRNA were recorded after this time-point.

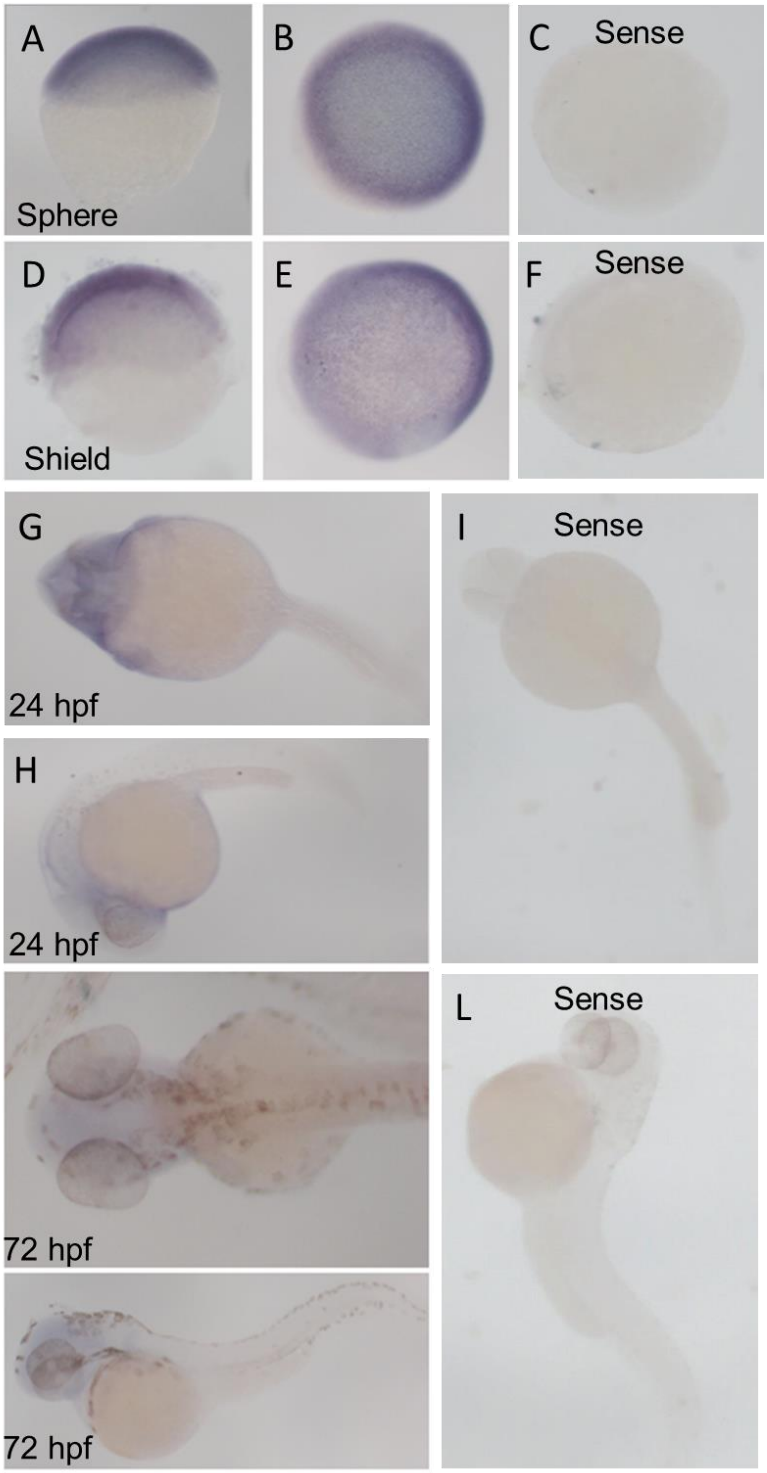

Fig. 3.3: Expression pattern of *nanor* in zebrafish embryos from the sphere stage to 72 hpf. WT mRNA expression of *nanor* by whole mount in situ hybridisation. High ubiquitous expression of *nanor* is seen at sphere stage (A lateral, B dorsal) and shield stage (D lateral, E dorsal). At 24 hpf expression has moved to anterior structures such as the head, eyes and brain (G ventral, H lateral). By 72 hpf expression has decreased but can still be seen in anterior structures (J dorsal, K lateral). Sense controls of sphere (C), shield (F), 24 hpf (I) and 72 hpf (L) shown alongside anti-sense *nanor* probes.

Results from in situ hybridisation show detectable *nanor* expression up to 72 hpf, localisation was ubiquitous during sphere and shield stage with restriction to anterior structures as development progresses and negligible expression beyond 48 hpf indicating a function in anterior structure formation during larval stages. *Nanor b* expression also showed rapid upregulation following the mid-blastula transition. Expression was down-regulated by 12 hpf and this gene appeared to go through a second wave of expression with high expression by 120 hpf indicating a later function of *nanor b.* Following mRNA quantification and localisation studies, attempts were made to identify downstream genes using gene editing technology to generate a mutant line.

3.4 Heritable targeting of *nanor* using TAL Effector Nucleases

Dr. O' Boyle, a previous member of our research group, generated successful knockdown of *nanor* by morpholino injection. This morpholino caused detrimental effects on embryo development with alterations in expression of the Nodal pathway genes including *pitx2a, lefty1* and *cyclops. Nanor* knockdown disrupted left/right signalling in the lateral plate mesoderm and increased *spaw* and *pitx2a* expression with reduced *lefty1*. Later in development, decreased mRNA expression of *cyclops, lefty1* and *pitx2a* was noted. Cardiac and neural defects as well as failure in separation of a single eye field into bilateral optic primordia during eye development were discovered. Expression of these genes were examined by in situ hybridisation and randomised expression was found in morphants. Dr. O' Boyle concluded that *nanor* is necessary for activation of Nodal-related genes in the lateral plate mesoderm and required to pattern the left/right axis (O' Boyle, 2008). However, many problems exist with the use of morpholino knockdown due to their transient nature as well as a high risk of off-target effects.

In order to explore the molecular interactions of *nanor*, established loss-of-function approach using transcription activator-like effector nucleases (TALENs) was used. This gene editing technology can be assembled to bind to almost any DNA sequence and result in generation of a stable, homozygous mutant line that can be passed on through generations (Boch et al., 2009; Christian et al., 2010). TALENs have been successfully applied in

a variety of organisms including yeast, Drosophila, zebrafish and human cell lines (Huang et al., 2011; Li et al., 2011; Miller et al., 2011; Sander et al., 2011; Reyon et al., 2013; Kobayashi et al., 2017).

TAL effectors bind DNA and when fused to a FokI nuclease, enable cleavage at specific target regions. FokI is fused to a C-terminus and cleaves as a dimer, therefore a pair of TAL subunits are required; one for the sense strand and one for the anti-sense strand of DNA sequence, with the FokI domains dimerising at a spacer region and inducing a double-strand break in the DNA, with the hope of non-homologous end joining inducing an insertion or deletion during the repair process. TALENs are generated by fusing an array of repeat-variable diresidues (RVDs) to generate a sequence specific DNA binding protein fused to FokI.

3.4.1 Sequence and Design of TALENs

TALEN pairs were designed to target exon 1 in the *nanor* gene and induce a premature stop codon using the guidelines outlined in Section 2.2.11 and the online TALEN targeter tool (https://tale-nt.cac.cornell.edu/node/add/talen). Candidates were aligned against the zebrafish genome using the Ensembl genome browser with TALENs that were chosen for manufacture meeting the recommended conditions outlined by Cermak et al. (2011). Two TALENs were manufactured and micro-injected (Table 3.2). A shorter spacer length was chosen for the second TALEN as this was reported to increase the efficiency of the TALEN (Christian et al., 2010).

Table 3.2: Target sequences of micro-injected TALENs.

	Left target sequence	Spacer	Right target sequence
TALEN 1	GGATGAAGGTGAAGATGCTC	CAGACGAGGCCAATAT	TAAAGTCTCACAAAGG
TALEN 2	GAAGGATCTCTCTCCT	CCATTTTATCAGTTT	TAAAGCTTTCATGCC

As *nanor* is only 626 base pairs in length with just four exons (Fig. 3.4), TALEN selection was limited. Exon 1 was chosen as the target site in the

exon as it met the criteria for TALEN design and the aim was to induce a premature stop codon as early as possible in the sequence to ensure knockout of the protein. TALEN target regions are shown in Fig. 3.4:

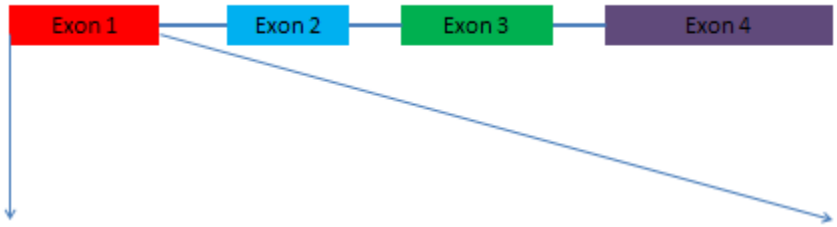

GAACACAGACGCAGAG**ATG**GACAGCGATTCAGCAAGCAGCGTTTAC
AGCGGATCTCAGAGCTCTGTGGAGGT**GAAGGATCTCTCTCCT**CCATTT
TATCAGTT**TAAAGCTTTCATGCC**TGT**GGATGAAGGTGAAGATGCTC**CA
GACGAGGCCAATAT**TAAAGTCTCACAAAGG**Tattattctgttctacatgactaa
ctgtatttgagtaaacaaacgactaataaacacaccactgtgcctgacacaaacactgcact
gaaactggactgttgtcatcctaaatcaggtGCTCTTGTGGAAACTGCAGACTCA
CTCCAGAGGAAAACGTTTGTTGTAGAGACATACCACAGGTaaaaaccttc
agcaaactgttcatacagcaaacagttcatacagcatcatgtcagagtctacaccgagtaat
atgctttgcttttcgtccaataggtGAAGCACAAATGTGGCCAGGTTAACGTATG
TTGCATAACAAACCACCCGGGGTTTGAGCTTGTCACTCTGAACCCAGA
CGTCCTGCAGGTGTCTTATTGCAGATATCAGGATGTTTATGGGAAGACA
CTCCCAGATCTCAACAGgttggttttaaagatccatcactgtgctctgtcgcttcagtaa
cattataatgaagtctgctaccgaacgttaatgcatcttatgtttattatctccatttctcctatc
aaacctcatgtaaattgagcaacatctgacctgacctgtgtttcattcagCCGTAACAGA
CACCTGGCATGTTTAAATTTCATCTTCTTGTGCTGGAGCGATGTGGGGC
AACAGACCAGAGCGGTGATTCCCTCATGTGTTGCTGGAAGAATGAGAC
AGAAACTCCCAGAAGGAAACGAAAACTACAATGGTTTATTTCCCCGTC
CACTTTAGGAGAAGACTTCTGTACTGAATCACGTGTGCTGTAAAATGCT
TCAAAATAAACTTGCGTACACAACAAA

Fig. 3.4: *Nanor* sequence and TALEN binding sites. Genomic sequence of *nanor*, exons are in capital letters and introns in lower case, start codon marked in green, TALEN 1 forward and reverse arms marked in blue and TALEN 2 forward and reverse arms marked in red.

3.4.2 TALEN assembly

TALENs were designed and assembled using Golden Gate cloning. Each subunit (forward and reverse) was constructed in two halves in which RVD's were ligated together during two Golden Gate reactions using two different plasmids. Golden Gate reaction 1 built RVD repeats 1-10 using pFUS A or pFUS B. Plasmids pFUS A and pFUS B were then ligated together with the last RVD in a second Golden Gate reaction into the vector containing the FokI domain using pTAL3-DD for the forward arm or pTAL3-RR for the reverse arm. All TALENs were sequenced to confirm correct insertion of RVDs and digestion with BamHI and XbaI were used to check TALEN size and ensure all RVDs had been correctly inserted (Fig. 3.5). Final TALEN constructs were also sent for sequencing to ensure that all RVDs were in place and in the correct order. Plasmid DNA was linearised and transcribed to generate 5' capped mRNA for micro-injection. Forward and reverse TALEN pairs were mixed in a 1:1 ratio followed by micro-injection of 1-cell stage zebrafish embryos at 100 pg or 200 pg doses, these embryos were the founder embryos (F_0).

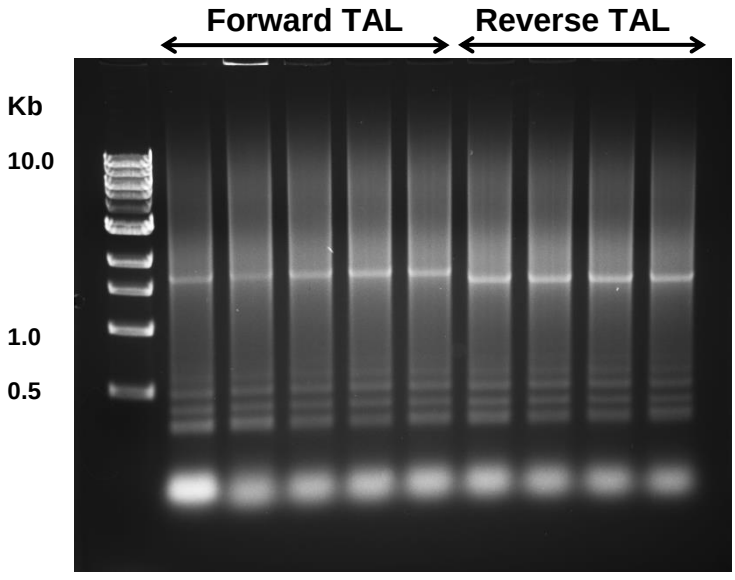

Fig. 3.5: Final TALEN constructs of forward and reverse arms targeting nanor exon 1. Clones of assembled forward and reverse arms of TALEN 2 shown in gel image. Successful products display a single faint band between 2-3 kb for TALENs of 12-22 RVDs accompanied by a characteristic smear and ladder effect due to the repetitive nature of RVD array.

3.5 TALEN 1 micro-injection and F_0 analysis

The first TALEN targeting exon 1 of *nanor* was micro-injected in approximately 300 embryos at the one-cell stage for each dose (100 pg and 200 pg) and approximately 100 embryos were micro-injected with phenol red as controls. Following micro-injection, embryos were scored at 48 hpf and developmental defects noted. Morphology was normal in over 75 % of 100 pg larvae and 70 % of the 200 pg larvae (Fig. 3.6). This absence of increased abnormalities with increasing dose indicated that TALEN 1 may have failed to produce any mutations in the embryos. However, this was not a clear indication of successful TALEN induced mutations.

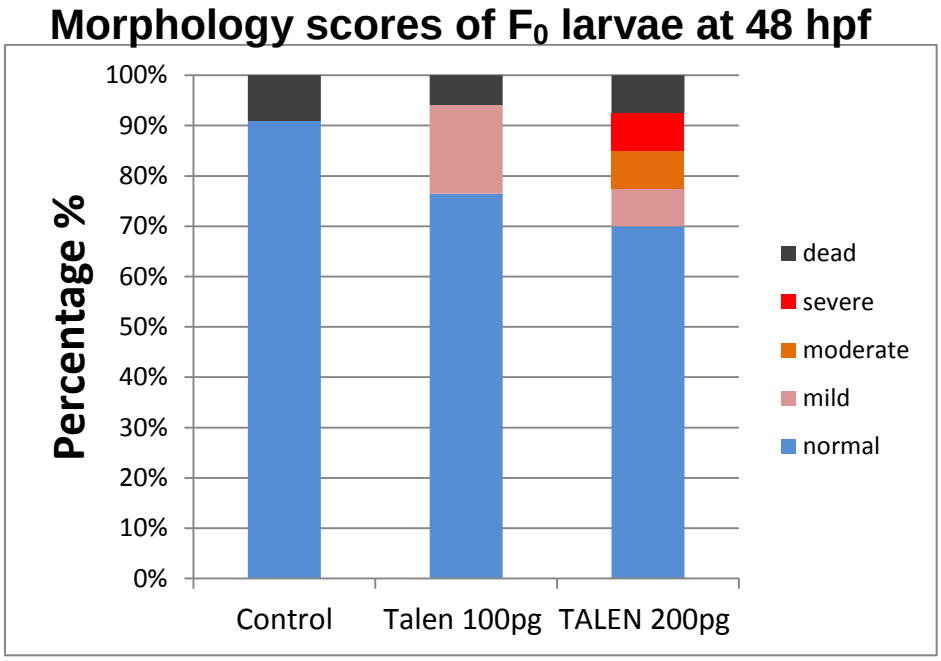

Fig. 3.6: Morphology scores of TALEN injected embryos at 48 hpf. At 100 pg most larvae presented with a normal phenotype (over 75%). Remaining larvae showed mild defects such as mild heart oedema or blood pooling. At 200 pg 70 % of larvae had a normal phenotype with remaining larvae showing mild, moderate or severe defects such as blood pooling, abnormal yolk sac and bent bodies, n = 40 embyros per group.

Therefore, following morphology scoring, genomic DNA samples from approximately 10 larvae from 100 pg and 200 pg micro-injected groups and 3-5 control larvae were extracted as described in Section 2.2.14. All sequences aligned with identical base matches to the wild-type reference

sequence in exon 1 showing that TALEN 1 micro-injection failed to induce any insertions or deletions in the spacer region (Fig. 3.7).

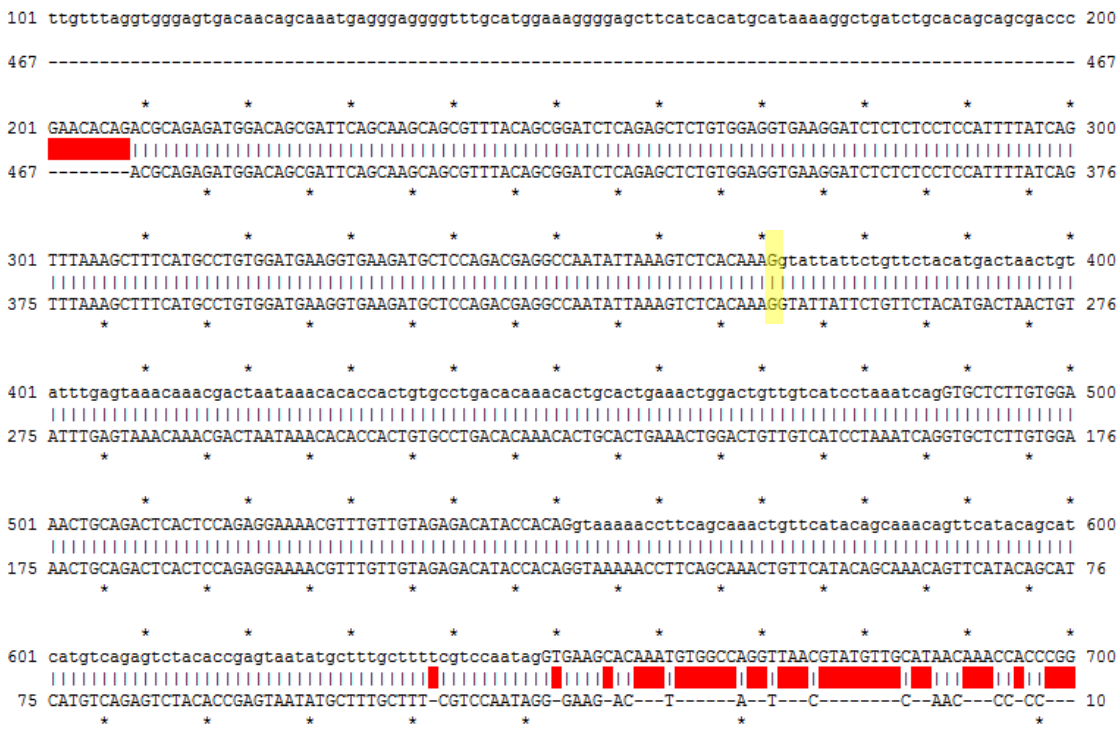

Fig. 3.7: Sequencing result following TALEN 1 micro-injection. An example of a TALEN 1 injected embryo sequencing result. Top sequence from base 101-700 is wild-type reference. Bottom sequence is aligned sequencing result from genomic DNA sample of an injected embryo. Red marks mis-matched bases. The beginning and end of a sequence always present with high background and several mismatched bases. This shows a perfect match to our reference sequence with no mutation as a result of TALEN 1. Exons are depicted by uppercase in the reference sequence. The end of exon 1 is highlighted in yellow.

Following these results it was clear that TALEN 1 had failed to induce any insertions or deletions in the spacer region. A new TALEN was designed to target exon 1.

3.6 TALEN 2 micro-injection and F_0 analysis

TALEN 2 was assembled as previously described in Section 3.1. Approximately 300 embryos were micro-injected with 100 pg of TALEN 2 mRNA and the same number of embryos injected with 200 pg of mRNA at the one-cell stage. Control embryos were micro-injected with phenol red.

Detailed morphology was scored at 48 hpf to record developmental defects. At 48 hpf approximately 10 morphologically normal TALEN-injected embryos per injected concentration and 3-5 sibling phenol-red micro-injected embryos were collected and genomic DNA extracted, PCR-amplified, purified and sent to Eurofins Genomics for sequencing the region of interest. Results are presented below.

3.6.1 F_0 founder morphology and genomic DNA collection

On micro-injection of the second TALEN by 48 hpf the majority of TALEN mutant embryos had mild, moderate or severe defects at the 200 pg dose and by 5 dpf approximately one-third of them had died. Defects observed primarily involved head formation and in more severe cases, bent bodies which were always accompanied with poor circulation and heart defects. Many larvae failed to develop a normal brain and had absent, underdeveloped or fused eyes. Moderate and severe phenotypes consistent with observations made in the *nanor* morpholino were noted; bent body axis or kinked tails with circulatory system defects as well as missing heads and brain oedema were recorded during scoring (Fig. 3.8).

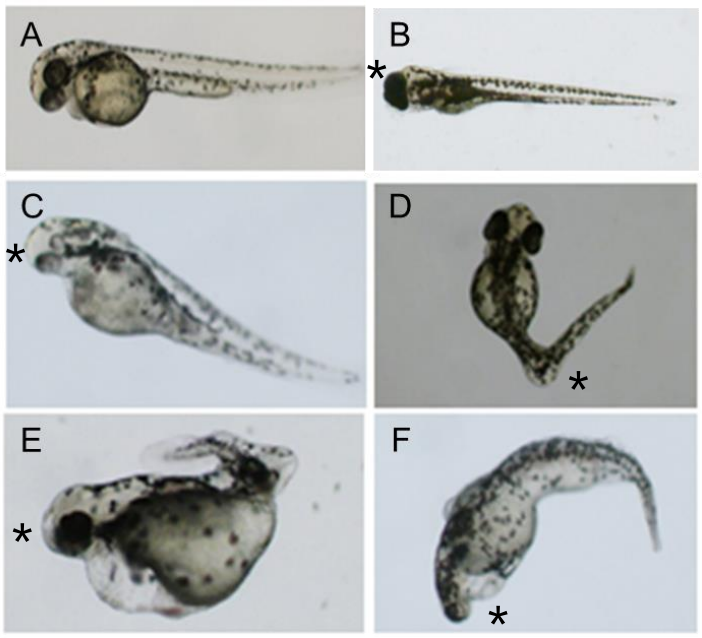

Fig. 3.8: Morphology of control and F_0 founder 48 hpf. When compared to healthy controls at 48 hpf (A) F_0 founders showed cyclopia (B) or underdeveloped eyes (C), kinked tails (D), underdeveloped brain, bent body axis and heart oedema (E), in most severe cases larvae did not develop any anterior structures (F).

In TALEN micro-injected embryos the severity of defects was clearly dose-dependent with more severe defects noted at the higher dose of 200 pg (Fig. 3.9). Phenol red injected embryos did not show any defects at 48 hpf but 10% of embryos did not survive to 48 hpf. At 100 pg, defects observed were mild in approximately 20% of larvae with 75% showing a normal phenotype. At 200 pg, less than 40% of larvae developed normally up to 48 hpf with 10% deaths and half of larvae presenting with mild, moderate or severe deformities.

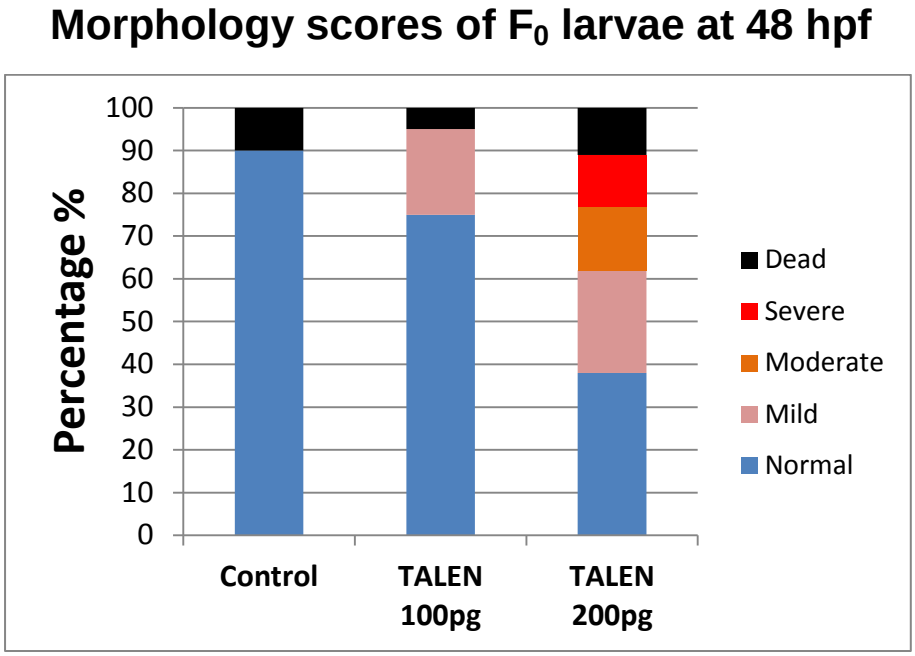

Fig. 3.9: Morphology scores of phenol red (control) or TALEN injected larvae at 48 hpf. Morphology scores at 48 hpf of control larvae (phenol red), 100 pg and 200 pg injected TALENS. A clear dose response was seen following TALEN injection. At 100 pg 5% of larvae were dead by 48 hpf and 20 % showed mild phenotypes such as underdeveloped eyes and bent body axis. At 200 pg approximately 25 % had mild, 15 % moderate, just over 10 % had a severe deformities with 10 % of larvae not surviving to 48 hpf, n = 100 per group.

3.6.2 F_0 genomic DNA sequencing

Extracted genomic DNA samples were PCR amplified using primers flanking the TALEN binding region. PCR products were then checked on an agarose gel. A single band of the expected size was seen in each lane on the electrophoresis gel, indicating specific primer amplification of the region of interest. The gel image shows amplified region of approximately 600 base pairs with no extra bands indicating high specificity of the primer pair.

Samples were purified and sent to Eurofins Genomics for sequencing (Fig. 3.10).

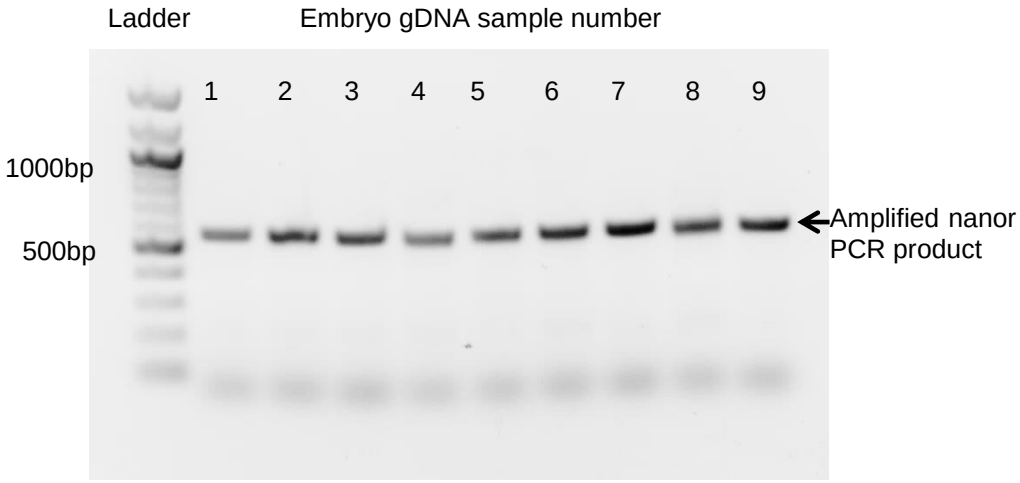

Fig. 3.10: Agarose gel electrophoresis image of PCR amplified genomic DNA samples. Agarose gel image of PCR amplified product of approximately 600 base pairs. All amplified genomic samples were checked on a gel before sending for sequencing to ensure correct and specific amplification of the genomic region of interest (TALEN targeting region). Single clear bands indicate successful amplification.

Genomic DNA was extracted from ten morphologically normal embryos from the 200 pg micro-injected group. Sequencing results showed five of the ten embryos had heterozygous sequence in exon 1 with the remaining larvae (5/10) having a wild-type genomic sequence. When base reads were aligned with the reference sequence large insertions and deletions in the spacer region were indicated (Fig. 3.11), however, this is not an accurate method to find exact positions of bases that have been inserted or deleted due to high noise from double peaks from the point of the first insertion or deletion as well as a high possibility of mosaicism in the embryonic genome following TALEN injection.

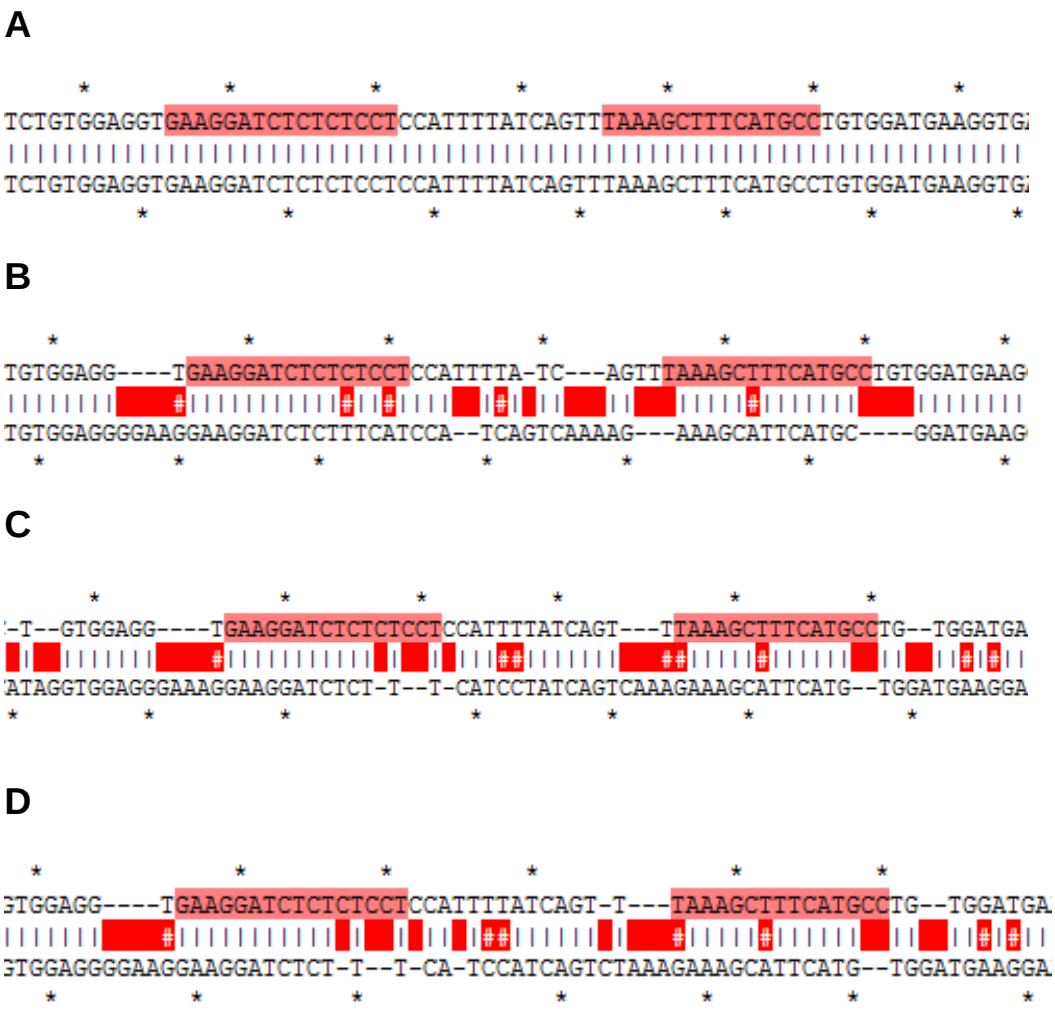

Fig. 3.11: F_0 alignments against wild-type reference sequence. Alignment to a wild-type reference sequence shows insertions/deletions in spacer region and extending from TALEN binding sites. Forward and reverse TALENs are highlighted in pink shading. Red marks mismatched bases. Some sequencing was a 100% match to reference sequence (A), others showed insertions or deletions and mismatched bases, B-D show all mismatches found. 3 mutated alignments were found across the 5 larvae.

If the first sequencing result was accurate only 50% of larvae carried TALEN induced mutations. All micro-injected fish would need to be screened to identify mutants from wild-types. Therefore, these F_0 fish were raised to adulthood and outcrossed with wild-type fish. The resulting F_1 embryos were screened by genotyping and high resolution melt analysis (HRMA) to distinguish wild-type from mutant founders as described in Section 2.2.18. Screening of F_0 genomic DNA samples was also completed by cloning to try

and identify insertions/deletions. However, this method would not identify if mutations had been passed on in the germline. Of 300 micro-injected embryos, 52 survived to adulthood.

Due to the difficulty in sequencing founder fish because of mosiacism (Fig. 3.12 B), it was necessary to clone samples of genomic DNA. Adult fish were anaesthetised and fin-clipped as described in Section 2.2.13. Using *nanor* exon 1 primers, a PCR product flanking the TALEN target region was PCR amplified and purified. These PCR products were then cloned into pGEM®-T easy vector using the Promega pGEM®-T Easy vector system I kit and transformed into *E.coli* for replication before purification and sequencing analysis.

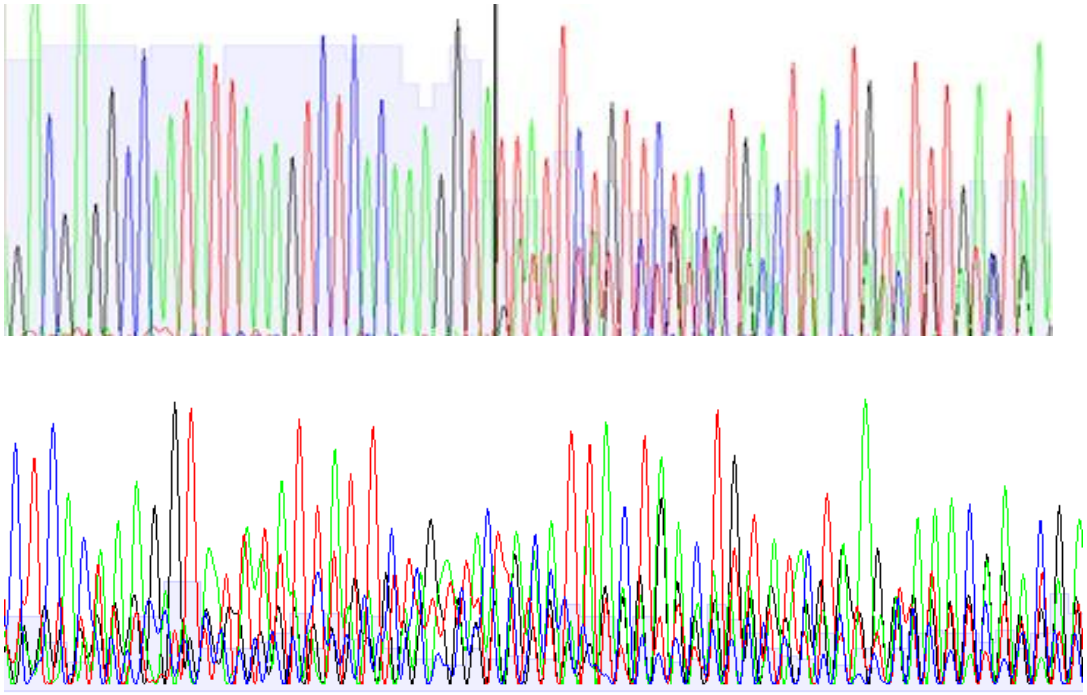

Fig. 3.12: Sequencing results of two F_0 founders. (A) Sequence begins with single peaks representing a homozygous read. When insertions/deletions are reached the sequence from that point on has double peaks representing a heterozygous mutant. (B) Difficulty in sequencing was due to mosiacism in some embryos resulting in multiple peaks in every base read which show a number of different genomic sequences in the sample. Cloning was used to overcome this problem.

Ten clones from each F_0 fish were picked and sequenced. Results from sequencing were disappointing and did not detect any insertions or deletions in the spacer region as expected. Instead a number of SNP's were found in the spacer region and TALEN binding sites as well as upstream or downstream in exon 1 of the gene (Fig. 3.13).

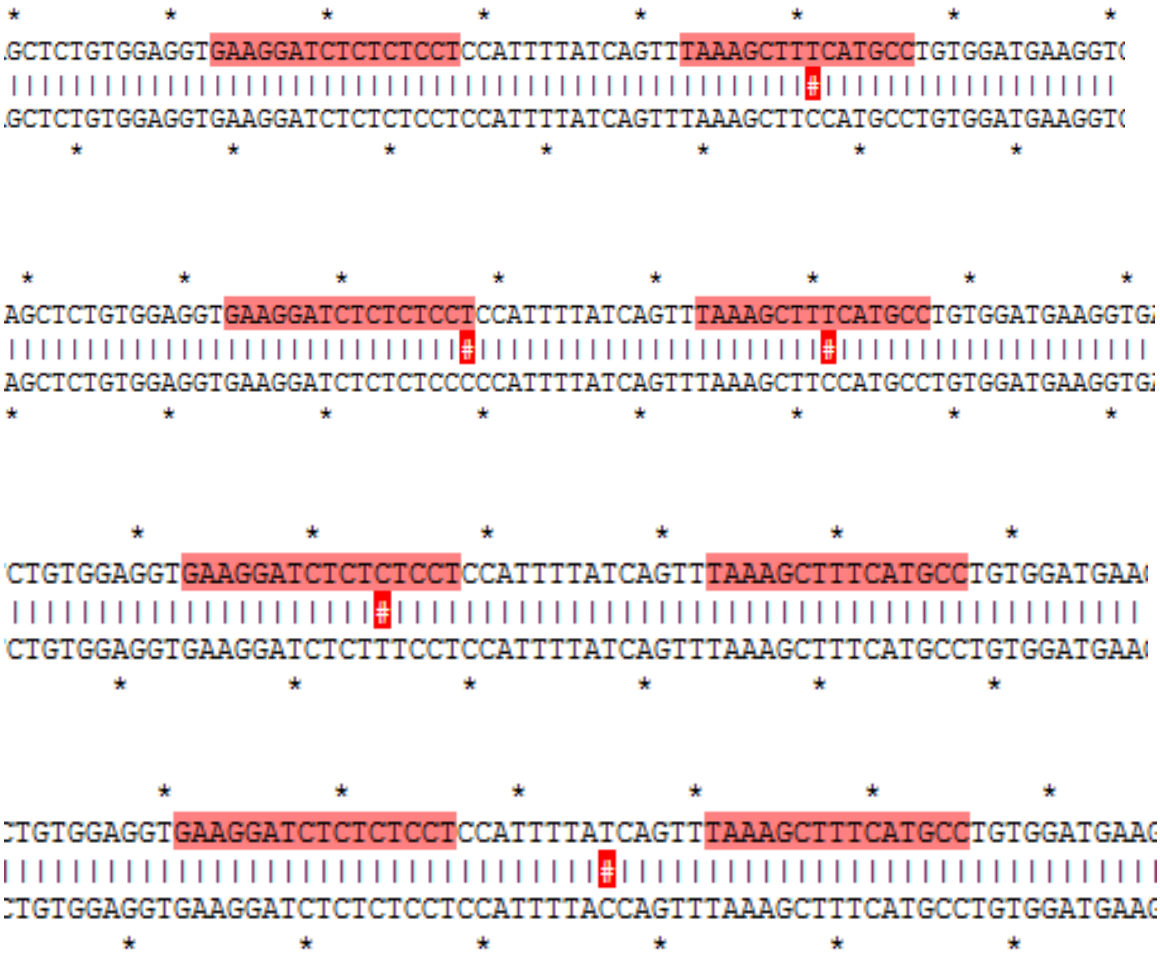

Fig. 3.13: Sequenced F_0 clones show SNPs in spacer and TALEN binding regions. Sequencing of clones showed SNPs present in spacer region and outside of this region when aligned with the wild-type reference sequence causing amino acid changes. TALEN binding sites are marked in pink. SNPs are highlighted in red. Spacer region is between the forward and reverse TALEN binding sites.

As well as identification of SNPs in the spacer region 4 base pair insertion was detected in F_0 clones (Fig. 3.14). This was detected in many founders and always on the exon/intron boundary, thus, this is the likely cause of the high background. Before TALEN design and micro-injection, three males and

three females from the tank to be injected were sequenced, none had this insertion. Following identification of this 4 base pair insertion, 15 more wild-type fish were picked from the adult wild-type families and this insertion was found in some of the wild-type genomes, therefore, I identified this insertion as naturally occurring and not induced by the TALEN.

In addition to the insertion, SNPs were detected in both F_0 clones and F_1 embryos that were not found in wild-type families. It is possible that these point mutations occurred as a result of TALEN micro-injection.

The disadvantage of using this cloning method of sequencing is it was not possible to identify germline mutations. Also, there was a possibility that sequenced clones failed to show all mutations that were present in fish. Therefore, further sequencing was completed on the F_1 generation where all fish would be wild-type or heterozygous mutants. In this generation the challenges faced by mosiacism in the F_0 founders would not pose a problem.

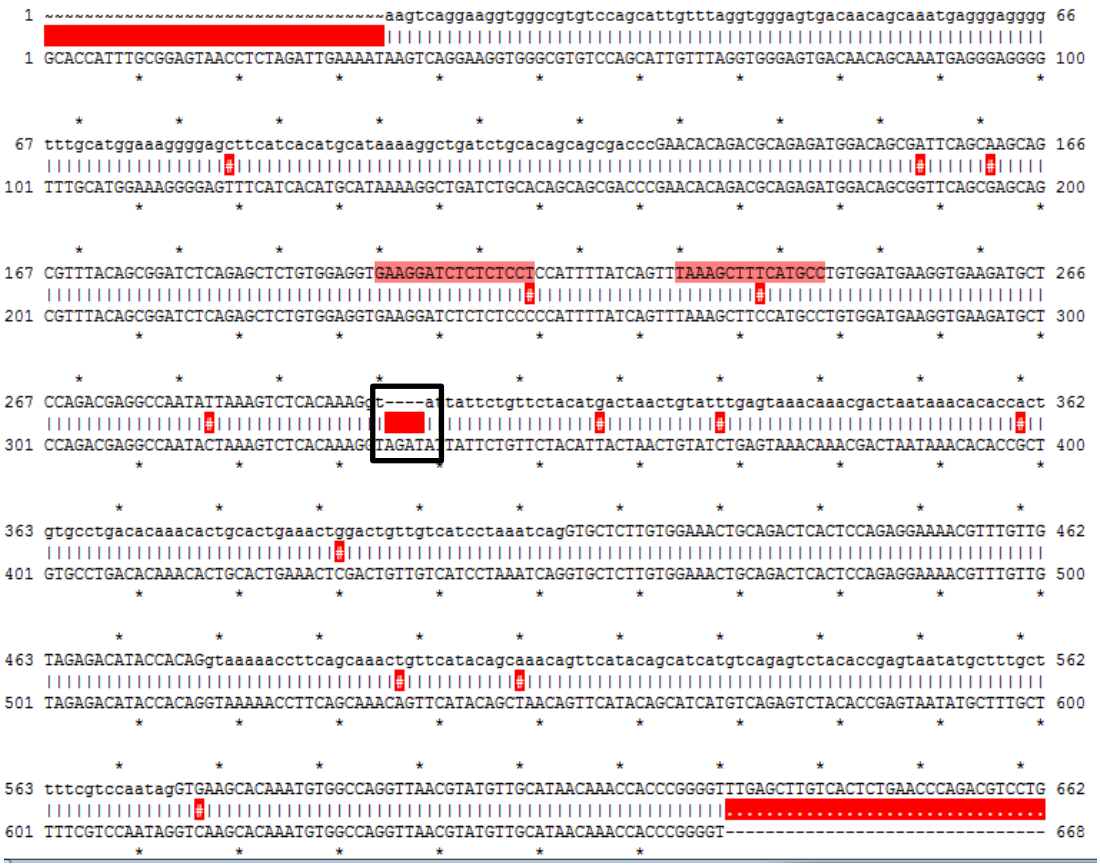

3.14: Sequenced F_0 clones show SNPs outside of the target region and a 4 base pair insertion. Sequencing of clones showed many SNPs present outside of the spacer region when aligned with wild-type reference sequence as well as a four base pair insertion at the beginning of the intron. TALEN binding sites are marked in pink. SNPs are highlighted in red. Insertion is marked by a black box. Exons are in capital letters and introns in lower case.

3.6.3 High Resolution Melt Analysis

HRMA was used to screen adult fish and make sure mutations were being passed on in the germline. Ten genomic DNA samples from outcrossed F_0 fish (10 F_1 embryos) were screened by melt curve analysis. Any larva that had an altered sequence from wild-type reference was flagged and the remaining F_1 embryos from this family kept as heterozygous mutants and raised to adulthood when individual wild-type and mutant fish within the family would be screened.

A primer pair with a very short amplicon (70 base pairs) flanking the region of interest, where the forward and reverse arm of the TALEN bound, was designed. The reverse primer was upstream of the 4 base pair insertion that

had been found in F_0 clones. This ensured no false positives would occur as a result of this naturally occurring insertion. Any induced mutations within this region would alter the G/C content of the amplicon, altering the melting temperature. Fig. 3.15 shows a representative image of one of the HRMA plates; five wild-type reference larvae were used on each plate with ten F_1 larvae per F_0 founder parent. Each line on the melt curve graphs represents one genomic DNA sequence or one F_1 larva. From this plate, it is clear that three larvae have been flagged as mutants with two different mutant genotypes (red and green lines), blue lines represent wild-type genomic DNA sequences. Parents of these three larvae were kept as mutant founders and their offspring raised as heterozygous mutant families. In total, 18 of 52 F_0 founders were flagged as mutants, therefore, these were outcrossed and 18 F_1 heterozygous families were raised to adulthood.

High Resolution Melt Analysis curve from F_1 embryos

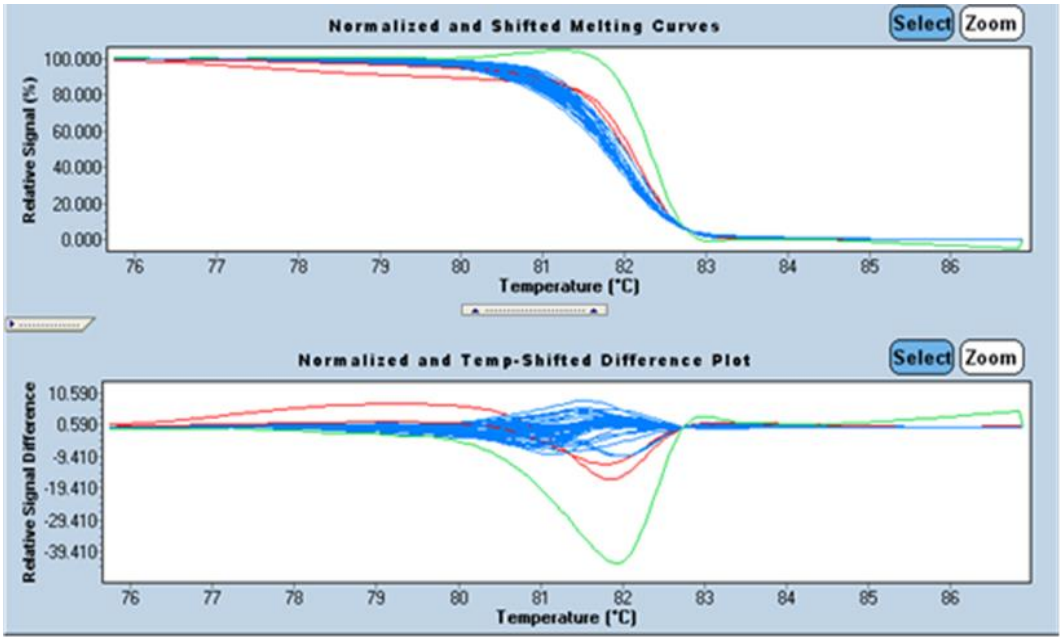

Fig. 3.15: High Resolution Melt Analysis curve from F_1 embryo genomic DNA at 1 dpf. The top graph shows the melting curve and the bottom graph is the temperature difference plot. Each line of the melt curve represents one larvae with genomic DNA extracted at 1 dpf. 10 larvae from each clutch were analysed; any parents that produced larvae flagged as mutants were kept as a TALEN F_0 founder and the remaining larvae raised to adulthood to generate the F_1 lineage. Blue lines represent wild-type sequences with reference wild-type run on the plate. Red lines represent two sibling larvae with altered sequence and green line represents one larva with a different mutated sequence. All families with only wild-type larvae were not raised to adulthood. Siblings of identified mutants were raised to adults.

Following confirmation of a mutated sequence in the targeted region by HRMA, embryos were raised to adults for generation of a mutant line. During all TALEN screening F_0, F_1 and F_2 generations were morphologically scored and compared to wild-type controls.

3.7 F_1 TALEN generation

3.7.1 F_1 TALEN morphology

Similar defects were recorded in F_1 larvae as observed in F_0 micro-injected embryos. Most defects were seen in anterior structures with more severe phenotypes involving bent body axis (Fig. 3.16). F_1 embryos whose parents had been identified as mutants with germline mutations were raised to adulthood, however, a high mortality was recorded and attempts to raise some families were unsuccessful with all remaining fish in some families having only wild-type genomic sequences.

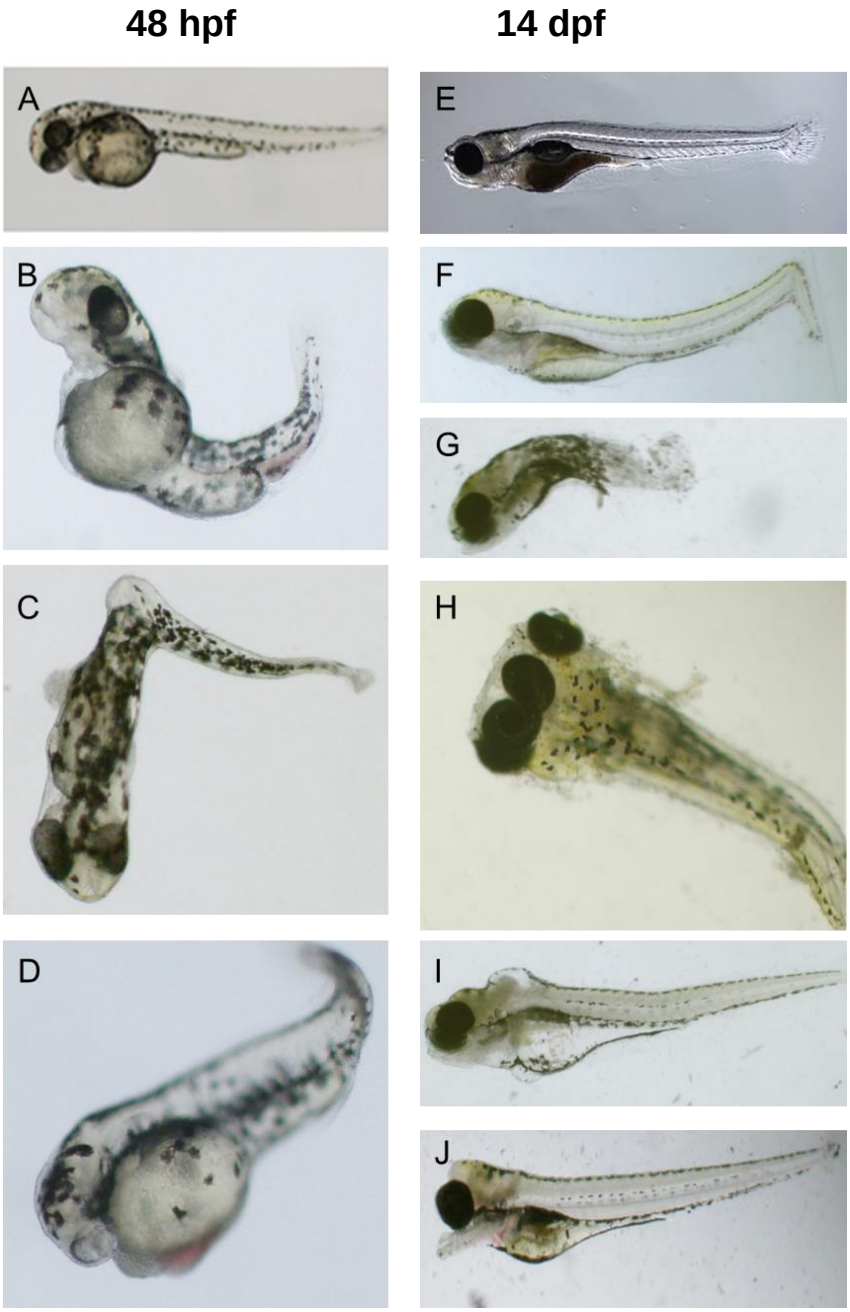

Fig. 3.16: F_1 mutant larval phenotype at 48 hpf and 14 dpf. When compared to 48 hpf control (A), mutant heterozygous larvae showed deformities such as (B) missing jaw and underdeveloped brain as well as poor circulation with bent body axis, (C) kinked tails with incorrect or no organ formation and (D) missing eyes and head with poor circulation. At 14 dpf when compared to control (E), some larvae had failed to develop a swim bladder and had kinked tails (F), gross morphological deformities (G), more than two eyes (H), incorrect heart and brain formation with oedema (I), and missing forebrains (J).

Mortality of F_1 larvae was recorded up to 48 hpf (Table 3.3). At 24 hpf 50% of F_1 embryos had died. This increased to 62% by 48 hpf with only 22% of larvae with a normal phenotype and the remaining 16% being deformed (Fig. 3.17). Defects observed were severe, involving eye and brain formation and included blood pooling and bent body axes.

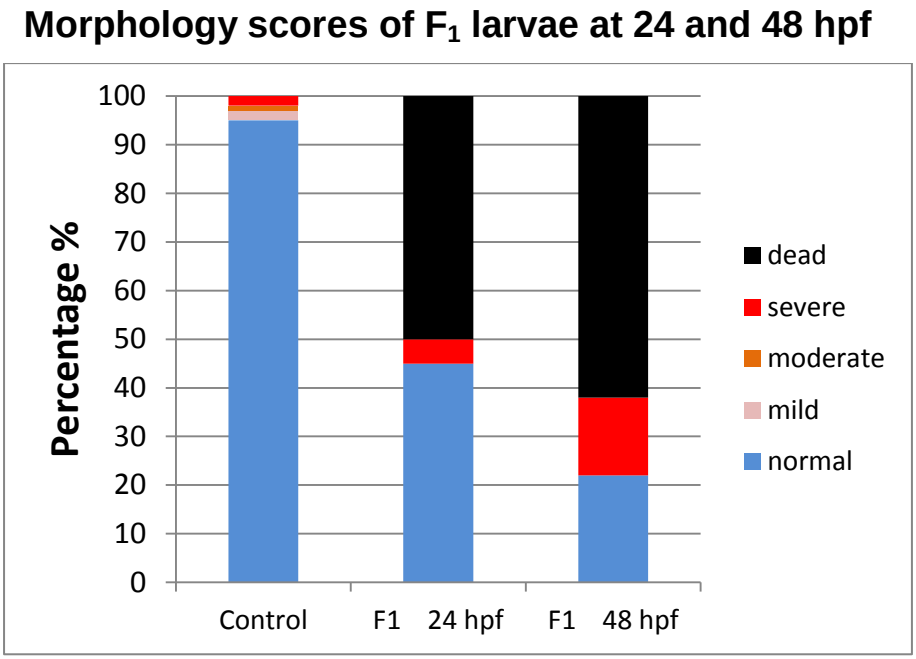

Fig. 3.17: Morphology scores of F_1 outcrossed larvae. F_1 larvae at 24 hpf had 50% death at time of scores, this increased to 60% by 48 hpf with only 20% of normal developing larvae and the final 20% with a severe phenotype, n = 100 per group.

3.7.2 F_1 TALEN sequencing

Embryos from 10 of these founders survived to adulthood (Table 3.4, n = 217 adults). F_1 fish that survived to adulthood were fin-clipped and genomic sequence was obtained.

Table 3.3: Survival to adulthood in the F_1 generation.

Tank number	Total embryo number	Total number at 6 hpf	Total number at 24 hpf	Total number at 48 hpf	Number surviving to adulthood
2	54	42	32	32	0
3	150	132	131	128	0
6	150	150	145	145	0
15	100	69	69	69	0
17	160	160	150	150	0
18	57	46	44	44	26
21	200	193	155	106	28
26	36	34	26	20	16
28	180	177	162	160	18
29	180	155	148	145	20
34	155	137	84	64	31
40	70	70	69	69	20
41	19	17	17	15	12
42	150	132	127	122	19
44	100	98	93	93	27
47	57	51	40	40	0
49	69	57	53	51	0
50	101	96	94	93	0

All fish that survived to adulthood from five of these families were wild-type and one family had a point mutation in the spacer region that resulted in no amino acid change. The remaining four families had mutations and amino acid changes in the spacer region. These mutations were all SNPs with no insertions or deletions (Fig. 3.18, Table 3.4).

Table 3.4: Mutant adult F_1 fish

Tank number	genotype	Number of adult fish	Number of mutants
18	Wild-type	26	0
21	Mutant	28	13
26	Mutant	16	8
28	Wild-type	18	0
29	Wild-type	20	0
34	Mutant	31	14
40	Wild-type	20	0
41	Mutant	12	5
42	Wild-type	19	0
44	Wild-type	27	0

A

```
CTGTGGAGGTGAAGGATCTCTCTCCTCCATTTTATCAGTTTAAAGCTTTCATGCCTGTGGATGAAG
                                  #
CTGTGGAGGTGAAGGATCTCTCTCCTCCATTCTATCAGTTTAAAGCTTTCATGCCTGTGGATGAAG
```

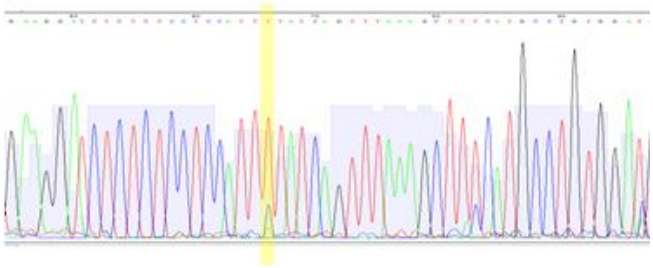

B

```
CTGTGGAGGTGAAGGATCTCTCTCCTCCATTTTATCAGTTTAAAGCTTTCATGCCTGTGGATGAAG
                                  #
CTGTGGAGGTGAAGGATCTCTCTCCTCCATTTTATCAGTATAAAGCTTTCATGCCTGTGGATGAAG
```

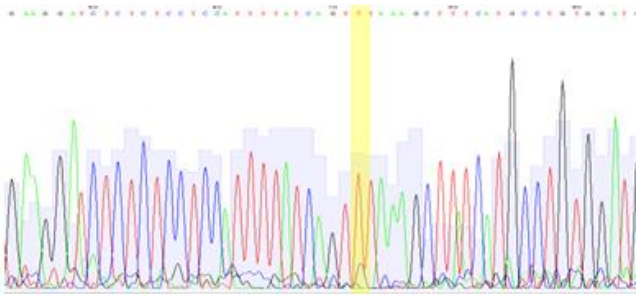

C

```
CTGTGGAGGTGAAGGATCTCTCTCCTCCATTTTATCAGTTTAAAGCTTTCATGCCTGTGGATGAAG
                                  #       ##
CTGTGGAGGTGAAGGATCTCTCTCCTCCATTCTATCAGTACAAAGCTTTCATGCCTGTGGATGAAG
```

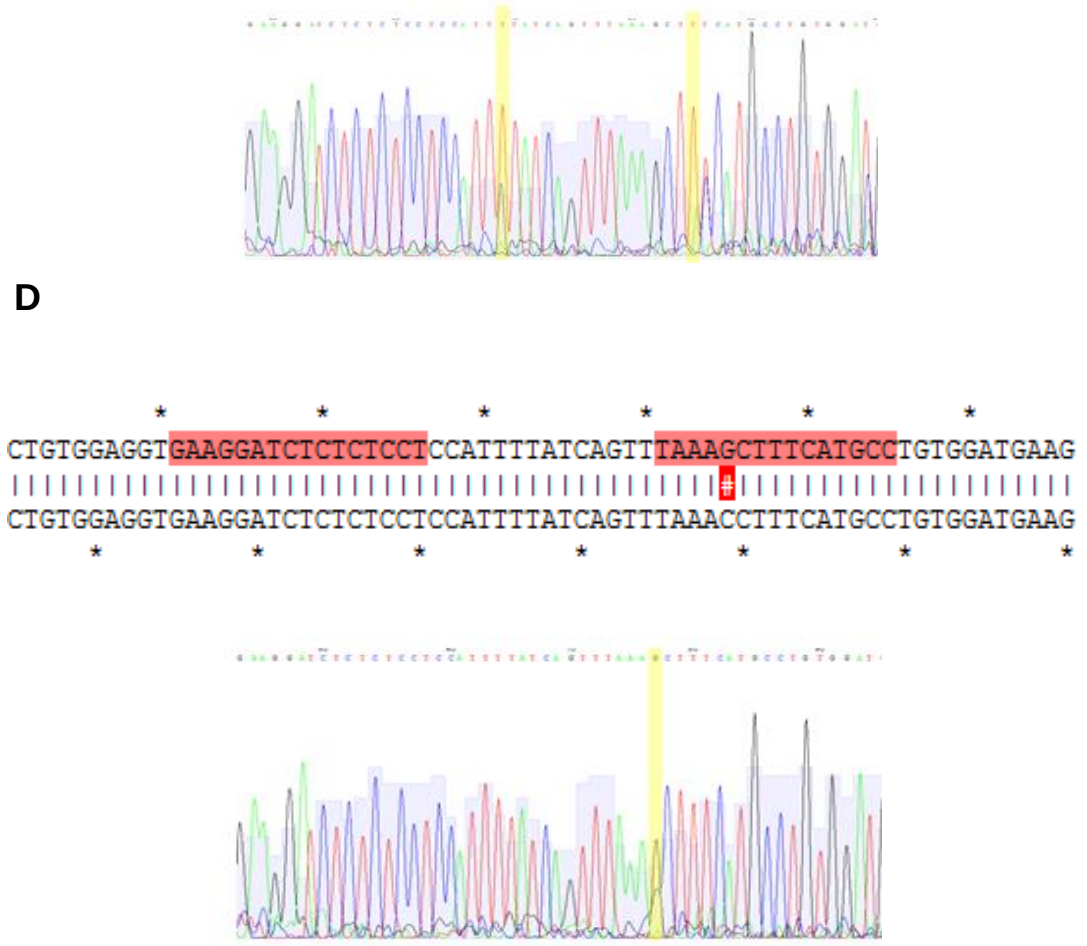

Fig. 3.18: SNPs found in F_1 adult genotyping. Single peaks show homozygous sequence regions with an occasional double peak marked in yellow representing point mutations. (A) family 21; (B) family 26; (C) family 34; (D) family 41. TALEN binding sites are marked in pink. SNPs are highlighted in red. Any fish without these SNPs were euthanised.

Predict Protein was used to predict the effect of these SNPs. These SNPs were predicted to cause severe effects on protein function indicating that protein function may be severely affected (Table 3.5).

Table 3.5: Prediction of effects of SNPS in four F_1 families using Predict Protein software.

Family number	Amino acid Change	Position	Predicted Severity	Number of fish
21	Phenylalanine - Serine	aa 26	Severe	10 male
	Tyrosine – Histidine	aa 32	Severe	4 female
26	Phenylalanine - Serine	aa 26	Severe	2 male
	Phenylalanine – Isoleucine	aa 29	Moderate	2 female
34	Phenylalanine – Tyrosine	aa 32	Severe	3 male 2 female
41	Alanine – Proline	aa 31	Severe	3 female 1 male

3.7.3 Nanor mRNA expression in F_1 heterozygous embryos

RNA was extracted from wild-type and F_1 embryos of a mixed population of wild-type (+/+), heterozygous mutants (+/-) and homozygous mutants (-/-) at sphere, shield, 24 hpf, 48 hpf and 72 hpf followed by *nanor* mRNA quantification by qPCR (Fig. 3.19). When compared to the same developmental stage in wild-type controls results show significant decreases in *nanor* mRNA expression at sphere, shield and 48 hpf stages. No significant differences were found at 24 hpf or 72 hpf. Data was analysed by One way ANOVA ($F_{(10, 33)} = 5.887$, $P < 0.0001$; Dunnett's post hoc test $P < 0.05$ sphere F_1 sphere, shield F_1 and 48 hpf F_1 vs. comparable wild-type control). This result gave further confidence that the mutants were altering *nanor* expression in the F_1 generation.

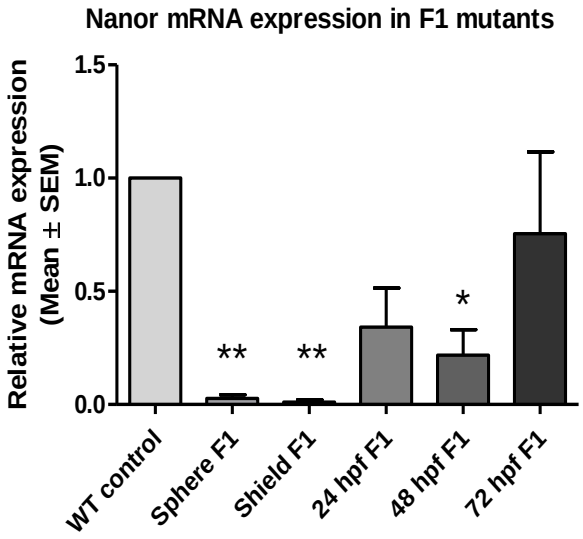

Fig. 3.19: *Nanor* mRNA expression during early development in wild-type and F_1 mutant embryos and larvae. *Nanor* was quantified at 128-cell, sphere, shield, 24 hpf, 48 hpf and 72 hpf in wild-type and TALEN F_1 embryos and larvae. When compared to wild-type larvae *nanor* mRNA expression was significantly decreased in F_1 mutant embryos at sphere and shield stage. Data are represented as mean ± SEM, * $P < 0.05$, ** $P < 0.01$, $n = 4$.

3.8 F_2 TALEN generation and mortality

To raise mutants for investigation of downstream genes of *nanor,* the four remaining F_1 heterozygote adult families with male and female siblings were incrossed. Mortality of F_2 embryos was scored; by 24 hpf 30% of embryos died and 60% were developing normally. By 48 hpf a severe phenotype was noted; 45% of larvae had died and 25% had severe deformities with only 20% classed as normal by 48 hpf (Fig. 3.20).

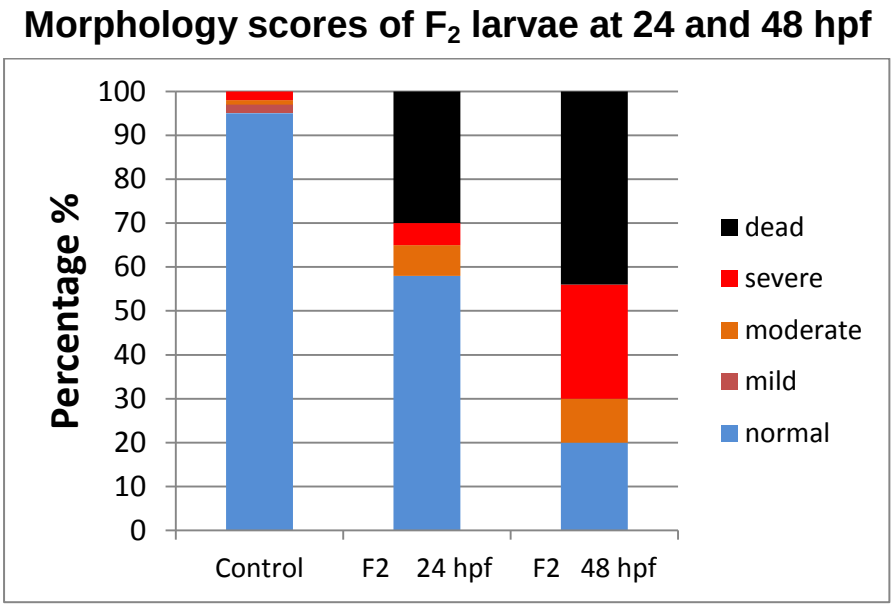

Fig. 3.20: F_2 morphology scores at 24 hpf and 48 hpf. Death rate of F_2 embryos was 30% by 24 hpf and over 40 % by 48 hpf. A severe phenotype was seen in most of the remaining F_2 embryos at 48 hpf, n = 100 embryos per group.

3.8.1 F_2 TALEN mortality

Incrosses were scored daily and deaths were recorded during the first two weeks of development. All TALEN families, with the exception of tank 34 which matched wild-type control survival, showed high mortality ranging from 30% - 60% by 48 hpf. Highest mortality was recorded in family 21; by 48 hpf 55 % of these embryos had died. Tank 26 and tank 41 showed 30% mortality by 48 hpf (Fig. 3.21).

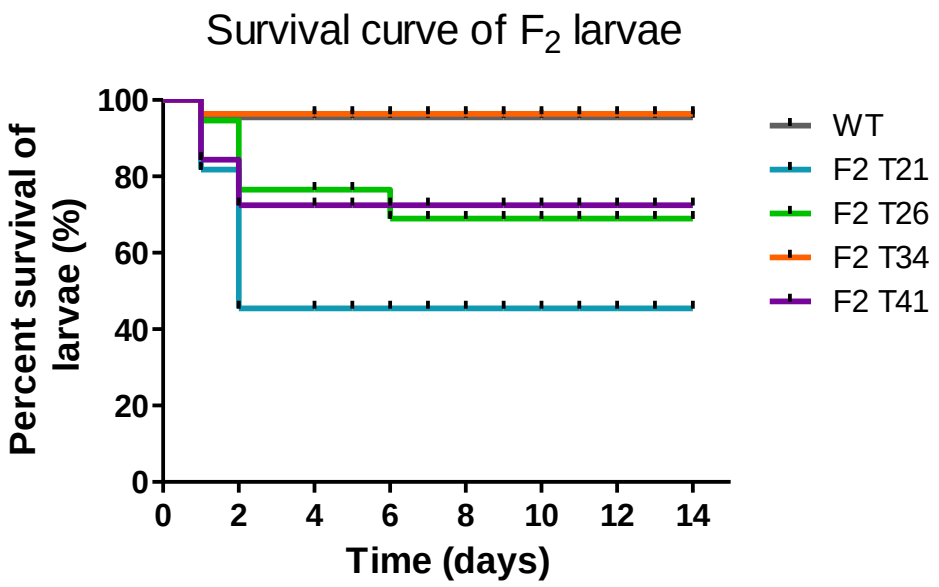

Fig. 3.21: Survival curve of F_2 homozygous larvae. The four heterozygous mutant TALEN families (T21, T26, T34, T41) were incrossed and embryos collected in an attempt to raise to adulthood. Each day larval deaths were recorded and graphed. T34 were the only family to have death numbers to match wild-type controls. The remaining families showed high mortality during the first 48 hours of development. T26 and T41 showed similar mortality with a quarter of all larvae dead within the first 48 hours of development. T21 showed the most severe mortality with just over half of all embryos dead within the first 48 hours.

3.8.2 F_2 TALEN sequencing

Twenty-six F_2 larvae from F_1 sibling incrosses were collected and genomic sequence was obtained (6-7 embryos from each F_1 family incross). Five out of 26 were homozygous carriers of SNPs, 3 were wild-type embryos and 18 were heterozygous carriers of SNPs. Many SNPs were found throughout exon 1 outside the spacer region as shown in Fig. 3.22.

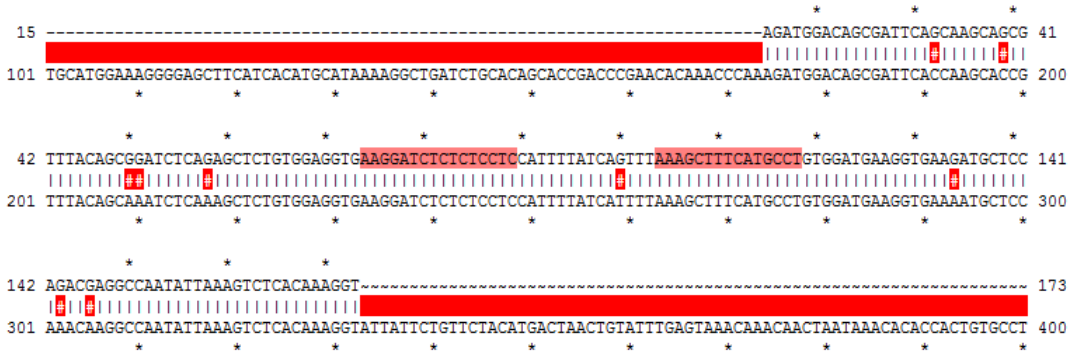

Fig. 3.22: An example of SNPs found in an F2 embryo. Alignment to reference sequence shows several SNPs in exon 1 of the *nanor* sequence. TALEN binding sites are marked in pink. SNPs are highlighted in red.

Remaining fish that did not die at larval stages were found to be homozygous wild-type fish and could not be used for further experimentation.

Due to mortality of many F_0, F_1 and F_2 larvae it is likely that the TALEN mutants with any indels present did not survive past embryo stages and mutations could not be passed to further generations.

3.9 Homozygous mutant generation summary

Following micro-injection of 300 embryos with 200 pg of TALEN 2, 52 F_0 founders were raised to adulthood. These were outcrossed with wild-type fish and genotyping of offspring identified 18 founders with mutations in the germline.

Of the 18 mutant adult founder fish, 8 produced non-viable offspring. The other 10 F_0 fish were outcrossed and their offspring raised to adults to generate F_1 heterozygous adults. Of these 10 F_1 families, five did not have any mutations in the spacer region and were considered to have off target mutations and one family had a point mutation in the spacer region but no amino acid changes. The remaining four families were incrossed but no mutants survived to adulthood. None of the SNPs in the spacer region were found to cause a premature stop codon in TALEN embryos. Attempts to raise mutants were not possible due to early mortality in these embryos. TALEN generation is summarised in Fig. 3.23.

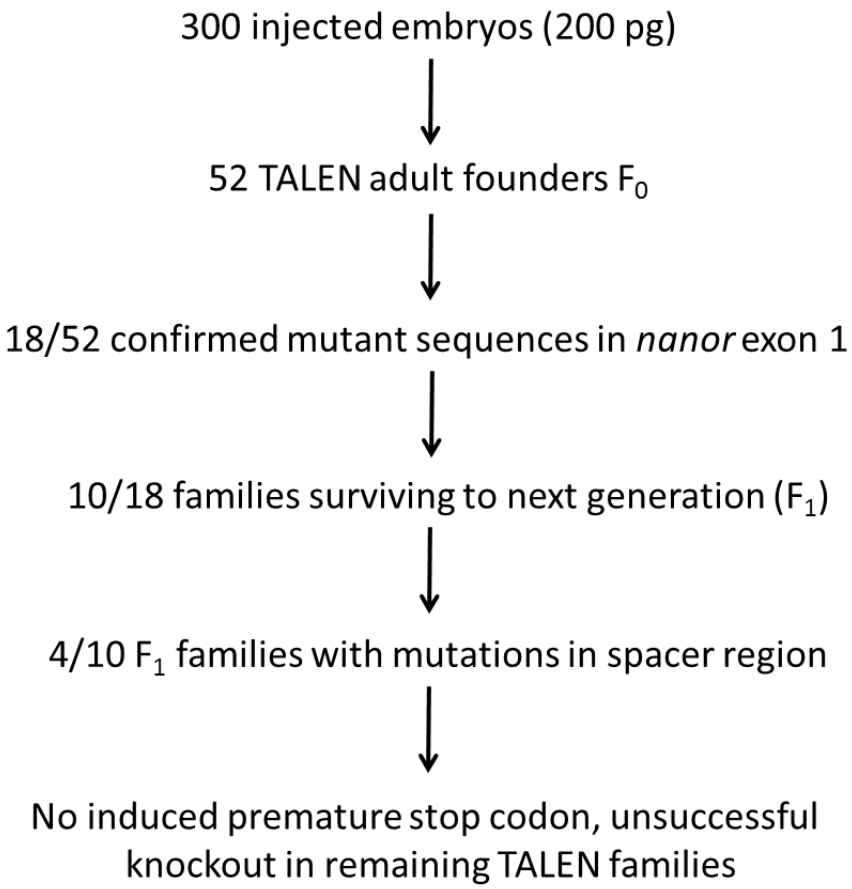

Fig. 3.23: Workflow of TALEN family generation.

3.10 Discussion

3.10.1 *Nanor* Bioinformatics

Investigation of *nanor* sequence in online genomic databases found P2X7-like purinoreceptor as the closest match by sequence homology. Kim et al., 2001 discovered 11 interacting proteins with human P2X7 receptor which enhance receptor function such as heat shock proteins, pannexins, laminin α3, integrin β2 and supervillin. Nanor and its paralogues were aligned to all known accessory proteins with no clear sequence homology to any of these. Therefore, it is unlikely that Nanor is an ortholog to any of the known human accessory proteins. From all bioinformatics and sequence homology investigations the only match to a characterised protein was partial sequence identity to a P2X7-like protein. *Nanor* may be an undiscovered paralog of the

P2X7–like protein in zebrafish. However sequence identity was low when compared to the human P2X7 protein sequence (27%).

3.10.2 *Nanor* mRNA expression

Previous investigations in the laboratory by Dr. Bree used semi-quantitative methods to show low expression of *nanor* at the 128 cell stage and upregulation at sphere stage. Dr. O' Boyle also reported high expression in dorsal forerunner cells which indicated an early function of *nanor* during embryogenesis. I quantified mRNA expression of *nanor* and *nanor b* by qPCR from 128-cell stage to 5 dpf which showed highest expression during sphere and shield stage and a second wave of *nanor b* expression up to 5 dpf. My in situ hybridisation results are also in agreement with Bree et al., 2005 and extend to 72 hpf which found high, ubiquitous expression during embryo stages which becomes restricted to anterior structures at larval stages with low expression by 72 hpf.

These reports and further studies by Lee et al. (2013); Perez-Camps et al. (2016) have established *nanor* as an early zygotic gene activated soon after the mid-blastula transition. My qPCR results may represent a later function of *nanor b* in larval development. Together these findings suggest an important function of *nanor* and *nanor b* during early development.

3.10.3 Nanor TALEN generation

Previous studies by Dr. O' Boyle knocked down *nanor* expression by morpholino injection. However, effects of a morpholino are transient, therefore, an effort was made to generate a stable, *nanor* knockout mutant line using TALEN technology. The morpholino studies had shown that *nanor* knockdown disrupted left/right signalling in the lateral plate mesoderm and neural patterning. Eye development and reduced neural structures were prominent morphological defects that were recorded in micro-injected larvae. Similar morphological defects were seen in TALEN-injected F_0 and subsequent F_1 and F_2 embryos and larvae, mainly involving anterior structures of the larvae.

The rationale for making a loss-of-function mutant line using TALENs derived from the ability of TALEN technology to generate a stable line that could be

passed on to subsequent generations. Although morpholinos had provided links to nanor function in left/right asymmetry development, there is also a risk of variation in responses between embryos as well as transient effects of morphilino injection and the risk of damage due to injection. The use of TALENs eliminated all of the disadvantages of morpholino use. All generations would inherit the same mutations with no risk of variation between siblings or damage from mechanical stress. Difficulties encountered during TALEN generation were due to high mortality throughout all generations of TALEN fish, therefore I was unable to generate a *nanor* knockout. As I did not find any insertions or deletions in the target region of F_1 or F_2 adult fish during gene sequencing, it is likely that any larvae that had these mutations died at early stages and as a result, mutations could not be passed on in the germline. As well as this the presence of a naturally occurring four-base pair insertion in the intron was responsible for misleading indications of a TALEN induced insertion/deletion in surviving mutant larvae. High mortality across generations and death of all mutant larvae further establishes *nanor* as an important gene during early development and loss of gene expression results in early embryonic lethality.

Point mutations in the spacer region in remaining heterozygous F_1 fish were predicted to have moderate or severe effects on Nanor protein function. Although these fish developed normally, attempts to pass on these mutations to the next generation resulted in embryonic lethality and it was not possible to raise them to adulthood. Therefore, maintenance of a heterozygous line was not possible in this study. While these identified SNP's are likely to account for high mortality seen across TALEN generations the possibility of off target effects causing mutations at other genomic locations should also be considered. This may also account for mortality in the F_2 mutants, however to confirm this further investigations using whole genome sequencing or next generation sequencing would be necessary in founders.

Difficulty in optimising TALEN generation came from many false positives in sequencing from a naturally occurring four base pair insertion in the intron. Sequencing results showed a heterozygous read and this was correctly attributed to an insertion or deletion. However, further investigation revealed

that this was naturally occurring. This occurred despite having sequenced the families prior to TALEN injection to avoid naturally occurring mutations in the region of interest. Sequencing of more wild-type fish identified this insertion in the genome. Therefore, sequencing of six fish proved to be insufficient to ensure detection of all naturally occurring mutations in this case. The mutated sequences flagged by HRMA are likely to be a result of point mutations in the spacer region and TALEN binding sites that were later identified in F_1 fish.

I was unsuccessful in producing a homozygous mutant line due to mortality in the F_2 generation. Although TALENs have a high success rate in generation of homozygous mutant lines some publications have reported TALEN knockout to be embryonic lethal and as a result, unable to generate stable mutant lines (Suzuki et al., 2013; Nakayama et al., 2015). These studies have used TALEN micro-injection similar to a morpholino micro-injection to prevent protein expression in the F_0 generation and embryos were subsequently used for functional studies on the targeted gene. The challenge with this model is due to mosiacism in the embryos. Multiple mutations could be present in one embryo as well as a high possibility that not all embryos will have induced mutations. One study attempted to overcome the challenge of mosiacism in the F_0 generation through injection at the oocyte stage prior to fertilisation followed by in vitro fertilisation. They state that this enabled the TALEN to take effect from an earlier stage to achieve a full knockout in Xenopus embryos (Miyamoto et al., 2015).

Following high mortality in my *nanor* mutant line, I then studied protein localisation and attempted to identify protein interactions at larval stages.

Results Chapter 4: Identification of Nanor Protein-Protein Interactions

4.1 Nanor protein expression in wild-type larvae

Identification of protein interactions is important to identify protein function and behaviour and enable characterisation of protein complexes and pathways. In the study of *nanor* identification of protein interactions would provide detailed information on *nanor* function.

A previous laboratory member, Melissa Walsh, studied protein expression by western blot from shield to 72 hpf in zebrafish larvae and using densitometric analysis reported similar expression from shield stage to 24 hpf which was then upregulated at 72 hpf (unpublished). However, protein localisation had never been visualised.

The aim of this chapter was to study protein expression and localisation and to identify interacting proteins, in an attempt to gain information about Nanor function.

4.1.1 Nanor protein localisation in wild-type larvae

Immunohistochemistry was used to visualise Nanor protein in the early embryo and larvae. As there were no available antibodies to study Nanor protein, a custom antiserum was raised in rabbit using the peptide, RMRQKLPEGNEN by Sigma-Genosys. The antibody was validated by Dr. O' Boyle and Melissa Walsh who reported that the antibody recognised both Nanor and Nanor b (unpublished). This antibody detected a protein of a single band (27kD) on western blot and I then visualised protein localisation by immunohistochemistry.

At sphere stage the protein was ubiquitously expressed and cytosolically localised (Fig. 4.1 A). By shield stage, expression was less uniform; immunohistochemical images show expression in all cells but with a higher expression in cells at the dorsal side during shield stage (Fig. 4.1 B, C). In cells with higher expression, the protein was seen with cytosolic localisation (Fig. 4.1 E). Expression in all other cells appeared closer to the cell

membrane. By 24 hpf protein expression can be clearly seen in anterior structures and in the vasculature around the heart with some expression in distal cells of the tail (Fig. 4.1 D).

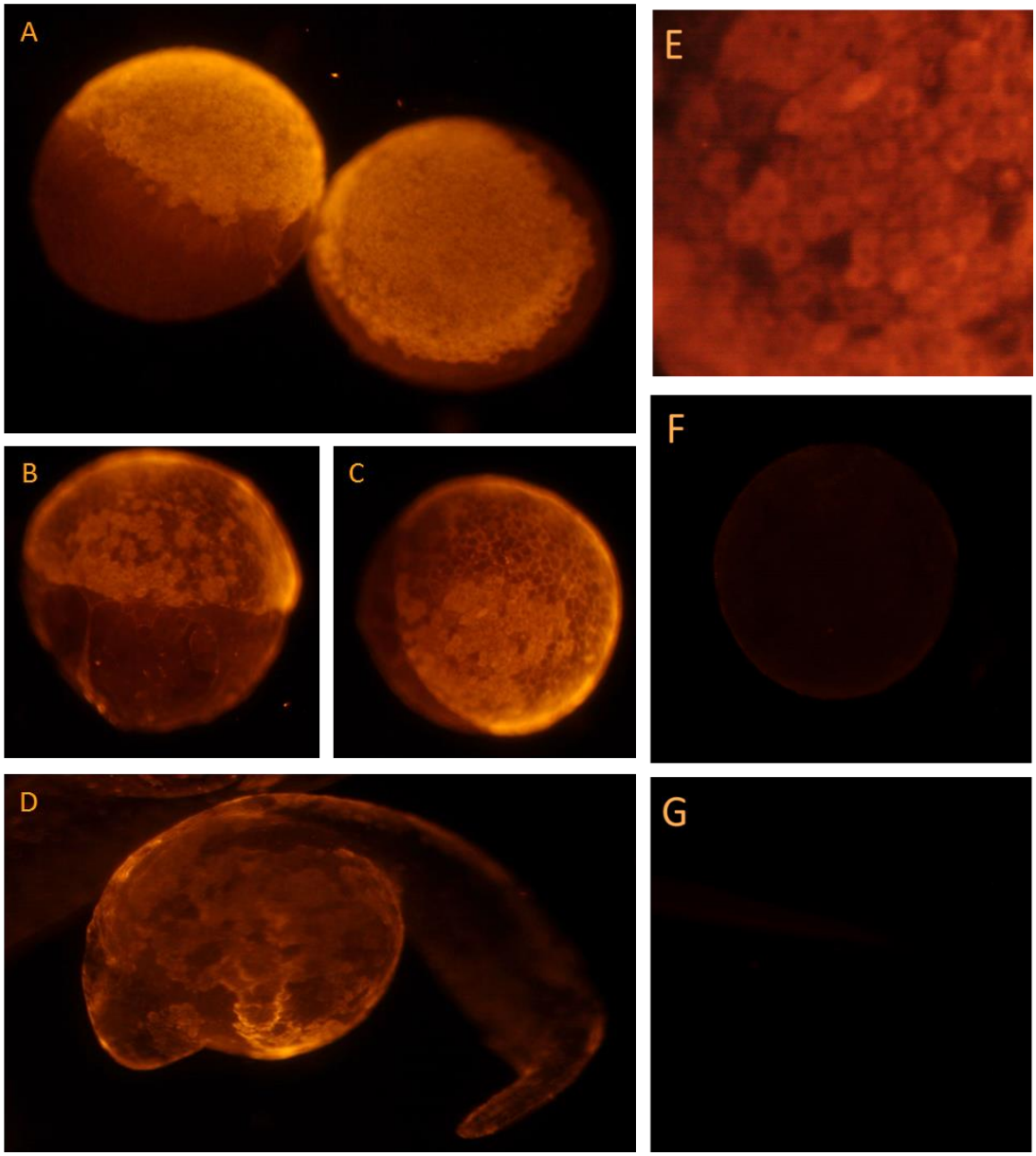

Fig. 4.1: Immunohistochemical images of whole mount Nanor expression in early development. Sphere (A, lateral, dorsal) and shield (B, lateral, C dorsal) stages showing cytosolic localisation of Nanor protein. Ubiquitous expression of Nanor protein is seen during sphere stage; by shield stage expression is seen in all cells with a cytosolic localisation in the cells at the dorsal side of the shield (E, with arrow to mark cytosolic localisation). At 24 hpf staining is seen in the vasculature of the heart and in anterior structures and distal ends of the developing tail (D, lateral). F Minus primary, G Minus secondary control images.

Confocal microscopy was then used to give a more detailed image of protein localisation. Tissue from older embryos and larvae (24-120 hpf) was sectioned at 20 micrometre thickness in a rostral to caudal direction prior to staining. Again at sphere stage, protein expression seems to be cytosolically localised (Fig. 4.2 A). From 24-120 hpf expression is found in all structures and localised in the cytosol; throughout the layers of the eye including the eye lens, the brain and extending caudally through the spinal column (Fig. 4.2 D-F). DAPI nuclear stain confirmed cytosolic expression of Nanor protein.

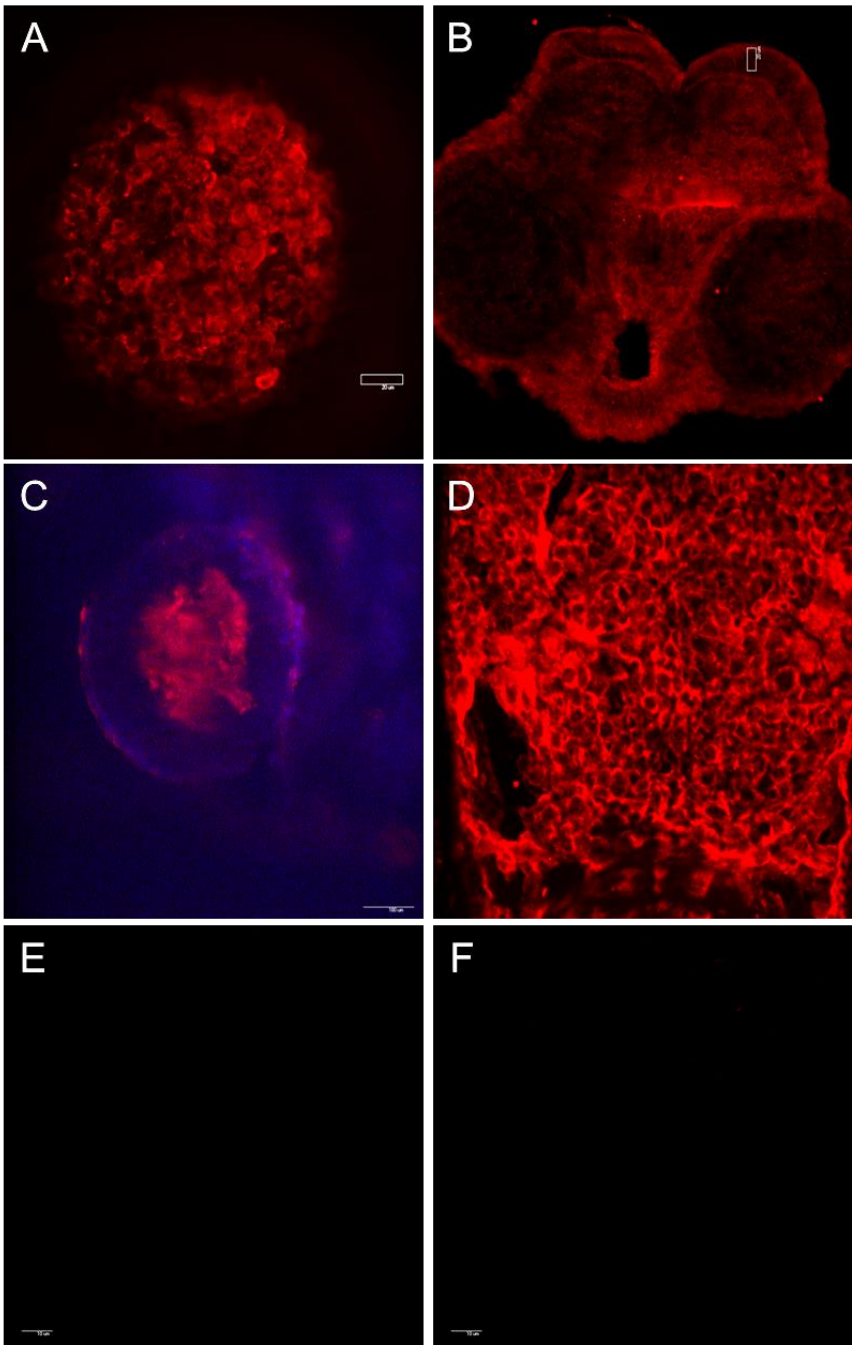

Fig. 4.2: Nanor protein localisation from sphere to 5 dpf by confocal microscopy. (A, animal pole) During sphere stage protein is ubiquitously expressed and cytosolically localised. (B, rostral) 1 dpf (C, lateral) eye lens (D, rostral) E, Minus primary, F Minus secondary control images. Scale bar 100 µM.

4.1.2 Nanor protein complex immunoprecipitation

Co-immunoprecipitation (Co-IP) followed by mass spectrometry was used to identify proteins that interact with Nanor in an effort to better understand protein function. Before Co-IP experiments began, a western blot in non-reducing conditions was run (Section 2.2.23) to identify possible Nanor protein complexes (Fig. 4.3). As a control, one lane of sphere stage protein under reducing conditions was run alongside the same protein sample under non-reducing conditions. Shield stage protein was also run on the gel as these two stages are when *nanor* mRNA expression is at its highest. The control lane showed a single immunoreactive band. Non-reducing lanes of sphere and shield stage showed a number of immunoreactive bands with different patterns at different stages possibly representing changing protein interactions as development progresses. These extra bands of higher molecular weight represent protein complexes.

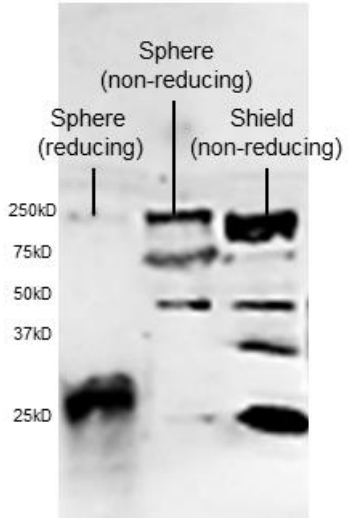

Fig. 4.3: Immunoreactive bands of Nanor western blot in reducing and non-reducing conditions. Samples at sphere and shield stage were run under non-reducing conditions (15% SDS-PAGE gel). As a control, a protein sample at sphere stage under reducing conditions was run. Reducing conditions gave a strong immunoreactive band at approximately 27 kD. The same protein sample under non-reducing conditions showed three higher molecular weight bands at 50, 75 and 250 kD. At shield stage under non-reducing conditions immunoreactive bands at 25, 35, 50, 75 and 200kD were seen.

The Sigma-Genosys Nanor antiserum was not purified, therefore, it was necessary to purify the serum to reduce the risk of high background in samples. This was achieved by affinity chromatography using the peptide that was originally used to immunise the rabbit for antiserum generation. The peptide was manufactured with the sequence RMRQKLPEGNEN with a cysteine added to the N-terminus to allow coupling to the residue: CRMRQKLPEGNEN. In total, three lots of antibody were purified from antiserum. An SDS-PAGE gel was run with the three purification lots alongside a reference antibody (desmoglein-2) of known concentration (250 µg/ml) to estimate purified anti-nanor antibody concentration (Fig. 4.4). The estimated concentrations from purification 1 and 2 were 50 µg/ml and from purification 3 was 100 µg/ml (Fig. 4.4).

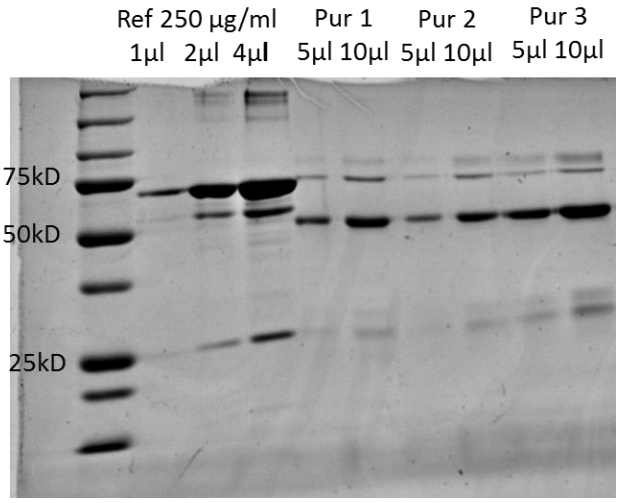

Fig. 4.4: Approximate quantification of antibody purification using a reference antibody (desmoglein-2) at a known concentration. Three purifications of nanor serum were quantified on a 15% SDS-PAGE gel with a known concentration of standard for reference. Purification 3 gave the highest yield. Estimated concentrations are as follows; purification 1: 50 µg/ml purification 2: 50 µg/ml purification 3: 100 µg/ml. IgG heavy chain / Fab fragment (50 kD), Fv fragment (25 kD), rlgG fragment / half IgG (75 kD), Fc fragment (50 kD). Thick band at approx. 65 kD in reference antibody is preservative sodium azide.

Although *nanor* mRNA expression is highest at sphere and shield stage, 96 hpf larvae were used for subsequent Co-IP experiments. The *nanor* paralog

(*nanor b*) is highly expressed at this stage and was previously reported by both Dr. O' Boyle and Melissa Walsh to be recognised by the antibody. This stage was chosen for two reasons; when optimising Co-IP experiments it was essential to have a high yield of protein. If sphere or shield stage were chosen for Co-IP experiments thousands of embryos would be required to achieve the same yield as two-hundred 96 hpf larvae. Secondly, at early stages there is a large protein yolk sac that interferes with western blots and mass spectrometry. Therefore, a de-yolking step is required up to approximately 72 hpf. This clean-up step further reduces the protein yield and using these stages carries an increased risk of yolk sac contamination, 96 hpf were used where a de-yolking step was not necessary.

Following antibody purification, Co-IP experiments were optimised to ensure successful capture of Nanor protein complexes to identify interacting proteins. Protein A/G beads were used for Co-IP and the same peptide that was used to purify the antibody was used for elution (Section 2.2.23). A western blot for Nanor protein was run to assess the properties (solubility, binding capacity, molecular weight) of the protein of interest (Fig. 4.5, Fig. 4.6). On this blot I ran a number of different samples as illustrated graphically in Fig. 4.5 and listed below;

1) Lysate before centrifugation at 14,000 g (soluble and insoluble fractions, whole tissue)

2) Re-suspended pellet following centrifugation at 14,000 g (insoluble material, cell debris)

3) S14,000 (soluble material following centrifugation at 14,000 g)

4) Unbound S14,000 following incubation with protein A/G beads and antibody (to check if all of Nanor protein is binding to the beads)

5) Supernatant from third PBS wash following antibody and protein binding to beads (to check if any protein or antibody is being washed from beads)

6) First eluate from beads following peptide elution (to check if protein is being eluted from beads)

7) Second elution from beads following repeat of peptide elution (to check if a second elution step is necessary)

8) Boiled bead samples after elution (to check if the antibody is remaining on the beads, and if any Nanor protein is being left bound to antibody on the beads)

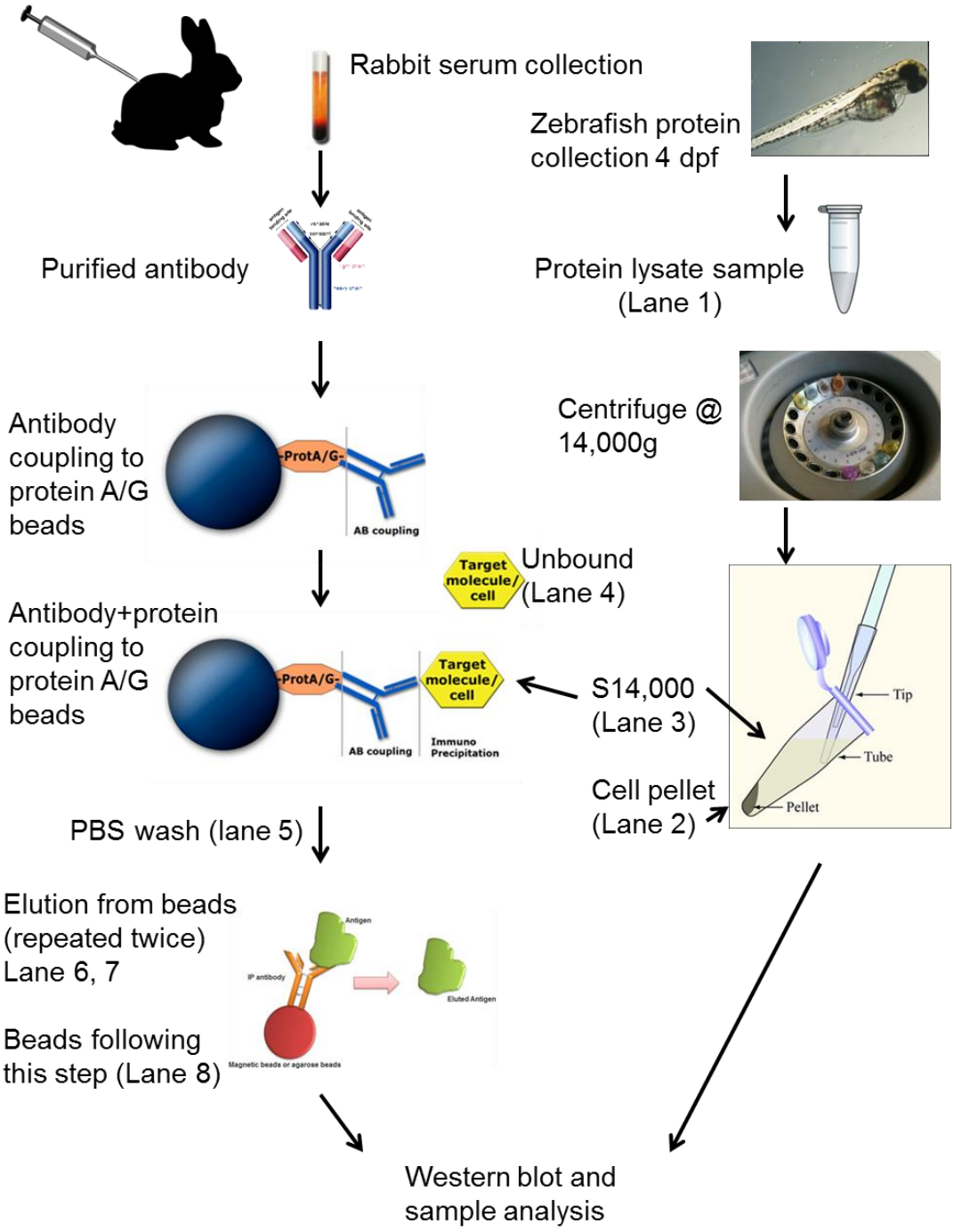

Fig. 4.5 Flow diagram of sample preparation and collection. Purified antibody was bound to protein A/G beads. 4 dpf zebrafish protein sample was collected (lysate) and centrifuged at 14,000g (S14,000). Soluble and insoluble fractions were run on a SDS-PAGE gel along with various samples from protein A/G beads with pull down of Nanor protein.

Results from this blot indicated that all of the Nanor protein was soluble due to detection in the S14,000 lane (lane 3) and no immunoreactive band in the resuspended cell debris pellet (lane 2) (Fig. 4.6). Lane 1 with the lysate showed several bands as well as a band at approximately 27 kD where I expect to see the Nanor protein band. S14,000 sample (lane 3) gave an identical band pattern. As a band was detected in the unbound material (lane 4) I can conclude that not all of the Nanor protein was binding to beads. This was possibly due to insufficient antibody on the protein A/G beads or not enough beads used, or may be because some of the protein complexes are unable to bind to the antibody. A sample of the wash supernatant (lane 5) showed that no antibody or Nanor protein was being washed off during PBS washes. Blots of the leftover beads showed that the antibody as well as non-specific proteins were still bound to the beads following elution with peptide and that none of the Nanor protein was left behind (lane 8-no band at approximately 27 kD). Blots of eluate from the beads initially appeared to have no Nanor protein (lane 6) but with increased exposure four very faint bands were seen (lane 6 - Fig. 4.6 B). This raised the possibility that a small amount of Nanor protein complexes were being successfully eluted off the beads using a peptide elution.

Beads were eluted with a Nanor peptide in the hope that the peptide would compete with Nanor protein complexes bound to the antibody, displace these protein complexes and consequently bind to the antibody. This peptide elution, if successful, would give a lower protein yield in the eluate, but would ensure high specificity and low background in the samples.

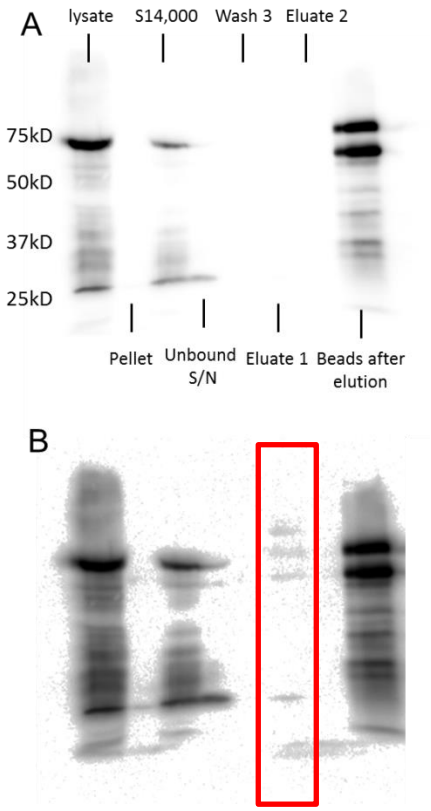

Fig. 4.6: Western blot for Nanor protein using Co-IP kit under normal and higher exposure (A) Western blot of lysate, cell pellet, S14,000, PBS wash, eluate 1 & 2 and protein A/G beads following elution. At first it appeared elution was unsuccessful. However, with increased exposure (B), four faint bands appeared in the first eluate. Four faint immunoreactive bands from eluate sample marked in red. Samples were run on a 15% SDS-PAGE gel.

To confirm that the bands I saw in the previous blot in the lysate, S14,000 and eluate 1 samples were specific to the protein of interest, I ran two samples on an SDS-PAGE gel followed by western blotting;

1) Peptide elution from protein A/G beads with antibody and protein sample bound (protein eluate)
2) Peptide elution from protein A/G beads with only antibody bound and no sample protein (antibody eluate)

This blot made it possible to identify bands that were from the antibody and bands that were from the protein sample. Ideally this blot would show no bands in the antibody eluate and a single band in the protein eluate. This would mean that no antibody was being stripped off the protein A/G beads and that the only immunoreactive band in the protein eluate was Nanor

protein. Unfortunately this was not the case, with several bands in both lanes. However, this western blot clearly distinguished between bands (Fig. 4.7). The protein lane appeared to have an extra band of the expected Nanor size which gave confidence that Nanor was binding to the antibody and was coming off with the peptide elution, but it was also evident that a large proportion of antibody was also being taken off the beads during peptide elution. It was necessary to optimise the protocol to avoid eluting the antibody off the protein A/G beads. Peptide elution times were shortened from 1 hour to 30 minutes.

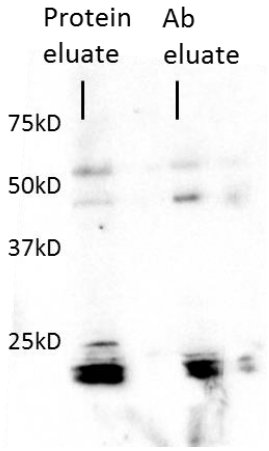

Fig. 4.7: Protein and antibody eluates off the protein A/G beads. A number of immunoreactive bands were seen from the antibody. In the protein eluate two extra bands at approximately 27 kD were found which may be due to nanor protein. Samples were run on a 10% SDS-PAGE gel followed by a western blot.

The remaining protein A/G bead samples from sample preparation of the previous blot were also run;

1) Beads with the antibody bound, (i.e. a sample of the antibody coupled protein A/G beads prior to adding the sample).

2) Beads with antibody bound following peptide elution, (i.e. without any protein sample added; this should identify if antibody is stripped from protein A/G beads by the peptide as well as bands which are coming from the antibody and not the protein sample)

3) Beads with antibody and protein bound following peptide elution, (i.e. protein A/G beads remaining after antibody and protein has been bound and eluted to identify if any protein has been left behind on beads and make sure the antibody has not been stripped from the beads).

Lanes from these samples gave identical patterns of bands with the expected IgG bands at 50 and 75 kD. No bands were seen at 27 kD, the expected size for Nanor (Fig. 4.8). The result gave confidence that no Nanor protein was being left behind on the beads following peptide elution due to no detection of a Nanor band at approximately 27 kD. The lack of extra bands in the protein sample lane indicates that nothing specific to Nanor antibody is being left behind on the beads. It also shows that all bands detected were from the antibody. This blot showed that although I was still getting a significant amount of antibody coming off with the peptide eluate, the majority of it was staying bound to the beads. Still further optimisation of the protocol was needed.

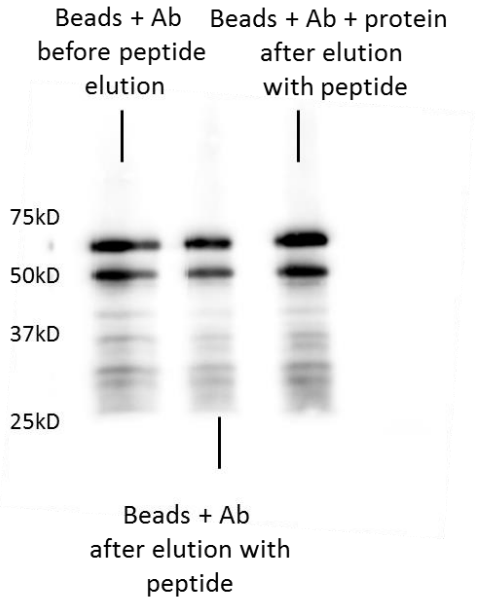

Fig. 4.8: Western blot of bead samples. No difference between lanes. All bands were IgG and not specific to Nanor. Strong immunoreactive bands were found to be due to the antibody and not protein. This shows that no Nanor protein is left behind on beads (15% SDS-PAGE gel). All lanes gave identical patterns of bands with the expected IgG bands at 50 and 75 kD. No bands were seen at 27 kD, the expected size for Nanor.

In order to reduce the background of the sample, I attempted to clear the S14,000 protein sample before adding it to antibody bound protein A/G beads. This would allow non-specific binders to the A/G beads to bind and be removed from the S14,000 and would reduce non-specific binding during sample preparation and Nanor protein complex capture. This was achieved by incubating S14,000 with 100 µL of protein A/G beads (without antibody) with agitation at 4°C for 30 minutes followed by a quick centrifugation and collection of the supernatant (S14,000), the beads used for clearing were discarded. A western blot was then run to compare samples; S14,000 alone (lane 1) and S14,000 after clearing through protein A/G beads (lane 4). Bead sample eluate 1 and eluate 2 of antibody alone (lane 2, 3) and antibody with protein bound eluate 1 and eluate 2 (lane 5, 6) were also run. These bead eluate samples would clearly identify bands coming from the antibody and bands from the protein sample. I was still attempting to optimise the peptide elution step and evidence of optimised protocol would show no bands in the bead and antibody (no protein) eluate 1 and 2 samples (lane 2 and 3). By running these samples it also enabled us to differentiate between antibody bands and protein bands around 25 kD. This blot (Fig. 4.9) showed a cleaner band following pre-clearing the S14,000, but also showed an extra band of higher molecular weight. This may be a Nanor protein complex. A difficulty in optimising the protocol came from the band sizes. Bands from Nanor at 27 kD were approximately the same size as light chain bands from the antibody. Therefore, antibody samples were almost always run on a blot to help to differentiate between these two bands by comparison between lanes. This blot also showed that the second repeat of peptide elution was an unnecessary step and that one elution step was sufficient to remove Nanor from the beads (27 kD band lane 5).

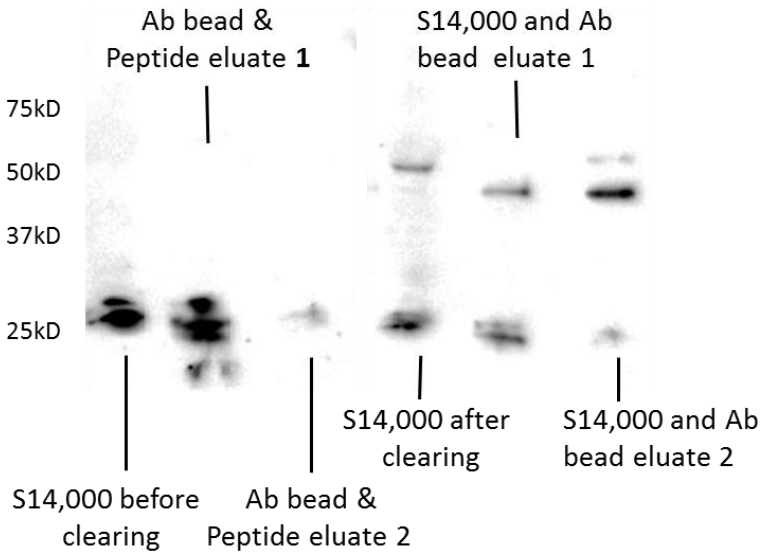

Fig. 4.9: Western blot of S14,000 and eluate samples. S14,000 was cleared before use by incubation with beads to remove non-specific binders to beads. Eluate samples showed Nanor protein had been eluted off the beads but when compared to antibody eluates shows that some of these bands were from the antibody and not the protein sample.

Blots of remaining samples of beads, PBS washes and unbound S14,000 from the previous blot were run on a western blot and showed a large amount of non-specific proteins had bound to beads (lane 1 - beads used for clearing S14,000), the antibody bound beads identified immunoreactive bands from the antibody (lane 2). A sample of the PBS wash confirmed that no Nanor protein or antibody was being washed off during wash steps (lane 3) and finally, a sample of S14,000 after incubation with protein A/G beads for Co-IP sample preparation showed that I was still not getting all Nanor protein bound to beads (lane 4) (Fig. 4.10).

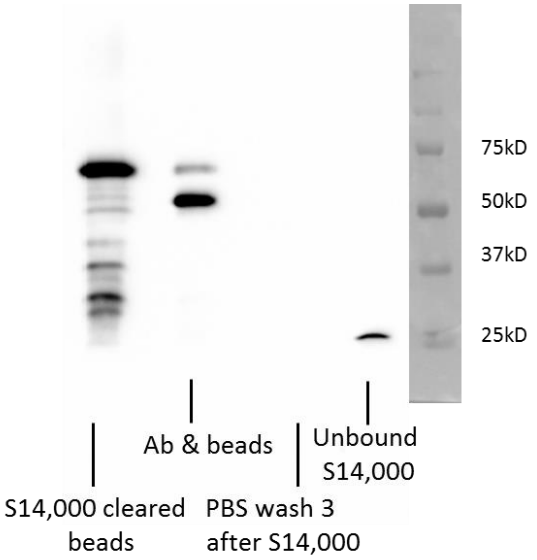

Fig. 4.10: Western blot of bead, PBS washes and unbound protein. This blot showed a number of non-specific proteins were binding to beads (S14,000 cleared beads), antibody was still left on beads following a peptide elution, although it appears a proportion of the antibody was coming off the beads (Ab and beads). PBS washes did not take any antibody or protein from the beads (Wash 3 after S14,000) and a significant amount of Nanor protein was still not binding to the beads (Unbound S14,000 lane).

The S14,000 sample had now been optimised to reduce non-specific binding to the beads. However, the amount of antibody coming off the beads in the elution step was still a concern. To control for this, only antibody and bead samples were run on a SDS-PAGE gel and stained with Coomassie Brilliant Blue (Fig. 4.11). Antibody bound beads were boiled and a sample of the eluate run in lane 2. A sample of the peptide eluate 1 and 2 from these beads were run in lanes 4 and 5. This would identify how much if any of the antibody was being eluted off the beads. In lane 7, the remaining beads after the elution steps were run. In this lane, it was hoped that a similar pattern would be seen to lane 2 (antibody would still be left on the beads). In the final lane (lane 9), the antibody supernatant after incubation with the beads was run. This would tell us if all of the antibody was binding to the beads. This gel showed that the peptide was taking almost all of the antibody off the beads and was not a suitable method of elution.

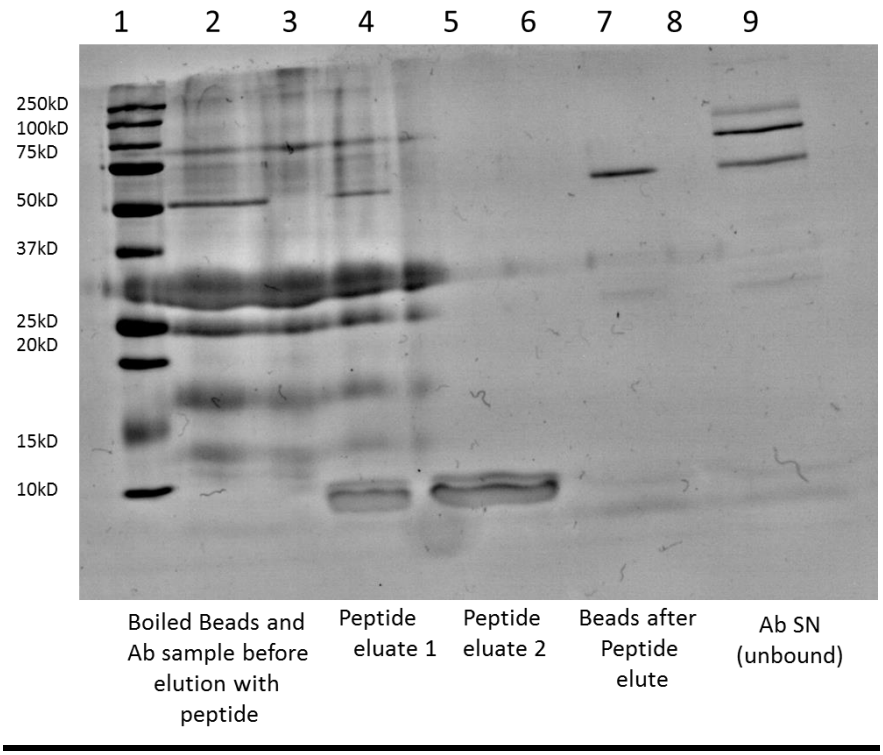

Fig. 4.11: SDS-PAGE gel stained with Coomassie Brilliant Blue showing bead eluates and unbound material. Nanor peptide was taking the majority of antibody off the beads. Almost all of the antibody was successfully binding to the beads but the majority of the antibody was being stripped off in the first peptide elution. Lane 1: protein standards, lane 2: beads with antibody bound, lane 3: empty, lane 4: peptide eluate of antibody bound beads, lane 5: second peptide eluate of antibody bound beads, lane 6: empty, lane 7: beads following peptide elution, lane 8: empty, lane 9: antibody supernatant (unbound antibody).

Following this gel, it was decided the best way to proceed was to elute with a low pH glycine buffer. All elutions from this point were completed using a glycine buffer in place of Nanor peptide.

Glycine elution is the most effective, non-denaturing elution buffer for dissociating most antibody-antigen interactions. Samples for mass spectrometry were prepared using cleared S14,000 followed by Co-immunoprecipitation and elution with glycine. Before sending samples for mass spectrometry an SDS-PAGE gel stained with Coomassie Brilliant Blue, as well as western blot of these samples was run (Fig. 4.12). Antibody and beads alone (no protein) was run alongside two lanes of protein elution 1 and elution 2. Results show very faint bands at 25 and 70 kD indicating bands from the antibody, however, the lane with the sample of protein elution 1 had

far more bands indicating protein complexes specific to the antibody. A control sample of eluate from antibody bound beads (no protein) was sent with the protein sample for mass spectrometric analysis. This would identify any contaminants in the sample or background from the antibody. These samples were sent to EMBL (40 µL eluate) for an in-solution digest and mass spectrometry to identify interacting proteins.

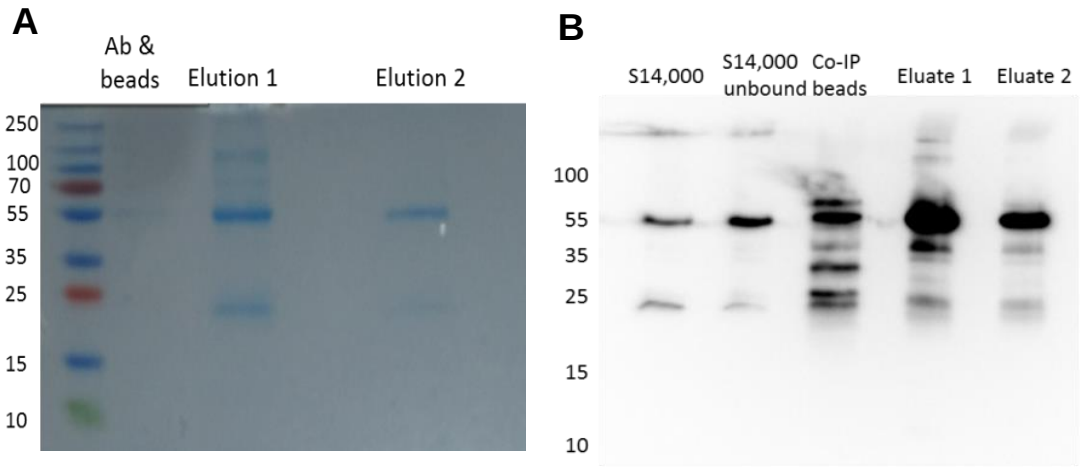

Fig. 4.12: Sample preparation and quality control prior to mass spec analysis by EMBL. (A) SDS-PAGE gel stained with Coomassie Brilliant Blue with bead and antibody as well as glycine eluates (B) Western blot of 1) S14,000 2) S14,000 unbound (protein that did not bind to the beads) 3) protein A/G beads following elution 4) glycine eluate 1 5) glycine eluate 2. Identical band sizes between S14,000 samples (lane 1, 2) and eluate 1 and 2 (lane 4, 5) show that these bands are protein complexes.

4.1.3 Mass spectrometry analysis

The samples were prepared with an in-solution tryptic digest and peptides were purified by a reverse phase cleaning step (OASIS) followed by analysis on Q-Exactive and processing using MaxQuant. Intensity based absolute quantification (iBAQ) values were used for the label-free quantification. The iBAQ corresponds to the sum of all the peptide intensities divided by the number of observable peptides of a protein. This method of quantification has been shown to have a higher precision and accuracy than absolute measures of known protein abundance by correcting for variation in peptide number or protein size and quantification of protein concentration

(Schwanhausser et al., 2013). This method can be used to estimate absolute copy numbers per cell.

Results from mass spectrometry gave 1,500 interacting proteins. However, none of these proteins were Nanor or any of its paralogues.

Table 4.1 Top 40 mass spectrometry hits from in solution digests of Co-IP protein complexes.

Rank	Protein name	Function
1	Betaine-homocysteine S-methyltransferase 1	Homocysteine metabolism
2	Delta-1-pyrroline-5-carboxylate synthase	Glutamate 5-kinase activity
3	Ferritin	Iron binding/transport
4	40S ribosomal protein S18	Structural constituent of ribosome
5	Ribosomal protein	Structural constituent of ribosome
6	Nucleosome assembly protein 1, like 1	Nucleosome assembly
7	C-terminal Binding Protein 1	NADP activity, transcription repressor
8	Ribosomal protein S9	rRNA binding, translation
9	Cleavage and polyadenylation specificity factor subunit 5	mRNA binding, processing
10	Ribosomal protein L17	Structural constituent of ribosome
11	Ribosomal protein S26	Structural constituent of ribosome
12	40S ribosomal protein S8	Structural constituent of ribosome
13	ATPase family, AAA domain-containing 3	ATPase family
14	Glutamine synthetase	ATP binding
15	Ribosomal protein S16 (RPS16)	Structural constituent of ribosome
16	Ribosomal protein L24	Structural constituent of ribosome
17	Ribosomal protein S11	Structural constituent of ribosome
18	40S ribosomal protein S4, X isoform	Structural constituent of ribosome

19	Ribosomal protein S3A	Structural constituent of ribosome
20	Ribosomal protein L4	Structural constituent of ribosome
21	Ribosomal protein S15a	Structural constituent of ribosome
22	Adducin 3 (Gamma)	Cytoskeleton, transport
23	Ribosomal protein L10	Structural constituent of ribosome
24	Ribosomal protein S2	Structural constituent of ribosome
25	UBX domain-containing protein 1	UBX domain containing protein
26	Ribosomal protein L7	Structural constituent of ribosome
27	Propionyl Coenzyme A carboxylase, beta polypeptide	Ligase activity
28	Beta B1-crystallin	Structural constituent of eye lens
29	Adducin 1 (Alpha)	Cytoskeleton, transport
30	60S ribosomal protein	Structural constituent of ribosome
31	60S ribosomal protein L18a	Structural constituent of ribosome
32	Ribosomal protein S29	Structural constituent of ribosome
33	Ribosomal protein L8	Structural constituent of ribosome
34	ATP-binding cassette, sub-family F, member 1	ATP binding
35	**14-3-3 protein beta/alpha-B**	**Protein domain specific binding**
36	60S ribosomal protein	Structural constituent of ribosome
37	small nuclear ribonucleoprotein	Spliceosomal snRNP assembly
38	60S ribosomal protein	Structural constituent of ribosome
39	Crystallin beta B1	mRNA, translation
40	Peptidyl-prolyl cis-trans isomerase	Protein folding

The majority of proteins were cytosolically expressed, which was in agreement with previously discussed immunohistochemical findings on protein expression. However, following mass spectrometry analysis Nanor or Nanor b paralogues failed to be identified from in-solution digests. When

Nanor was not detected, output was reanalysed. Depending on how data is processed slight variations in protein identification can result. Therefore, data were processed using an alternative software (isobarquant), but Nanor was not detected in this analysis either. As isobarquant already applies thresholds, the initial Mascot files that isobarquant uses were reviewed and even in those files Nanor was not found.

Following results from mass spectrometry, the protein sequence originally used to synthesise the Nanor antibody, and subsequently used to purify the antibody from serum was BLAST aligned against the zebrafish protein and genome database. The top 10 hits against the zebrafish database are listed below (Table 4.2). There were many possible off-target hits with high sequence similarity, including 3 proteins in the top 10 hits with the same molecular weight as Nanor. The possibility that the antibody was binding to an off-target protein now had to be considered and investigated.

Table 4.2 Top 10 hits with high sequence identity to the custom made anti-nanor antibody.

	Protein name	Query cover	Identity %	Molecular weight (kD)
1	Nanor	100	100	25
2	Diacylglycerol Kinase alpha	66	88	82
3	Zinc finger CCCH domain			
	containing protein 14	66	88	74
4	Transcription factor p65 X1	50	100	66
5	Transmembrane protein 74B	83	70	25
6	Protein MIS12 homolog	83	70	25
7	Nanor B	100	58	25
8	RNA pseudouridylate synthase	50	100	17
9	GTPase IMAP family member 8	100	86	89
10	Glutamine and serine protein 1	83	70	187

14-3-3 protein α/β B was also a hit but only in the top 500 output results.

As Nanor is a small protein and the sample was so complex, it was possible that the few peptides that derived from the tryptic digest escaped analysis. Therefore, it was necessary to send a gel where the immunoreactive band would be excised and analysed by mass spectrometry (Fig. 4.13). The same procedure as in Section 2.2.23 was run for Co-IP and the maximum volume of eluate was loaded onto the gel under reducing conditions. An SDS-PAGE gel stained with Coomassie Brilliant Blue was then sent to EMBL for analysis.

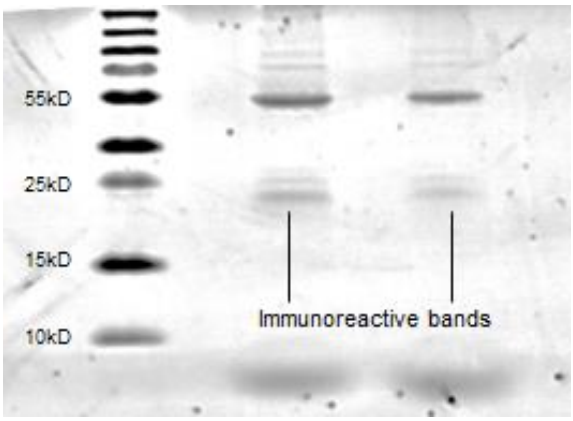

Fig. 4.13: Reducing gel showing immunoreactive bands for nanor antibody. SDS-PAGE gel stained with Coomassie Brilliant Blue of samples sent for mass spec analysis. Immunoreactive band was cut out and sent for mass spectrometry analysis to identify the protein that the antibody was binding.

Three proteins were detected from the excised immunoreactive band; 14-3-3 protein β/α-B, Tyrosine 3-monooxygenase/tryptophan 5-monooxygenase activation protein β polypeptide like and Zinc finger CCCH domain-containing protein 14. 14-3-3 protein β/α B was identified as the most abundantly expressed protein from mass spec results from the excised band with 54% sequence coverage from peptide identification (Fig. 4.14).

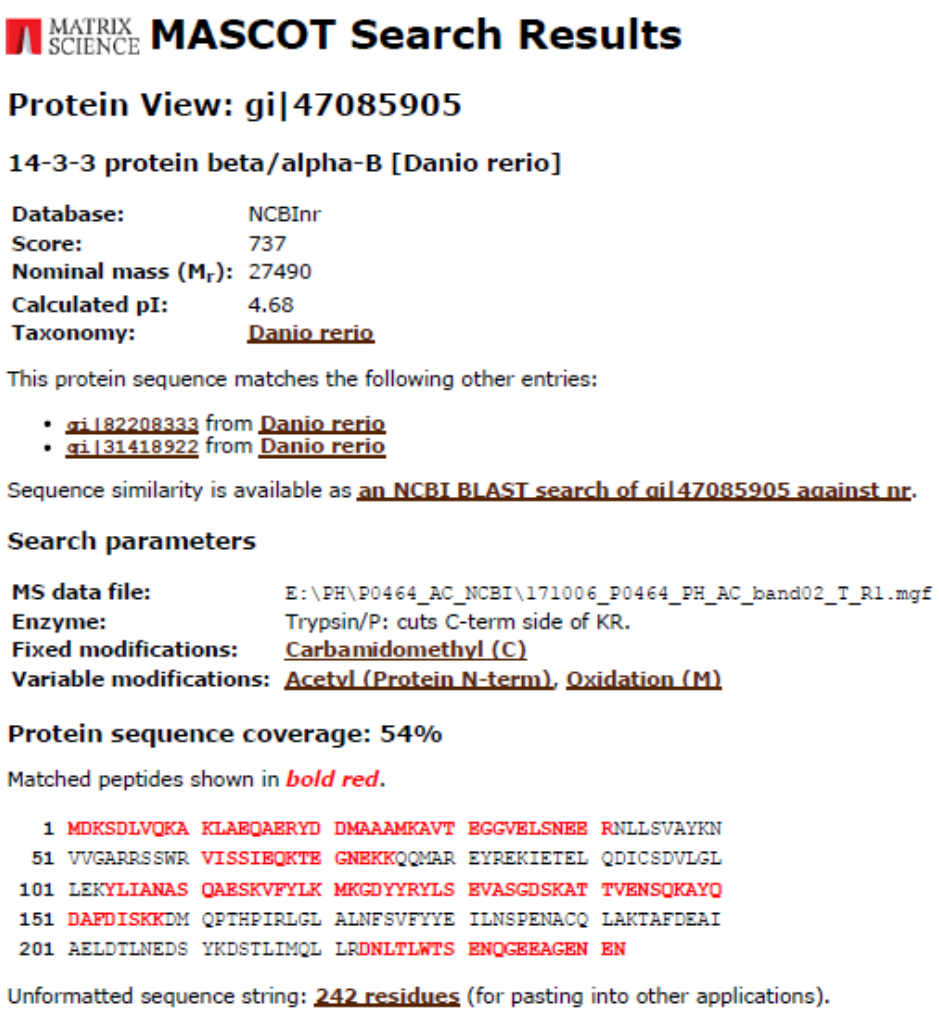

MATRIX SCIENCE **MASCOT Search Results**

Protein View: gi|47085905

14-3-3 protein beta/alpha-B [Danio rerio]

Database:	NCBInr
Score:	737
Nominal mass (M_r):	27490
Calculated pI:	4.68
Taxonomy:	Danio rerio

This protein sequence matches the following other entries:

- gi|82208333 from Danio rerio
- gi|31418922 from Danio rerio

Sequence similarity is available as an NCBI BLAST search of gi|47085905 against nr.

Search parameters

MS data file:	E:\PH\P0464_AC_NCBI\171006_P0464_PH_AC_band02_T_R1.mgf
Enzyme:	Trypsin/P: cuts C-term side of KR.
Fixed modifications:	Carbamidomethyl (C)
Variable modifications:	Acetyl (Protein N-term), Oxidation (M)

Protein sequence coverage: 54%

Matched peptides shown in ***bold red***.

```
  1 MDKSDLVQKA KLAEQAERYD DMAAAMKAVT EGGVELSNEE RNLLSVAYKN
 51 VVGARRSSWR VISSIEQKTE GNEKKQQMAR EYREKIETEL QDICSDVLGL
101 LEKYLIANAS QAESKVFYLK MKGDYYRYLS EVASGDSKAT TVENSQKAYQ
151 DAFDISKKDM QPTHPIRLGL ALNFSVFYYE ILNSPENACQ LAKTAFDEAI
201 AELDTLNEDS YKDSTLIMQL LRDNLTLWTS ENQGEEAGEN EN
```

Unformatted sequence string: 242 residues (for pasting into other applications).

Fig. 4.14: Mascot search results reveal 14-3-3 protein β/α-B as the most abundant protein in the excised band.

When these three hits were further investigated, 83% sequence identity with 97% query cover was found between the two most abundant proteins (Fig. 4.15). These two genes are members of the 14-3-3 superfamily, therefore it is possible that these top 2 hits resulted from the same peptide sequence identification.

14-3-3 protein beta/alpha-B [Danio rerio]

Sequence ID: NP_998310.1 Length: 242 Number of Matches: 1

See 2 more title(s)

Tyrosine 3-monooxygenase/tryptophan 5-monooxygenase activation protein, beta polypeptide like

Range 1: 1 to 235 GenPept Graphics Next Match Previous Match

Score	Expect	Method	Identities	Positives	Gaps
409 bits(1051)	3e-146	Compositional matrix adjust.	195/235(83%)	220/235(93%)	0/235(0%)

```
Query  1    MDKSELVQKAKLAEQAERYDDMAAAMKAVTEGDIELSNEERNLLSVAYKNVVGARRSSWR  60
            MDKS+LVQKAKLAEQAERYDDMAAAMKAVTEG +ELSNEERNLLSVAYKNVVGARRSSWR
Sbjct  1    MDKSDLVQKAKLAEQAERYDDMAAAMKAVTEGGVELSNEERNLLSVAYKNVVGARRSSWR  60

Query  61   VVSSIEQKMEGSDKKQQMVKEYREKIEKELKEICNDVLVLLDKYLIPKATPAESRVFYLK  120
            V+SSIEQK EG++KKQQM +EYREKIE EL++IC+DVL LL+KYLI  A+ AES+VFYLK
Sbjct  61   VISSIEQKTEGNEKKQQMAREYREKIETELQDICSDVLGLLEKYLIANASQAESKVFYLK  120

Query  121  MKGDYFRYLAEVAVGEEKNSIIGNSQEAYKDAFEISKAEMQPTHPIRLGLALNFSVFYYE  180
            MKGDY+RYL+EVA G+ K + + NSQ+AY+DAF+ISK +MQPTHPIRLGLALNFSVFYYE
Sbjct  121  MKGDYYRYLSEVASGDSKATTVENSQKAYQDAFDISKKDMQPTHPIRLGLALNFSVFYYE  180

Query  181  ILNSPEQACKLAKTAFDEAIAELDSLNEESYKDSTLIMQLLRDNLTLWTSDNQGE  235
            ILNSPE AC+LAKTAFDEAIAELD+LNE+SYKDSTLIMQLLRDNLTLWTS+NQGE
Sbjct  181  ILNSPENACQLAKTAFDEAIAELDTLNEDSYKDSTLIMQLLRDNLTLWTSENQGE  235
```

Fig. 4.15: Alignment of 14-3-3 protein beta/alpha-B with Tyrosine 3-monooxygenase/tryptophan 5-monooxygenase activation protein, beta polypeptide like. 83% identity with 93% query cover was found between the two protein identifications.

14-3-3 protein α/β-B is a 27kDa protein which is approximately the same molecular weight as Nanor. When aligned with Nanor sequence, only 25% identity and 11% query cover was found and 45% identity with Nanor b with only 7% query cover. However, when 14-3-3 α/β-B was aligned with the peptide used for antibody synthesis, results show 66% sequence identity with 75% query cover (Fig. 4.16).

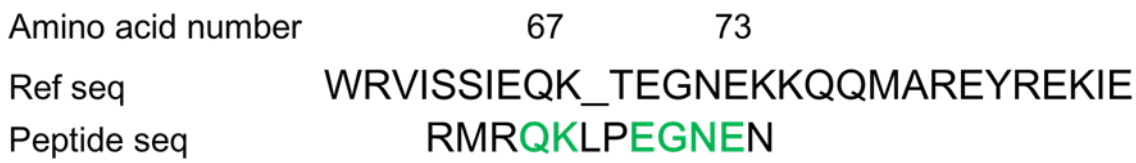

Fig. 4.16: Alignment of 14-3-3 protein α/β B with peptide sequence used to synthesis anti-nanor antiserum. Sequence matches shown in green.

When compared to initial results from in-solution digests of the eluate this protein was in the top 40 expressed proteins out of just over 1,500 proteins

detected (Table 4.1). As well as this protein, many known interaction partners were also detected, such as A-kinase anchoring protein, Abl-interactor, myosin 1C, mitogen activated protein kinase 1, histone deacetylase 1, 3 and 4, cell division cycle protein 5-like (CDC5-like) and Ras homolog guanine nucleotide exchange factor (GEF) to name a few. Therefore, I can conclude that although the Co-IP protocol was optimised for this antibody and mass spectrometry analysis was completed with protein interaction partners being identified, the antibody was binding to an off-target protein and therefore, protein interactions with Nanor were not successfully identified. As there was no alternative antibody available and this antibody had been custom made, it was not possible to continue with identification of protein interactions.

4.2 Discussion

4.2.1 Protein studies on Nanor

Melissa Walsh studied protein expression by western blot from shield to 72 hpf and used densitometric analysis to quantify expression. She reported similar expression from shield to 24 hpf which was then upregulated at 72 hpf (unpublished). Immunohistochemical studies in this thesis agree with this; expression at sphere and shield stage could clearly be seen, but this was then upregulated from 3-5 dpf with stronger staining found cytosolically in all developing structures. This is in contrast to qPCR findings; results show highest expression at sphere and shield stage followed by rapid down-regulation by 24 hpf. *Nanor b* then goes through a second wave of expression up to 120 hpf with no expression of *nanor.*

I attempted to identify interacting proteins with Nanor using a custom made anti-Nanor antibody. Non-denaturing conditions were used to avoid breakdown of these protein complexes followed by elution using a Nanor peptide; the same peptide that was used to manufacture the antibody. This peptide elution, if successfully optimised, would have ensured high specificity in the eluate. However, optimisation of this Co-IP protocol resulted in switching to a glycine elution. This disadvantage of this elution meant that

there was a higher risk of background (non-specific binders) in the sample. However, I controlled for this event by using cleared S14,000 protein sample to reduce background binding to beads, as well as sending a control sample to account for contaminants and background noise.

Mass spectrometry results have cast doubt on the validity of protein studies completed by Melissa Walsh who reported the antibody to bind to Nanor and Nanor b paralogues. Does the antibody recognise Nanor or Nanor b at any stage of development? My results have proven that the antibody is not detecting either paralogue at 4 dpf. The only way to validate this research question would be to send a number of development stages from sphere to 5 dpf for mass spectrometry analysis to identify the immunoreactive band at approximately 27 kD.

A splice blocking morpholino was injected at one-cell stage by Dr. O' Boyle. He did not find complete knockdown of the protein and reported a 36% decrease in expression measured by western blot and explains this discrepancy due to knockdown of only *nanor* with *nanor b* expression being unaffected and therefore, protein expression was still detectable in western blots. Following my mass spectrometry findings, it is likely that the reduced protein expression reported is not due to knockdown of Nanor with detection of Nanor b on western blots, but due to the antibody detecting an off-target protein, 14-3-3 α/β-B protein, which was unaffected by morpholino injection.

The results from mass spectrometry invalidate all previous work involving this custom made anti-nanor antibody. Therefore, western blots and immunohistochemistry for Nanor staining were invalid. Initial validation of the antibody by previous students involved the standard method of detection of a single immunoreactive band by western blot. When a single band was seen, it was concluded that no off-target binding was occurring. However, following BLAST alignment of this epitope against the zebrafish genome, it is clear that there is a high risk of off-target effects due to high sequence similarity within the genome. Therefore in this case, this method of validating antibody specificity was not sufficient. Although the antibody may still detect Nanor during sphere and shield stage, when *nanor* mRNA is most highly

expressed, mass spectrometry results have conclusively shown that at the chosen stage (4 dpf) the antibody was binding to off target proteins with no detection of Nanor protein.

There have been several publications in the last decade which question the specificity of many commercially available antibodies and even variations between batches and lot numbers have been found. These publications argue that there are insufficient validation practices widely accepted in research today (Rhodes and Trimmer, 2006; Pradidarcheep et al., 2008; Couchman, 2009; Perkel, 2014; Schonbrunn, 2014; Baker, 2015). Many argue that the inability to reproduce results come from false positives or negatives from antibodies which are not properly validated, and that all antibodies will cross-react to varying extents. Therefore, it is essential to approach results with scepticism. One publication used six widely used muscarinic receptor antibodies which gave selective staining on sections. However, they found none produced bands of the expected size on western blots and none showed any changes in western blots or immunohistochemistry between wild-type and knock-out mice. This casts doubts into the validity of current knowledge on the family of muscarinic receptors. This study recommends a necessity for staining or western blot showing altered expression patterns of the protein of interest in different tissues and the use of knockout lines where possible (Pradidarcheep et al., 2008).

In the case of the Nanor antibody, validation was run by western blot with results of a single band of the correct size followed by overexpression mRNA studies showing an increase in protein following *nanor* mRNA micro-injection. I also confirmed this single band detection myself by running a western blot and reproducing previous results of a single band of the expected size. As this has now been proven to be insufficient in antibody validation, this casts further doubt on widely accepted antibody validation techniques.

Problems in using animals to produce anti-sera come from the possibility of antibodies against contaminants from the immunogen or antigens that the

animal has been previously exposed (Schonbrunn, 2014). My results from Co-IP experiments would support arguments made against antibody validation practices and would also argue a more robust validation method is essential, such as negative controls in western blots or immunohistochemistry staining in samples which are deficient for the protein of interest. Evidence of identical staining patterns using two antibodies with the same target protein binding to different epitopes in the protein of interest are necessary, as well as more detailed specification sheets of commercially available antibodies which provide all the validation criteria that have been met (Rhodes and Trimmer, 2006; Pradidarcheep et al., 2008; Couchman, 2009; Perkel, 2014; Schonbrunn, 2014; Baker, 2015).

4.2.2 Function and expression of 14-3-3 proteins

The 14-3-3 proteins are a family of dimeric multi-functional adaptor proteins which are highly conserved and responsible for regulating several systems in organisms such as intracellular signalling, cell cycle, apoptosis and transcription. They control transport of proteins between the nucleus and cytoplasm and to mitochondria (Muslin, 2004). They are abundantly expressed in eukaryotic organisms (7 isoforms) and found in all cell types (Aitken, 2002). Many intracellular proteins are known to contain 14-3-3 binding motifs and this family has been found to bind to several protein kinases and scaffolding proteins with roles in signal transduction (Fantl et al., 1994; Liu et al., 1996; Fanger et al., 1998). 14-3-3 proteins in Xenopus are required during early development and regulate FGF signalling. 14-3-3 β/α B has been shown to be among the most abundant 14-3-3 protein expressed in the early embryo and is cytosolically localised (Lau et al., 2006). At shield stage the beta isoform is known to be strongly expressed and by 18 hours high expression is found in developing neural structures and floor plate extending to the tail (Besser et al., 2007). These findings would agree with immunohistochemistry staining previously shown. When aligned with Nanor sequence 14-3-3 protein α/β-B showed little sequence similarity to Nanor or Nanor B paralogues. However, high similarity to the peptide used for antibody synthesis was found.

Identification of protein-protein interactions was not possible with the custom made anti-Nanor antibody, therefore, I then attempted to identify upstream genes of Nanor. This would provide clues to the function of Nanor in addition to which signalling cascades Nanor plays a role.

Results Chapter 5: Identification of Upstream Genes and Signalling Events of *Nanor*

As interacting proteins and downstream genes could not be identified by immunoprecipitation and TALEN knockout, I then attempted to identify upstream genes and upstream left/right asymmetry events such as calcium influx and FGF signalling on *nanor* expression. To do this I used both pharmacological methods and zebrafish mutant lines and investigated gene expression. Pharmacological block of calcium channels using isradipine and FGF signalling inhibition using SU5402 identified links between *nanor* expression, calcium signalling and FGF signalling. To determine if *nanor* was downstream of cilia formation and asymmetry development, I used *elipsa* ciliary mutants with defective cilia formation and Kupffer's vesicle functioning. I then used *plakoglobin* mutants with defective junction formation to investigate if *nanor* was affected in other left/right asymmetry mutant lines.

5.1 Effect of Pharmacological Blockade of Calcium Channels and FGF Signalling on *Nanor* Expression.

The expression of *nanor* in dorsal forerunner cells (Bree et al., 2005) and the findings that *nanor* knockdown led to altered expression patterns of genes in the Nodal pathway (O' Boyle, 2008), suggest that *nanor* is upstream of Nodal signalling. O'Boyle (2008) found that the Nodal homolog, *spaw,* was increased in the lateral plate mesoderm and *lefty1* and *lefty2* decreased, which resulted in increased downstream *pitx2a* in the left lateral plate mesoderm in *nanor* morphants. He concluded that *nanor* is a regulator of Nodal signalling and necessary for activation of left/right asymmetry genes in the lateral plate mesoderm, similar to genes which are highly expressed in Kupffer's vesicle such as *polaris, polycystin 2, ncx4a, ttrap* and *atp1a2a*. Therefore, it was of interest to find if *nanor* was downstream of even earlier signalling events such as calcium signalling and FGF signalling in the establishment and function of Kupffer's vesicle, the organ of asymmetry.

Calcium influx into dorsal forerunner cells and Kupffer's vesicle cells is an important event before and during Nodal pathway activation necessary for left/right patterning of all vertebrate model organisms (mouse, chick,

Xenopus, zebrafish; Section 1.3.4). Inhibition of these calcium fluxes at early stages prior to Kupffer's vesicle formation has been shown to result in loss of asymmetry development and incorrect dorsal forerunner cell migration with loss of Kupffer's vesicle formation (Schneider et al., 2008). Inhibition of these calcium currents once the vesicle has been formed were shown to have similar effects on asymmetry development with incorrect Nodal signalling and expression in the lateral plate mesoderm in zebrafish and mice (Francescatto et al., 2010).

At the cellular level FGFs regulate proliferation, migration, differentiation, and metabolism. They play key roles in epiblast and endoderm lineages and organogenesis at later stages (Ornitz and Itoh, 2015). Numerous studies have also shown that FGF signalling is required for successful morphogenesis and ciliogenesis of Kupffer's vesicle from 10-12 hpf (Melby et al., 1996; Amack et al., 2007; Neugebauer et al., 2009). During Kupffer's vesicle function it has been shown that inhibition of FGF signalling will result in loss of left-sided calcium elevation in the vesicle leading to incorrect Nodal signalling (Tanaka et al., 2005).

My hypothesis for this study was that *nanor* is upstream of *spaw* and *lefty1* but downstream of very early events in Kupffer's vesicle formation such as calcium influx and FGF signalling. I tested this hypothesis by inhibition of calcium flux and FGF signalling through pharmacological block during dorsal forerunner cell migration (6-12 hpf) or during Kupffer's vesicle functioning (12-24 hpf). As well as quantifying *nanor* expression, three important asymmetry genes (*southpaw, lefty1 and one-eyed pinhead)* were chosen for quantification.

Spaw is the earliest known marker of left/right asymmetry in the zebrafish and is expressed in the left lateral plate mesoderm at 10 somites, which developmentally is later than the onset of *nanor* expression. This gene has been established as a downstream target of *nanor*. Morpholino knockdown by Dr. O' Boyle resulted in increased *spaw* expression in the lateral plate mesoderm of morphant embryos (O'Boyle, 2008).

The expression of downstream Nodal inhibitor *lefty1* was then examined. At 22 somites, expression is found along the notochord, left heart field and left diencephalon (Meno et al., 1998). Previous morpholino work in the lab has reported that *nanor* knockdown resulted in bilateral patterning and distribution, as well as a decrease in *lefty1 expression*.

One-eyed pinhead (oep) is upstream of Nodal signalling and essential for formation of anterior axial mesoderm, endoderm and ventral neuroectoderm. *Nanor* mRNA expression at 24 hpf has been found to be most highly expressed in ventral neuroectoderm. *Oep* was not investigated in *nanor* morphants but is known to be upstream of Nodal signalling and in many ciliary mutant models is reported to show no alteration in expression, suggesting it is an early expressed gene and upstream of ciliary mutants and Nodal signalling.

Before mRNA expression studies began, toxicity of both drugs were investigated through larval morphology screening and behavioural tracking (locomotor activity). Each drug was administered at doubling concentrations from 6-24 hpf to establish a dose that was non-lethal up to 5 dpf and did not prevent formation of major structures such as the head and tail.

5.1.1 Isradipine and SU5402 dose selection

Isradipine was administered at 10 µM, 20 µM or 40 µM . At 10 µM the drug resulted in mainly cardiac defects in larval stages ranging from mild to severe (Fig. 5.1 B). At 20 µM exposure to the drug resulted in moderate to severe defects, oedema and pooling around the heart (Fig. 5.1 C). At the highest dose the drug resulted in severe cardiac oedema and blood pooling in almost all larvae and defects in circulation. Delayed development and moderate defects in head and eye formation were also seen (Fig. 5.1 D). No deaths were recorded at the lowest dose with 6% deaths at 20 µM and 50% mortality in 40 µM by 48 hpf (Fig. 5.1 E). Therefore, the 10 µM dose was used for subsequent experiments.

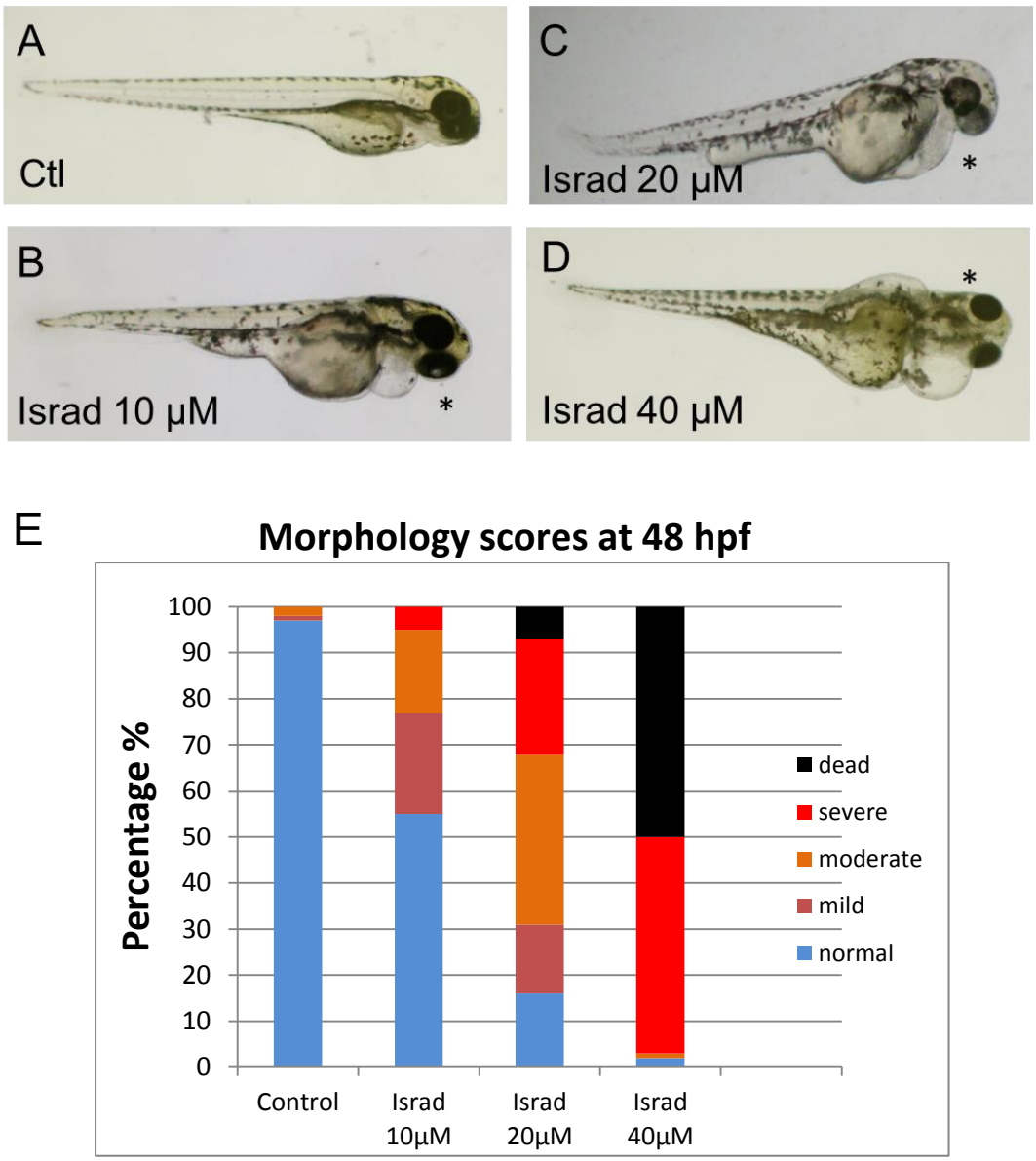

Fig. 5.1: Morphology defects observed and scores following isradipine exposure. Mild, moderate and severe defects were seen following isradipine treatment from 6 – 24 hpf. Isradipine at 10 µM (B) caused mainly heart defects ranging from mild to severe effects. At 20 µM (C) moderate and severe phenotypes were seen including heart oedema and poor circulation as well as deformed yolk sac. At 40 µM (D) the drug caused a severe phenotype in larvae including heart and brain oedema with underdeveloped eyes and poor circulation. Defects in images marked by an asterisks (*) and represent larvae at 72 hpf. (E) Morphology scoring at 48 hpf: At the lowest dose, 10 µM 60% of larvae presented with a normal phenotype with all other larvae showing mild to severe heart defects. At 20 µM, most larvae had mild – severe defects with only 15% presenting with a normal phenotype. At 40 µM, by 2 dpf 50% of larvae had died while most of the remaining larvae had severe deformities, n = 100 embryos per group.

SU5402 was administered at 12.5 μM , 25 μM , or 50 μM, and had a severe effect on larval morphology (Fig. 5.2). At the lowest dose (12.5 μM) the majority of embryos and larvae survived to 5 dpf but failed to develop normal body axis (Fig. 5.2 B) with mild, moderate and severe defects noted. At 25 μM, the majority of surviving larvae had mild, moderate and severe defects including bent body axis and oedema in the heart and brain (Fig. 5.2 C). At the highest dose (50 μM) the few larvae that survived failed to develop a tail, head or heart (Fig. 5.2 D). At 12.5 μM, SU5402 resulted in 10% deaths, 25 μM resulted in 50% deaths by 48 hpf and at 50 μM, 90% of larvae had died by 48 hpf with remaining larvae dead by 120 hpf. SU5402 was used at 12.5 μM for subsequent behavioural and qPCR experiments.

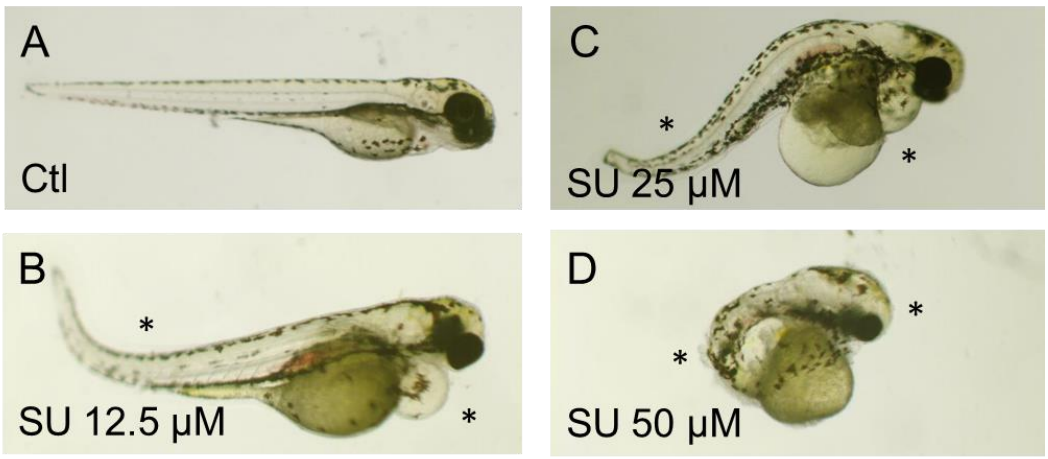

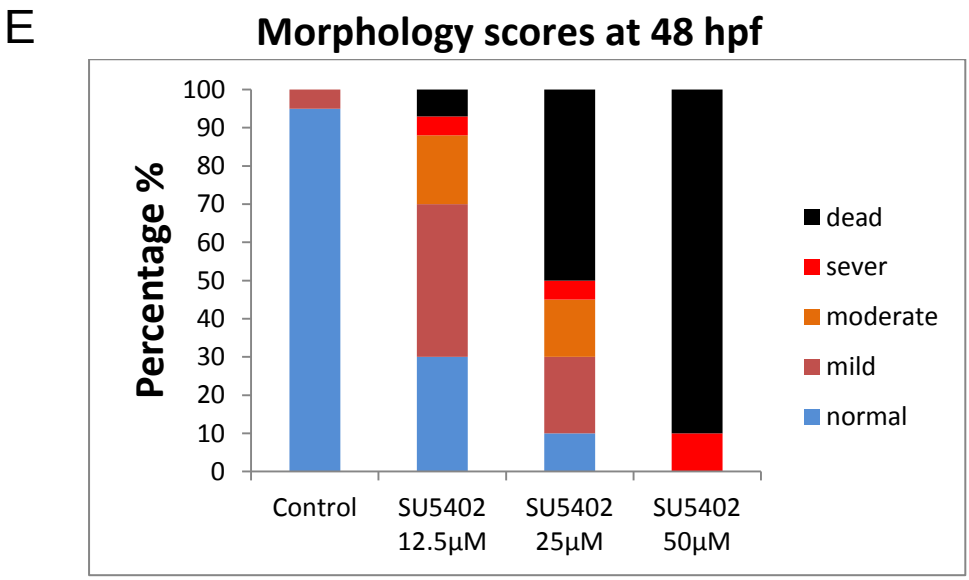

Fig. 5.2: Morphology defects observed and scores following SU5402 exposure. Mild, moderate and severe defects were seen following isradipine treatment from 6 – 24 hpf. (B) Embryos treated with 12.5 µM SU5402 were moderately deformed with bent tails, blood pooling and oedema around the heart. At 25 µM (C) the larvae were severely deformed showing bent bodies, yolk sac deformities and incorrect heart development (heart string) with poor circulation and at the highest dose (50 µM) surviving larvae failing to develop a head or tail with absent anterior organs and posterior structures (D). Defects in images marked by an asterisks (*) and represent larvae at 72 hpf. (E) Morphology scores at 48 hpf: 12.5 µM, SU5402 caused mainly mild defects in body axis formation (40%) with 30 % of larvae with a normal phenotype. At 25 µM, half of larvae had died with a further 40% with developmental defects. At 50 µM, 90% of larvae were dead by 48 hpf. The remaining larvae had severe defects and all were dead by 5 dpf, n = 100 embryos per group.

Behavioural effects of these drugs were recorded at 120 hpf using locomotor activity testing following morphology scoring and dose selection; the lowest dose of each drug was chosen for locomotor activity testing (10 μM isradipine and 12.5 μM SU5402 - Fig. 5.3). When larvae at this stage go from light to dark it triggers a startle response and any effects on locomotor activity are clearly visible. The test was run with 10 minute alternating light-dark cycles over a 50 minute period (Fig. 5.3 A). Two timepoints were chosen to investigate the critical developmental stages for calcium channels and FGF signalling. Initial treatment timepoints studied embryo stages; during the initial 48 hours of development (from 6-24 hpf and 24-48 hpf for both drug treatments). This showed the critical timepoint for calcium channels and FGF signalling to be during the initial 24 hours of development. Locomotor activity of 6 - 24 hpf isradipine-treated larvae was greatly reduced when compared to healthy controls (Fig. 5.3; One way ANOVA $F_{(4, 10)} = 14.21$, $P = 0.0004$; Tukey's post hoc test, $P < 0.01$ isradipine 6-24 hpf vs. 5 dpf control). There was also a partial reduction in locomotor activity when isradipine was administered from 24 – 48 hpf although this was not significantly different to controls. Following FGF inhibition using SU5402, very little movement was recorded after 6 - 24 hpf treatment (Fig. 5.3; One way ANOVA $F_{(4, 10)} = 14.21$, $P = 0.0004$; Tukey's post hoc test, $P < 0.01$ vs. control). SU5402 had no effect in 24 – 48 hpf treated larvae on locomotor activity at 5 dpf when compared to controls.

The results for both drugs show a more severe effect during the first 24 hours of development (Fig. 5.3 B). After the first 24 hours of development, effects of blocking calcium channels is less severe although still causes a partial reduction in locomotion at 5 dpf. FGF inhibition after 24 hpf appears to be completely reversible by 5 dpf and had no effect on locomotor activity three days after drug withdrawal. The results of locomotor testing clearly showed calcium channel and FGF signalling inhibition had detrimental effect during the first 24 hours of development, with significant decreases in locomotor activity when tested at 5 dpf. Following these results, qPCR studies were broken down into two shorter timepoints before 24 hpf;

preceding Kupffer's vesicle formation (6-12 hpf) and subsequent to Kupffer's vesicle formation (12-24 hpf).

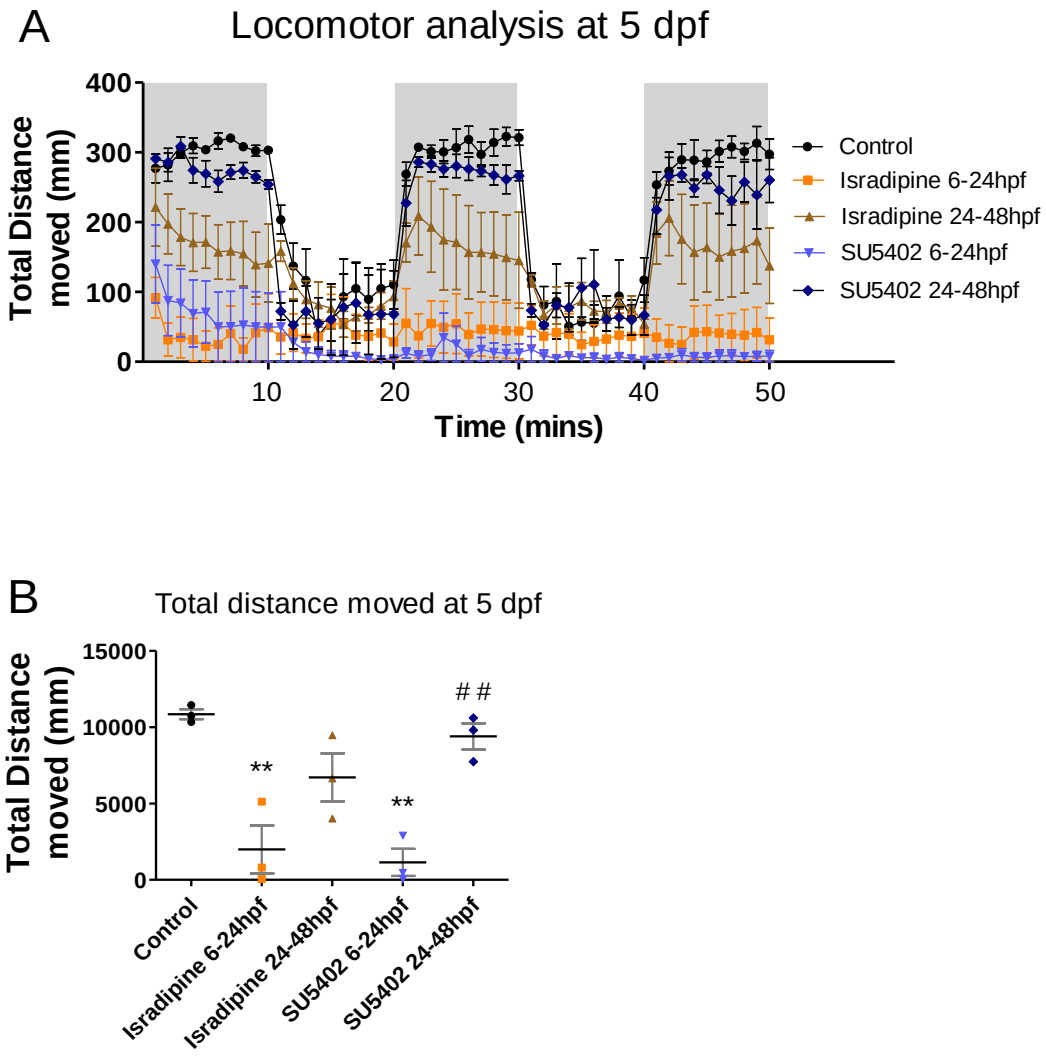

Fig. 5.3: Locomotor activity at 5 dpf following isradipine and SU5402 treatment. Locomotor testing consisted of a 50 minute tracking with 10 minute alternating light to dark cycles (A). Total distance moved over the course of the test is also shown (B). Isradipine treatment during the first 24 hours of development caused severe locomotor deficits at 5 dpf. SU5402 during the same treatment timepoint was also significantly lower than controls. Data are represented as (A) mean ± SEM and (B) mean ± SEM, n = 3. **P < 0.01 vs. control larvae. ## P<0.01 vs. SU5402 6-24 hpf.

5.1.2 *Nanor, spaw, lefty1 and oep* mRNA expression following calcium channel inhibition

Expression of *nanor* was examined after disruption of calcium channels using pharmacological block by isradipine, during dorsal forerunner cell migration or during Kupffer's vesicle functioning. Isradipine treatment from 6-12 hpf caused a significant increase in *nanor* expression at 24 hpf (Fig. 5.4 A; One-way ANOVA $F_{(2, 6)} = 7.941$, $P = 0.0206$, Dunnett's post-hoc test $P < 0.05$ isradipine 6-12 hpf vs. control), whereas there was no significant change in expression of *spaw, lefty1* or *oep*. When treated at 12-24 hpf there was a small increase in mean *nanor* expression but this increase was not statistically significant. Again, no changes were seen in *spaw, lefty1* or *oep* at this later time-point (Fig. 5.4).

This shows a clear relationship between calcium influx and regulation of *nanor* expression and suggests a very early function of *nanor* during embryogenesis. *Spaw* showed little effect following drug administration at both time-points (Fig. 5.4 B; One-way ANOVA $F_{(2, 6)} = 3.083$, $P = 0.120$). Similarly, no changes in *lefty1* (Fig. 5.4 C; One-way ANOVA $F_{(2, 6)} = 0.9551$, $P = 0.4364$) or *oep* (Fig. 5.4 D; One-way ANOVA $F_{(2, 6)} = 1.183$, $P = 0.3689$) were noted.

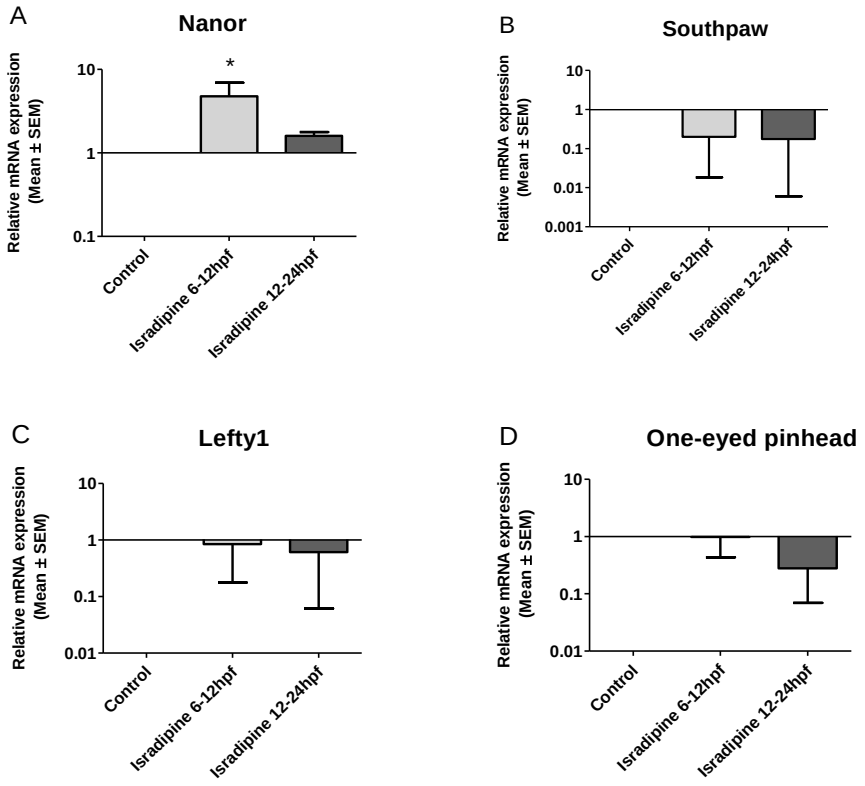

Fig. 5.4: Effect of calcium channel block on *nanor, spaw, lefty1* and *oep* expression before and after Kupffer's vesicle formation, *Nanor* showed an increase in expression at 24 hpf in response to calcium channel block from 6 – 12 hpf ($P < 0.05$ vs. 24 hpf control) also seen at the later timepoint (12-24 hpf) but was not significantly increased. *Spaw, lefty1, oep* showed no changes in relative expression when compared to controls at 24 hpf although they failed to reach statistical significance. Controls were untreated sibling embryos at 24 hpf, n = 3 with at least 50 embryos in each biological replicate. Data are represented as mean ± SEM.

5.1.3 *Nanor, spaw, lefty1 and oep* mRNA expression following FGF signalling inhibition

Following SU5402 administration, to inhibit FGF signalling, *nanor* expression was significantly upregulated when compared to controls at both treatment timepoints, indicating FGF signalling has an inhibitory effect on *nanor* both during Kupffer's vesicle formation and during vesicle function (Fig. 5.5 A; One-way ANOVA; $F_{(2, 12)} = 10.38$, $P = 0.0024$, Dunnett's post hoc test $P < 0.01$ SU5402 6-12 hpf, 12-24 hpf vs. control). Mean values of *spaw* gene expression in all three replicates were lower than controls, however, this decrease was not found to be statistically significant prior to and following

vesicle formation due to variation in fold changes between biological replicates (Fig. 5.5 B; $F_{(2, 6)}$ = 2.470, *P* = 0.1649). Similarly, no significant changes were found in *oep* in response to FGF inhibition, although a slight decrease was seen (Fig. 5.5 D; $F_{(2, 6)}$ = 2.376, *P* = 0.1738) with *lefty1* showing no changes at either timepoint (Fig. 5.5 C; $F_{(2, 6)}$ = 0.5172, P = 0.6206).

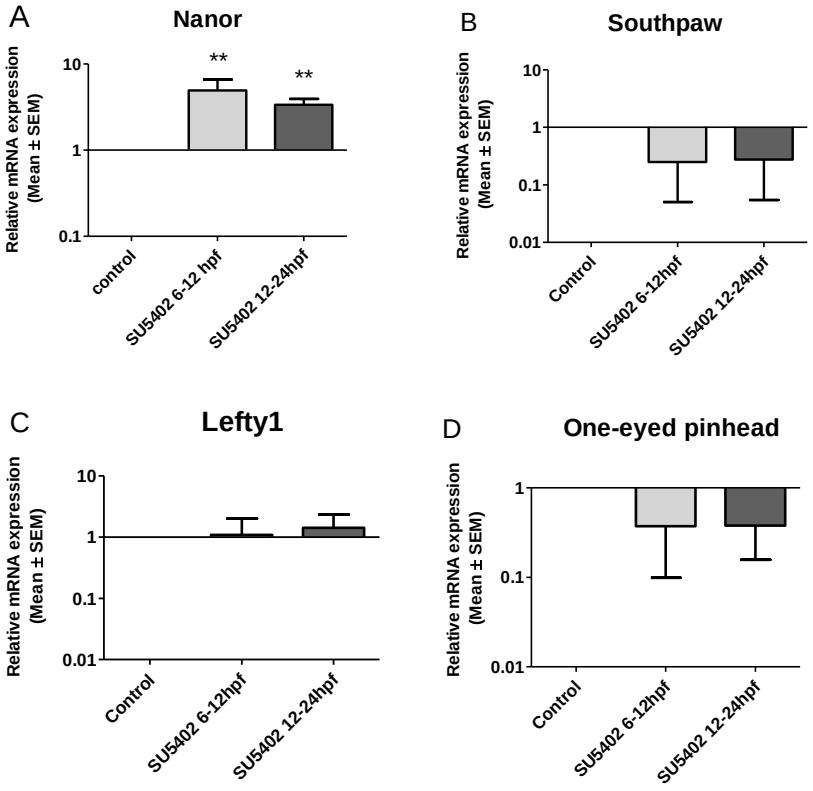

Fig. 5.5: Effect of FGF signalling inhibition on *nanor, spaw, lefty1* and *oep* expression before and after Kupffer's vesicle formation. (A) *nanor* expression was increased at 24 hpf following FGF inhibition before and after Kupffer's vesicle formation (*P* < 0.01 vs. 24 hpf control) (B) *Spaw* expression was slightly decreased but did not reach statistical significance (C) *Lefty1* and (D) o*ep* also failed to reach statistical significance at both treatment timepoints, n ≥ 3. mRNA was quantified at 24 hpf. Controls were untreated sibling embryos at 24 hpf. Data are represented as mean ± SEM.

Having measured changes in *nanor* and Nodal gene expression following pharmacological block of calcium channels and FGF signalling, I then went on to investigate gene expression in *elipsa* and *plakoglobin* mutant embryos and larvae.

5.2 Effects of the Elipsa mutation on *nanor* and left-right asymmetry gene expression

I examined *nanor* mRNA expression in the *elipsa* mutant line which has well established functions in left/right asymmetry development as described in Section 1.3.5, as well as the expression of other important asymmetry genes; *spaw, lefty1* and *oep*. To examine if *nanor* is downstream of cilia formation and function, expression was examined in *elipsa* mutants.

In this study and all *elipsa* experiments, wild-type control embryos were used during sphere and shield stage. At 48 hpf and 72 hpf controls were a mixed population of +/+ (wild-type) and +/- sibling embryos. Mutant embryos at sphere and shield stage were a mixed population of +/+, +/- and -/- as it is impossible to differentiate between these genotypes at early stages. At 48 hpf and 72 hpf mutants were all homozygous mutants (-/-) which can be clearly identified by their phenotype of curled tails.

5.2.1 Nanor mRNA expression in *elipsa* mutants

When *nanor* mRNA was quantified by qPCR, increased expression was found at sphere stage in *elipsa* mutants compared to wild-type controls; this is also the stage at which wild-type *nanor* expression is highest (Fig. 5.6 A; One way ANOVA; $F_{(7, 16)} = 4.541$, $P = 0.0058$; Dunnett's post hoc test $P < 0.05$ *elipsa* sphere vs. wild-type sphere). *Nanor b* expression was also quantified in these mutants and a significant increase in expression was found in *elipsa* mutants at sphere stage with no significant changes at later stages (Fig. 5.6 B; One way ANOVA; $F_{(7, 16)} = 7.533$, $P = 0.0038$; Dunnett's post hoc test $P < 0.01$ *elipsa* sphere vs. wild-type sphere).

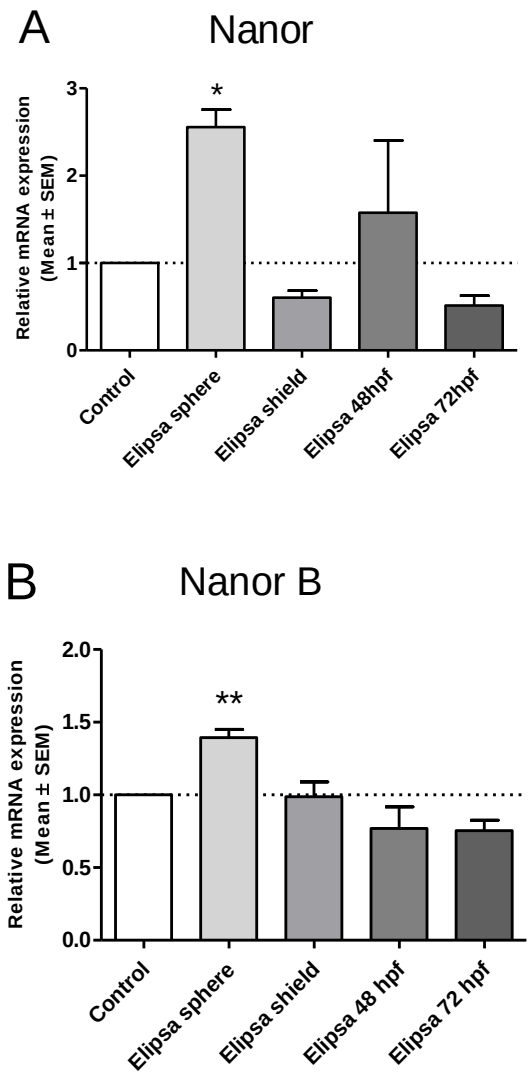

Fig. 5.6: Nanor expression in *elipsa* mutants. *Nanor* expression (A) was significantly increased in *elipsa* mutants at sphere stage ($P < 0.05$ vs. sphere wild-type) with no difference at later developmental stages. *Nanor b* expression (B) was also significantly increased at sphere stage when compared to wild-type controls ($P < 0.01$ vs. sphere wild-type). Data are represented as mean ± SEM, n = 3 with 25-50 embryos and larvae per biological replicate. Control embryos were wild-type embryos and +/+ or +/- larvae at the same stage.

5.2.2 *Spaw, lefty1* and *oep* mRNA expression in *elipsa* mutants

Spaw, Lefty 1 and *oep* were quantified at sphere stage and 72 hpf to examine if these three left/right asymmetry genes were affected in *elipsa* ciliary mutants. Little effect was found on *spaw* with no significant differences when compared to controls, although a slight decrease was noted at sphere stage (Fig. 5.7 A; One way ANOVA; $F_{(2, 6)} = 2.138$, $P = 0.1990$). *Lefty 1* which

is downstream of *spaw,* was quantified and found to be significantly down regulated at 72 hpf with no change at sphere stage when compared to wild-type controls (Fig. 5.7 B; One way ANOVA $F_{(2, 6)} = 5.15$, $P = 0.0499$; Dunnett's post hoc test $P < 0.05$ *elipsa* 72 hpf vs. wild-type 72 hpf). *Oep* showed no changes at either stage when compared to controls (Fig. 5.7 C; One way ANOVA; $F_{(2, 6)} = 1.681$, $P = 0.2633$).

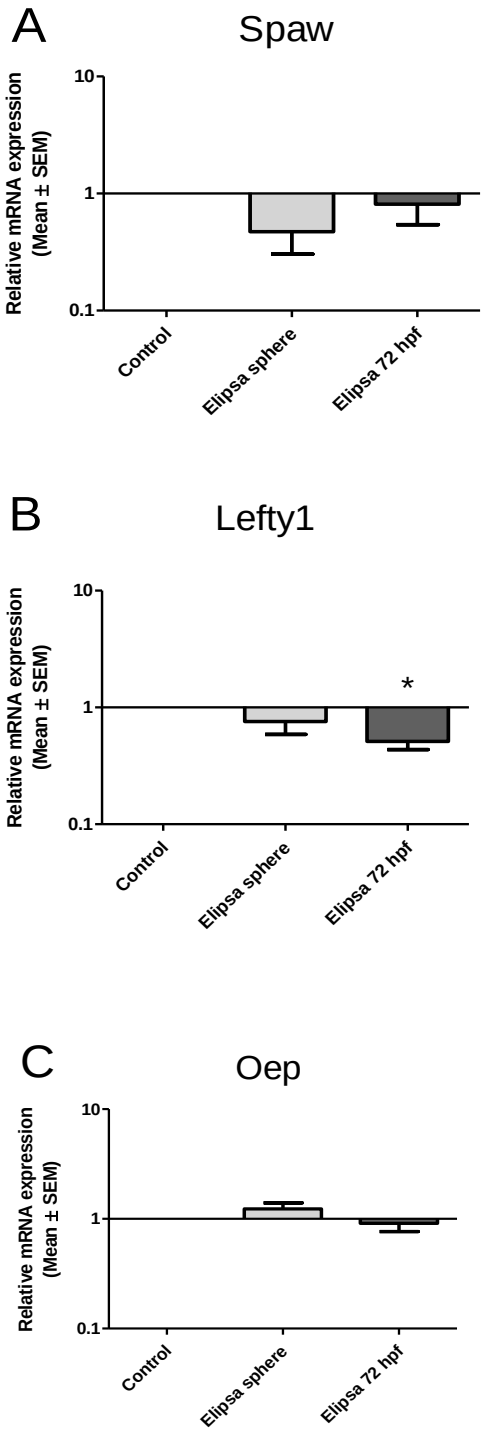

Fig. 5.7: *Spaw, lefty1* and *oep* mRNA expression in *elipsa* mutants. When compared to control larvae (A) *spaw* expression was slightly decreased (B) with significant down-regulation of *lefty1* at 72 hpf ($P < 0.05$ vs. 72 hpf control) (C) and no change in expression of *oep* when compared to controls, n=3 with 25-50 embryos and larvae per biological replicate. Control embryos were wild-type embryos and +/+ or +/- larvae at the same stage. Data are represented as mean ± SEM.

5.2.3 *Nanor* mRNA localisation in *elipsa* mutants

Following mRNA quantification I examined the pattern of *nanor* expression in *elipsa* mutants by in situ hybridisation. Wild-type and heterozygous siblings were used as controls at larval stages as heterozygous siblings cannot be deciphered phenotypically from their wild-type sibling. Sense controls for each developmental stage are shown in Fig. 5.8 and results for *nanor* expression in *elipsa* mutants are summarised in Table 5.1.

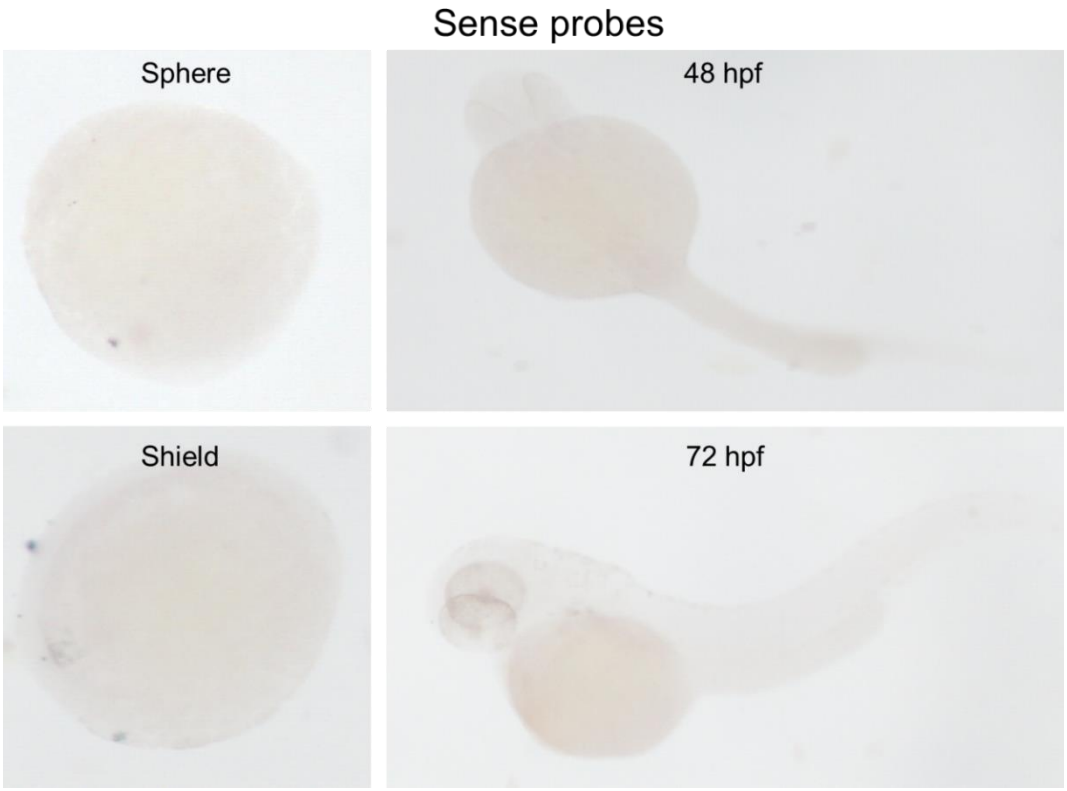

Fig. 5.8: Sense controls of all *elipsa* ISH *nanor* images. Sphere, shield, 48 hpf and 72 hpf show no staining with sense control *nanor* probes.

At sphere stage, when compared to controls, approximately a quarter of embryos show extremely high expression of *nanor.* This is in agreement with increased mRNA expression measured earlier by qPCR. Some individual cells could be seen with extra dark staining; this pattern was sporadic in the embryo at this stage (Fig. 5.9 C, D). Other *elipsa* embryos showed an unusual distribution of *nanor* mRNA (Fig. 5.9 E, F); in the control group mRNA is ubiquitously expressed, however, in *elipsa* embryos expression

appeared to be higher at the distal point of the cell population in what will become the germ ring of the embryo at 6 hpf (Fig. 5.9 F *).

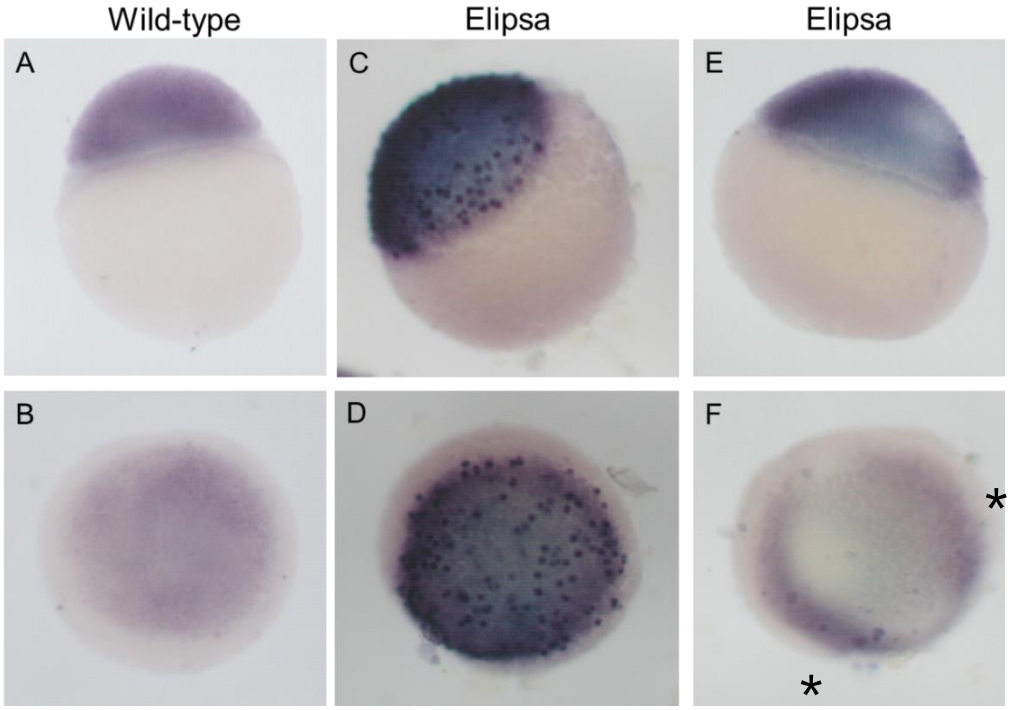

Fig. 5.9: ISH images showing altered *nanor* expression in *elipsa* mutants at sphere stage. When compared to controls (A, lateral, B, dorsal) *nanor* expression was increased in 26% of *elipsa* mutants(C lateral, D dorsal) with some cells showing very high expression in a sporadic pattern. The rest of the *elipsa* embryos show normal levels of expression but with irregular patterning strongest at the germ ring (E, lateral, F, dorsal indicated by asterisks)

Little disruption to *nanor* patterning is seen at shield stage but there appeared to be alterations in expression levels at this stage. In wild-type embryos, *nanor* expression is ubiquitously expressed at shield stage. Some *elipsa* mutants at this stage showed very high expression when compared to controls (Fig. 5.10 C, D) and other mutants showed normal levels of expression but with slight disruption in distribution (Fig. 5.10 E, F).

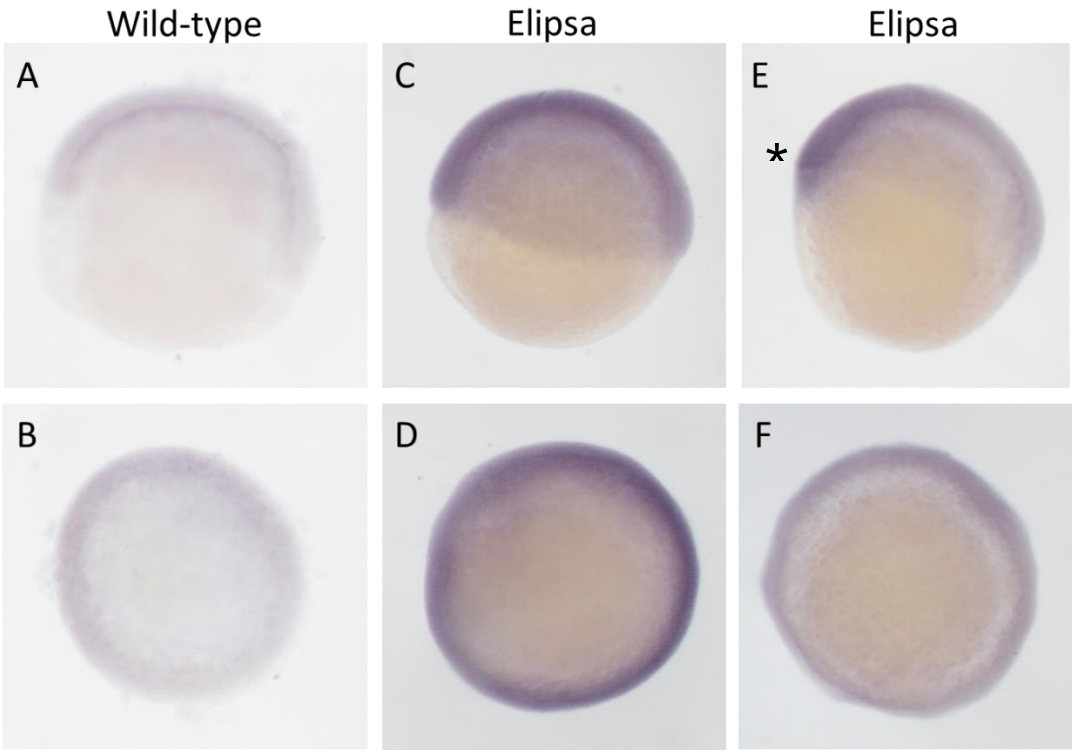

Fig. 5.10: ISH images showing altered *nanor* expression in *elipsa* mutants at shield stage. When compared to controls (A lateral, B dorsal) *nanor* expression was increased in 39% of *elipsa* mutants (C lateral, D dorsal). The rest of the *elipsa* embryos show normal levels of expression but with slight changes in patterning (E lateral, F dorsal), unlike wild-type controls *nanor* expression was not evenly expressed in the embryo.

By 24 hpf, *nanor* is restricted to anterior structures with very little detection by 72 hpf in controls. Again, mutants at 48 hpf show very strong staining with higher expression in the vasculature of the heart when compared to controls (Fig. 5.11 C-F).

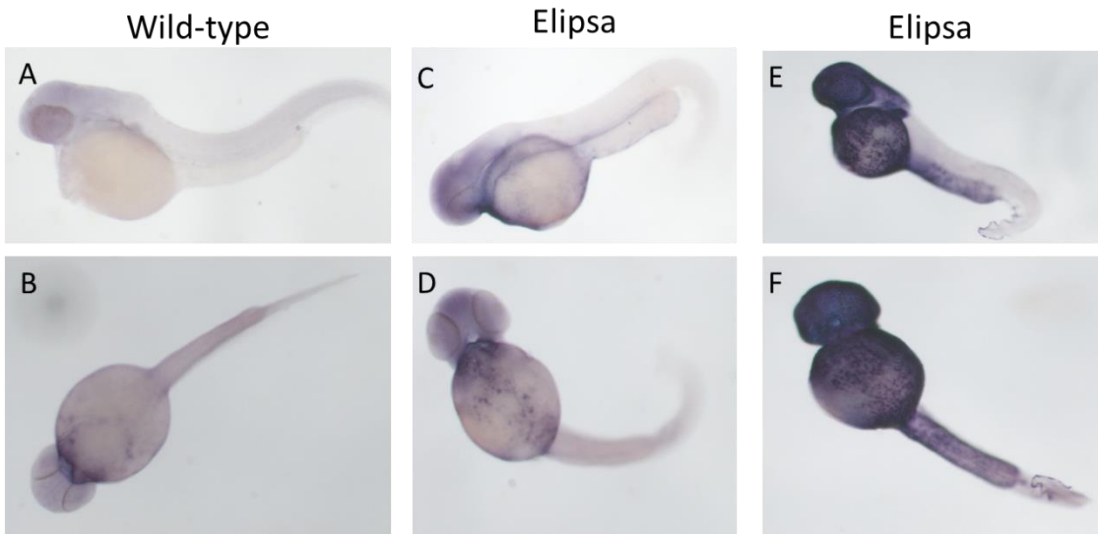

Fig. 5.11: ISH images showing altered *nanor* expression in *elipsa* mutants at 48 hpf. When compared to controls (A, lateral, B, ventral) the majority of *elipsa* larvae (77%) had slightly increased *nanor* expression compared to controls in the anterior region including the brain, eyes, and heart with the same mRNA distribution as controls (C lateral, D ventral). *nanor* expression was increased in 14% of *elipsa* mutants with very dark staining of the head, eyes, heart and yolk sac (E lateral, F ventral).

By 72 hpf expression is negligible in wild-type larvae, mutants presented with higher expression in anterior structures with staining seen at the developing heart and surrounding vasculature. Although expression at these stages does not appear to be disorganised in mutants, a clear increase in expression was noted (Fig. 5.12 C-F).

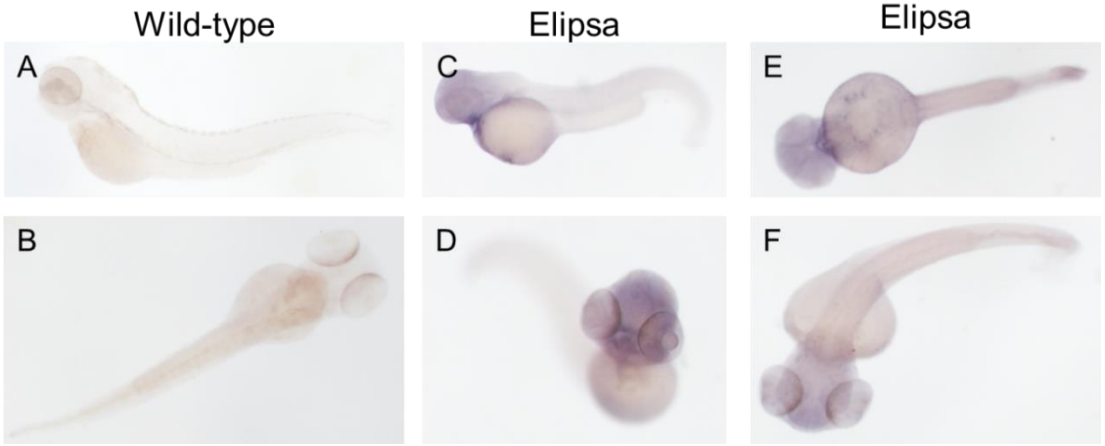

Fig. 5.12: ISH images showing altered *nanor* expression in *elipsa* mutants at 72 hpf. When compared to controls (A, lateral, B, ventral), *nanor* expression was increased in 26% of *elipsa* mutants with dark staining of the head, eyes, heart and yolk sac (C lateral, D rostral). All *elipsa* larvae had increased *nanor* expression compared to controls in the anterior region with the same mRNA distribution as controls. (E ventral, F dorsal).

Table 5.1: Percentage (and numbers) of wild-type and *elipsa* mutant embryos and larvae with light, medium or dark staining at sphere, shield, 48 hpf and 72 hpf.

Group	Light stain	Medium stain	Dark stain
WT sphere	0	100% (50/50)	0
Elipsa sphere +/+ +/- -/-	0	74% (23/31)	26% (8/31)
WT shield	0	100% (38/38)	0
Elipsa shield +/+ +/- -/-	0	61% (27/44)	39% (16/44)
WT 48 hpf +/+ +/-	5% (2/42)	81% (34/42)	14% (6/42)
Elipsa 48 hpf -/-	7% (3/39)	77% (30/39)	16% (6/39)
WT 72 hpf +/+ +/-	100% (49/49)	0	0
Elipsa 72 hpf -/-	0	73% (40/55)	27% (15/55)

In situ hybridisation and qPCR studies have shown altered *nanor* and *nanor b* expression in mutants, indicating that *elipsa* is upstream of *nanor*.

5.3 Effects of the plakoglobin SA12692 mutation on *nanor* mRNA expression

Plakoglobin is a gene that is important for the formation of desmosomes, adherens junctions and gap junctions in cardiac muscle. Mutations in *plakoglobin* have been linked to sudden adult death syndrome in adults (Kaplan et al., 2004). A review by Mercola (2003) linked gap junction communication, along with monocilia and calcium channels as essential signalling components that are necessary for asymmetry development in an embryo. In agreement with this publication RNA sequencing analysis by Tracy Lynskey in our research group has found that 11 genes involved in cilium assembly are upregulated in the SA12692 *plakoglobin* mutant (Tracy Lynskey, personal communication, June 2017). As *plakoglobin* has been linked to cilium assembly and asymmetry development (Martin et al., 2009; Verstraeten et al., 2016) and *nanor* mRNA expression is seen in cardiac muscle, as well as observing cardiovascular defects following TALEN and morpholino injection, I quantified *nanor* expression in the SA12692 *plakoglobin* mutant line. As this mutation is not embryonic lethal,

homozygous mutants were available for these experiments and wild-type siblings at the same stage of development were used as controls.

When compared to wild-type controls, this homozygous mutant line showed increased *nanor* expression at sphere stage and 24 hpf which was only statistically significant at 24 hpf (Fig. 5.13 A; One way ANOVA $F_{(3, 8)} = 9.762$, $P = 0.0047$; Tukey's post hoc test $P < 0.05$ *plakoglobin* 24 hpf vs. wild-type 24 hpf). *Nanor b* expression was quantified at later developmental timepoints as high mRNA expression was found up to 120 hpf in wild-type larvae. Significant increased expression was found in mutants with upregulation of *nanor b* (Fig. 5.13 B; One way ANOVA $F_{(5, 12)} = 23.97$, $P < 0.0001$; Tukey's post hoc test $P < 0.001$ *plakoglobin* 72 hpf vs. wild-type 72 hpf). *Nanor b* expression was significantly increased at 72 hpf with non-statistically significant increases also seen at sphere stage, 24 hpf and 48 hpf.

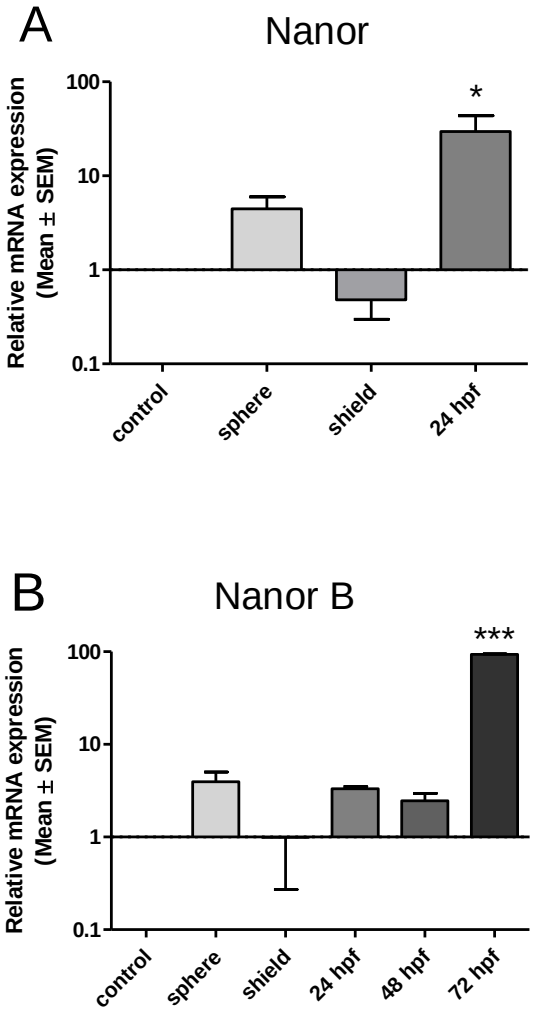

Fig. 5.13: *Nanor* and *nanor b* mRNA expression in *plakoglobin* mutant embryos and larvae. (A) *Nanor* mRNA expression at sphere, shield and 24 hpf. Increased mRNA was found at sphere stage and 24 hpf ($P < 0.05$ vs. wild-type control). However, sphere stage failed to reach statistical significance. (B) *Nanor b* mRNA expression at sphere, shield, 24, 48 and 72 hpf. Significantly increased mRNA was found at 72 hpf ($P<0.001$ vs. wild-type 72 hpf) with increased expression also at sphere stage, 24 hpf and 48 hpf, n = 3 with 50 – 80 embryos or larvae per biological replicate. Data are represented as mean ± SEM.

5.4 Discussion

Results from this study identified upstream genes and signalling events from *nanor*. In pharmacological studies calcium channel block at early stages from 6-24 hpf resulted in an increase in *nanor* expression showing *nanor* is downstream of calcium signalling and is influenced by calcium influx at very early developmental stages. FGF signalling inhibition at 6-12 hpf and 12-24 hpf also resulted in an increase in *nanor* expression at 24 hpf showing *nanor*

is downstream of FGF signalling. *Nanor* and *nanor b* were also increased in ciliary *elipsa* mutants and *plakoglobin* mutants which show both *nanor* paralogues to be downstream of TRAF3IP1 and *plakoglobin* genes.

Significant advances in understanding the function of *nanor* were provided by Dr. O' Boyle who successfully knocked down Nanor protein by morpholinos. His studies on morphants provided the first link to asymmetry development. Embryos showed altered Nodal signalling and disruption in the lateral plate mesoderm with increases in *spaw* and *pitx2a* and decreased *lefty1* and *lefty2* expression. Morphant phenotype at larval stages showed asymmetry defects with incorrect heart development, as well as defects in neural structure development.

5.4.1 Pharmacological block of calcium channels and FGF signalling through isradipine and SU5402 drug treatment

Dorsal forerunner cells are known to give rise to Kupffer's vesicle, the organ of asymmetry (Melby et al., 1996). These cells are dependent on FGF signalling calcium channels for correct vesicle formation and function. Loss of either signalling event will result in disrupted Nodal signalling and left/right asymmetry defects at larval stages (Kreiling et al., 2008; Schneider et al., 2008).

Calcium channel inhibition using isradipine

Blocking calcium channels using isradipine between 6 and 12 hpf during dorsal forerunner cell migration resulted in increased *nanor* expression and no change in expression of *spaw, lefty1 and oep*. No significant changes were found at the later treatment timepoint of 12 - 24 hpf when compared to controls. These results show *nanor* to be sensitive to calcium influx during dorsal forerunner cell migration, where *nanor* is known to be expressed, and show Nodal gene expression levels to have no change in response to calcium inhibition during the initial 24 hours of development.

Two independent studies have found disruption of asymmetry development following pharmacological block of calcium fluxes using thapsigargin; in both studies Kupffer's vesicle formation was disrupted resulting in bilateral expression of asymmetrical genes (*spaw, lefty1, lefty2, pitx2*) which resulted

in randomised organ laterality (Kreiling et al., 2008; Schneider et al., 2008). My results from qPCR studies found *nanor* was the only gene which had an increase in expression before and after Kupffer's vesicle formation with a significant increase at the earlier timepoint during calcium channel inhibition. Increased *nanor* expression suggests that calcium influx has an inhibitory effect on *nanor* expression. The larger response at the earlier timepoint show that calcium channels have a greater effect on *nanor* expression during the first 12 hours of development and gives us clues as to where in the asymmetry development pathway *nanor* acts. It has been discovered that dorsal forerunner cells in Xenopus and zebrafish go through a calcium sensitive stage and inhibition will result in failure of Kupffer's vesicle formation (Schneider et al., 2008). This may also account for the larger responses in expression seen at the earlier treatment timepoint prior to vesicle formation. Even after drug withdrawal it is possible that the vesicle was unable to correctly function due to failure of dorsal forerunner cells to correctly migrate. Mutations that have been found in kidney disease which result in inhibition of calcium flux have also been shown to result in left/right asymmetry defects. These findings were also reported in rodent models (*Polycystin 2* knockouts) (Nauli et al., 2003).

FGF signalling inhibition using SU5402

Inhibition of FGF receptors using SU5402 resulted in increased expression of *nanor* whether administered during dorsal forerunner cell migration or following Kupffer's vesicle formation, a larger effect was seen during earlier administration (from 6-12 hpf) similar to the effects of calcium channel inhibition. This shows that *nanor* is downstream of FGF signalling and is influenced by FGF signalling during Kupffer's vesicle formation and functioning. *Spaw* and *oep* showed a slight decrease but were not significantly down-regulated and *lefty1* expression showed no change in either group. To my knowledge, this study was the first study to quantify relative changes in Nodal gene expression following disruption to left/right asymmetry development.

A study by Tanaka et al. (2005) has shown FGF to be crucial for secretion of Nodal vesicular parcels which carry sonic hedgehog and retinoic acid, as

well as having an important role in asymmetric calcium signalling on the left side of the node in mice. Therefore, it is not surprising that similar results were seen in response to both drug treatments. In zebrafish, FGF has been linked to correct cilia formation in Kupffer's vesicle. FGF receptors 1, 2 and 3 were also shown to be localised on cilia with knockdown of these receptors resulting in the bilateral expression of *spaw*. Tanaka et al. (2005) used SU5402 to show FGF proteins are not capable of generating a left/right axis alone, and instead trigger the calcium influx and release of Nodal vesicular parcels containing retinoic acid and sonic hedgehog in the node. In mice, homozygous FGF8 knockouts failed to develop beyond gastrula stage. Heterozygous mutants in that study were found to have abnormal left/right patterning similar to defects noted when I blocked FGF signalling in embryos and lack Nodal expression in the left lateral plate mesoderm (Meyers and Martin, 1999). Studies have shown the importance of FGF in calcium signalling as well as the importance of both of these events on cilia formation and functioning. My results agree with these findings; gene changes followed similar response patterns in both drug studies which would agree with studies that have found FGF signalling to be essential for activation of calcium influx to a cell.

At later stages, FGF functions at the lateral plate mesoderm in left/right organisation from 11 - 24 hpf. A previous publication used SU5402 in rabbits and reported bilateral and decreased *Nodal* expression in the lateral plate mesoderm with similar findings in chick (Fischer et al., 2002). In that study analysis was done using in situ hybridisation. This method is a useful tool to visualise mRNA distribution but a less accurate method of quantifying gene expression. My qPCR studies show a slight decrease in *spaw* and *oep* with no effect on *lefty1*. qPCR is a more robust and precise method of measuring changes in gene expression which may explain discrepancy between my qPCR results and Fischer et al., (2002). The use of different animal models may also account for the variation in expression between both studies.

5.4.2 *Nanor* and *Nodal* gene expression in *elipsa* mutants.

Nanor mRNA expression in *elipsa* mutants

Increased expression of *nanor* at sphere stage in *elipsa* mutants show *nanor* to be downstream of the TRAF3IP1 gene and agree with previously discussed pharmacological experiments which inhibit correct asymmetry development through calcium channel block and FGF signalling inhibition, which all show an increase in *nanor* expression. This is in agreement with the *elipsa* in situ hybridisation staining; a quarter of sphere stage embryos show increased *nanor* mRNA expression, which accounts for roughly a quarter of embryos which are homozygous mutants. Disrupted expression of *nanor* in mutants at sphere stage was found which indicated that the TRAF3IP1 gene may be necessary for correct localisation of *nanor* during early embryo stages.

No significant upregulation was found at shield stage during qPCR studies, although in situ showed increased expression through staining intensity in roughly a third of embryos which indicate that expression may be increased at this stage also. As embryos were a mixed population with two heterozygous mutant parents, it may account for less significant changes at shield stage; mixed population of *elipsa* mutants would give a smaller effect in qPCR studies and varying numbers in in situ hybridisation. This dampening effect on gene expression changes during qPCR studies may account for only significant changes found at sphere stage and not later in development.

Larval stages in *elipsa* mutants showed no significant changes in qPCR studies. However, a clear increase in gene expression can be seen in in situ hybridisation experiments in 72 hpf larvae with all larvae showing more intense staining than their respective controls in all anterior structures including the brain, eyes and heart. Discrepancy between these findings may be attributed to a mixed population of heterozygous and wild-type control siblings which may have had an effect of decreased significant changes between homozygous mutants, although qPCR is a more robust measure of

changes in gene expression as opposed to variations noted through staining intensity.

Pharmacology and *elipsa* mutant experiments studied *nanor* and Nodal gene expression using embryos and larvae with disrupted left/right asymmetry and similar findings were reported across both experiments. Results show that *nanor* is influenced by cilia formation and Kupffer's vesicle function and gives further confidence that *nanor* has a role in left/right asymmetry. I was able to establish *nanor* as a downstream gene to *elipsa* and downstream of calcium currents and FGF signalling prior to Kupffer's vesicle formation and during Kupffer's vesicle functioning. As these experiments used embryos with defects in left/right asymmetry development, it is possible that *nanor* may play an inhibitory role in Kupffer's vesicle formation and Nodal signalling, and appeared to have the opposite response to Nodal genes during these experiments.

Spaw mRNA expression in *elipsa* mutants

Spaw is one of the earliest known markers of left/right asymmetry and requires Kupffer's vesicle for correct patterning and distribution. The gene controls both visceral organ and diencephalic formation (Long et al., 2003). No significant changes in *spaw* expression were found during qPCR studies, although at early stages a slight decrease is seen in *elipsa* mutants and pharmacology experiments. Although no significant changes in levels of expression were found, it is likely that *spaw* pattern of expression would be disrupted as shown in other ciliary mutants. Altered *spaw* expression was reported in *joi* mutants in zebrafish which are a left/right asymmetry mutant line and result in randomised expression on both sides of the lateral plate mesoderm as opposed to just the left side as found in wild-type embryos (Kobayashi et al., 2010). Similarly in *flanders* mutants and *ccdc151* morphants, which both disrupt cilia formation, *spaw* was found with randomised distribution on both sides of the lateral plate mesoderm (Hjeij et al., 2014). Smith et al. (2011) noted bilateral expression of *spaw* in *lin/bmpr1aa* mutants coupled with reduced *lefty1* expression in the midline. Although there are numerous publications on ciliary mutants and morphants that report disruption of *spaw* distribution and decreased expression through

in situ hybridisation screens, to my knowledge this is the first study to quantify expression in *elipsa* mutants. Although a slight decrease was also found by qPCR in mutants, this was not statistically significant. Similarly, pharmacological block of calcium channels and FGF signalling did not report a significant change in expression.

Lefty1 mRNA expression in elipsa mutants

Lefty1 as previously discussed is downstream of *spaw* and in *elipsa* mutants was found to be significantly down-regulated at 72 hpf. In mice, *Lefty1* is initially expressed at the 3-4 somite stage on the left side of the lateral plate mesoderm, however, in *ccdc40* mutants delayed expression of *Lefty1* was found with no expression at 3-4 somite stage when the gene should first be detected, and bi-lateral expression at later stages with reduced expression of *lefty1* noted in in situ hybridisation experiments. This study concluded that their ciliary mutant showed a delayed and reduced initiation of the gene (Sugrue and Zohn, 2017). In mice, the IFT46 mutant, which is very similar to the *elipsa* mutant used in my study, reported *lefty1* to be bilaterally expressed but did not quantify mRNA expression (Lee et al., 2015). My qPCR studies on Nodal gene expression quantified *lefty1* expression in a ciliary mutant for the first time and found significantly decreased expression consistent with many observations made in in situ hybridisation studies from previous publications.

Oep mRNA expression in elipsa mutants

Kupffer's vesicle formation is dependent on Nodal signalling components exemplified by *oep*; an epidermal growth factor-CFC co-receptor. *Oep* is necessary for dorsal forerunner cells to organise and form Kupffer's vesicle (Essner et al., 2005). Mutants of *oep* have resulted in a failure of Nodal signalling in the embryo; they do not asymmetrically express *lefty1* in the diencephalon, heart and gut, as well as overall organisation of the anterior-posterior axis (Gritsman et al., 1999). The mutant is reported to display an identical phenotype to *squint* and *cyclops* mutants which are Nodal related genes (Rebagliati et al., 1998; Sampath et al., 1998). *Oep* mutants were shown to have defective Kupffer's vesicle morphogenesis and affect downstream left/right gene expression. No change in expression was

expected in these studies as they are upstream of Kupffer's vesicle formation and Nodal signalling. If *nanor* was also upstream of these events, it was expected that responses would be similar between *nanor* and *oep* expression in larvae. *Oep* is highly expressed at early stage pre-mid blastula transition due to maternal transcripts. In *elipsa* mutants, I report no change in expression of *oep* consistent with pharmacology experiment results. I conclude that the gene is upstream of *elipsa* and not affected in ciliary mutants or following pharmacological inhibition of asymmetry development, although an alteration in expression pattern cannot be ruled out in mutants.

5.4.3 Plakoglobin SA12692 mutant line

Plakoglobin is a cytoplasmic component of desmosomes that also has roles in adherens junctions and gap junction formation located within intercalated discs of cardiac muscle and skin that tightly join adjacent cells. Mutations of this gene are linked to arrhythmogenic right ventricular cardiomyopathy. The gene also has a signalling role and has been linked to Wnt signalling (Karnovsky and Klymkowsky, 1995). Knockdown of *plakoglobin* was found to cause morphological heart defects such as heart size, oedema and reflux of blood between heart chambers as well as a twisted tail in zebrafish larvae (Martin et al., 2009). I found mild, moderate and severe cardiac defects following morphology scoring of TALEN injected larvae (Chapter 3) consistent with previous studies in the lab by Dr. O'Boyle who found *nanor* morphant larvae to have incorrect formation of the outflow tract of the heart, as well as incorrect looping of the heart during development. A significant increase in *nanor* at sphere stage was observed in *plakoglobin* mutants with significant upregulation of *nanor b* at sphere stage and 72 hpf. This shows that *nanor* is downstream of *plakoglobin*. It has been proposed that minor situs defects as a result of incorrect cilia formation or function present only as cardiac conditions and that the heart is the most sensitive organ at situs defects (Norris, 2012). *Plakoglobin* has also been linked to gap junction formation which has been shown to be an essential factor in left/right asymmetry development and may contribute to signalling from the node to the lateral plate mesoderm (Levin and Mercola, 1998; Mercola, 2003).

This result implicated *nanor* in heart formation and may act with or downstream of *plakoglobin*. In situ hybridisation studies in *elipsa* mutants which show an increase in nanor expression have also shown strong staining in the vasculature of the heart. This is in agreement with both morpholino and TALEN morphology scoring which noted defects in heart and circulation at 2 dpf. Dr. O' Boyle previously noted incorrect looping of the heart and outflow tract in Nanor morphants (O'Boyle, 2008).

5.4.4 Conclusion

Nanor was found to be downstream of both *elipsa*; a protein required for ciliogenesis and crucial for formation of Kupffer's vesicle and *plakoglobin*; a protein involved in heart formation with signalling roles in the Wnt pathway and left/right asymmetry development. *Spaw* and *lefty1* show slight decreases in *elipsa* mutants, with a significant decrease in *lefty1* expression after Kupffer's vesicle formation consistent with *spaw* being an earlier activated gene than downstream *lefty1*. No change in *oep* was found at either treatment timepoint. I conclude that *spaw* and *lefty1* are downstream of *elipsa* and *oep* is upstream of the TRAF3IP1 gene.

Pharmacology experiments and mutant experiments agree for the most part; *nanor* expression was increased in drug exposed embryos following blockade of calcium channels and FGF signalling. Little effect is seen in Nodal gene expression although altered expression patterns cannot be ruled out. *Spaw* was slightly decreased in *elipsa* and SU5402-exposed embryos and larvae, however, failed to reach significant down-regulation. This shows a similar response in both pharmacological and mutant models. *Lefty1* was down-regulated in mutants with no significant effect following pharmacological disruption of calcium channels or FGF inhibition before and after Kupffer's vesicle formation. *Oep* showed no changes following calcium channel block and FGF inhibition and was not altered in *elipsa* mutants. This suggests that *oep* is upstream and not affected by these early calcium fluxes or FGF signalling and is upstream of *elipsa* and not affected in ciliary mutant lines, this is consistent with early gene expression prior to the mid-blastula transition. Ciliary mutant and pharmacological disrupted asymmetry development are well known to disrupt Nodal signalling at embryonic and

larval stages. However, no studies have investigated changes in levels of gene expression. My findings show that although gene distribution has been shown to be altered in embryos and larvae, very small changes in relative expression of Nodal genes are seen.

These results have given further indications that *nanor* is involved in left/right asymmetry development and have shown *nanor* to be early activated and downstream of calcium fluxes and FGF signalling, as well as the TRAF3IP1 gene and *plakoglobin* gene. Nanor did not follow the expected response in these studies. Disruption to left/right asymmetry development was expected to result in decreased Nodal gene expression and a similar response in *nanor* expression. However, this was not the case and *nanor* showed significant increases during testing with *Nodal* signalling remaining unchanged and in some cases showing decreased expression. This may indicate an inhibitory role of *nanor* in Nodal signalling as we now know that FGF signalling and calcium influx has a dampening effect on *nanor* expression. I can also conclude that *nanor* is a very early acting gene in left/right asymmetry development due to a significant response to calcium inhibition from 6 – 12 hpf as opposed to 12 – 24 hpf.

Results Chapter 6: Development of a Neuroprotective and Neurorestorative Drug Screening Model of Parkinson's Disease

Calcium channels were previously linked to early asymmetry development and found to be upstream of *nanor* expression but have also been implicated as a potential neuroprotective drug treatment through calcium channel inhibition in Parkinson's disease. This study tested the neuroprotective and neurorestorative potential of previously used calcium channel inhibitor, isradipine, as well as monoamine oxidase inhibitor, rasagiline and tetracycline antibiotic, minocycline, on a Parkinson's disease model due to recent findings of neuroprotective effects in patients.

Parkinson's disease is the second most common neurodegenerative disorder characterised by loss of dopaminergic neurons from the nigrostriatial pathway and formation of α-synuclein aggregates known as Lewy bodies. The disease is thought to be due to a combination of genetic and environmental factors resulting in oxidative stress, mitochondrial dysfunction, Lewy body formation and neuroinflammation (Jenner and Olanow, 2006). There is an urgent, unmet need for neuroprotective or, ideally, neurorestorative treatments. The gold-standard treatment of the disease, L-DOPA, is merely symptomatic and does not slow or halt disease progression (Cotzias et al., 1969) Part of the failure to develop novel treatment for the disease is attributed to the lack of suitable animal models with high-throughput drug screening potential which can screen neuroprotective and neurorestorative drug treatments.

6.1 Aims of this study

The aim of this study was to induce locomotor deficit and neuronal loss in zebrafish larvae using 6-OHDA, in order to use this model for drug screening in zebrafish larvae up to 5 dpf. In particular, the aim was to investigate the ability of drugs not only to protect dopaminergic neurons but to restore them following 6-OHDA-induced loss. To this end, four drugs; L-DOPA, isradipine, minocycline or rasagiline were administered to Parkinson's disease models

and tested for neuroprotective and neurorestorative effects on morphology, locomotor activity and dopamine neuronal cell survival (Fig. 2.4 for experimental design).

6.2 Developing a 6-OHDA model of Parkinson's disease

Before I began testing neuroprotective or neurorestorative effects of novel drugs in the treatment of Parkinson's disease, the effects of 6-OHDA alone or L-DOPA alone were first assessed to confirm that I could replicate reported findings by Feng et al., (2014).

6.2.1 Effects of 6-OHDA and L-DOPA on morphology

I first tested for acute toxicity of 6-OHDA (250 μM) and L-DOPA (1mM) by assessing morphology in zebrafish larvae each day for three days post-treatment (3 to 5 dpf). Whereas L-DOPA did not cause any morphological defects, exposure to 6-OHDA caused mild morphological defects such as delayed development and cardiac oedema and blood pooling at 3-, 4- and 5 dpf, with defects at 4 dpf being similar to those at 3 dpf (Fig. 6.1 A-D). No moderate or severe developmental effects were noted, and morphology scores were significantly different to controls only at 3 dpf (Fig. 6.1 E; Kruskal-Wallis ANOVA ($\chi 2$ (2) = 11.2; P = 0.0037; Dunn's post hoc test P < 0.01, 6-OHDA vs. control at 3 dpf). However, 13% of larvae in the 6-OHDA group died by 5 dpf (Fig. 6.1 E).

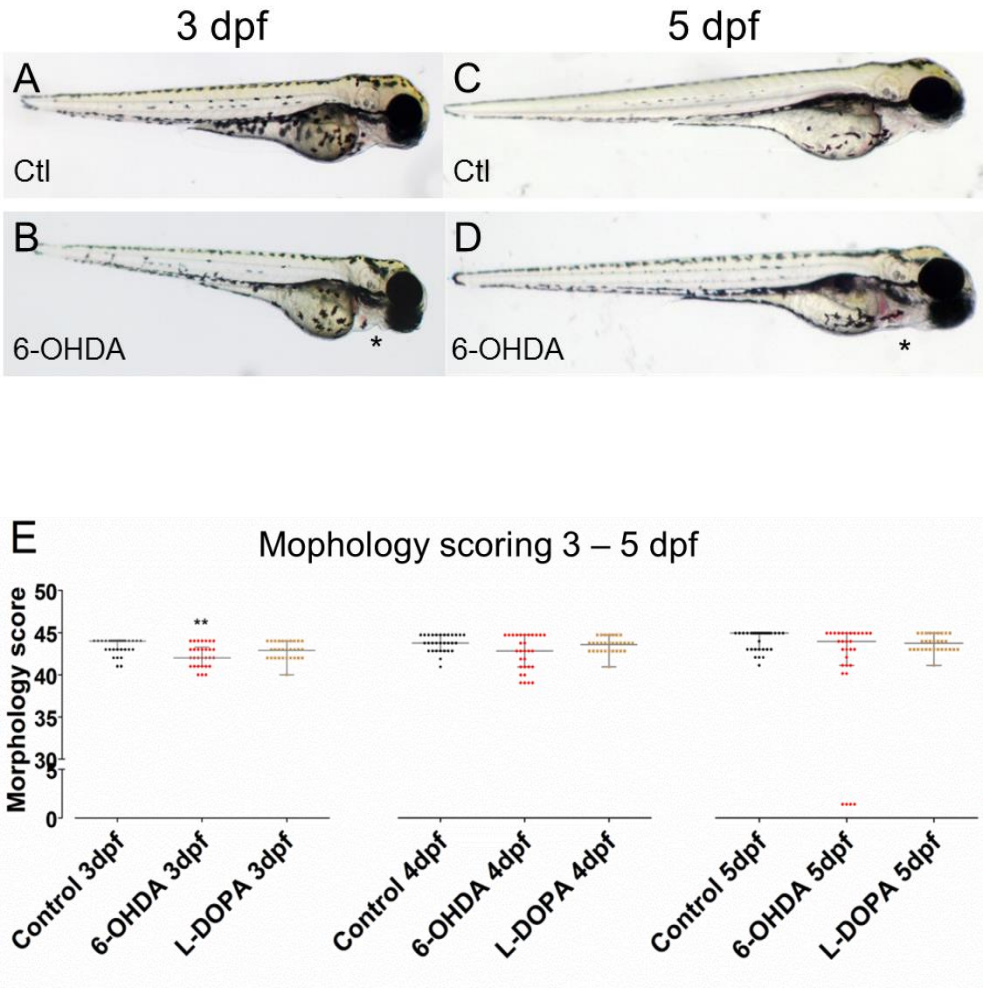

Fig. 6.1: Effects of 6-OHDA and L-DOPA on development. When compared with controls (Ctl) at 3 dpf (A) heart oedema and blood pooling (*) were seen in 6-OHDA (250 µM)-treated larvae (B). At 5 dpf larvae in the 6-OHDA-treated group (D) had delayed development such as slow development of the swim bladder along with cardiac oedema and blood pooling (*) compared to 5 dpf control (C). (E) Morphology scores at 3 dpf, 4 dpf, and 5 dpf in control, 6-OHDA and L-DOPA treated groups. L-DOPA had no effect on development however 6-OHDA groups had significantly lower body score at 3 dpf. Data are represented as median and interquartile range with n = 30 larvae per group; $^{**}P < 0.01$ vs. control.

6.2.2 Effects of 6-OHDA on Locomotor activity and Dopaminergic Neurons

Next, I assessed dopaminergic cell survival and locomotor activity following 6-OHDA exposure for three days, as a basis for testing neuroprotective drugs, or for 32 h as a basis for testing neurorestorative drugs (Fig. 2.4 for timeline). In addition, I examined the ability of L-DOPA to reverse the effects of 6-OHDA in both of these paradigms. Either the 3-day or 32-hour exposure to 6-OHDA caused a reduction in locomotor activity and a loss of dopaminergic neurons throughout the dopaminergic clusters of the brain.

The retinal pigmented epithelium of the eye has intense tyrosine hydroxylase positive staining, because melanin is downstream of tyrosine hydroxylase in the catecholamine synthesis pathway; this was unaffected by 6-OHDA exposure (Fig. 6.2). In the control group, dopaminergic neurons were clearly seen throughout the zebrafish brain with the expected clustered pattern of cell populations in the pretectum, ventral thalamus, posterior tuberculum and hypothalamus. In contrast, exposure to 6-OHDA caused a substantial loss of dopaminergic neurons, with few to no surviving cells (Fig. 6.2 A-O). When assessed using 10 minute light: dark cycles at 5 dpf, larvae moved more in the dark, with transition to the dark phase triggering movement. Exposure to 6-OHDA, for either 3 days or 32 hours resulted in a loss of locomotor activity (Fig. 6.3). The reduction in locomotor activity caused by the three-day exposure to 6-OHDA (48-120 hpf) was statistically significant (Fig. 6.3; one-way ANOVA $F_{(5,12)} = 6.251$, $P = 0.0045$; Tukey's post hoc test $P < 0.05$ 6-OHDA 3 days vs. control). Interestingly, the locomotor activity deficit caused by exposure to 6-OHDA for 32 h (48-80 hpf) was similar to that caused by the longer three-day exposure (Tukey's post hoc test $P < 0.05$ 6-OHDA 32 h vs. control), thus providing a paradigm for testing functional restoration potential of test drugs.

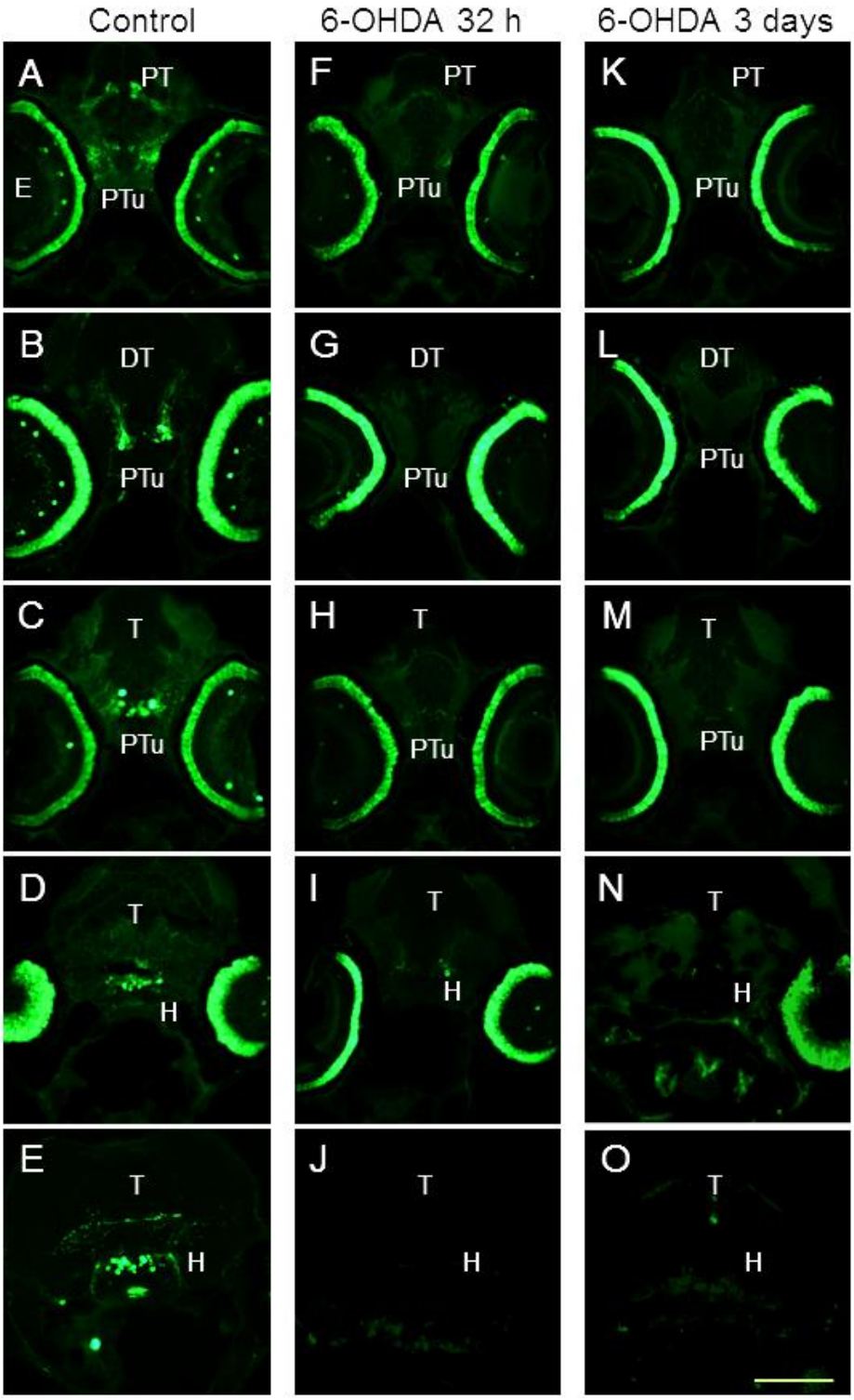

Fig. 6.2: Dopaminergic cell loss throughout the brain following 6-OHDA exposure for 32 h or 3 days. Control larvae at 5 dpf have expected dopamine cell populations in the pretectum (A), posterior tuberculum (A, B, C) and hypothalamus (D, E). Corresponding brain regions in 6-OHDA 32 h exposed larvae (F, G, H, I, J) or 3 day exposed larvae (K, L, M, N, O) showed huge dopaminergic neuronal loss throughout the brain (DT, dorsal thalamus; H, hypothalamus; PT, pretectum; PTu, posterior tuberculum; T, tegmentum; Scale bar = 100 µM).

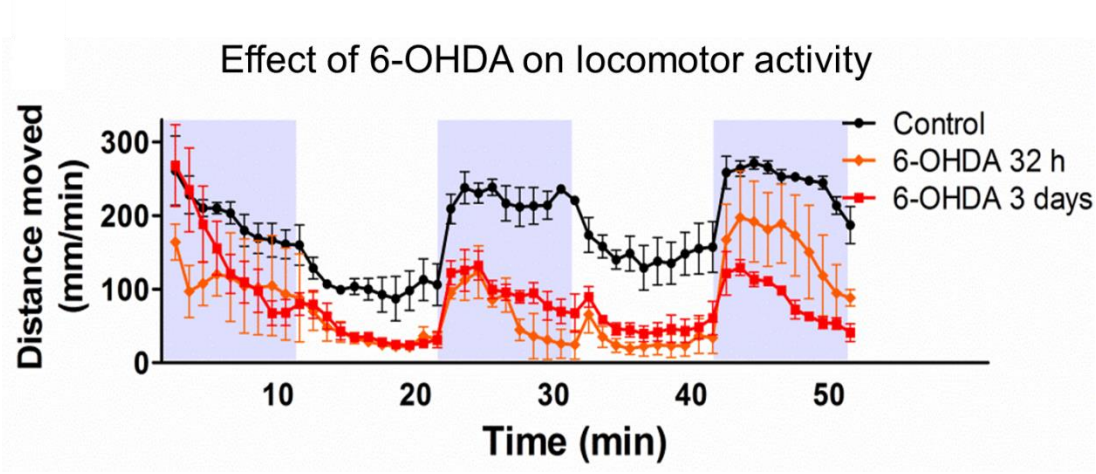

Fig. 6.3: Effect of 6-OHDA on locomotor activity. Distance moved over time in dark (shaded) and light conditions shows that larvae move more in the dark, with severe loss of movement in the dark phase in both 32-hour and 3-day 6-OHDA-treated larvae; n = 3 separate experiments with 10 larvae per experiment. Data are represented as mean ± SEM.

6.2.3 Effects of L-DOPA on Locomotor Activity and Dopaminergic Neurons in 6-OHDA-treated larvae

In contrast to the partial reversal by L-DOPA of the 6-OHDA-induced locomotor deficit (Fig. 6.4 A), L-DOPA was unable to prevent or restore the loss of dopaminergic neurons caused by exposure to 6-OHDA (Fig. 6.5 A-F) when tested at 5 dpf. The neuronal losses due to 6-OHDA were statistically significant (Fig. 6.5 G; Kruskal-Wallis ANOVA ($\chi 2$ (4) = 13.5; P = 0.0091; Dunn's post hoc test $P < 0.05$ 6-OHDA vs. control; L-DOPA groups ns vs. relevant 6-OHDA groups). This indicates that a 32 h exposure to 6-OHDA is sufficient to induce substantial neuronal loss with no recovery of neuronal cell numbers by 5 dpf, 40 h after withdrawal of the toxin. L-DOPA co-treatment did not prevent neuronal loss due to the three-day 6-OHDA exposure (Fig. 6.5 E). Nor did post-treatment with L-DOPA following washout of 6-OHDA reverse the neuronal loss due to 32 h exposure to 6-OHDA (Fig. 6.5 F). Thus, the effect of L-DOPA in this zebrafish model is similar to those observed clinically showing an improvement of locomotor function with no improvement in dopaminergic neuronal loss.

L-DOPA partially restored locomotor activity in both neuroprotective and neurorestorative treatment groups (Fig. 6.4 A, B; 6-OHDA+L-DOPA ns vs. any group), with movement intermediate between that of the control and the relevant 6-OHDA groups. The drug alone had no toxic effects with no significant difference in total distance moved when compared to controls (Fig. 6.4 B).

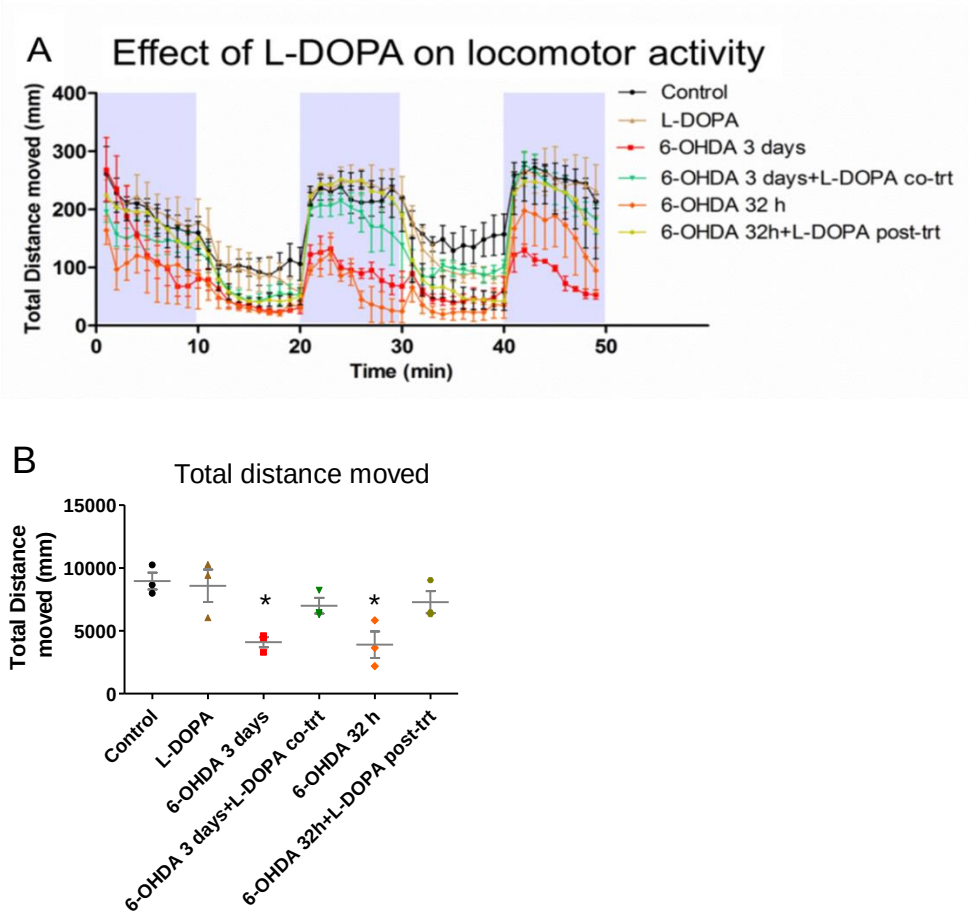

Fig. 6.4: Effect of 6-OHDA and L-DOPA on dopaminergic cell count and locomotor activity. (A) Locomotor testing at 5 dpf over a 50 min alternating light: dark cycle. (B) Total distance moved over the 50 min test found decreased locomotor activity in both 6-OHDA groups when compared to controls. L-DOPA treatment in both neuroprotective and neurorestorative groups had a partial rescue of locomotor activity; n = 3 separate experiments with 10 larvae per experiment. Data are represented as mean ± SEM; **P* < 0.05 vs. control.

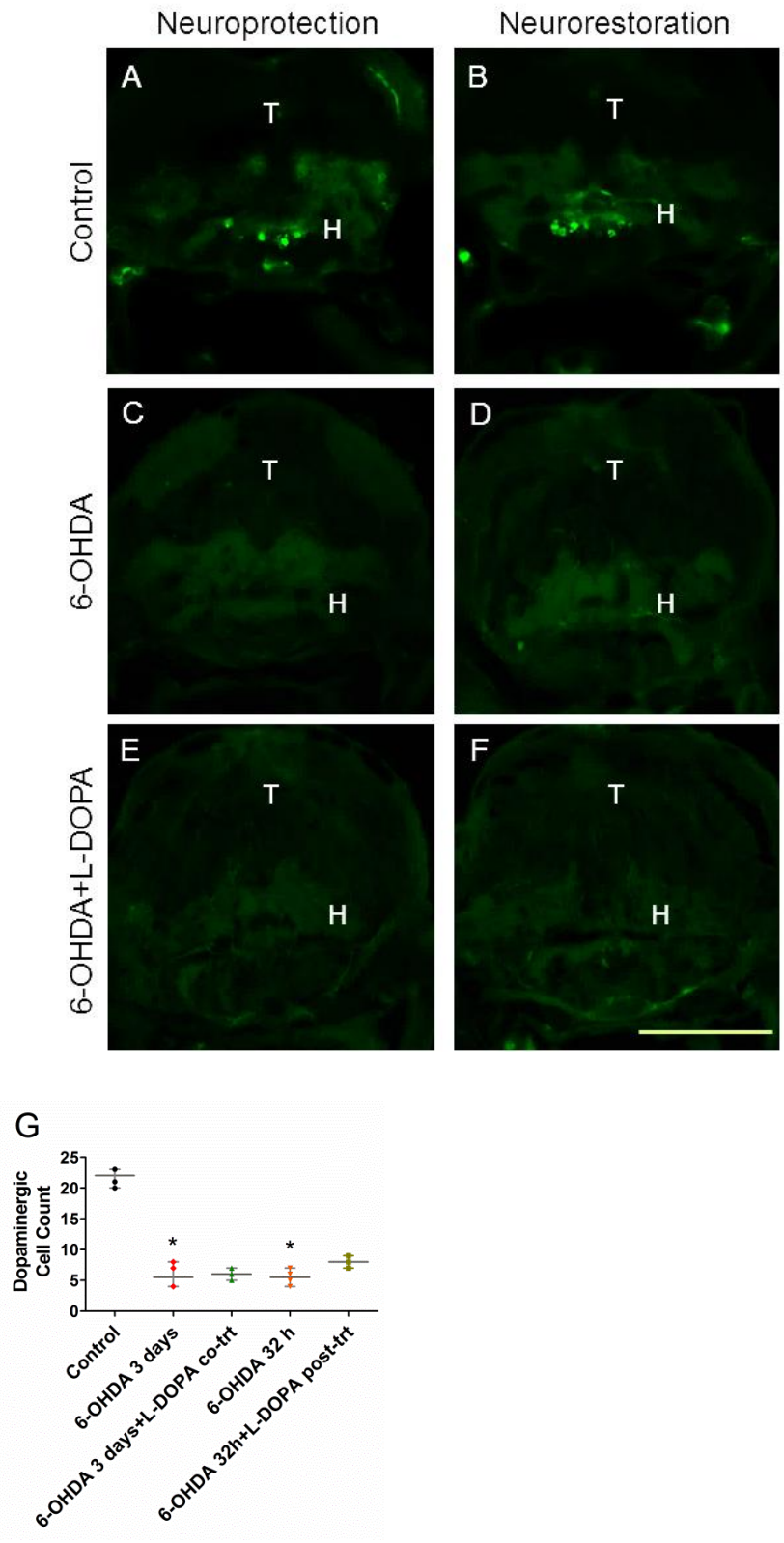

Fig. 6.5: Effect of L-DOPA on dopaminergic cell survival in 6-OHDA treated larvae. Compared with their respective controls (A, B) 3-day (C) or 32-hour (D) 6-OHDA treatment caused dopaminergic neuronal loss, L-DOPA co-treatment (E) or post-treatment (F) did not protect from or restore cell loss. (H, hypothalamus; T, tegmentum; Scale bar 100 µM). (G) Dopaminergic cell count data are represented as median with range, n = 4 per group.

6.3 Testing neuroprotective and neurorestorative potential of drug treatments

Three drugs were chosen to test neuroprotective or neurorestorative potential in a 6-OHDA neurotoxic model of Parkinson's disease. All three drugs were chosen due to recent publications which reported neuroprotective properties in animal models or Parkinson's disease patients.

6.3.1 Toxicity screening and drug dose selection of isradipine, minocycline and rasagiline

Before testing the neuroprotective or neurorestorative ability of the test drugs, the toxicity of each test drug was assessed, when administered from 48 hpf to 120 hpf, by scoring morphology each day and assessing locomotor activity at 5 dpf. No defects were recorded in minocycline (10 μM) or rasagiline (1 μM) treated groups; morphology scores were similar to controls (Fig. 6.6 G), and these drugs had no effect on locomotor activity (Fig. 6.7 A). Whereas isradipine at 10 μM caused severe heart oedema (Fig. 6.6 C, F), the 1 μM concentration was much less toxic; it caused mild heart oedema and mild blood pooling in approximately 20% of treated larvae (Fig. 6.6 B, E). Morphology scores were only significantly different to controls at 5 dpf (Fig. 6.6 G; Kruskal Wallis ANOVA $\chi 2$ (3) =9.558; P = 0.0227; Tukey's post hoc test $P < 0.05$ isradipine vs. control at 5 dpf). Therefore, the 1 μM concentration of isradipine was chosen for further investigations. None of the drugs affected locomotor activity compared to controls (Fig. 6.7 A, B; one-way ANOVA $F_{(3, 31)} = 2.851$, P = 0.0533; Dunn's post hoc test all groups ns vs. control). Thus, I tested these drugs for neuroprotection and neurorestoration.

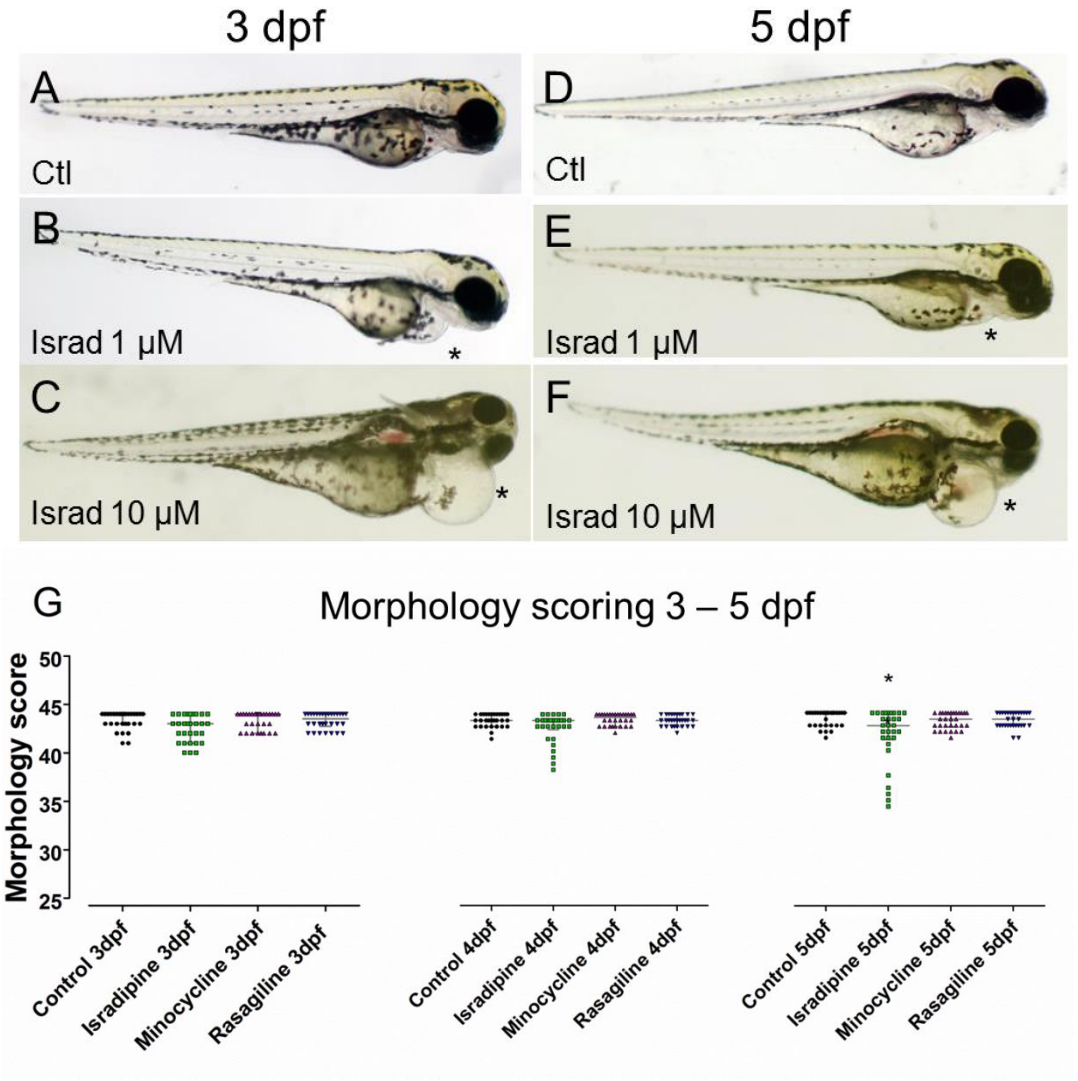

Fig. 6.6: Effects of test drugs alone on morphology up to 5 dpf. Compared with control larvae at 3 dpf (A) and 5 dpf (D) larvae treated with isradipine (10 µM) had severe cardiac oedema at 3 dpf (C*) and 5 dpf (F*), whereas only some larvae in the 1 µM isradipine group had mild oedema (*B and E). (G) Morphology was scored in isradipine, minocycline and rasagiline treated embryos at 3 dpf, 4 dpf, and 5 dpf. At 5 dpf isradipine-treated larvae had significantly lower morphology scores than controls. Data are represented as median and interquartile range with n = 30 larvae per group; *P < 0.05 vs. control.

Locomotor activity testing of each drug at the chosen dose showed no significant changes when compared to other drug treatment groups or the control group as shown in Fig. 6.7. Following toxicity testing, neuroprotective and neurorestorative screen of each drug was assessed.

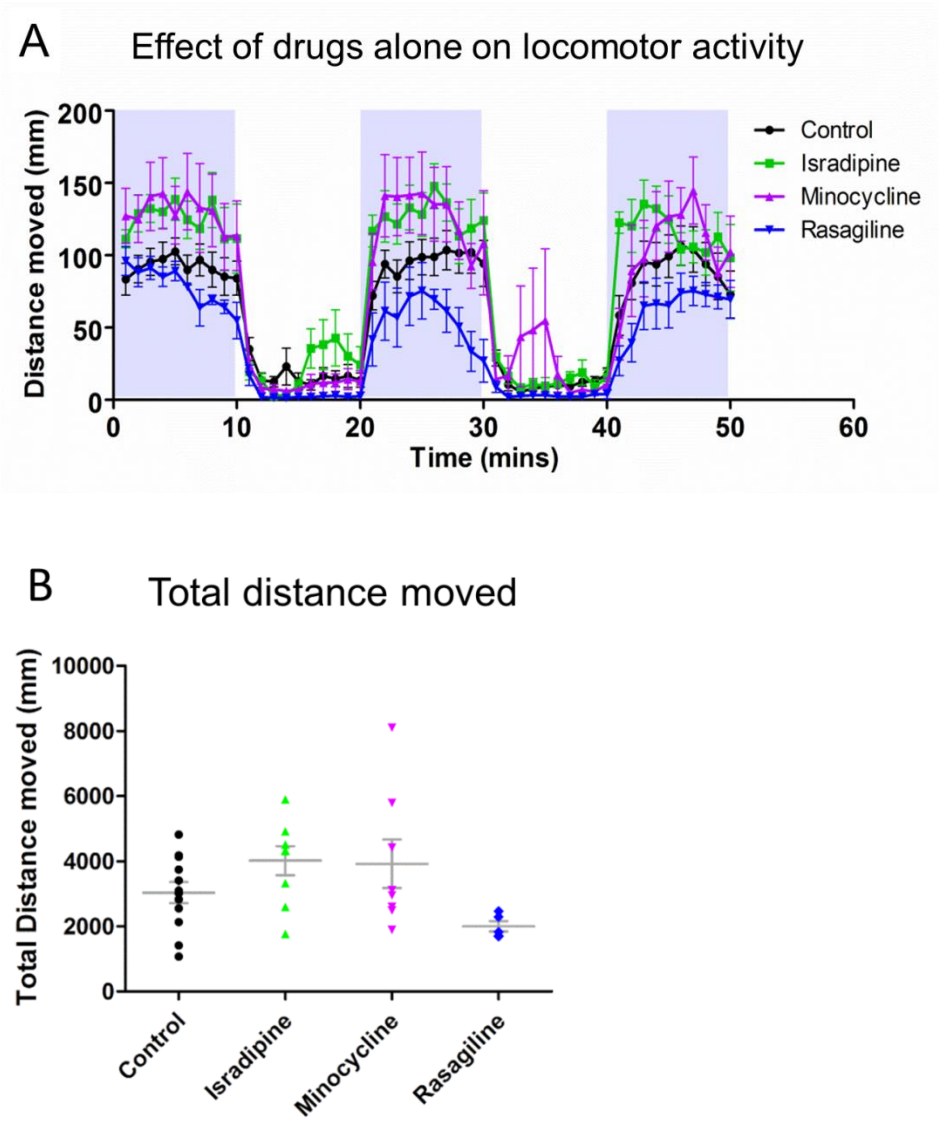

Fig. 6.7: Effect of each test drug alone on locomotor activity. (A) Locomotor activity was assessed at 5 dpf over a 50 min alternating light: dark cycle. (B) Total distance moved was similar in all groups with no significant changes in movement between any of the groups. Data are represented as mean ± SEM, n ≥ 5 separate experiments with 10 larvae per experiment.

6.3.2 Neuroprotective effects of isradipine, minocycline and rasagiline

To test if isradipine, minocycline or rasagiline were neuroprotective, I co-administered these drugs with 6-OHDA for three days (2 to 5 dpf). Locomotor activity and dopaminergic cell counts were assessed at 5 dpf. Co-treatment with isradipine did not prevent the 6-OHDA-induced loss of dopaminergic

neurons (Fig. 6.8 B, C, F; Kruskal-Wallis ANOVA ($\chi 2$ (4) = 21.18; P = 0.0003; Dunn's post hoc test P < 0.05 isradipine vs. control; ns vs. 6-OHDA), whereas pre-treatment with minocycline or rasagiline protected the dopaminergic neurons (Fig. 6.8 D-F, Dunn's post hoc test P < 0.05 vs. 6-OHDA; ns vs. control), demonstrating that minocycline and rasagiline protect dopaminergic neurons, whereas isradipine does not. Overall there were significant differences in distance moved between treatment groups (one-way ANOVA, $F_{(4,\ 18)}$ = 6.435, P = 0.0021). Isradipine co-treatment did not improve locomotor activity in 6-OHDA treated larvae; distance moved was similar to the 6-OHDA only group and significantly lower than controls (Tukey's post-hoc test, P < 0.05 vs. controls). In contrast, larvae co-treated with minocycline moved as much as controls, and significantly more than the 6-OHDA-only group (Fig. 6.8 G, H; Tukey's post-hoc test P < 0.05 vs. 6-OHDA). Similarly, movement of larvae co-treated with 6-OHDA and rasagiline was similar to controls and was significantly higher than in the 6-OHDA-only group (Fig. 6.8 G, H; Tukey's post-hoc test P < 0.05 vs. 6-OHDA), demonstrating functional protection by minocycline and rasagiline in this 6-OHDA zebrafish model of Parkinson's disease and consistent with the dopaminergic cell imaging findings.

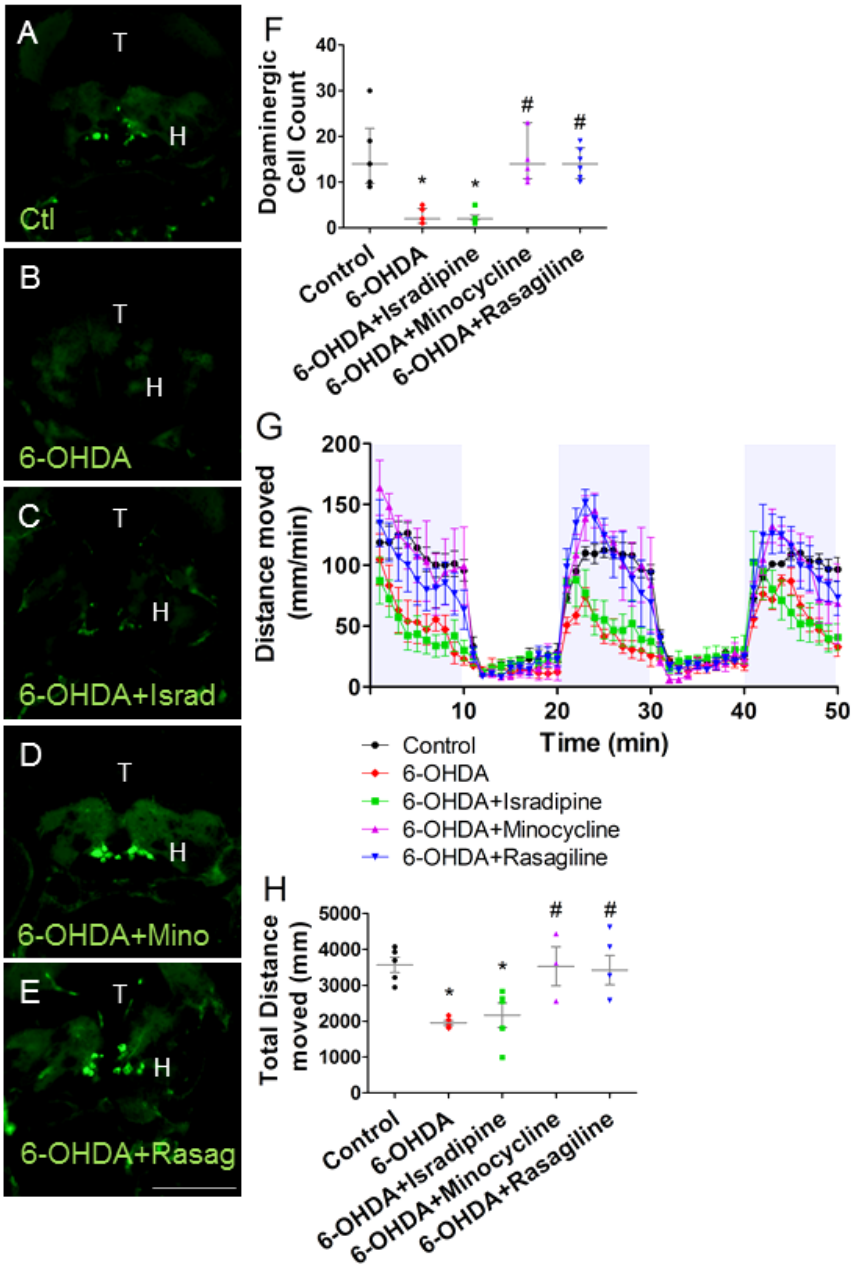

Fig. 6.8: Neuroprotective effects of test drugs. Compared to control (A) 6-OHDA treatment (B) caused dopaminergic loss. Treatment with isradipine (C) did not prevent 6-OHDA-induced dopaminergic cell loss, whereas minocycline (D) or rasagiline (E) treatment was neuroprotective. Scale bar 100 µM ; H, hypothalamus; T, tegmentum. (F) Dopaminergic cell counts following immunohistochemical analysis. Data are represented as median with range, n = 6 larvae per group; **P* < 0.05 vs. control; #*P* < 0.05 vs. 6-OHDA. (G) Distance moved over time in dark (shaded) and light shows that larvae move more in the dark, with severe loss of movement in the dark phase in 6-OHDA treated larvae, which was prevented by co-treatment with rasagiline or minocycline but not with isradipine. Total distance moved over the 50-minute trial (H), shows overall effects of treatments. Data are represented as mean ± SEM, n = 5 separate experiments with 10 larvae per experiment, except minocycline group for which there were 3 separate experiments; **P* < 0.05 vs. control; #*P* < 0.05 vs. 6-OHDA.

6.3.3 Neurorestorative effect of isradipine, minocycline and rasagiline

Having found that co-treatment with rasagiline or minocycline protected dopaminergic neurons from 6-OHDA effects, I wished to determine whether they could restore locomotor activity and dopaminergic cells in larvae pre-treated with 6-OHDA. Having established that exposure to 6-OHDA from 48 hpf to 80 hpf induced similar deficits in locomotor activity and dopaminergic neurons, at 5 dpf, to the longer, 3 day, exposure (Fig. 6.9), I then initiated treatment with isradipine, rasagiline, or minocycline at 80 hpf, just after withdrawal of the 6-OHDA. Treatment with these drugs continued until 120 hpf. There was a significant effect of treatment on dopaminergic cell number (Fig. 6.9 A-F; Kruskal-Wallis ANOVA ($\chi 2$ (4) = 23.72; $P < 0.0001$). Rasagiline treatment from 80 hpf to 120 hpf rescued dopaminergic neurons by 5 dpf (Dunn's post hoc test $P = 0.0005$ vs. 6-OHDA, ns vs. control), whereas treatment with isradipine did not (Dunn's post hoc test $P < 0.05$ vs. control, ns vs. 6-OHDA). Although cell numbers in the minocycline group were similar to controls (Dunn's post-hoc test $P > 0.999$) numbers were not significantly higher than in the 6-OHDA group (Dunn's post-hoc test $P = 0.1097$), indicating a partial recovery of neuronal cell numbers. Overall, there were significant differences in locomotor activity between treatment groups (Fig. 6.9 G, H; one-way ANOVA $F (4, 10) = 8.267$, $P = 0.0033$). Treatment with isradipine from 80 to 120 hpf failed to improve the 6-OHDA-induced locomotor deficit (Fig. 6.9 H; Tukey's post hoc test, $P < 0.05$ vs. control), whereas minocycline or rasagiline treatment restored movement to control levels (Fig. 6.9 H; Tukey's post hoc test, $P < 0.05$ vs. 6-OHDA). Together with the neuronal cell immunohistochemical findings, these results demonstrate that rasagiline restores both locomotor function and dopaminergic neurons in zebrafish larvae, whereas isradipine does not. Minocycline fully restores locomotor function but did not fully restore dopaminergic neurons to control levels.

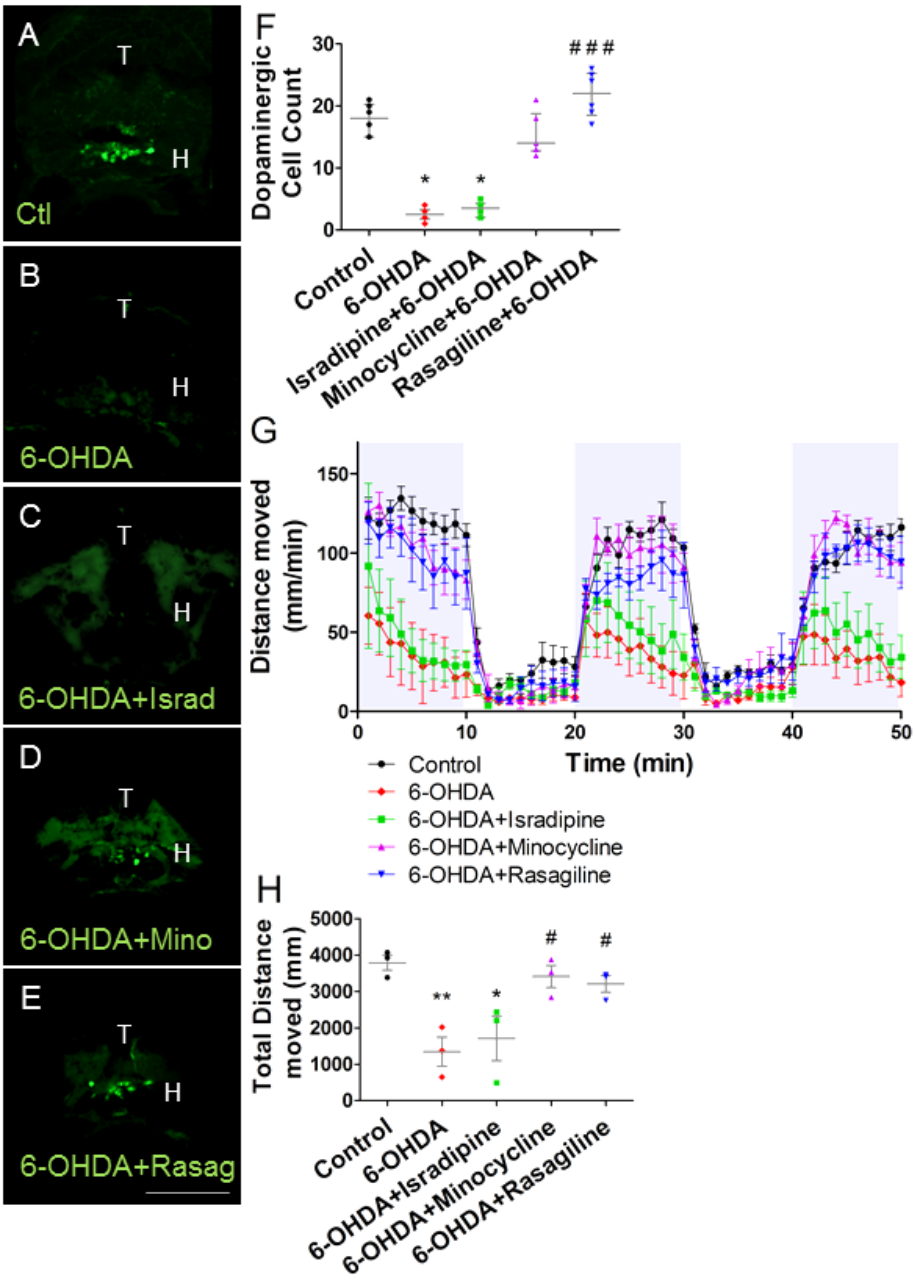

Fig. 6.9: Neurorestorative effects of test drugs. Compared to control (A) 32-hour 6-OHDA treatment (B) caused dopaminergic neuron loss. Subsequent treatment with isradipine (C) did not rescue 6-OHDA-induced dopaminergic cell loss, whereas minocycline partially restored dopaminergic neurons (D) and rasagiline (E) treatment was fully neurorestorative. Scale bar 100 µM ; H, hypothalamus; T, tegmentum. (F) Dopaminergic cell count data are represented as median with range, n = 6 larvae per group; **P* < 0.05 vs. control; ###*P* < 0.0005 vs. 6-OHDA. (G) Distance moved over time in dark (shaded) and light conditions shows that larvae move more in the dark, with severe loss of movement in the dark phase in 6-OHDA treated larvae, which was rescued by post-treatment with rasagiline or minocycline but not with isradipine. Total distance moved per 50-minute trial (H), shows overall effects of treatments. Data are represented as mean ± SEM, n = 3 separate experiments with 10 larvae per experiment; **P* < 0.05 vs. control; ***P* < 0.01 vs. control; #*P* < 0.05 vs. 6-OHDA.

6.4 Discussion

In this study I demonstrate the value of zebrafish larvae for screening putative treatments for Parkinson's disease. For the first time I have shown that exposure of zebrafish larvae to 6-OHDA for 32 hours can induce similar deficits to a 3-day exposure regimen. This allowed me to assess the neurorestorative as well as neuroprotective effects of drug treatments in 5 dpf zebrafish larvae, with the potential for high-throughput screening. Both minocycline and rasagiline demonstrated neuroprotective and neurorestorative properties in this model with no effect of isradipine treatment and only symptomatic effects of L-DOPA.

6.4.1 6-OHDA model and neurodegeneration

In agreement with published reports (Parng et al., 2007; Feng et al., 2014) I found 6-OHDA, when administered for three days, beginning at 48 hpf, produced both robust deficits in locomotor activity and extensive dopaminergic neuronal loss in zebrafish larvae. Significantly, I was also able to demonstrate locomotor deficits and dopaminergic neuronal loss following a shorter, 32 h, exposure to 6-OHDA, thus allowing me to subsequently treat with putative neurorestorative drugs and assess locomotor activity and dopaminergic neurons at 5 dpf. To my knowledge this is the first report of such studies in zebrafish larvae up to 5 dpf; previous studies have tested for neuroprotection at this early larval stage but not for neurorestoration (Zhang et al., 2011; Feng et al., 2014; 2015; 2017). Chong et al. (2013) induced locomotor deficit following two days of 6-OHDA treatment; however they began exposure at 24 hpf. Feng et al. (2014) were unable to induce locomotor deficit in their system following two days of 6-OHDA exposure beginning at 48 hpf and found only significant decreases following 6-OHDA exposure for a minimum of 3 days. Locomotor activity was tracked over 10 minutes with no alternating light and dark cycles. The increased sensitivity of this system may be due to the use of 10-minute dark phases to stimulate movement, coupled with the increased length of locomotor testing.

6.4.2 L-DOPA

The finding that L-DOPA co-treatment could partially restore the 6-OHDA induced locomotor activity deficit is similar to that of Feng et al. (2014).

Despite this, L-DOPA could not prevent dopaminergic neuronal loss in 6-OHDA-treated larvae. This lack of protection of neurons is similar to findings in a zebrafish LRRK2 morpholino knockdown model (Sheng et al., 2010). However, in this morphant authors were unable to monitor locomotor activity as the morphant phenotype was severe; in addition, morpholino effects are typically transient, lasting no more than a few days because the antisense morpholino is diluted by new RNA in surviving larvae. As an alternative knockdown these authors deleted the WD40 domain of zebrafish LRRK2 by splice morpholino and found loss of dopaminergic neurons in the diencephalon and locomotor deficit. In this morphant, L-DOPA rescued locomotor activity but not neuronal loss when treated from 5 – 6 dpf, with locomotor activity measured over 30 seconds (Liu et al., 2008).

Although the majority of studies report a beneficial effect of L-DOPA with significant symptomatic relief, there are a number of conflicting reports which have found a deleterious effect of L-DOPA by selectively damaging dopaminergic neurons through oxidative damage. It has been hypothesised that dopamine aldehyde, the metabolite of dopamine following breakdown by MAO, is toxic to dopaminergic neurons by causing mitochondrial damage to the cell and that monoamine oxidase inhibitors may be an effective treatment to save remaining neurons (Burke et al., 2004). In agreement with this, Stednitz et al. (2015) found that 1 mM L-DOPA exposure in zebrafish larvae caused neuronal loss. This group studied green fluorescent protein (GFP) tagged dopamine transporter neurons in live larvae and found a significant reduction in dopamine transporter expressing neurons as well as an increase in oxidative stress markers following L-DOPA exposure. However, treatment with selegiline, a monoamine oxidase inhibitor, did not cause any improvement of neuronal survival or oxidative stress markers and they suggest that L-DOPA toxicity is caused by overproduction of dopamine itself and not by dopamine aldehyde (Stednitz et al., 2015). In my study, I report no toxic effect of L-DOPA between control and treated embryos. Stednitz et al. (2015) report a depression of locomotor activity following L-DOPA treatment given a 24 hour recovery period. The difference in locomotor activity findings may be due to different time of treatment; Stednitz and

colleagues treated for one day starting at 5 dpf, whereas my treatments were from 2 to 5 dpf.

Despite conflicting findings, the majority are in favour of a beneficial effect of L-DOPA for symptomatic relief of Parkinson's disease. As well as zebrafish and Drosophila animal models of Parkinson's disease, the majority of published literature use rodent models which also report symptomatic relief with no neuroprotective effect (Grigoriadis et al., 1996; Henry et al., 1998; Ponten et al., 2013). My findings correspond to clinical use of L-DOPA to improve movement without neuroprotection and are a further validation of a zebrafish 6-OHDA model for screening of novel treatments for Parkinson's disease.

6.4.3 Isradipine

Calcium channels in recent years have been linked to disease progression through calcium overload and oxidative stress. L-type calcium channels are essential for regulation of dopaminergic neuronal firing and are responsible for the majority of calcium currents entering dopaminergic neurons. In particular, dopamine neurons in the substantia nigra are heavily reliant on the pacemaking activity of these channels for calcium influx into the cell. This is in contrast to dopamine cells in the ventral tegmental area which may explain why these cells are less affected in Parkinson's disease (Puopolo et al., 2007; Guzman et al., 2010; Khaliq and Bean, 2010). One hypothesis on disease pathology states that calcium entry during channel pacemaking requires ATP supplied by mitochondria. Reactive oxygen species are produced as a result of oxidative phosphorylation leading to oxidant stress in the cell. Supporting this theory; genetic models of PARK7 knockout mice have been shown to have increased metabolic stress generated by L-type calcium channels, an effect that was completely abolished by the calcium channel blocker isradipine (Guzman et al., 2010).

Isradipine was put forward for clinical trials for Parkinson's disease, based on the observation that patients treated for hypertension with calcium channel blockers had a lower risk of developing Parkinson's disease (Becker et al., 2008; Ritz et al., 2010; Pasternak et al., 2012). In addition, in vitro and in vivo

animal studies on rodents and primates were promising (Kupsch et al., 1996; Chan et al., 2007; Ilijic et al., 2011). As isradipine is specific to L-type calcium channels it was hypothesised that treatment would protect and rescue dopaminergic cells through inhibition of calcium influx into the cell which would otherwise lead to neuronal vulnerability and subsequent cell death (Kruman and Mattson, 1999; Durante et al., 2004). Despite this, I failed to find any protective or restorative effect in the 6-OHDA zebrafish model, and isradipine itself caused mild heart oedema. Although Ilijic et al. (2011) found that isradipine was neuroprotective in a 6-OHDA mouse model, a recent study by Ortner et al. (2017) found that at therapeutic or even supra-therapeutic doses isradipine was not neuroprotective in their 6-OHDA mouse model of Parkinson's disease. They reason that this is because vascular calcium channels are more sensitive to isradipine than those in the substantia nigra. My findings of mild oedema in zebrafish, without any neuroprotection would agree with this interpretation. These results also correspond to preliminary results from a phase II study in patients which failed to show an effect of this drug as a treatment for Parkinson's disease at the maximum tolerated dose of 10 mg after 52 weeks (Parkinson Study, 2013). In addition, there are several studies which did not find an association between calcium channel blocker use and protection from Parkinson's disease (Ton et al., 2007; Louis et al., 2009; Simon et al., 2010). Therefore, this negative finding with isradipine may be a better reflection of the clinical effects than previous animal studies.

In this Parkinson's disease study, as well as left/right asymmetry studies, during toxicity testing, isradipine was administered at 10 μM. In Parkinson's disease experiments, the drug at this dose was toxic over three days of drug treatment (from 48 hpf – 120 hpf) and resulted in moderate and severe cardiac oedema in zebrafish larvae at 120 hpf therefore, a lower dose was chosen (1 μM) for neuroprotective and neurorestorative testing in Parkinson's disease models. In left/right asymmetry studies, isradipine was administered from 6 – 24 hpf and showed far less toxicity. When morphologically scored at 48 hpf, 55 % of larvae had developed normally, with 20 % showing mild, 20% moderate and 5 % severe defects. Along with

cardiac oedema, the drug when administered before 24 hpf resulted in mild and moderate defects in head and eye formation. These results have shown higher toxicity of isradipine following 72 hours of exposure in the Parkinson's study versus 18 hours of exposure in left/right asymmetry studies irrespective of developmental stage.

6.4.4 Minocycline

There has been increasing evidence for the role of neuroinflammation in neurodegenerative diseases in recent years (De Virgilio et al., 2016). Therefore, there has been an increased interest in the possible neuroprotective effects of anti-inflammatory drugs, with many reports of neuroprotection in genetic and neurotoxic animal models of neurodegenerative diseases through inhibition of microglial activation, anti-apoptotic properties and inhibition of reactive oxygen species production (Ramsey and Tansey, 2014).

Minocycline has been found to be anti-inflammatory, anti-apoptotic, and anti-oxidant in cell culture and animal models (Garrido-Mesa et al., 2013). It is known to inhibit the release of cytochrome C into the cytosol (Zhu et al., 2002) leading to inhibition of caspase-1 and caspase-3, as well as iNOS (Chen et al., 2000). The drug also inhibits microglial activation following 6-OHDA exposure in mice and protects dopaminergic neurons as well as projections to the striatum (He et al., 2001) and this effect may be due to inhibition of the generation of reactive oxygen species by NADPH oxidases (NOX), particularly NOX2 (Hernandes et al., 2013). As well as neuroprotection in 6-OHDA exposed mice, the drug has demonstrated neuroprotective properties in many different animal models. For example, zinc-sulphate exposed rats with targeted loss of dopamine from the nigrostriatal pathway and increased microglial activation in the substantia nigra were treated with minocycline. That study reported reductions in behavioural impairment, dopamine neuronal loss, microglial activation and oxidative stress, demonstrating neuroprotective effects against Zinc-induced degeneration (Kumar et al., 2016). Zhu et al. (2002) report similar protective effects through inhibition of cytochrome C in amylotrophic lateral sclerosis mice. The drug was also found to be neuroprotective against

maneb/paraquat mice models of the disease; in this study minocycline at 30 mg/kg protected against loss of dopaminergic neurons and reduced microglia activation (Dixit et al., 2013). The same neuroprotective properties have been reported in a rodent MPTP model (Wu et al., 2002). Similar findings were found in Drosophila knockdown models of Parkinson's disease where minocycline (0.5 mM) increased locomotor activity and protect LRRK knockdown and wild-type controls from paraquat toxicity indicated by decreased oxidative stress markers (Quintero-Espinosa et al., 2017). Neuroprotective effects of the drug have also been shown in a 6-OHDA zebrafish model (Feng et al., 2014) as well as in an oxidation-induced apoptosis model in zebrafish through L-hydroxyglutaric acid exposure. This study was attempting to develop a high-throughput in vivo model for anti-oxidant drugs such as lipoic acid, minocycline, isatin, cortisone and D-methionine (Parng et al., 2006). Despite numerous studies reporting neuroprotective effects of minocycline none of these studies tested for a neurorestorative effect of the drug. My findings are in agreement with Quintero et al. (2006) who reported that treatment of rodents with minocycline before 6-OHDA-induced loss of dopaminergic neurons was neuroprotective, and treatment with minocycline after 6-OHDA lesion reduced the loss of neurons, but the neurorestorative effect was not statistically significant.

There are many animal studies in support of minocycline drug treatment for Parkinson's disease; while the majority of Parkinson's disease models have reported minocycline to successfully treat disease pathology, one study found unsuccessful treatment including worsening of Parkinson's disease symptoms and enhanced cell death in monkeys following exposure to minocycline (Diguet et al., 2004).

During zebrafish development, NOX2 is stably expressed in the brain by 24 hpf (Weaver et al., 2016), and microglia colonise zebrafish brain between 2.5 and 4.5 dpf, with increased apoptosis causing increased colonization (Casano et al., 2016; Xu et al., 2016). Therefore, it is plausible that the neuroprotection and partial neurorestoration in this study was due to inhibition of NOX2 and microglia. I found that minocycline far exceeded the

efficacy of L-DOPA in neuroprotective and neurorestorative treatment groups during locomotor testing and dopaminergic neuron survival; movement was restored to control levels and large dopamine cell populations were found throughout the zebrafish midbrain as a result of drug treatment. This finding agrees with studies in animal models of the disease which reported an improvement in symptoms of Parkinson's disease. Although very promising results have been found in animal models, to date no clinical benefit has been found in patients (Kieburtz et al., 2008).

In clinical studies, minocycline did not improve motor symptoms after 12 or 18 months (Ravina et al., 2006; Kieburtz et al., 2008) in a small trial (66 to 67 patients in each treatment arm) although a longer trial period may be needed to assess the benefits of this drug in protection or symptomatic treatment of this disease. In patients with Parkinsonian related multiple systems atrophy, it reduced microglial activation in the small sub-group tested but it did not improve motor function (n = 8; (Dodel et al., 2010)). Although the preclinical evidence is promising, further clinical evidence is needed to determine whether minocycline is beneficial in Parkinson's disease patients.

6.4.5 Rasagiline

The MAO B inhibitor, rasagiline, has proven to be a well-tolerated, effective drug improving motor symptoms as monotherapy in early Parkinson's disease or in combination therapy as an adjunct to levodopa at more advanced stages where the drug inhibits the catabolism of dopamine which prolongs the effects of L-DOPA (Olanow et al., 2009; Weintraub et al., 2016).

In contrast to humans, which have two MAO isoforms MAO A and MAO B, zebrafish have only one form of MAO which displays approximately 70% sequence identity to both MAO A and B in the human genome (Setini et al., 2005). Functionally, the zebrafish MAO is also intermediate between MAO A and MAO B (Arslan and Edmondson, 2010). In the current study, mean distance moved in the rasagiline (1 μM) treated larvae was slightly lower than in the control group, although this decrease was not significant. Hyperserotonergic effects have been reported in zebrafish using deprenyl with hypolocomotion and increased 5HT levels when deprenyl was given at

high doses (> 10 μM) and for a longer duration of seven days treatment rather than three days treatment in my study (Sallinen et al., 2009). Although the IC50 for rasagiline in zebrafish has not been reported, in humans it is similar to deprenyl (Geha et al., 2001), therefore I would expect that the effects of the two drugs in zebrafish would be broadly equivalent. Given that I did not find a difference in locomotion, nor was there any cardiac oedema or other morphological signs of toxicity, it is unlikely that it caused hyperserotonergic effects in this study. In addition, in humans, rasagiline alone at therapeutic doses has not been reported to cause serotonin syndrome (Chen, 2011; Fernandes et al., 2011), and no correlation was found between rasagiline treatment, in combination with anti-depressants, and serotonin syndrome in 93 Parkinson's patients over a 36 week period in a clinical trial (Smith et al., 2015).

Rasagiline has been shown to be neuroprotective in vitro (Goggi et al., 2000) and was shown to protect SH-SY5Y neuroblastoma cells from apoptosis (Maruyama et al., 2001). Neuroprotection has also been reported in primates and rodents (Kupsch et al., 2001; Blandini et al., 2004), and Sagi et al. (2007) have shown that rasagiline restored dopaminergic neurons when given subsequent to the neurotoxin MPTP. Blandini et al. (2004) found the same neuroprotection in a 6-OHDA rodent model treated with 0.8 mg/kg of rasagiline. The S-isomer of rasagiline is 1000-fold less potent as a MAO-B inhibitor (Youdim and Weinstock, 2001), yet has been reported to protect dopaminergic cells in vitro and in vivo (Maruyama et al., 2001; Youdim et al., 2001). These findings led to the hypothesis that the neuroprotective effect is due to intrinsic anti-apoptotic properties and not due to its action on monoamine oxidase (Youdim et al., 2001; Akao et al., 2002).

My findings that rasagiline both protects and restores neurons from the effects of 6-OHDA, and normalises locomotor activity, agree with the findings in the cell culture and animal studies above. To my knowledge this is the first report of the neuroprotective and neurorestorative effects of rasagiline in zebrafish.

In clinical studies, rasagiline monotherapy has been found to improve motor scores when compared to placebo groups at a dose of 1 mg / day and reported improved Unified Parkinson's Disease Rating Scale (UPDRS) score (Siderowf et al., 2002; Olanow et al., 2009); however, it did not have any effect on cognitive impairment in Parkinson's patients in a small recent trial (Weintraub et al., 2016). Therefore, it is not yet known whether the neuroprotective evidence from animal studies will be confirmed in the clinic. In another study, beneficial effects on disease symptoms were found at 1 mg a day but no difference to placebo was found at 2mg a day (Olanow et al., 2009). It is now approved as a monotherapy or in combination with other drugs for the symptomatic treatment of the disease and seems to be an efficacious and well-tolerated drug treatment (Stocchi et al., 2015).

6.4.6 Conclusion

Despite a clearer understanding of Parkinson's disease pathology, treatment to date is merely symptomatic; the ultimate goal is to protect against further degeneration and worsening of symptoms. The ability to screen drugs in a relatively high-throughput fashion is key to progress. This study aimed to further develop zebrafish as a model suitable for high-throughput drug screening for Parkinson's disease. Findings for minocycline and rasagiline mirror those of studies in rodents and primates, and although, unlike studies in rodents, isradipine was not neuroprotective in zebrafish, this may better reflect the clinical situation. Thus, I have developed a zebrafish model suitable for high-throughput screening of both putative neuroprotective and neurorestorative therapies for the treatment of Parkinson's disease. This model enabled fast, efficient drug screening that modelled all the principal characteristics of the disease including dopaminergic neuronal loss and locomotor deficit.

Chapter 7: Discussion

The work presented in this thesis aimed to demonstrate the tractability of the zebrafish as a valuable tool for both genetic and pharmacological studies in vertebrate development and disease. The findings in this thesis determined the expression, localisation and function of *nanor* and further strengthened previously reported links to left/right asymmetry development. Early signalling events in left/right patterning such as calcium signalling and FGF signalling were found to be upstream events to *nanor* expression. Calcium channels have also been of recent interest due to neuroprotective and neurorestorative properties of calcium channel inhibitors in Parkinson's disease. This study investigated these findings in a zebrafish 6-OHDA Parkinson's disease model as well as two novel drug treatments in Parkinson's disease, monoamine oxidase inhibitor (rasagiline) and tetracycline antibiotic (minocycline).

Although nanor has three orthologues, these are in lower vertebrates and in invertebrates, with little homology to mammalian proteins. Sequence similarity to a P2X7-like receptor in a genus of fish was the closest sequence match across species. However, low homology to the human P2X7 receptor (27%), and the presence of identified P2X receptors in the zebrafish genome, together with the absence of transmembrane motifs in *nanor* make it unlikely that *nanor* is a zebrafish P2X7 receptor. Similarly, a lack of sequence homology to any P2X7 accessory proteins known to date, mean it is unlikely that *nanor* is an accessory protein for this receptor. Investigation of Nanor protein sequence revealed that Nanor has the potential to be membrane-bound and can be regulated by several kinases. However, because Nanor is a small protein and it has no major domains, other than phosphorylation sites, it is difficult to predict its function through bioinformatic investigations.

Huge upregulation of *nanor* mRNA expression following the mid-blastula transition has been found in this study as well as other studies (Bree et al., 2005; Lee et al., 2013; Perez-Camps et al., 2016). Other genes with a similar expression pattern have functions in cell migration, mesoderm development,

tissue morphogenesis and determination of left/right asymmetry, suggesting that *nanor* may have an important, early function. Localisation in anterior structures implicates potential roles in anterior structure development such as the head, eyes, brain and heart. This is in agreement with previous reports by Dr. O' Boyle who reported defects in brain and eye formation following *nanor* knockdown by morpholino injection along with incorrect cardiac looping caused by a disruption of nodal signalling in the lateral plate mesoderm as well as defects seen in TALEN-injected larvae that were recorded during morphology scoring. Failure of TALEN micro-injection to generate a homozygous mutant line due to embryonic lethality also indicates that *nanor* is an important gene necessary for embryo development.

I set out to investigate protein-protein interactions using co-immunoprecipation with mass spectrometry to identify interacting proteins. Unfortunately problems with the Nanor antibody resulted in unsuccessful identification of Nanor protein interactions. Although there are considerable problems with the antibody, it is possible that Nanor is detected at stages of highest expression, during shield and shield stage, confirming cytosolic location as shown though immunohistochemical staining. However, to confirm this it would be necessary to excise the immunoreactive band from an SDS-PAGE gel and identify the protein at sphere and shield stages through mass spectrometry analysis.

As *nanor* was shown to be sensitive to calcium influx during a period of dorsal forerunner cell migration and these cells are also known to go through a calcium sensitive stage which is necessary for correct migration, this further establishes a function for *nanor* in dorsal forerunner cell movement and Kupffer's vesicle functioning. Due to reports from Dr. O' Boyle of a function of *nanor* in asymmetry development as well as a disruption of Nodal signalling in the lateral plate mesoderm, I was expecting that disruption of Kupffer's vesicle and dorsal forerunner cell migration would reduce *nanor* expression. Surprisingly, *nanor* showed an increase in expression when calcium influx to a cell is inhibited. Similarly *nanor* shows increased expression in response to FGF signalling inhibition during Kupffer's vesicle formation and functioning. As FGF signalling has been established as

upstream to calcium signalling, it is not surprising a similar response is seen in both studies. These results may indicate an inhibitory role of *nanor* in left/right asymmetry development. If this hypothesis of an inhibitory effect on Nodal signalling was correct, increased *nanor* expression may result in opposite findings to knockdown effects of a *nanor* morphilino. However, in some cases similar responses may be seen following knockdown/knockout and overexpression studies by mRNA injection. Previous overexpression studies have been carried out by Dr. O' Boyle and Melissa Walsh during antibody validation as discussed in Section 4.2.1. During this time, morphology defects were also recorded and included cyclopia, disrupted brain structures, and bent bodies. Therefore, disruption to *nanor* gene expression through no expression or over-expression studies has previously been shown to result in the same morphological defects and therefore, may also result in a similar response in gene expression following disruption to homeostasis.

Although little response of nodal-related genes was seen in *elipsa* mutants*, plakoglobin* or isradipine/SU5402 treated embryos, it is likely that a disruption to gene localisation resulted in embryos. Further investigation through in situ hybridisation is needed to confirm.

Elipsa ciliary mutants (TRAF3IP1 gene) have disrupted left/right asymmetry formation due to incorrect cilia formation in Kupffer's vesicle. My study found increased *nanor* in this mutant line. Similarly *plakoglobin* mutants showed increased *nanor* expression, due to links to cilia formation and Kupffer's vesicle function, it is also not surprising that similar responses were seen in both mutant lines. Taken together, pharmacology and mutant experiments indicate a potential early position for *nanor* in the *nodal* signalling cascade. FGF signalling triggers calcium signalling and Kuppfer's vesicle formation which may be where *nanor* has a function along with genes activated early on in the left/right asymmetry development pathway such as TRAF3IP1 gene*, plakoglobin, polaris* and *left/right dynein*. Downstream Nodal signalling is then activated which establishes asymmetric gene expression in the lateral plate mesoderm. Downstream targets control correct left/right asymmetry of developing organs in the zebrafish larvae (Fig. 7.1).

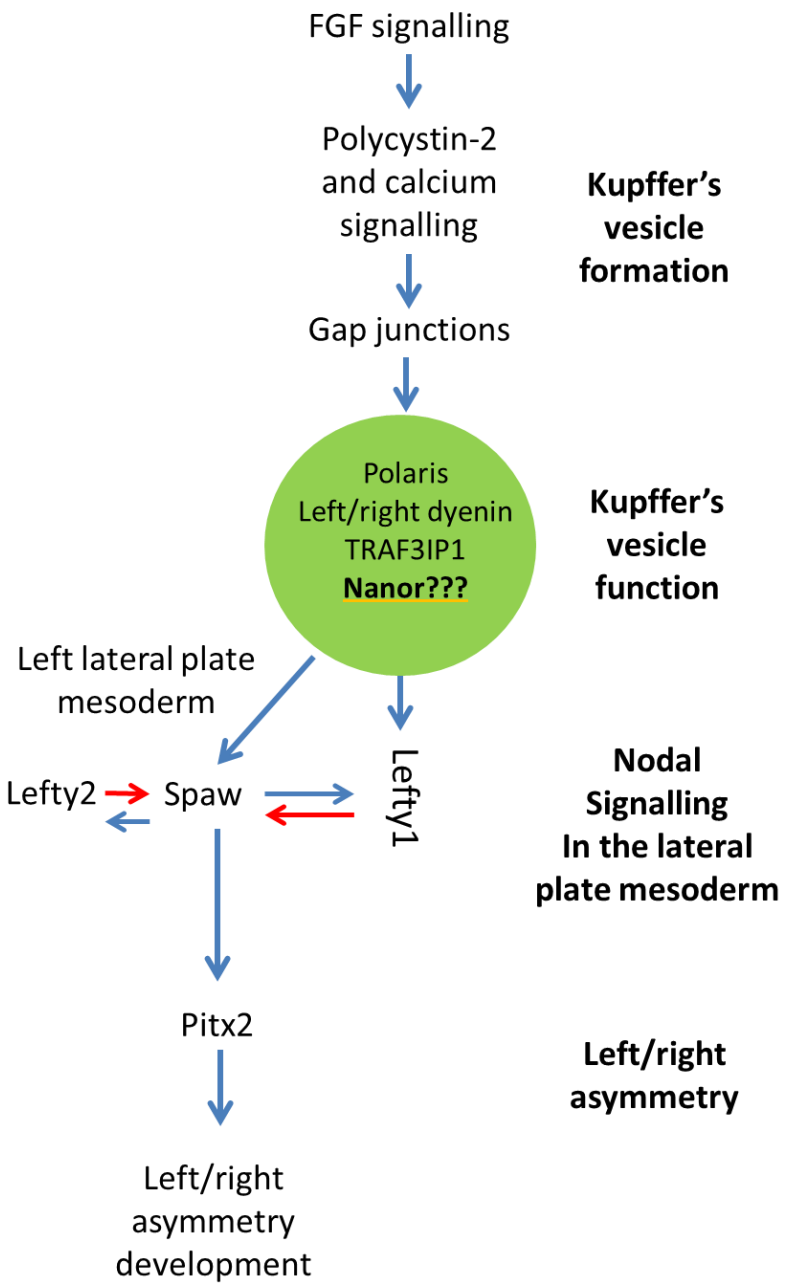

Fig. 7.1: Image showing potential position of *nanor* as well as a simplified signalling cascade leading to asymmetry development. Image constructed using Mercola (2003 ENREF 215) as reference with modifications to indicate when *nanor* may function. Although not all essential genes are included, this image shows a potential position for *nanor* expression in the Nodal signalling pathway.

Calcium channel inhibitors, such as isradipine, have also been used to study neurodegenerative diseases as well as in asymmetry studies. It was reported

in rodent models that these inhibitors were neuroprotective against the loss of dopaminergic neurons. However, to date, clinical findings do not report any beneficial effect of these drugs in patients. Also in my zebrafish model, I found no neuroprotective or neurorestorative effect and my findings appear to more closely model the clinical situation. In contrast, minocycline and rasagiline showed neuroprotective and neurorestorative properties in a 6-OHDA zebrafish model. These results have shown potential for high-throughput screening of neuroprotective and neurorestorative drugs in zebrafish larvae. Larvae show huge potential and are suitable for robotic screening of drug discovery in Parkinson's disease.

Future directions

As it appears knockout of the *nanor* gene is embryonic lethal, further work in this study should aim to identify protein-protein interactions with Nanor through co-immunoprecipitation and mass spectrometry analysis. This would successfully identify interacting proteins and indicate possible signalling roles for *nanor*. To do this, it is necessary to attempt to generate a custom-made anti-nanor antibody. This would require animal immunisation with a redesigned Nanor peptide followed by careful and thorough antibody validation. Careful design of a new peptide would need to avoid sequences with a high risk of cross-reactivity in the protein sample, also peptide length would need to be optimised. A longer peptide sequence will increase immunogenicity but also increase the risk of cross-reactivity and a shorter peptide will improve specificity but may not be immunogenic to the Nanor protein. Peptide selection would have to be correctly validated and aligned to the zebrafish genome to ensure there is a low risk of off-target binding as discussed in Chapter 4.2.1.

Further work on calcium channels and FGF signalling inhibition experiments would give a clear understanding of the extent of inhibition of these signalling events. Nodal signalling investigations in these models should investigate gene localisation by in situ hybridisation to confirm disrupted gene organisation as reported by others. Also further investigations should be

completed to confirm disrupted Kupffer's vesicle formation in embryos following isradipine and SU5402 drug administration.

This validated 6-OHDA zebrafish model of Parkinson's disease could be further utilised to investigate the mechanism of action of the drugs which prevent and restore dopamine neuron loss. For example quantification of inflammatory gene expression changes, such as IL-1β and TNF-α following drug administration. This would give a clear indication of the anti-inflammatory effects of novel drug treatments in Parkinson's disease. This 6-OHDA model has proven to be a valuable model that could be used for high-throughput drug screening of neuroprotective and neurorestorative Parkinson's disease drug treatments in future pre-clinical screening.

The findings in this thesis successfully applied gene editing techniques and pharmacological treatment to study early develop in zebrafish as well as neurotoxic modelling of neurodegenerative disease, Parkinson's disease and subsequent drug screening for disease treatment through toxicity, behavioural and molecular investigations. This has clearly shown the potential and versatility of zebrafish in advancing the field of a range of research fields including early development and neurodegenerative diseases.

Chapter 8: Bibliography

AANES, H., WINATA, C. L., LIN, C. H., CHEN, J. P., SRINIVASAN, K. G., LEE, S. G., LIM, A. Y., HAJAN, H. S., COLLAS, P., BOURQUE, G., GONG, Z., KORZH, V., ALESTROM, P. & MATHAVAN, S. 2011. Zebrafish mRNA sequencing deciphers novelties in transcriptome dynamics during maternal to zygotic transition. *Genome Res,* 21**,** 1328-38.

ADINOLFI, E., KIM, M., YOUNG, M. T., DI VIRGILIO, F. & SURPRENANT, A. 2003. Tyrosine phosphorylation of HSP90 within the P2X7 receptor complex negatively regulates P2X7 receptors. *J Biol Chem,* 278**,** 37344-51.

AGATHON, A., THISSE, C. & THISSE, B. 2003. The molecular nature of the zebrafish tail organizer. *Nature,* 424**,** 448-52.

AITKEN, A. 2002. Functional specificity in 14-3-3 isoform interactions through dimer formation and phosphorylation. Chromosome location of mammalian isoforms and variants. *Plant Mol Biol,* 50**,** 993-1010.

AKAO, Y., MARUYAMA, W., YI, H., SHAMOTO-NAGAI, M., YOUDIM, M. B. H. & NAOI, M. 2002. An anti-Parkinson's disease drug, N-propargyl-1(R)-aminoindan (rasagiline), enhances expression of anti-apoptotic Bcl-2 in human dopaminergic SH-SY5Y cells. *Neuroscience Letters,* 326**,** 105-108.

ALAM, M. & SCHMIDT, W. J. 2002. Rotenone destroys dopaminergic neurons and induces parkinsonian symptoms in rats. *Behav Brain Res,* 136**,** 317-24.

ALEXANDER, J., ROTHENBERG, M., HENRY, G. L. & STAINIER, D. Y. 1999. casanova plays an early and essential role in endoderm formation in zebrafish. *Dev Biol,* 215**,** 343-57.

AMACK, J. D., WANG, X. & YOST, H. J. 2007. Two T-box genes play independent and cooperative roles to regulate morphogenesis of ciliated Kupffer's vesicle in zebrafish. *Dev Biol,* 310**,** 196-210.

AOKI, F., WORRAD, D. M. & SCHULTZ, R. M. 1997. Regulation of transcriptional activity during the first and second cell cycles in the preimplantation mouse embryo. *Dev Biol,* 181**,** 296-307.

ARIAS-CARRION, O., STAMELOU, M., MURILLO-RODRIGUEZ, E., MENENDEZ-GONZALEZ, M. & POPPEL, E. 2010. Dopaminergic reward system: a short integrative review. *Int Arch Med,* 3**,** 24.

ARSLAN, B. K. & EDMONDSON, D. E. 2010. Expression of zebrafish (Danio rerio) monoamine oxidase (MAO) in Pichia pastoris: purification and comparison with human MAO A and MAO B. *Protein Expr Purif,* 70**,** 290-297.

BAKER, M. 2015. Antibody anarchy: A call to order. *Nature,* 527**,** 545-51.

BARR, M. M., DEMODENA, J., BRAUN, D., NGUYEN, C. Q., HALL, D. H. & STERNBERG, P. W. 2001. The Caenorhabditis elegans autosomal dominant polycystic kidney disease gene homologs lov-1 and pkd-2 act in the same pathway. *Curr Biol,* 11**,** 1341-6.

BECK, S., LE GOOD, J. A., GUZMAN, M., BEN HAIM, N., ROY, K., BEERMANN, F. & CONSTAM, D. B. 2002. Extraembryonic proteases regulate Nodal signalling during gastrulation. *Nat Cell Biol,* 4**,** 981-5.

BECKER, C., JICK, S. S. & MEIER, C. R. 2008. Use of antihypertensives and the risk of Parkinson disease. *Neurology,* 70**,** 1438-1444.

BENNETT, M. C., BISHOP, J. F., LENG, Y., CHOCK, P. B., CHASE, T. N. & MOURADIAN, M. M. 1999. Degradation of alpha-synuclein by proteasome. *J Biol Chem,* 274**,** 33855-8.

BENOIT, B., HE, C. H., ZHANG, F., VOTRUBA, S. M., TADROS, W., WESTWOOD, J. T., SMIBERT, C. A., LIPSHITZ, H. D. & THEURKAUF, W. E. 2009. An essential role for the RNA-binding protein Smaug during the Drosophila maternal-to-zygotic transition. *Development,* 136**,** 923-32.

BERG, D., SCHWEITZER, K. J., LEITNER, P., ZIMPRICH, A., LICHTNER, P., BELCREDI, P., BRUSSEL, T., SCHULTE, C., MAASS, S., NAGELE, T., WSZOLEK, Z. K. & GASSER, T. 2005. Type and frequency of mutations in the LRRK2 gene in familial and sporadic Parkinson's disease*. *Brain,* 128**,** 3000-11.

BERRY, C., LA VECCHIA, C. & NICOTERA, P. 2010. Paraquat and Parkinson's disease. *Cell Death Differ,* 17**,** 1115-25.

BESSER, J., BAGOWSKI, C. P., SALAS-VIDAL, E., VAN HEMERT, M. J., BUSSMANN, J. & SPAINK, H. P. 2007. Expression analysis of the family of 14-3-3 proteins in zebrafish development. *Gene Expr Patterns,* 7**,** 511-20.

BETARBET, R., SHERER, T. B., MACKENZIE, G., GARCIA-OSUNA, M., PANOV, A. V. & GREENAMYRE, J. T. 2000. Chronic systemic pesticide exposure reproduces features of Parkinson's disease. *Nat Neurosci,* 3**,** 1301-6.

BEYER, M., GIMSA, U., EYUPOGLU, I. Y., HAILER, N. P. & NITSCH, R. 2000. Phagocytosis of neuronal or glial debris by microglial cells: upregulation of MHC class II expression and multinuclear giant cell formation in vitro. *Glia,* 31**,** 262-6.

BEYER, T., THUMBERGER, T., SCHWEICKERT, A. & BLUM, M. 2012. Connexin26-mediated transfer of laterality cues in Xenopus. *Biol Open,* 1**,** 473-81.

BIANCO, C., ADKINS, H. B., WECHSELBERGER, C., SENO, M., NORMANNO, N., DE LUCA, A., SUN, Y., KHAN, N., KENNEY, N., EBERT, A., WILLIAMS, K. P., SANICOLA, M. & SALOMON, D. S. 2002. Cripto-1 activates nodal- and ALK4-dependent and -independent signaling pathways in mammary epithelial Cells. *Mol Cell Biol,* 22**,** 2586-97.

BILGIC, B., PFEFFERBAUM, A., ROHLFING, T., SULLIVAN, E. V. & ADALSTEINSSON, E. 2012. MRI estimates of brain iron concentration in normal aging using quantitative susceptibility mapping. *Neuroimage,* 59**,** 2625-35.

BISGROVE, B. W., SNARR, B. S., EMRAZIAN, A. & YOST, H. J. 2005. Polaris and Polycystin-2 in dorsal forerunner cells and Kupffer's vesicle are required for specification of the zebrafish left-right axis. *Dev Biol,* 287**,** 274-88.

BLANDINI, F., ARMENTERO, M. T., FANCELLU, R., BLAUGRUND, E. & NAPPI, G. 2004. Neuroprotective effect of rasagiline in a rodent model of Parkinson's disease. *Experimental Neurology,* 187**,** 455-459.

BLOCK, M. L. & HONG, J. S. 2007. Chronic microglial activation and progressive dopaminergic neurotoxicity. *Biochem Soc Trans,* 35**,** 1127-32.

BOCH, J., SCHOLZE, H., SCHORNACK, S., LANDGRAF, A., HAHN, S., KAY, S., LAHAYE, T., NICKSTADT, A. & BONAS, U. 2009. Breaking the code of DNA binding specificity of TAL-type III effectors. *Science,* 326**,** 1509-12.

BOKA, G., ANGLADE, P., WALLACH, D., JAVOY-AGID, F., AGID, Y. & HIRSCH, E. C. 1994. Immunocytochemical analysis of tumor necrosis factor and its receptors in Parkinson's disease. *Neurosci Lett,* 172**,** 151-4.

BONIFATI, V., ROHE, C. F., BREEDVELD, G. J., FABRIZIO, E., DE MARI, M., TASSORELLI, C., TAVELLA, A., MARCONI, R., NICHOLL, D. J., CHIEN, H. F., FINCATI, E., ABBRUZZESE, G., MARINI, P., DE GAETANO, A., HORSTINK, M. W., MAAT-KIEVIT, J. A., SAMPAIO, C., ANTONINI, A., STOCCHI, F., MONTAGNA, P., TONI, V., GUIDI, M., DALLA LIBERA, A., TINAZZI, M., DE PANDIS, F., FABBRINI, G., GOLDWURM, S., DE KLEIN, A., BARBOSA, E., LOPIANO, L., MARTIGNONI, E., LAMBERTI, P., VANACORE, N., MECO, G., OOSTRA, B. A. & ITALIAN PARKINSON GENETICS, N. 2005. Early-onset parkinsonism associated with PINK1 mutations: frequency, genotypes, and phenotypes. *Neurology,* 65**,** 87-95.

BONINI, N. M. & GIASSON, B. I. 2005. Snaring the function of alpha-synuclein. *Cell,* 123**,** 359-61.

BOROVAC, J. A. 2016. Side effects of a dopamine agonist therapy for Parkinson's disease: a mini-review of clinical pharmacology. *Yale J Biol Med,* 89**,** 37-47.

BOROVINA, A., SUPERINA, S., VOSKAS, D. & CIRUNA, B. 2010. Vangl2 directs the posterior tilting and asymmetric localization of motile primary cilia. *Nat Cell Biol,* 12**,** 407-12.

BOUWMEESTER, T., KIM, S., SASAI, Y., LU, B. & DE ROBERTIS, E. M. 1996. Cerberus is a head-inducing secreted factor expressed in the anterior endoderm of Spemann's organizer. *Nature,* 382**,** 595-601.

BOYER, L. A., LEE, T. I., COLE, M. F., JOHNSTONE, S. E., LEVINE, S. S., ZUCKER, J. P., GUENTHER, M. G., KUMAR, R. M., MURRAY, H. L., JENNER, R. G., GIFFORD, D. K., MELTON, D. A., JAENISCH, R. & YOUNG, R. A. 2005. Core transcriptional regulatory circuitry in human embryonic stem cells. *Cell,* 122**,** 947-56.

BRAAK, H., DEL TREDICI, K., RUB, U., DE VOS, R. A., JANSEN STEUR, E. N. & BRAAK, E. 2003. Staging of brain pathology related to sporadic Parkinson's disease. *Neurobiol Aging,* 24**,** 197-211.

BRADFORD, M. M. 1976. A rapid and sensitive method for the quantitation of microgram quantities of protein utilizing the principle of protein-dye binding. *Anal Biochem,* 72**,** 248-54.

BRANNEN, K. C., PANZICA-KELLY, J. M., DANBERRY, T. L. & AUGUSTINE-RAUCH, K. A. 2010. Development of a zebrafish embryo teratogenicity assay and quantitative prediction model. *Birth Defects Res B Dev Reprod Toxicol,* 89**,** 66-77.

BREE, R. T., MCLOUGHLIN, S., JIN, S. W., MCMEEL, O. M., STAINIER, D. Y., GREALY, M. & BYRNES, L. 2005. nanor, a novel zygotic gene, is

expressed initially at the midblastula transition in zebrafish. *Biochem Biophys Res Commun,* 333**,** 722-8.

BRETAUD, S., ALLEN, C., INGHAM, P. W. & BANDMANN, O. 2007. p53-dependent neuronal cell death in a DJ-1-deficient zebrafish model of Parkinson's disease. *J Neurochem,* 100**,** 1626-35.

BRUNDIN, P., LI, J. Y., HOLTON, J. L., LINDVALL, O. & REVESZ, T. 2008. Research in motion: the enigma of Parkinson's disease pathology spread. *Nat Rev Neurosci,* 9**,** 741-5.

BUCHMAN, A. S., NAG, S., SHULMAN, J. M., LIM, A. S., VANDERHORST, V. G., LEURGANS, S. E., SCHNEIDER, J. A. & BENNETT, D. A. 2012. Locus coeruleus neuron density and parkinsonism in older adults without Parkinson's disease. *Mov Disord,* 27**,** 1625-31.

BURKE, W. J., LI, S. W., CHUNG, H. D., RUGGIERO, D. A., KRISTAL, B. S., JOHNSON, E. M., LAMPE, P., KUMAR, V. B., FRANKO, M., WILLIAMS, E. A. & ZAHM, D. S. 2004. Neurotoxicity of MAO metabolites of catecholamine neurotransmitters: Role in neurodegenerative diseases. *Neurotoxicology,* 25**,** 101-115.

BURRE, J., SHARMA, M., TSETSENIS, T., BUCHMAN, V., ETHERTON, M. R. & SUDHOF, T. C. 2010. Alpha-synuclein promotes SNARE-complex assembly in vivo and in vitro. *Science,* 329**,** 1663-7.

BUSSING, I., SLACK, F. J. & GROSSHANS, H. 2008. let-7 microRNAs in development, stem cells and cancer. *Trends Mol Med,* 14**,** 400-9.

CANNON, J. R., TAPIAS, V., NA, H. M., HONICK, A. S., DROLET, R. E. & GREENAMYRE, J. T. 2009. A highly reproducible rotenone model of Parkinson's disease. *Neurobiol Dis,* 34**,** 279-90.

CARRADORI, S., D'ASCENZIO, M., CHIMENTI, P., SECCI, D. & BOLASCO, A. 2014. Selective MAO-B inhibitors: a lesson from natural products. *Mol Divers,* 18**,** 219-43.

CARTWRIGHT, J. H., PIRO, O. & TUVAL, I. 2004. Fluid-dynamical basis of the embryonic development of left-right asymmetry in vertebrates. *Proc Natl Acad Sci U S A,* 101**,** 7234-9.

CASANO, A. M., ALBERT, M. & PERI, F. 2016. Developmental Apoptosis Mediates Entry and Positioning of Microglia in the Zebrafish Brain. *Cell Rep,* 16**,** 897-906.

CEPEDA, C., BUCHWALD, N. A. & LEVINE, M. S. 1993. Neuromodulatory actions of dopamine in the neostriatum are dependent upon the excitatory amino acid receptor subtypes activated. *Proc Natl Acad Sci U S A,* 90**,** 9576-80.

CERMAK, T., DOYLE, E. L., CHRISTIAN, M., WANG, L., ZHANG, Y., SCHMIDT, C., BALLER, J. A., SOMIA, N. V., BOGDANOVE, A. J. & VOYTAS, D. F. 2011. Efficient design and assembly of custom TALEN and other TAL effector-based constructs for DNA targeting. *Nucleic Acids Res,* 39**,** e82.

CHAN, C. S., GUZMAN, J. N., ILIJIC, E., MERCER, J. N., RICK, C., TKATCH, T., MEREDITH, G. E. & SURMEIER, D. J. 2007. 'Rejuvenation' protects neurons in mouse models of Parkinson's disease. *Nature,* 447**,** 1081-1085.

CHAPMAN, E. J. & CARRINGTON, J. C. 2007. Specialization and evolution of endogenous small RNA pathways. *Nat Rev Genet,* 8**,** 884-96.

CHEN, H., ZHANG, S. M., HERNAN, M. A., SCHWARZSCHILD, M. A., WILLETT, W. C., COLDITZ, G. A., SPEIZER, F. E. & ASCHERIO, A. 2003. Nonsteroidal anti-inflammatory drugs and the risk of Parkinson disease. *Arch Neurol,* 60**,** 1059-64.

CHEN, J. J. 2011. Pharmacologic safety concerns in Parkinson's disease: facts and insights. *Int J Neurosci,* 121 Suppl 2**,** 45-52.

CHEN, M., ONA, V. O., LI, M., FERRANTE, R. J., FINK, K. B., ZHU, S., BIAN, J., GUO, L., FARRELL, L. A., HERSCH, S. M., HOBBS, W., VONSATTEL, J. P., CHA, J. H. & FRIEDLANDER, R. M. 2000. Minocycline inhibits caspase-1 and caspase-3 expression and delays mortality in a transgenic mouse model of Huntington disease. *Nat Med,* 6**,** 797-801.

CHOCRON, S., VERHOEVEN, M. C., RENTZSCH, F., HAMMERSCHMIDT, M. & BAKKERS, J. 2007. Zebrafish Bmp4 regulates left-right asymmetry at two distinct developmental time points. *Dev Biol,* 305**,** 577-88.

CHONG, C. M., ZHOU, Z. Y., RAZMOVSKI-NAUMOVSKI, V., CUI, G. Z., ZHANG, L. Q., SA, F., HOI, P. M., CHAN, K. & LEE, S. M. 2013. Danshensu protects against 6-hydroxydopamine-induced damage of PC12 cells in vitro and dopaminergic neurons in zebrafish. *Neurosci Lett,* 543**,** 121-125.

CHRISTIAN, M., CERMAK, T., DOYLE, E. L., SCHMIDT, C., ZHANG, F., HUMMEL, A., BOGDANOVE, A. J. & VOYTAS, D. F. 2010. Targeting DNA double-strand breaks with TAL effector nucleases. *Genetics,* 186**,** 757-61.

CIECHANOVER, A. 1998. The ubiquitin-proteasome pathway: on protein death and cell life. *EMBO J,* 17**,** 7151-60.

CLARK, I. E., DODSON, M. W., JIANG, C., CAO, J. H., HUH, J. R., SEOL, J. H., YOO, S. J., HAY, B. A. & GUO, M. 2006. Drosophila pink1 is required for mitochondrial function and interacts genetically with parkin. *Nature,* 441**,** 1162-6.

COLLER, J. & PARKER, R. 2004. Eukaryotic mRNA decapping. *Annu Rev Biochem,* 73**,** 861-90.

COOPER, M. S. & D'AMICO, L. A. 1996. A cluster of noninvoluting endocytic cells at the margin of the zebrafish blastoderm marks the site of embryonic shield formation. *Dev Biol,* 180**,** 184-98.

COSTA-JUNIOR, H. M., SARMENTO VIEIRA, F. & COUTINHO-SILVA, R. 2011. C terminus of the P2X7 receptor: treasure hunting. *Purinergic Signal,* 7**,** 7-19.

COTZIAS, G. C., PAPAVASI.PS & GELLENE, R. 1969. Modification of Parkinsonism - Chronic Treatment with L-Dopa. *New England Journal of Medicine,* 280**,** 337-338.

COUCHMAN, J. R. 2009. Commercial antibodies: the good, bad, and really ugly. *J Histochem Cytochem,* 57**,** 7-8.

DAHANUKAR, A., WALKER, J. A. & WHARTON, R. P. 1999. Smaug, a novel RNA-binding protein that operates a translational switch in Drosophila. *Mol Cell,* 4**,** 209-18.

DAHLEM, T. J., HOSHIJIMA, K., JURYNEC, M. J., GUNTHER, D., STARKER, C. G., LOCKE, A. S., WEIS, A. M., VOYTAS, D. F. & GRUNWALD, D. J. 2012. Simple methods for generating and

detecting locus-specific mutations induced with TALENs in the zebrafish genome. *PLoS Genet,* 8**,** e1002861.

DAUER, W. & PRZEDBORSKI, S. 2003. Parkinson's disease: Mechanisms and models. *Neuron,* 39**,** 889-909.

DAWSON, T. M. & DAWSON, V. L. 2003. Molecular pathways of neurodegeneration in Parkinson's disease. *Science,* 302**,** 819-22.

DAWSON, T. M., DAWSON, V. L. & SNYDER, S. H. 1993. Nitric oxide as a mediator of neurotoxicity. *NIDA Res Monogr,* 136**,** 258-71; discussion 271-3.

DAWSON, T. M., KO, H. S. & DAWSON, V. L. 2010. Genetic animal models of Parkinson's disease. *Neuron,* 66**,** 646-61.

DAY, B. J., PATEL, M., CALAVETTA, L., CHANG, L. Y. & STAMLER, J. S. 1999. A mechanism of paraquat toxicity involving nitric oxide synthase. *Proc Natl Acad Sci U S A,* 96**,** 12760-5.

DE LAU, L. M. & BRETELER, M. M. 2006. Epidemiology of Parkinson's disease. *Lancet Neurol,* 5**,** 525-35.

DE RENZIS, S., ELEMENTO, O., TAVAZOIE, S. & WIESCHAUS, E. F. 2007. Unmasking activation of the zygotic genome using chromosomal deletions in the Drosophila embryo. *PLoS Biol,* 5**,** e117.

DE VIRGILIO, A., GRECO, A., FABBRINI, G., INGHILLERI, M., RIZZO, M. I., GALLO, A., CONTE, M., ROSATO, C., APPIANI, M. C. & DE VINCENTIIS, M. 2016. Parkinson's disease: Autoimmunity and neuroinflammation. *Autoimmun Rev,* 15**,** 1005-1011.

DELONG, M. R. & WICHMANN, T. 2007. Circuits and circuit disorders of the basal ganglia. *Arch Neurol,* 64**,** 20-4.

DIGUET, E., GROSS, C. E., TISON, F. & BEZARD, E. 2004. Rise and fall of minocycline in neuroprotection: need to promote publication of negative results. *Experimental Neurology,* 189**,** 1-4.

DIXIT, A., SRIVASTAVA, G., VERMA, D., MISHRA, M., SINGH, P. K., PRAKASH, O. & SINGH, M. P. 2013. Minocycline, levodopa and MnTMPyP induced changes in the mitochondrial proteome profile of MPTP and maneb and paraquat mice models of Parkinson's disease. *Biochim Biophys Acta,* 1832**,** 1227-40.

DODEL, R., SPOTTKE, A., GERHARD, A., REUSS, A., REINECKER, S., SCHIMKE, N., TRENKWALDER, C., SIXEL-DORING, F., HERTING, B., KAMM, C., GASSER, T., SAWIRES, M., GESER, F., KOLLENSPERGER, M., SEPPI, K., KLOSS, M., KRAUSE, M., DANIELS, C., DEUSCHL, G., BOTTGER, S., NAUMANN, M., LIPP, A., GRUBER, D., KUPSCH, A., DU, Y. S., TURKHEIMER, F., BROOKS, D. J., KLOCKGETHER, T., POEWE, W., WENNING, G., SCHADE-BRITTINGER, C., OERTEL, W. H. & EGGERT, K. 2010. Minocycline 1-Year Therapy in Multiple-System-Atrophy: Effect on Clinical Symptoms and [C-11] (R)-PK11195 PET (MEMSA-Trial). *Movement Disorders,* 25**,** 97-107.

DOUGAN, S. T., WARGA, R. M., KANE, D. A., SCHIER, A. F. & TALBOT, W. S. 2003. The role of the zebrafish nodal-related genes squint and cyclops in patterning of mesendoderm. *Development,* 130**,** 1837-51.

DRECHSEL, D. A. & PATEL, M. 2008. Role of reactive oxygen species in the neurotoxicity of environmental agents implicated in Parkinson's disease. *Free Radic Biol Med,* 44**,** 1873-86.

DU, Y., GUO, Q., SHAN, M., WU, Y., HUANG, S., ZHAO, H., HONG, H., YANG, M., YANG, X., REN, L., PENG, J., SUN, J., ZHOU, H., LI, S. & SU, B. 2016. Spatial and Temporal Distribution of Dopaminergic Neurons during Development in Zebrafish. *Front Neuroanat,* 10**,** 115.

DU, Y. S., MA, Z. Z., LIN, S. Z., DODEL, R. C., GAO, F., BALES, K. R., TRIARHOU, L. C., CHERNET, E., PERRY, K. W., NELSON, D. L. G., LUECKE, S., PHEBUS, L. A., BYMASTER, F. P. & PAUL, S. M. 2001. Minocycline prevents nigrostriatal dopaminergic neurodegeneration in the MPTP model of Parkinson's disease. *Proceedings of the National Academy of Sciences of the United States of America,* 98**,** 14669-14674.

DUBRULLE, J., MCGREW, M. J. & POURQUIE, O. 2001. FGF signaling controls somite boundary position and regulates segmentation clock control of spatiotemporal Hox gene activation. *Cell,* 106**,** 219-32.

DUNICAN, D. S., RUZOV, A., HACKETT, J. A. & MEEHAN, R. R. 2008. xDnmt1 regulates transcriptional silencing in pre-MBT Xenopus embryos independently of its catalytic function. *Development,* 135**,** 1295-302.

DURANTE, P., CARDENAS, C. G., WHITTAKER, J. A., KITAI, S. T. & SCROGGS, R. S. 2004. Low-threshold L-type calcium channels in rat dopamine neurons. *J Neurophysiol,* 91**,** 1450-1454.

EKSTRAND, M. I., TERZIOGLU, M., GALTER, D., ZHU, S., HOFSTETTER, C., LINDQVIST, E., THAMS, S., BERGSTRAND, A., HANSSON, F. S., TRIFUNOVIC, A., HOFFER, B., CULLHEIM, S., MOHAMMED, A. H., OLSON, L. & LARSSON, N. G. 2007. Progressive parkinsonism in mice with respiratory-chain-deficient dopamine neurons. *Proc Natl Acad Sci U S A,* 104**,** 1325-30.

ESSNER, J. J., AMACK, J. D., NYHOLM, M. K., HARRIS, E. B. & YOST, H. J. 2005. Kupffer's vesicle is a ciliated organ of asymmetry in the zebrafish embryo that initiates left-right development of the brain, heart and gut. *Development,* 132**,** 1247-60.

FAN, H. C., CHEN, S. J., HARN, H. J. & LIN, S. Z. 2013. Parkinson's disease: from genetics to treatments. *Cell Transplant,* 22**,** 639-52.

FANGER, G. R., WIDMANN, C., PORTER, A. C., SATHER, S., JOHNSON, G. L. & VAILLANCOURT, R. R. 1998. 14-3-3 proteins interact with specific MEK kinases. *J Biol Chem,* 273**,** 3476-83.

FANTL, W. J., MUSLIN, A. J., KIKUCHI, A., MARTIN, J. A., MACNICOL, A. M., GROSS, R. W. & WILLIAMS, L. T. 1994. Activation of Raf-1 by 14-3-3 proteins. *Nature,* 371**,** 612-4.

FARKAS, E., DE JONG, G. I., DE VOS, R. A., JANSEN STEUR, E. N. & LUITEN, P. G. 2000. Pathological features of cerebral cortical capillaries are doubled in Alzheimer's disease and Parkinson's disease. *Acta Neuropathol,* 100**,** 395-402.

FEARNLEY, J. M. & LEES, A. J. 1991. Aging and Parkinsons-Disease - Substantia-Nigra Regional Selectivity. *Brain,* 114**,** 2283-2301.

FELDMAN, B., GATES, M. A., EGAN, E. S., DOUGAN, S. T., RENNEBECK, G., SIROTKIN, H. I., SCHIER, A. F. & TALBOT, W. S. 1998. Zebrafish organizer development and germ-layer formation require nodal-related signals. *Nature,* 395**,** 181-5.

FENG, C. W., WEN, Z. H., HUANG, S. Y., HUNG, H. C., CHEN, C. H., YANG, S. N., CHEN, N. F., WANG, H. M., HSIAO, C. D. & CHEN, W. F. 2014. Effects of 6-hydroxydopamine exposure on motor activity and biochemical expression in zebrafish (Danio rerio) larvae. *Zebrafish,* 11**,** 227-239.

FERNANDES, C., REDDY, P. & KESSEL, B. 2011. Rasagiline-induced serotonin syndrome. *Mov Disord,* 26**,** 766-767.

FERRANTE, R. J., SCHULZ, J. B., KOWALL, N. W. & BEAL, M. F. 1997. Systemic administration of rotenone produces selective damage in the striatum and globus pallidus, but not in the substantia nigra. *Brain Res,* 753**,** 157-62.

FERRARI, D., PIZZIRANI, C., ADINOLFI, E., LEMOLI, R. M., CURTI, A., IDZKO, M., PANTHER, E. & DI VIRGILIO, F. 2006. The P2X7 receptor: a key player in IL-1 processing and release. *J Immunol,* 176**,** 3877-83.

FETT, M. E., PILSL, A., PAQUET, D., VAN BEBBER, F., HAASS, C., TATZELT, J., SCHMID, B. & WINKLHOFER, K. F. 2010. Parkin is protective against proteotoxic stress in a transgenic zebrafish model. *PLoS One,* 5**,** e11783.

FISCHER, A., VIEBAHN, C. & BLUM, M. 2002. FGF8 acts as a right determinant during establishment of the left-right axis in the rabbit. *Curr Biol,* 12**,** 1807-16.

FITZGERALD, J. C. & PLUN-FAVREAU, H. 2008. Emerging pathways in genetic Parkinson's disease: autosomal-recessive genes in Parkinson's disease--a common pathway? *FEBS J,* 275**,** 5758-66.

FRANCESCATTO, L., ROTHSCHILD, S. C., MYERS, A. L. & TOMBES, R. M. 2010. The activation of membrane targeted CaMK-II in the zebrafish Kupffer's vesicle is required for left-right asymmetry. *Development,* 137**,** 2753-62.

FURTADO, M. B., SOLLOWAY, M. J., JONES, V. J., COSTA, M. W., BIBEN, C., WOLSTEIN, O., PREIS, J. I., SPARROW, D. B., SAGA, Y., DUNWOODIE, S. L., ROBERTSON, E. J., TAM, P. P. & HARVEY, R. P. 2008. BMP/SMAD1 signaling sets a threshold for the left/right pathway in lateral plate mesoderm and limits availability of SMAD4. *Genes Dev,* 22**,** 3037-49.

GAINETDINOV, R. R., FUMAGALLI, F., WANG, Y. M., JONES, S. R., LEVEY, A. I., MILLER, G. W. & CARON, M. G. 1998. Increased MPTP neurotoxicity in vesicular monoamine transporter 2 heterozygote knockout mice. *J Neurochem,* 70**,** 1973-8.

GARRIDO-MESA, N., ZARZUELO, A. & GALVEZ, J. 2013. Minocycline: far beyond an antibiotic. *Br J Pharmacol,* 169**,** 337-352.

GASSER, A. I., KALBE, E., CALABRESE, P., KESSLER, J., VON ALLMEN, G. & ROSSIER, P. 2011. French translation and normation of the Parkinson Neuropsychometric Dementia Assessment (PANDA). *J Neurol Sci,* 310**,** 189-93.

GEHA, R. M., REBRIN, I., CHEN, K. & SHIH, J. C. 2001. Substrate and inhibitor specificities for human monoamine oxidase A and B are influenced by a single amino acid. *J Biol Chem,* 276**,** 9877-9882.

GERFEN, C. R., ENGBER, T. M., MAHAN, L. C., SUSEL, Z., CHASE, T. N., MONSMA, F. J., JR. & SIBLEY, D. R. 1990. D1 and D2 dopamine

receptor-regulated gene expression of striatonigral and striatopallidal neurons. *Science,* 250**,** 1429-32.

GERHARD, A., PAVESE, N., HOTTON, G., TURKHEIMER, F., ES, M., HAMMERS, A., EGGERT, K., OERTEL, W., BANATI, R. B. & BROOKS, D. J. 2006. In vivo imaging of microglial activation with [11C](R)-PK11195 PET in idiopathic Parkinson's disease. *Neurobiol Dis,* 21**,** 404-12.

GIAIME, E., SUNYACH, C., DRUON, C., SCARZELLO, S., ROBERT, G., GROSSO, S., AUBERGER, P., GOLDBERG, M. S., SHEN, J., HEUTINK, P., POUYSSEGUR, J., PAGES, G., CHECLER, F. & ALVES DA COSTA, C. 2010. Loss of function of DJ-1 triggered by Parkinson's disease-associated mutation is due to proteolytic resistance to caspase-6. *Cell Death Differ,* 17**,** 158-69.

GIRALDEZ, A. J. 2010. microRNAs, the cell's Nepenthe: clearing the past during the maternal-to-zygotic transition and cellular reprogramming. *Curr Opin Genet Dev,* 20**,** 369-75.

GIRALDEZ, A. J., MISHIMA, Y., RIHEL, J., GROCOCK, R. J., VAN DONGEN, S., INOUE, K., ENRIGHT, A. J. & SCHIER, A. F. 2006. Zebrafish MiR-430 promotes deadenylation and clearance of maternal mRNAs. *Science,* 312**,** 75-9.

GOGGI, J., THEOFILOPOULOS, S., RIAZ, S. S., JAUNIAUX, E., STERN, G. M. & BRADFORD, H. F. 2000. The neuronal survival effects of rasagiline and deprenyl on fetal human and rat ventral mesencephalic neurones in culture. *Neuroreport,* 11**,** 3937-3941.

GRIGORIADIS, N., SIMEONIDOU, C., PARASHOS, S. A., ALBANI, M. & GUIBA-TZIAMPIRI, O. 1996. Ontogenetic development of the locomotor response to levodopa in the rat. *Pediatr Neurol,* 14**,** 41-5.

GRITSMAN, K., ZHANG, J., CHENG, S., HECKSCHER, E., TALBOT, W. S. & SCHIER, A. F. 1999. The EGF-CFC protein one-eyed pinhead is essential for nodal signaling. *Cell,* 97**,** 121-32.

GROISMAN, I., JUNG, M. Y., SARKISSIAN, M., CAO, Q. & RICHTER, J. D. 2002. Translational control of the embryonic cell cycle. *Cell,* 109**,** 473-83.

GU, B. J., ZHANG, W., WORTHINGTON, R. A., SLUYTER, R., DAO-UNG, P., PETROU, S., BARDEN, J. A. & WILEY, J. S. 2001. A Glu-496 to Ala polymorphism leads to loss of function of the human P2X7 receptor. *J Biol Chem,* 276**,** 11135-42.

GUZMAN, J. N., SANCHEZ-PADILLA, J., WOKOSIN, D., KONDAPALLI, J., ILIJIC, E., SCHUMACKER, P. T. & SURMEIER, D. J. 2010. Oxidant stress evoked by pacemaking in dopaminergic neurons is attenuated by DJ-1. *Nature,* 468**,** 696-U119.

HABER, S. N. & CALZAVARA, R. 2009. The cortico-basal ganglia integrative network: the role of the thalamus. *Brain Res Bull,* 78**,** 69-74.

HABER, S. N., FUDGE, J. L. & MCFARLAND, N. R. 2000. Striatonigrostriatal pathways in primates form an ascending spiral from the shell to the dorsolateral striatum. *J Neurosci,* 20**,** 2369-82.

HABER, S. N., KUNISHIO, K., MIZOBUCHI, M. & LYND-BALTA, E. 1995. The orbital and medial prefrontal circuit through the primate basal ganglia. *J Neurosci,* 15**,** 4851-67.

HALLIWELL, B. 2001. Role of free radicals in the neurodegenerative diseases: therapeutic implications for antioxidant treatment. *Drugs Aging,* 18**,** 685-716.

HALLIWELL, B. & GUTTERIDGE, J. M. 1986. Oxygen free radicals and iron in relation to biology and medicine: some problems and concepts. *Arch Biochem Biophys,* 246**,** 501-14.

HAMADA, H., MENO, C., WATANABE, D. & SAIJOH, Y. 2002. Establishment of vertebrate left-right asymmetry. *Nat Rev Genet,* 3**,** 103-13.

HAMATANI, T., CARTER, M. G., SHAROV, A. A. & KO, M. S. 2004. Dynamics of global gene expression changes during mouse preimplantation development. *Dev Cell,* 6**,** 117-31.

HARTL, F. U., BRACHER, A. & HAYER-HARTL, M. 2011. Molecular chaperones in protein folding and proteostasis. *Nature,* 475**,** 324-32.

HARVEY, S. A., SEALY, I., KETTLEBOROUGH, R., FENYES, F., WHITE, R., STEMPLE, D. & SMITH, J. C. 2013. Identification of the zebrafish maternal and paternal transcriptomes. *Development,* 140**,** 2703-10.

HAUSER, R. A., ABLER, V., EYAL, E. & ELIAZ, R. E. 2016. Efficacy of rasagiline in early Parkinson's disease: a meta-analysis of data from the TEMPO and ADAGIO studies. *Int J Neurosci,* 126**,** 942-946.

HAYCRAFT, C. J., BANIZS, B., AYDIN-SON, Y., ZHANG, Q., MICHAUD, E. J. & YODER, B. K. 2005. Gli2 and Gli3 localize to cilia and require the intraflagellar transport protein polaris for processing and function. *PLoS Genet,* 1**,** e53.

HE, Y., APPEL, S. & LE, W. 2001. Minocycline inhibits microglial activation and protects nigral cells after 6-hydroxydopamine injection into mouse striatum. *Brain Res,* 909**,** 187-193.

HENGARTNER, M. O. 2000. The biochemistry of apoptosis. *Nature,* 407**,** 770-6.

HENRY, B., CROSSMAN, A. R. & BROTCHIE, J. M. 1998. Characterization of enhanced behavioral responses to L-DOPA following repeated administration in the 6-hydroxydopamine-lesioned rat model of Parkinson's disease. *Experimental Neurology,* 151**,** 334-342.

HENRY, C. J., HUANG, Y., WYNNE, A. M. & GODBOUT, J. P. 2009. Peripheral lipopolysaccharide (LPS) challenge promotes microglial hyperactivity in aged mice that is associated with exaggerated induction of both pro-inflammatory IL-1beta and anti-inflammatory IL-10 cytokines. *Brain Behav Immun,* 23**,** 309-17.

HERNAN, M. A., TAKKOUCHE, B., CAAMANO-ISORNA, F. & GESTAL-OTERO, J. J. 2002. A meta-analysis of coffee drinking, cigarette smoking, and the risk of Parkinson's disease. *Ann Neurol,* 52**,** 276-84.

HERNANDES, M. S., SANTOS, G. D., CAFE-MENDES, C. C., LIMA, L. S., SCAVONE, C., MUNHOZ, C. D. & BRITTO, L. R. 2013. Microglial cells are involved in the susceptibility of NADPH oxidase knockout mice to 6-hydroxy-dopamine-induced neurodegeneration. *PLoS One,* 8**,** e75532.

HERPIN, A., LELONG, C. & FAVREL, P. 2004. Transforming growth factor-beta-related proteins: an ancestral and widespread superfamily of cytokines in metazoans. *Dev Comp Immunol,* 28**,** 461-85.

HIROKAWA, N., TANAKA, Y. & OKADA, Y. 2009. Left-right determination: involvement of molecular motor KIF3, cilia, and nodal flow. *Cold Spring Harb Perspect Biol,* 1**,** a000802.

HIRSCH, E. C., HUNOT, S., DAMIER, P. & FAUCHEUX, B. 1998. Glial cells and inflammation in Parkinson's disease: a role in neurodegeneration? *Ann Neurol,* 44**,** S115-20.

HJEIJ, R., ONOUFRIADIS, A., WATSON, C. M., SLAGLE, C. E., KLENA, N. T., DOUGHERTY, G. W., KURKOWIAK, M., LOGES, N. T., DIGGLE, C. P., MORANTE, N. F., GABRIEL, G. C., LEMKE, K. L., LI, Y., PENNEKAMP, P., MENCHEN, T., KONERT, F., MARTHIN, J. K., MANS, D. A., LETTEBOER, S. J., WERNER, C., BURGOYNE, T., WESTERMANN, C., RUTMAN, A., CARR, I. M., O'CALLAGHAN, C., MOYA, E., CHUNG, E. M., CONSORTIUM, U. K., SHERIDAN, E., NIELSEN, K. G., ROEPMAN, R., BARTSCHERER, K., BURDINE, R. D., LO, C. W., OMRAN, H. & MITCHISON, H. M. 2014. CCDC151 mutations cause primary ciliary dyskinesia by disruption of the outer dynein arm docking complex formation. *Am J Hum Genet,* 95**,** 257-74.

HOGLINGER, G. U., CARRARD, G., MICHEL, P. P., MEDJA, F., LOMBES, A., RUBERG, M., FRIGUET, B. & HIRSCH, E. C. 2003. Dysfunction of mitochondrial complex I and the proteasome: interactions between two biochemical deficits in a cellular model of Parkinson's disease. *J Neurochem,* 86**,** 1297-307.

HONG, S. K. & DAWID, I. B. 2009. FGF-dependent left-right asymmetry patterning in zebrafish is mediated by Ier2 and Fibp1. *Proc Natl Acad Sci U S A,* 106**,** 2230-5.

HOWE, J. A. & NEWPORT, J. W. 1996. A developmental timer regulates degradation of cyclin E1 at the midblastula transition during Xenopus embryogenesis. *Proc Natl Acad Sci U S A,* 93**,** 2060-4.

HOWE, K., CLARK, M. D., TORROJA, C. F., TORRANCE, J., BERTHELOT, C., MUFFATO, M., COLLINS, J. E., HUMPHRAY, S., MCLAREN, K., MATTHEWS, L., MCLAREN, S., SEALY, I., CACCAMO, M., CHURCHER, C., SCOTT, C., BARRETT, J. C., KOCH, R., RAUCH, G. J., WHITE, S., CHOW, W., KILIAN, B., QUINTAIS, L. T., GUERRA-ASSUNCAO, J. A., ZHOU, Y., GU, Y., YEN, J., VOGEL, J. H., EYRE, T., REDMOND, S., BANERJEE, R., CHI, J., FU, B., LANGLEY, E., MAGUIRE, S. F., LAIRD, G. K., LLOYD, D., KENYON, E., DONALDSON, S., SEHRA, H., ALMEIDA-KING, J., LOVELAND, J., TREVANION, S., JONES, M., QUAIL, M., WILLEY, D., HUNT, A., BURTON, J., SIMS, S., MCLAY, K., PLUMB, B., DAVIS, J., CLEE, C., OLIVER, K., CLARK, R., RIDDLE, C., ELLIOT, D., THREADGOLD, G., HARDEN, G., WARE, D., BEGUM, S., MORTIMORE, B., KERRY, G., HEATH, P., PHILLIMORE, B., TRACEY, A., CORBY, N., DUNN, M., JOHNSON, C., WOOD, J., CLARK, S., PELAN, S., GRIFFITHS, G., SMITH, M., GLITHERO, R., HOWDEN, P., BARKER, N., LLOYD, C., STEVENS, C., HARLEY, J., HOLT, K., PANAGIOTIDIS, G., LOVELL, J., BEASLEY, H., HENDERSON, C., GORDON, D., AUGER, K., WRIGHT, D., COLLINS, J., RAISEN, C., DYER, L., LEUNG, K., ROBERTSON, L., AMBRIDGE, K., LEONGAMORNLERT, D., MCGUIRE, S., GILDERTHORP, R., GRIFFITHS, C., MANTHRAVADI, D., NICHOL, S., BARKER, G., et al.

2013. The zebrafish reference genome sequence and its relationship to the human genome. *Nature,* 496**,** 498-503.

HU, Y., FISETTE, P. L., DENLINGER, L. C., GUADARRAMA, A. G., SOMMER, J. A., PROCTOR, R. A. & BERTICS, P. J. 1998. Purinergic receptor modulation of lipopolysaccharide signaling and inducible nitric-oxide synthase expression in RAW 264.7 macrophages. *J Biol Chem,* 273**,** 27170-5.

HUANG, P., XIAO, A., ZHOU, M., ZHU, Z., LIN, S. & ZHANG, B. 2011. Heritable gene targeting in zebrafish using customized TALENs. *Nat Biotechnol,* 29**,** 699-700.

HUNOT, S., BRUGG, B., RICARD, D., MICHEL, P. P., MURIEL, M. P., RUBERG, M., FAUCHEUX, B. A., AGID, Y. & HIRSCH, E. C. 1997. Nuclear translocation of NF-kappaB is increased in dopaminergic neurons of patients with parkinson disease. *Proc Natl Acad Sci U S A,* 94**,** 7531-6.

HUNOT, S., DUGAS, N., FAUCHEUX, B., HARTMANN, A., TARDIEU, M., DEBRE, P., AGID, Y., DUGAS, B. & HIRSCH, E. C. 1999. FcepsilonRII/CD23 is expressed in Parkinson's disease and induces, in vitro, production of nitric oxide and tumor necrosis factor-alpha in glial cells. *J Neurosci,* 19**,** 3440-7.

HUNOT, S. & HIRSCH, E. C. 2003. Neuroinflammatory processes in Parkinson's disease. *Ann Neurol,* 53 Suppl 3**,** S49-58; discussion S58-60.

ILIJIC, E., GUZMAN, J. N. & SURMEIER, D. J. 2011. The L-type channel antagonist isradipine is neuroprotective in a mouse model of Parkinson's disease. *Neurobiol Dis,* 43**,** 364-371.

INDEN, M., KITAMURA, Y., TAKEUCHI, H., YANAGIDA, T., TAKATA, K., KOBAYASHI, Y., TANIGUCHI, T., YOSHIMOTO, K., KANEKO, M., OKUMA, Y., TAIRA, T., ARIGA, H. & SHIMOHAMA, S. 2007. Neurodegeneration of mouse nigrostriatal dopaminergic system induced by repeated oral administration of rotenone is prevented by 4-phenylbutyrate, a chemical chaperone. *J Neurochem,* 101**,** 1491-1504.

INGERSLEV, H. C., PETTERSEN, E. F., JAKOBSEN, R. A., PETERSEN, C. B. & WERGELAND, H. I. 2006. Expression profiling and validation of reference gene candidates in immune relevant tissues and cells from Atlantic salmon (Salmo salar L.). *Mol Immunol,* 43**,** 1194-201.

JAMES, G. & BUTT, A. M. 2001. P2X and P2Y purinoreceptors mediate ATP-evoked calcium signalling in optic nerve glia in situ. *Cell Calcium,* 30**,** 251-9.

JANA, N. R. 2012. Protein homeostasis and aging: role of ubiquitin protein ligases. *Neurochem Int,* 60**,** 443-7.

JANABI, N., CHABRIER, S. & TARDIEU, M. 1996. Endogenous nitric oxide activates prostaglandin F2 alpha production in human microglial cells but not in astrocytes: a study of interactions between eicosanoids, nitric oxide, and superoxide anion (O2-) regulatory pathways. *J Immunol,* 157**,** 2129-35.

JANKOVIC, J. 1984. Progressive Supranuclear Palsy - Clinical and Pharmacologic Update. *Neurologic Clinics,* 2**,** 473-486.

JEANG, K. T. 2012. RNAi in the regulation of mammalian viral infections. *BMC Biol,* 10**,** 58.

JENNER, P. & OLANOW, C. W. 2006. The pathogenesis of cell death in Parkinson's disease. *Neurology,* 66**,** S24-36.

JIN, X., MOHIELDIN, A. M., MUNTEAN, B. S., GREEN, J. A., SHAH, J. V., MYKYTYN, K. & NAULI, S. M. 2014. Cilioplasm is a cellular compartment for calcium signaling in response to mechanical and chemical stimuli. *Cell Mol Life Sci,* 71**,** 2165-78.

KALINDERI, K., BOSTANTJOPOULOU, S. & FIDANI, L. 2016. The genetic background of Parkinson's disease: current progress and future prospects. *Acta Neurol Scand,* 134**,** 314-326.

KANAVOURAS, K., TZATZARAKIS, M. N., MASTORODEMOS, V., PLAITAKIS, A. & TSATSAKIS, A. M. 2011. A case report of motor neuron disease in a patient showing significant level of DDTs, HCHs and organophosphate metabolites in hair as well as levels of hexane and toluene in blood. *Toxicol Appl Pharmacol,* 256**,** 399-404.

KANE, D. A. & KIMMEL, C. B. 1993. The zebrafish midblastula transition. *Development,* 119**,** 447-56.

KAPLAN, S. R., GARD, J. J., PROTONOTARIOS, N., TSATSOPOULOU, A., SPILIOPOULOU, C., ANASTASAKIS, A., SQUARCIONI, C. P., MCKENNA, W. J., THIENE, G., BASSO, C., BROUSSE, N., FONTAINE, G. & SAFFITZ, J. E. 2004. Remodeling of myocyte gap junctions in arrhythmogenic right ventricular cardiomyopathy due to a deletion in plakoglobin (Naxos disease). *Heart Rhythm,* 1**,** 3-11.

KARNOVSKY, A. & KLYMKOWSKY, M. W. 1995. Anterior axis duplication in Xenopus induced by the over-expression of the cadherin-binding protein plakoglobin. *Proc Natl Acad Sci U S A,* 92**,** 4522-6.

KEMP, J. M. & POWELL, T. P. 1971. The connexions of the striatum and globus pallidus: synthesis and speculation. *Philos Trans R Soc Lond B Biol Sci,* 262**,** 441-57.

KHALIQ, Z. M. & BEAN, B. P. 2010. Pacemaking in dopaminergic ventral tegmental area neurons: depolarizing drive from background and voltage-dependent sodium conductances. *J Neurosci,* 30**,** 7401-13.

KIEBURTZ, K., TILLEY, B., RAVINA, B., GALPERN, W., SHANNON, K., TANNER, C., WOOTEN, G. F. & INVESTIGATORS, N. N.-P. 2008. A pilot clinical trial of creatine and minocycline in early Parkinson disease: 18-month results. *Clinical Neuropharmacology,* 31**,** 141-150.

KIM, S. U. & DE VELLIS, J. 2005. Microglia in health and disease. *J Neurosci Res,* 81**,** 302-13.

KIMELMAN, D., KIRSCHNER, M. & SCHERSON, T. 1987. The events of the midblastula transition in Xenopus are regulated by changes in the cell cycle. *Cell,* 48**,** 399-407.

KIMMEL, C. B., BALLARD, W. W., KIMMEL, S. R., ULLMANN, B. & SCHILLING, T. F. 1995. Stages of embryonic development of the zebrafish. *Dev Dyn,* 203**,** 253-310.

KITADA, T., ASAKAWA, S., HATTORI, N., MATSUMINE, H., YAMAMURA, Y., MINOSHIMA, S., YOKOCHI, M., MIZUNO, Y. & SHIMIZU, N. 1998. Mutations in the parkin gene cause autosomal recessive juvenile parkinsonism. *Nature,* 392**,** 605-8.

KNOTT, C., STERN, G. & WILKIN, G. P. 2000. Inflammatory regulators in Parkinson's disease: iNOS, lipocortin-1, and cyclooxygenases-1 and -2. *Mol Cell Neurosci,* 16**,** 724-39.

KOBAYASHI, D., IIJIMA, N., HAGIWARA, H., KAMURA, K., TAKEDA, H. & YOKOYAMA, T. 2010. Characterization of the medaka (Oryzias latipes) primary ciliary dyskinesia mutant, jaodori: Redundant and distinct roles of dynein axonemal intermediate chain 2 (dnai2) in motile cilia. *Dev Biol,* 347**,** 62-70.

KOBAYASHI, Y., HAYASHI, R., QUANTOCK, A. J. & NISHIDA, K. 2017. Generation of a TALEN-mediated, p63 knock-in in human induced pluripotent stem cells. *Stem Cell Res,* 25**,** 256-265.

KREILING, J. A., BALANTAC, Z. L., CRAWFORD, A. R., REN, Y., TOURE, J., ZCHUT, S., KOCHILAS, L. & CRETON, R. 2008. Suppression of the endoplasmic reticulum calcium pump during zebrafish gastrulation affects left-right asymmetry of the heart and brain. *Mech Dev,* 125**,** 396-410.

KRUMAN, II & MATTSON, M. P. 1999. Pivotal role of mitochondrial calcium uptake in neural cell apoptosis and necrosis. *J Neurochem,* 72**,** 529-540.

KUMAR, V., SINGH, B. K., CHAUHAN, A. K., SINGH, D., PATEL, D. K. & SINGH, C. 2016. Minocycline Rescues from Zinc-Induced Nigrostriatal Dopaminergic Neurodegeneration: Biochemical and Molecular Interventions. *Mol Neurobiol,* 53**,** 2761-77.

KUPSCH, A., SAUTTER, J., GOTZ, M. E., BREITHAUPT, W., SCHWARZ, J., YOUDIM, M. B., RIEDERER, P., GERLACH, M. & OERTEL, W. H. 2001. Monoamine oxidase-inhibition and MPTP-induced neurotoxicity in the non-human primate: comparison of rasagiline (TVP 1012) with selegiline. *J Neural Transm (Vienna),* 108**,** 985-1009.

KUPSCH, A., SAUTTER, J., SCHWARZ, J., RIEDERER, P., GERLACH, M. & OERTEL, W. H. 1996. 1-Methyl-4-phenyl-1,2,3,6-tetrahydropyridine-induced neurotoxicity in non-human primates is antagonized by pretreatment with nimodipine at the nigral, but not at the striatal level. *Brain Research,* 741**,** 185-196.

LAI, B. C., MARION, S. A., TESCHKE, K. & TSUI, J. K. 2002. Occupational and environmental risk factors for Parkinson's disease. *Parkinsonism Relat Disord,* 8**,** 297-309.

LANGLEY, A. R., SMITH, J. C., STEMPLE, D. L. & HARVEY, S. A. 2014. New insights into the maternal to zygotic transition. *Development,* 141**,** 3834-41.

LANGSTON, J. W. & BALLARD, P. A., JR. 1983. Parkinson's disease in a chemist working with 1-methyl-4-phenyl-1,2,5,6-tetrahydropyridine. *N Engl J Med,* 309**,** 310.

LAOUKILI, J., PERRET, E., WILLEMS, T., MINTY, A., PARTHOENS, E., HOUCINE, O., COSTE, A., JORISSEN, M., MARANO, F., CAPUT, D. & TOURNIER, F. 2001. IL-13 alters mucociliary differentiation and ciliary beating of human respiratory epithelial cells. *J Clin Invest,* 108**,** 1817-24.

LAU, J. M., WU, C. & MUSLIN, A. J. 2006. Differential role of 14-3-3 family members in Xenopus development. *Dev Dyn,* 235**,** 1761-76.

LAWSON, L. J., PERRY, V. H., DRI, P. & GORDON, S. 1990. Heterogeneity in the distribution and morphology of microglia in the normal adult mouse brain. *Neuroscience,* 39**,** 151-70.

LEE, M. S., HWANG, K. S., OH, H. W., JI-AE, K., KIM, H. T., CHO, H. S., LEE, J. J., YEONG KO, J., CHOI, J. H., JEONG, Y. M., YOU, K. H., KIM, J., PARK, D. S., NAM, K. H., AIZAWA, S., KIYONARI, H., SHIOI, G., PARK, J. H., ZHOU, W., KIM, N. S. & KIM, C. H. 2015. IFT46 plays an essential role in cilia development. *Dev Biol,* 400**,** 248-57.

LEE, M. T., BONNEAU, A. R., TAKACS, C. M., BAZZINI, A. A., DIVITO, K. R., FLEMING, E. S. & GIRALDEZ, A. J. 2013. Nanog, Pou5f1 and SoxB1 activate zygotic gene expression during the maternal-to-zygotic transition. *Nature,* 503**,** 360-4.

LENHART, K. F., LIN, S. Y., TITUS, T. A., POSTLETHWAIT, J. H. & BURDINE, R. D. 2011. Two additional midline barriers function with midline lefty1 expression to maintain asymmetric Nodal signaling during left-right axis specification in zebrafish. *Development,* 138**,** 4405-10.

LEVIN, M. & MERCOLA, M. 1998. Gap junctions are involved in the early generation of left-right asymmetry. *Dev Biol,* 203**,** 90-105.

LI, T., HUANG, S., JIANG, W. Z., WRIGHT, D., SPALDING, M. H., WEEKS, D. P. & YANG, B. 2011. TAL nucleases (TALNs): hybrid proteins composed of TAL effectors and FokI DNA-cleavage domain. *Nucleic Acids Res,* 39**,** 359-72.

LIANG, H. L., NIEN, C. Y., LIU, H. Y., METZSTEIN, M. M., KIROV, N. & RUSHLOW, C. 2008. The zinc-finger protein Zelda is a key activator of the early zygotic genome in Drosophila. *Nature,* 456**,** 400-3.

LIU, Y. C., ELLY, C., YOSHIDA, H., BONNEFOY-BERARD, N. & ALTMAN, A. 1996. Activation-modulated association of 14-3-3 proteins with Cbl in T cells. *J Biol Chem,* 271**,** 14591-5.

LIU, Z., WANG, X., YU, Y., LI, X., WANG, T., JIANG, H., REN, Q., JIAO, Y., SAWA, A., MORAN, T., ROSS, C. A., MONTELL, C. & SMITH, W. W. 2008. A Drosophila model for LRRK2-linked parkinsonism. *Proc Natl Acad Sci U S A,* 105**,** 2693-8.

LOH, Y. H., WU, Q., CHEW, J. L., VEGA, V. B., ZHANG, W., CHEN, X., BOURQUE, G., GEORGE, J., LEONG, B., LIU, J., WONG, K. Y., SUNG, K. W., LEE, C. W., ZHAO, X. D., CHIU, K. P., LIPOVICH, L., KUZNETSOV, V. A., ROBSON, P., STANTON, L. W., WEI, C. L., RUAN, Y., LIM, B. & NG, H. H. 2006. The Oct4 and Nanog transcription network regulates pluripotency in mouse embryonic stem cells. *Nat Genet,* 38**,** 431-40.

LONG, S., AHMAD, N. & REBAGLIATI, M. 2003. The zebrafish nodal-related gene southpaw is required for visceral and diencephalic left-right asymmetry. *Development,* 130**,** 2303-16.

LOUIS, E. D., BENITO-LEON, J., BERMEJO-PAREJA, F. & NEUROLOGICAL DISORDERS IN CENTRAL SPAIN STUDY, G. 2009. Antihypertensive agents and risk of Parkinson's disease, essential tremor and dementia: a population-based prospective study (NEDICES). *Neuroepidemiology,* 33**,** 286-292.

LU, X., LI, J. M., ELEMENTO, O., TAVAZOIE, S. & WIESCHAUS, E. F. 2009. Coupling of zygotic transcription to mitotic control at the Drosophila mid-blastula transition. *Development,* 136**,** 2101-10.

MA, J., FLEMR, M., STRNAD, H., SVOBODA, P. & SCHULTZ, R. M. 2013. Maternally recruited DCP1A and DCP2 contribute to messenger RNA degradation during oocyte maturation and genome activation in mouse. *Biol Reprod,* 88**,** 11.

MA, S. Y., CILIAX, B. J., STEBBINS, G., JAFFAR, S., JOYCE, J. N., COCHRAN, E. J., KORDOWER, J. H., MASH, D. C., LEVEY, A. I. & MUFSON, E. J. 1999. Dopamine transporter-immunoreactive neurons decrease with age in the human substantia nigra. *J Comp Neurol,* 409**,** 25-37.

MANNING-BOG, A. B., MCCORMACK, A. L., LI, J., UVERSKY, V. N., FINK, A. L. & DI MONTE, D. A. 2002. The herbicide paraquat causes up-regulation and aggregation of alpha-synuclein in mice: paraquat and alpha-synuclein. *J Biol Chem,* 277**,** 1641-4.

MARTIN, E. D., MORIARTY, M. A., BYRNES, L. & GREALY, M. 2009. Plakoglobin has both structural and signalling roles in zebrafish development. *Dev Biol,* 327**,** 83-96.

MARUYAMA, W., YOUDIM, M. B. & NAOI, M. 2001. Antiapoptotic properties of rasagiline, N-propargylamine-1(R)-aminoindan, and its optical (S)-isomer, TV1022. *Ann N Y Acad Sci,* 939**,** 320-329.

MATHAVAN, S., LEE, S. G., MAK, A., MILLER, L. D., MURTHY, K. R., GOVINDARAJAN, K. R., TONG, Y., WU, Y. L., LAM, S. H., YANG, H., RUAN, Y., KORZH, V., GONG, Z., LIU, E. T. & LUFKIN, T. 2005. Transcriptome analysis of zebrafish embryogenesis using microarrays. *PLoS Genet,* 1**,** 260-76.

MCGEER, P. L., ITAGAKI, S., BOYES, B. E. & MCGEER, E. G. 1988. Reactive microglia are positive for HLA-DR in the substantia nigra of Parkinson's and Alzheimer's disease brains. *Neurology,* 38**,** 1285-91.

MCGRATH, J. & BRUECKNER, M. 2003. Cilia are at the heart of vertebrate left-right asymmetry. *Curr Opin Genet Dev,* 13**,** 385-92.

MCKINLEY, E. T., BARANOWSKI, T. C., BLAVO, D. O., CATO, C., DOAN, T. N. & RUBINSTEIN, A. L. 2005. Neuroprotection of MPTP-induced toxicity in zebrafish dopaminergic neurons. *Brain Res Mol Brain Res,* 141**,** 128-37.

MCNAUGHT, K. S., BELIZAIRE, R., ISACSON, O., JENNER, P. & OLANOW, C. W. 2003. Altered proteasomal function in sporadic Parkinson's disease. *Exp Neurol,* 179**,** 38-46.

MEEKER, N. D., HUTCHINSON, S. A., HO, L. & TREDE, N. S. 2007. Method for isolation of PCR-ready genomic DNA from zebrafish tissues. *Biotechniques,* 43**,** 610, 612, 614.

MELBY, A. E., WARGA, R. M. & KIMMEL, C. B. 1996. Specification of cell fates at the dorsal margin of the zebrafish gastrula. *Development,* 122**,** 2225-37.

MELO, K. M., OLIVEIRA, R., GRISOLIA, C. K., DOMINGUES, I., PIECZARKA, J. C., DE SOUZA FILHO, J. & NAGAMACHI, C. Y. 2015. Short-term exposure to low doses of rotenone induces developmental, biochemical, behavioral, and histological changes in fish. *Environ Sci Pollut Res Int,* 22**,** 13926-38.

MELTON, C., JUDSON, R. L. & BLELLOCH, R. 2010. Opposing microRNA families regulate self-renewal in mouse embryonic stem cells. *Nature,* 463**,** 621-6.

MENDEZ, R. & RICHTER, J. D. 2001. Translational control by CPEB: a means to the end. *Nat Rev Mol Cell Biol,* 2**,** 521-9.

MENO, C., SHIMONO, A., SAIJOH, Y., YASHIRO, K., MOCHIDA, K., OHISHI, S., NOJI, S., KONDOH, H. & HAMADA, H. 1998. lefty-1 is required for left-right determination as a regulator of lefty-2 and nodal. *Cell,* 94**,** 287-97.

MERCOLA, M. 2003. Left-right asymmetry: nodal points. *J Cell Sci,* 116**,** 3251-7.

MEYERS, E. N. & MARTIN, G. R. 1999. Differences in left-right axis pathways in mouse and chick: functions of FGF8 and SHH. *Science,* 285**,** 403-6.

MILLER, J. C., TAN, S., QIAO, G., BARLOW, K. A., WANG, J., XIA, D. F., MENG, X., PASCHON, D. E., LEUNG, E., HINKLEY, S. J., DULAY, G. P., HUA, K. L., ANKOUDINOVA, I., COST, G. J., URNOV, F. D., ZHANG, H. S., HOLMES, M. C., ZHANG, L., GREGORY, P. D. & REBAR, E. J. 2011. A TALE nuclease architecture for efficient genome editing. *Nat Biotechnol,* 29**,** 143-8.

MIYAMOTO, K., SUZUKI, K. T., SUZUKI, M., SAKANE, Y., SAKUMA, T., HERBERG, S., SIMEONE, A., SIMPSON, D., JULLIEN, J., YAMAMOTO, T. & GURDON, J. B. 2015. The Expression of TALEN before Fertilization Provides a Rapid Knock-Out Phenotype in Xenopus laevis Founder Embryos. *PLoS One,* 10**,** e0142946.

MOGI, M., HARADA, M., KONDO, T., RIEDERER, P., INAGAKI, H., MINAMI, M. & NAGATSU, T. 1994a. Interleukin-1 beta, interleukin-6, epidermal growth factor and transforming growth factor-alpha are elevated in the brain from parkinsonian patients. *Neurosci Lett,* 180**,** 147-50.

MOGI, M., HARADA, M., RIEDERER, P., NARABAYASHI, H., FUJITA, K. & NAGATSU, T. 1994b. Tumor necrosis factor-alpha (TNF-alpha) increases both in the brain and in the cerebrospinal fluid from parkinsonian patients. *Neurosci Lett,* 165**,** 208-10.

MORENS, D. M., GRANDINETTI, A., REED, D., WHITE, L. R. & ROSS, G. W. 1995. Cigarette smoking and protection from Parkinson's disease: false association or etiologic clue? *Neurology,* 45**,** 1041-51.

MOYER, J. H., LEE-TISCHLER, M. J., KWON, H. Y., SCHRICK, J. J., AVNER, E. D., SWEENEY, W. E., GODFREY, V. L., CACHEIRO, N. L., WILKINSON, J. E. & WOYCHIK, R. P. 1994. Candidate gene associated with a mutation causing recessive polycystic kidney disease in mice. *Science,* 264**,** 1329-33.

MULLER, T. 2015. Catechol-O-methyltransferase inhibitors in Parkinson's disease. *Drugs,* 75**,** 157-74.

MURCIA, N. S., RICHARDS, W. G., YODER, B. K., MUCENSKI, M. L., DUNLAP, J. R. & WOYCHIK, R. P. 2000. The Oak Ridge Polycystic Kidney (orpk) disease gene is required for left-right axis determination. *Development,* 127**,** 2347-55.

MUSLIN, A. J., LAU, J. 2004. *Differential Functions of 14-3-3 Isoforms in Vertebrate Development*, Elsevier.

NAKAYAMA, T., FISHER, M., NAKAJIMA, K., ODELEYE, A. O., ZIMMERMAN, K. B., FISH, M. B., YAOITA, Y., CHOJNOWSKI, J. L., LAUDERDALE, J. D., NETLAND, P. A. & GRAINGER, R. M. 2015. Xenopus pax6 mutants affect eye development and other organ systems, and have phenotypic similarities to human aniridia patients. *Dev Biol,* 408**,** 328-44.

NARENDRA, D. P., JIN, S. M., TANAKA, A., SUEN, D. F., GAUTIER, C. A., SHEN, J., COOKSON, M. R. & YOULE, R. J. 2010. PINK1 is selectively stabilized on impaired mitochondria to activate Parkin. *PLoS Biol,* 8**,** e1000298.

NAULI, S. M., ALENGHAT, F. J., LUO, Y., WILLIAMS, E., VASSILEV, P., LI, X., ELIA, A. E., LU, W., BROWN, E. M., QUINN, S. J., INGBER, D. E. & ZHOU, J. 2003. Polycystins 1 and 2 mediate mechanosensation in the primary cilium of kidney cells. *Nat Genet,* 33**,** 129-37.

NELLORE, J. & P, N. 2015. Paraquat exposure induces behavioral deficits in larval zebrafish during the window of dopamine neurogenesis. *Toxicol Rep,* 2**,** 950-956.

NEUGEBAUER, J. M., AMACK, J. D., PETERSON, A. G., BISGROVE, B. W. & YOST, H. J. 2009. FGF signalling during embryo development regulates cilia length in diverse epithelia. *Nature,* 458**,** 651-4.

NEUGEBAUER, J. M. & YOST, H. J. 2014. FGF signaling is required for brain left-right asymmetry and brain midline formation. *Dev Biol,* 386**,** 123-34.

NEWPORT, J. & KIRSCHNER, M. 1982. A major developmental transition in early Xenopus embryos: II. Control of the onset of transcription. *Cell,* 30**,** 687-96.

NICOT, N., HAUSMAN, J. F., HOFFMANN, L. & EVERS, D. 2005. Housekeeping gene selection for real-time RT-PCR normalization in potato during biotic and abiotic stress. *J Exp Bot,* 56**,** 2907-14.

NONAKA, S., TANAKA, Y., OKADA, Y., TAKEDA, S., HARADA, A., KANAI, Y., KIDO, M. & HIROKAWA, N. 1998. Randomization of left-right asymmetry due to loss of nodal cilia generating leftward flow of extraembryonic fluid in mice lacking KIF3B motor protein. *Cell,* 95**,** 829-37.

NORRIS, D. P. 2012. Cilia, calcium and the basis of left-right asymmetry. *BMC Biol,* 10**,** 102.

O'BOYLE, S. 2008. *The activation of zygotic genes at the midblastula transition and the developmental role on one such novel gene, nanor, in the zebrafish embryo.* PhD, National University of Ireland, Galway.

OBESO, J. A., RODRIGUEZ-OROZ, M. C., CHANA, P., LERA, G., RODRIGUEZ, M. & OLANOW, C. W. 2000. The evolution and origin of motor complications in Parkinson's disease. *Neurology,* 55**,** S13-20; discussion S21-3.

OERTEL, W. H. 2017. Recent advances in treating Parkinson's disease. *F1000Res,* 6**,** 260.

OKUDA, Y., OGURA, E., KONDOH, H. & KAMACHI, Y. 2010. B1 SOX coordinate cell specification with patterning and morphogenesis in the early zebrafish embryo. *PLoS Genet,* 6**,** e1000936.

OLANOW, C. W., RASCOL, O., HAUSER, R., FEIGIN, P. D., JANKOVIC, J., LANG, A., LANGSTON, W., MELAMED, E., POEWE, W., STOCCHI,

F., TOLOSA, E. & INVESTIGATORS, A. S. 2009. A Double-Blind, Delayed-Start Trial of Rasagiline in Parkinson's Disease. *New England Journal of Medicine,* 361**,** 1268-1278.

OLBRICH, H., HAFFNER, K., KISPERT, A., VOLKEL, A., VOLZ, A., SASMAZ, G., REINHARDT, R., HENNIG, S., LEHRACH, H., KONIETZKO, N., ZARIWALA, M., NOONE, P. G., KNOWLES, M., MITCHISON, H. M., MEEKS, M., CHUNG, E. M., HILDEBRANDT, F., SUDBRAK, R. & OMRAN, H. 2002. Mutations in DNAH5 cause primary ciliary dyskinesia and randomization of left-right asymmetry. *Nat Genet,* 30**,** 143-4.

OLSON, K. E. & GENDELMAN, H. E. 2016. Immunomodulation as a neuroprotective and therapeutic strategy for Parkinson's disease. *Current Opinion in Pharmacology,* 26**,** 87-95.

OMORI, Y., ZHAO, C., SARAS, A., MUKHOPADHYAY, S., KIM, W., FURUKAWA, T., SENGUPTA, P., VERAKSA, A. & MALICKI, J. 2008. Elipsa is an early determinant of ciliogenesis that links the IFT particle to membrane-associated small GTPase Rab8. *Nat Cell Biol,* 10**,** 437-44.

ORNITZ, D. M. & ITOH, N. 2015. The Fibroblast Growth Factor signaling pathway. *Wiley Interdiscip Rev Dev Biol,* 4**,** 215-66.

ORTNER, N. J., BOCK, G., DOUGALIS, A., KHARITONOVA, M., DUDA, J., HESS, S., TULUC, P., POMBERGER, T., STEFANOVA, N., PITTERL, F., CIOSSEK, T., OBERACHER, H., DRAHEIM, H. J., KLOPPENBURG, P., LISS, B. & STRIESSNIG, J. 2017. Lower Affinity of Isradipine for L-Type Ca2+ Channels during Substantia Nigra Dopamine Neuron-Like Activity: Implications for Neuroprotection in Parkinson's Disease. *J Neurosci,* 37**,** 6761-6777.

PAISAN-RUIZ, C., JAIN, S., EVANS, E. W., GILKS, W. P., SIMON, J., VAN DER BRUG, M., LOPEZ DE MUNAIN, A., APARICIO, S., GIL, A. M., KHAN, N., JOHNSON, J., MARTINEZ, J. R., NICHOLL, D., CARRERA, I. M., PENA, A. S., DE SILVA, R., LEES, A., MARTI-MASSO, J. F., PEREZ-TUR, J., WOOD, N. W. & SINGLETON, A. B. 2004. Cloning of the gene containing mutations that cause PARK8-linked Parkinson's disease. *Neuron,* 44**,** 595-600.

PALACINO, J. J., SAGI, D., GOLDBERG, M. S., KRAUSS, S., MOTZ, C., WACKER, M., KLOSE, J. & SHEN, J. 2004. Mitochondrial dysfunction and oxidative damage in parkin-deficient mice. *J Biol Chem,* 279**,** 18614-22.

PARKER, M. O., BROCK, A. J., WALTON, R. T. & BRENNAN, C. H. 2013. The role of zebrafish (Danio rerio) in dissecting the genetics and neural circuits of executive function. *Front Neural Circuits,* 7**,** 63.

PARKINSON STUDY, G. 2013. Phase II safety, tolerability, and dose selection study of isradipine as a potential disease-modifying intervention in early Parkinson's disease (STEADY-PD). *Mov Disord,* 28**,** 1823-1831.

PARNG, C., ROY, N. M., TON, C., LIN, Y. & MCGRATH, P. 2007. Neurotoxicity assessment using zebrafish. *J Pharmacol Toxicol Methods,* 55**,** 103-112.

PARNG, C. L., TON, C., LIN, Y. X., ROY, N. M. & MCGRATH, P. 2006. A zebrafish assay for identifying neuroprotectants in vivo. *Neurotoxicology and Teratology,* 28**,** 509-516.

PASTERNAK, B., SVANSTROM, H., NIELSEN, N. M., FUGGER, L., MELBYE, M. & HVIID, A. 2012. Use of calcium channel blockers and Parkinson's disease. *Am J Epidemiol,* 175**,** 627-635.

PEREZ-CAMPS, M., TIAN, J., CHNG, S. C., SEM, K. P., SUDHAHARAN, T., TEH, C., WACHSMUTH, M., KORZH, V., AHMED, S. & REVERSADE, B. 2016. Quantitative imaging reveals real-time Pou5f3-Nanog complexes driving dorsoventral mesendoderm patterning in zebrafish. *Elife,* 5.

PERKEL, J. M. 2014. The antibody challenge. *Biotechniques,* 56**,** 111-4.

PICCOLO, S., AGIUS, E., LEYNS, L., BHATTACHARYYA, S., GRUNZ, H., BOUWMEESTER, T. & DE ROBERTIS, E. M. 1999. The head inducer Cerberus is a multifunctional antagonist of Nodal, BMP and Wnt signals. *Nature,* 397**,** 707-10.

POLYMEROPOULOS, M. H., LAVEDAN, C., LEROY, E., IDE, S. E., DEHEJIA, A., DUTRA, A., PIKE, B., ROOT, H., RUBENSTEIN, J., BOYER, R., STENROOS, E. S., CHANDRASEKHARAPPA, S., ATHANASSIADOU, A., PAPAPETROPOULOS, T., JOHNSON, W. G., LAZZARINI, A. M., DUVOISIN, R. C., DI IORIO, G., GOLBE, L. I. & NUSSBAUM, R. L. 1997. Mutation in the alpha-synuclein gene identified in families with Parkinson's disease. *Science,* 276**,** 2045-7.

PONTEN, H., KULLINGSJO, J., SONESSON, C., WATERS, S., WATERS, N. & TEDROFF, J. 2013. The dopaminergic stabilizer pridopidine decreases expression of L-DOPA-induced locomotor sensitisation in the rat unilateral 6-OHDA model. *European Journal of Pharmacology,* 698**,** 278-285.

PRADIDARCHEEP, W., LABRUYERE, W. T., DABHOIWALA, N. F. & LAMERS, W. H. 2008. Lack of specificity of commercially available antisera: better specifications needed. *J Histochem Cytochem,* 56**,** 1099-111.

PRAETORIUS, H. A., FROKIAER, J., NIELSEN, S. & SPRING, K. R. 2003. Bending the primary cilium opens Ca2+-sensitive intermediate-conductance K+ channels in MDCK cells. *J Membr Biol,* 191**,** 193-200.

PRIYADARSHI, A., KHUDER, S. A., SCHAUB, E. A. & PRIYADARSHI, S. S. 2001. Environmental risk factors and Parkinson's disease: a metaanalysis. *Environ Res,* 86**,** 122-7.

PUOPOLO, M., RAVIOLA, E. & BEAN, B. P. 2007. Roles of subthreshold calcium current and sodium current in spontaneous firing of mouse midbrain dopamine neurons. *J Neurosci,* 27**,** 645-56.

QUIK, M. 2004. Smoking, nicotine and Parkinson's disease. *Trends Neurosci,* 27**,** 561-8.

QUINTERO-ESPINOSA, D., JIMENEZ-DEL-RIO, M. & VELEZ-PARDO, C. 2017. Knockdown transgenic Lrrk Drosophila resists paraquat-induced locomotor impairment and neurodegeneration: A therapeutic strategy for Parkinson's disease. *Brain Res,* 1657**,** 253-261.

QUINTERO, E. M., WILLIS, L., SINGLETON, R., HARRIS, N., HUANG, P., BHAT, N. & GRANHOLM, A. C. 2006. Behavioral and morphological

effects of minocycline in the 6-hydroxydopamine rat model of Parkinson's disease. *Brain Res,* 1093**,** 198-207.

RAMSEY, C. P. & TANSEY, M. G. 2014. A survey from 2012 of evidence for the role of neuroinflammation in neurotoxin animal models of Parkinson's disease and potential molecular targets. *Exp Neurol,* 256**,** 126-132.

RAPPOLD, P. M., CUI, M., CHESSER, A. S., TIBBETT, J., GRIMA, J. C., DUAN, L., SEN, N., JAVITCH, J. A. & TIEU, K. 2011. Paraquat neurotoxicity is mediated by the dopamine transporter and organic cation transporter-3. *Proc Natl Acad Sci U S A,* 108**,** 20766-71.

RAVINA, B., KIEBURTZ, K., TILLEY, B., SHANNON, K., TANNER, C., WOOTEN, F., RACETTE, B., DEPPEN, P., DEWEY, R. B., HAYWARD, B., SCOTT, B., FIELD, J., CARTER, J., BRODSKY, M., ANDREWS, P., MANYAM, B., WHETTECKEY, J., RAO, J., COOK, M., AMINOFF, M. J., CHRISTINE, C., ROTH, J., NANCE, M., PARASHOS, S., PETERSON, S., SHANNON, K., JAGLIN, J., SINGER, C., PEREZ, M. A., BLENKE, A., HAUSER, R., MCCLAIN, T., DAWSON, T., DUNLOP, B., PAHWA, R., LYONS, K., PARSONS, A., LEEHEY, M., BAINBRIDGE, J., SHULMAN, L., WEINER, W., PABST, K., ELBLE, R., YOUNG, C., SETHI, K., DILL, B., MARTIN, W., MCINNES, G., CALABRESE, V. P., ROBERGE, P., HAMILL, R., HOMAN, C., BODIS-WOLLNER, I. G., HAYES, E., ROSS, G. W., TERASHITA, S., WOOTEN, G. F., TRUGMAN, J., KELLER, M. F., SAGE, J. I., CAPUTO, D., FANG, J., SHEARON, D., JENNINGS, D., KELSEY, T., JENNINGS, D., KELSEY, T., WOJCIESZEK, J., FEIGIN, A., WATTS, R. L., STOVER, N., MCMURRAY, R., ALBIN, R., WERNETTE, K., SIDEROWF, A., REICHWEIN, S., SIMON, D., TARSY, D., TINTNER, R., HUNTER, C., LEWITT, P., DEANGELIS, M., BURNS, R. S., SHILL, H., DANIELSON, J., MARLOR, L., ADLER, C., LIND, M., GORELL, J., KRSTEVSKA, S., FLEWELLEN, M., SCHNEIDER, J., SENDEK, S., GOLLOMP, S., VERNON, G., COFFEY, D., LEBLANC, P., LEW, M. F., WU, A., KAWAI, C., et al. 2006. A randomized, double-blind, futility clinical trial of creatine and minocycline in early Parkinson disease. *Neurology,* 66**,** 664-671.

RAYA, A. & IZPISUA BELMONTE, J. C. 2004. Sequential transfer of left-right information during vertebrate embryo development. *Curr Opin Genet Dev,* 14**,** 575-81.

RAYA, A., KAWAKAMI, Y., RODRIGUEZ-ESTEBAN, C., IBANES, M., RASSKIN-GUTMAN, D., RODRIGUEZ-LEON, J., BUSCHER, D., FEIJO, J. A. & IZPISUA BELMONTE, J. C. 2004. Notch activity acts as a sensor for extracellular calcium during vertebrate left-right determination. *Nature,* 427**,** 121-8.

REBAGLIATI, M. R., TOYAMA, R., HAFFTER, P. & DAWID, I. B. 1998. cyclops encodes a nodal-related factor involved in midline signaling. *Proc Natl Acad Sci U S A,* 95**,** 9932-7.

REEVE, A., SIMCOX, E. & TURNBULL, D. 2014. Ageing and Parkinson's disease: why is advancing age the biggest risk factor? *Ageing Res Rev,* 14**,** 19-30.

REYON, D., MAEDER, M. L., KHAYTER, C., TSAI, S. Q., FOLEY, J. E., SANDER, J. D. & JOUNG, J. K. 2013. Engineering customized TALE

nucleases (TALENs) and TALE transcription factors by fast ligation-based automatable solid-phase high-throughput (FLASH) assembly. *Curr Protoc Mol Biol,* Chapter 12**,** Unit 12 16.

RHODES, K. J. & TRIMMER, J. S. 2006. Antibodies as valuable neuroscience research tools versus reagents of mass distraction. *J Neurosci,* 26**,** 8017-20.

RINK, E. & WULLIMANN, M. F. 2001. The teleostean (zebrafish) dopaminergic system ascending to the subpallium (striatum) is located in the basal diencephalon (posterior tuberculum). *Brain Res,* 889**,** 316-330.

RINK, E. & WULLIMANN, M. F. 2002a. Connections of the ventral telencephalon and tyrosine hydroxylase distribution in the zebrafish brain (Danio rerio) lead to identification of an ascending dopaminergic system in a teleost. *Brain Research Bulletin,* 57**,** 385-387.

RINK, E. & WULLIMANN, M. F. 2002b. Development of the catecholaminergic system in the early zebrafish brain: an immunohistochemical study. *Brain Res Dev Brain Res,* 137**,** 89-100.

RITZ, B., RHODES, S. L., QIAN, L., SCHERNHAMMER, E., OLSEN, J. H. & FRIIS, S. 2010. L-type calcium channel blockers and Parkinson disease in Denmark. *Ann Neurol,* 67**,** 600-606.

ROSS, G. W., ABBOTT, R. D., PETROVITCH, H., WHITE, L. R. & TANNER, C. M. 2000. Relationship between caffeine intake and parkinson disease. *JAMA,* 284**,** 1378-9.

ROUGET, C., PAPIN, C., BOUREUX, A., MEUNIER, A. C., FRANCO, B., ROBINE, N., LAI, E. C., PELISSON, A. & SIMONELIG, M. 2010. Maternal mRNA deadenylation and decay by the piRNA pathway in the early Drosophila embryo. *Nature,* 467**,** 1128-32.

RUBINSZTEIN, D. C., MARINO, G. & KROEMER, G. 2011. Autophagy and aging. *Cell,* 146**,** 682-95.

RYAN, A. K., BLUMBERG, B., RODRIGUEZ-ESTEBAN, C., YONEI-TAMURA, S., TAMURA, K., TSUKUI, T., DE LA PENA, J., SABBAGH, W., GREENWALD, J., CHOE, S., NORRIS, D. P., ROBERTSON, E. J., EVANS, R. M., ROSENFELD, M. G. & IZPISUA BELMONTE, J. C. 1998. Pitx2 determines left-right asymmetry of internal organs in vertebrates. *Nature,* 394**,** 545-51.

SACHS, C. & JONSSON, G. 1975. Effects of 6-hydroxydopamine on central noradrenaline neurons during ontogeny. *Brain Res,* 99**,** 277-91.

SADEGHIAN, M., MULLALI, G., POCOCK, J. M., PIERS, T., ROACH, A. & SMITH, K. J. 2016. Neuroprotection by safinamide in the 6-hydroxydopamine model of Parkinson's disease. *Neuropathol Appl Neurobiol,* 42**,** 423-435.

SAGI, Y., MANDEL, S., AMIT, T. & YOUDIM, M. B. 2007. Activation of tyrosine kinase receptor signaling pathway by rasagiline facilitates neurorescue and restoration of nigrostriatal dopamine neurons in post-MPTP-induced parkinsonism. *Neurobiol Dis,* 25**,** 35-44.

SAITO, K. 2013. The epigenetic regulation of transposable elements by PIWI-interacting RNAs in Drosophila. *Genes Genet Syst,* 88**,** 9-17.

SALLINEN, V., SUNDVIK, M., REENILA, I., PEITSARO, N., KHRUSTALYOV, D., ANICHTCHIK, O., TOLEIKYTE, G., KASLIN, J.

& PANULA, P. 2009. Hyperserotonergic phenotype after monoamine oxidase inhibition in larval zebrafish. *J Neurochem,* 109**,** 403-415.

SAMPATH, K., RUBINSTEIN, A. L., CHENG, A. M., LIANG, J. O., FEKANY, K., SOLNICA-KREZEL, L., KORZH, V., HALPERN, M. E. & WRIGHT, C. V. 1998. Induction of the zebrafish ventral brain and floorplate requires cyclops/nodal signalling. *Nature,* 395**,** 185-9.

SANDER, J. D., CADE, L., KHAYTER, C., REYON, D., PETERSON, R. T., JOUNG, J. K. & YEH, J. R. 2011. Targeted gene disruption in somatic zebrafish cells using engineered TALENs. *Nat Biotechnol,* 29**,** 697-8.

SCHAPIRA, A. H. 2011. Monoamine oxidase B inhibitors for the treatment of Parkinson's disease: a review of symptomatic and potential disease-modifying effects. *CNS Drugs,* 25**,** 1061-71.

SCHIER, A. F. 2003. Nodal signaling in vertebrate development. *Annu Rev Cell Dev Biol,* 19**,** 589-621.

SCHIER, A. F. & GIRALDEZ, A. J. 2006. MicroRNA function and mechanism: insights from zebra fish. *Cold Spring Harb Symp Quant Biol,* 71**,** 195-203.

SCHIER, A. F. & SHEN, M. M. 2000. Nodal signalling in vertebrate development. *Nature,* 403**,** 385-9.

SCHMIDT, D. E., EBERT, M. H., LYNN, J. C. & WHETSELL, W. O., JR. 1997. Attenuation of 1-methyl-4-phenylpyridinium (MPP+) neurotoxicity by deprenyl in organotypic canine substantia nigra cultures. *J Neural Transm (Vienna),* 104**,** 875-85.

SCHMITZ, B., PAPAN, C. & CAMPOS-ORTEGA, J. A. 1993. Neurulation in the anterior trunk region of the zebrafish Brachydanio rerio. *Roux Arch Dev Biol,* 202**,** 250-259.

SCHNEIDER, I., HOUSTON, D. W., REBAGLIATI, M. R. & SLUSARSKI, D. C. 2008. Calcium fluxes in dorsal forerunner cells antagonize beta-catenin and alter left-right patterning. *Development,* 135**,** 75-84.

SCHONBRUNN, A. 2014. Editorial: Antibody can get it right: confronting problems of antibody specificity and irreproducibility. *Mol Endocrinol,* 28**,** 1403-7.

SCHOSSER, A., CALATI, R., SERRETTI, A., MASSAT, I., KOCABAS, N. A., PAPAGEORGIOU, K., LINOTTE, S., MENDLEWICZ, J., SOUERY, D., ZOHAR, J., JUVEN-WETZLER, A., MONTGOMERY, S. & KASPER, S. 2012. The impact of COMT gene polymorphisms on suicidality in treatment resistant major depressive disorder--a European multicenter study. *Eur Neuropsychopharmacol,* 22**,** 259-66.

SCHWANHAUSSER, B., BUSSE, D., LI, N., DITTMAR, G., SCHUCHHARDT, J., WOLF, J., CHEN, W. & SELBACH, M. 2013. Corrigendum: Global quantification of mammalian gene expression control. *Nature,* 495**,** 126-7.

SCHWARZ, J. 2003. Rationale for dopamine agonist use as monotherapy in Parkinson's disease. *Curr Opin Neurol,* 16 Suppl 1**,** S27-33.

SELEMON, L. D. & GOLDMAN-RAKIC, P. S. 1990. Topographic intermingling of striatonigral and striatopallidal neurons in the rhesus monkey. *J Comp Neurol,* 297**,** 359-76.

SEMOTOK, J. L., COOPERSTOCK, R. L., PINDER, B. D., VARI, H. K., LIPSHITZ, H. D. & SMIBERT, C. A. 2005. Smaug recruits the

CCR4/POP2/NOT deadenylase complex to trigger maternal transcript localization in the early Drosophila embryo. *Curr Biol,* 15**,** 284-94.

SETINI, A., PIERUCCI, F., SENATORI, O. & NICOTRA, A. 2005. Molecular characterization of monoamine oxidase in zebrafish (Danio rerio). *Comp Biochem Physiol B Biochem Mol Biol,* 140**,** 153-161.

SHEN, M. M. & SCHIER, A. F. 2000. The EGF-CFC gene family in vertebrate development. *Trends Genet,* 16**,** 303-9.

SHENG, D. L., QU, D. B., KWOK, K. H. H., NG, S. S., LIM, A. Y. M., AW, S. S., LEE, C. W. H., SUNG, W. K., TAN, E. K., LUFKIN, T., JESUTHASAN, S., SINNAKARUPPAN, M. & LIU, J. J. 2010. Deletion of the WD40 Domain of LRRK2 in Zebrafish Causes Parkinsonism-Like Loss of Neurons and Locomotive Defect. *Plos Genetics,* 6.

SHERER, T. B., BETARBET, R. & GREENAMYRE, J. T. 2002. Environment, mitochondria, and Parkinson's disease. *Neuroscientist,* 8**,** 192-7.

SHERMOEN, A. W. & O'FARRELL, P. H. 1991. Progression of the cell cycle through mitosis leads to abortion of nascent transcripts. *Cell,* 67**,** 303-10.

SHIMURA, H., HATTORI, N., KUBO, S., MIZUNO, Y., ASAKAWA, S., MINOSHIMA, S., SHIMIZU, N., IWAI, K., CHIBA, T., TANAKA, K. & SUZUKI, T. 2000. Familial Parkinson disease gene product, parkin, is a ubiquitin-protein ligase. *Nat Genet,* 25**,** 302-5.

SIDEROWF, A., STERN, M., SHOULSON, I., KIEBURTZ, K., OAKES, D., DAY, D., SHINAMAN, A., PLUMB, S., FAHN, S., BLINDAUER, K., LEW, M., HURTIG, H., LLOYD, M., HAUSER, R., GAUGER, L., GOLBE, L., WOJCIESZEK, J., BELDEN, J., FEIGIN, A., KLIMEK, M. L., SHANNON, B., ONDO, W., HUNTER, C., CALABRESE, V., ALLEN, C., BERRY, D., GARDINER, I., MIYASAKI, J., DEL RIZZO, L., MENDIS, T., MENDIS, N., GRAY, P., HUBBLE, J., BETCHER, K., PAHWA, R., MOLHO, E., BROWN, D., SHULMAN, L., RAJPUT, A., EWANISHIN, M., STACY, M., WILLIAMSON, K., BERTONI, J., PETERSON, C., TUITE, P., EBBITT, B., SHANNON, K., JAGLIN, J., TANNER, C., MAREK, K., STAVRIS, K., AMINOFF, M. J., DIMINNO, M., DOWLING, G., KANG, U. J., RICHMAN, J., SETHI, K., MARTIN, W., KING, P., MCINNES, G., ADLER, C., LEWITT, P., DEANGELIS, M., SCHEAR, M., GORDON, M. F., WINNICK, R., FELDMAN, R., THOMAS, C. A., CONN, K., BROCHT, A., CHADWICK, C., CONNOLLY, J., DAIGNEAULT, S., EBERLY, S., BAUSCH, M., JOSEPHSON, L., OLIVA, R., SCHWID, S., LANG, A., COX, C., IRVINE, C., NUTT, J., WHITE, W., OREN, S., LEVY, R., EYAL, E., LADKANI, D., HOUCK, W. & GRP, P. S. 2002. A controlled trial of rasagiline in early Parkinson disease - The TEMPO study. *Archives of Neurology,* 59**,** 1937-1943.

SIMOLA, N., MORELLI, M. & CARTA, A. R. 2007. The 6-hydroxydopamine model of Parkinson's disease. *Neurotox Res,* 11**,** 151-67.

SIMON, K. C., GAO, X., CHEN, H., SCHWARZSCHILD, M. A. & ASCHERIO, A. 2010. Calcium channel blocker use and risk of Parkinson's disease. *Mov Disord,* 25**,** 1818-1822.

SINGLETON, A. B., FARRER, M., JOHNSON, J., SINGLETON, A., HAGUE, S., KACHERGUS, J., HULIHAN, M., PEURALINNA, T., DUTRA, A., NUSSBAUM, R., LINCOLN, S., CRAWLEY, A., HANSON, M.,

MARAGANORE, D., ADLER, C., COOKSON, M. R., MUENTER, M., BAPTISTA, M., MILLER, D., BLANCATO, J., HARDY, J. & GWINN-HARDY, K. 2003. alpha-Synuclein locus triplication causes Parkinson's disease. *Science,* 302**,** 841.

SMITH, K. A., NOEL, E., THURLINGS, I., REHMANN, H., CHOCRON, S. & BAKKERS, J. 2011. Bmp and nodal independently regulate lefty1 expression to maintain unilateral nodal activity during left-right axis specification in zebrafish. *PLoS Genet,* 7**,** e1002289.

SMITH, K. M., EYAL, E., WEINTRAUB, D. & INVESTIGATORS, A. 2015. Combined rasagiline and antidepressant use in Parkinson disease in the ADAGIO study: effects on nonmotor symptoms and tolerability. *JAMA Neurol,* 72**,** 88-95.

SMITH, L. P. 2003. Steady the course of Parkinson's disease. *Nurs Manage,* 34**,** 35-9.

SNYDER, H., MENSAH, K., THEISLER, C., LEE, J., MATOUSCHEK, A. & WOLOZIN, B. 2003. Aggregated and monomeric alpha-synuclein bind to the S6' proteasomal protein and inhibit proteasomal function. *J Biol Chem,* 278**,** 11753-9.

SONG, J., OH, S. P., SCHREWE, H., NOMURA, M., LEI, H., OKANO, M., GRIDLEY, T. & LI, E. 1999. The type II activin receptors are essential for egg cylinder growth, gastrulation, and rostral head development in mice. *Dev Biol,* 213**,** 157-69.

SOONG, N. W., HINTON, D. R., CORTOPASSI, G. & ARNHEIM, N. 1992. Mosaicism for a specific somatic mitochondrial DNA mutation in adult human brain. *Nat Genet,* 2**,** 318-23.

STANCHEVA, I. & MEEHAN, R. R. 2000. Transient depletion of xDnmt1 leads to premature gene activation in Xenopus embryos. *Genes Dev,* 14**,** 313-27.

STEDNITZ, S. J., FRESHNER, B., SHELTON, S., SHEN, T., BLACK, D. & GAHTAN, E. 2015. Selective toxicity of L-DOPA to dopamine transporter-expressing neurons and locomotor behavior in zebrafish larvae. *Neurotoxicology and Teratology,* 52**,** 51-56.

STOCCHI, F., FOSSATI, C. & TORTI, M. 2015. Rasagiline for the treatment of Parkinson's disease: an update. *Expert Opin Pharmacother,* 16**,** 2231-41.

SU, Y. Q., SUGIURA, K., WOO, Y., WIGGLESWORTH, K., KAMDAR, S., AFFOURTIT, J. & EPPIG, J. J. 2007. Selective degradation of transcripts during meiotic maturation of mouse oocytes. *Dev Biol,* 302**,** 104-17.

SUGRUE, K. F. & ZOHN, I. E. 2017. Mechanism for generation of left isomerism in Ccdc40 mutant embryos. *PLoS One,* 12**,** e0171180.

SULLIVAN-BROWN, J., SCHOTTENFELD, J., OKABE, N., HOSTETTER, C. L., SERLUCA, F. C., THIBERGE, S. Y. & BURDINE, R. D. 2008. Zebrafish mutations affecting cilia motility share similar cystic phenotypes and suggest a mechanism of cyst formation that differs from pkd2 morphants. *Dev Biol,* 314**,** 261-75.

SUMI, T., TSUNEYOSHI, N., NAKATSUJI, N. & SUEMORI, H. 2008. Defining early lineage specification of human embryonic stem cells by the orchestrated balance of canonical Wnt/beta-catenin, Activin/Nodal and BMP signaling. *Development,* 135**,** 2969-79.

SUN, N., LIANG, J., ABIL, Z. & ZHAO, H. 2012. Optimized TAL effector nucleases (TALENs) for use in treatment of sickle cell disease. *Mol Biosyst,* 8**,** 1255-63.

SUN, Y. & OBERLEY, L. W. 1996. Redox regulation of transcriptional activators. *Free Radic Biol Med,* 21**,** 335-48.

SUPATTO, W., FRASER, S. E. & VERMOT, J. 2008. An all-optical approach for probing microscopic flows in living embryos. *Biophys J,* 95**,** L29-31.

SURPRENANT, A., RASSENDREN, F., KAWASHIMA, E., NORTH, R. A. & BUELL, G. 1996. The cytolytic P2Z receptor for extracellular ATP identified as a P2X receptor (P2X7). *Science,* 272**,** 735-8.

SUZUKI, K. T., ISOYAMA, Y., KASHIWAGI, K., SAKUMA, T., OCHIAI, H., SAKAMOTO, N., FURUNO, N., KASHIWAGI, A. & YAMAMOTO, T. 2013. High efficiency TALENs enable F0 functional analysis by targeted gene disruption in Xenopus laevis embryos. *Biol Open,* 2**,** 448-52.

SVOBODA, P. & FLEMR, M. 2010. The role of miRNAs and endogenous siRNAs in maternal-to-zygotic reprogramming and the establishment of pluripotency. *EMBO Rep,* 11**,** 590-7.

SWERDLOW, R. H. 1998. Is NADH effective in the treatment of Parkinson's disease? *Drugs Aging,* 13**,** 263-8.

TADROS, W. & LIPSHITZ, H. D. 2009. The maternal-to-zygotic transition: a play in two acts. *Development,* 136**,** 3033-42.

TAKAHASHI, K. & YAMANAKA, S. 2006. Induction of pluripotent stem cells from mouse embryonic and adult fibroblast cultures by defined factors. *Cell,* 126**,** 663-76.

TAM, O. H., ARAVIN, A. A., STEIN, P., GIRARD, A., MURCHISON, E. P., CHELOUFI, S., HODGES, E., ANGER, M., SACHIDANANDAM, R., SCHULTZ, R. M. & HANNON, G. J. 2008. Pseudogene-derived small interfering RNAs regulate gene expression in mouse oocytes. *Nature,* 453**,** 534-8.

TAM, P. P. & LOEBEL, D. A. 2007. Gene function in mouse embryogenesis: get set for gastrulation. *Nat Rev Genet,* 8**,** 368-81.

TANAKA, Y., ENGELENDER, S., IGARASHI, S., RAO, R. K., WANNER, T., TANZI, R. E., SAWA, A., V, L. D., DAWSON, T. M. & ROSS, C. A. 2001. Inducible expression of mutant alpha-synuclein decreases proteasome activity and increases sensitivity to mitochondria-dependent apoptosis. *Hum Mol Genet,* 10**,** 919-26.

TANAKA, Y., OKADA, Y. & HIROKAWA, N. 2005. FGF-induced vesicular release of Sonic hedgehog and retinoic acid in leftward nodal flow is critical for left-right determination. *Nature,* 435**,** 172-7.

TANG, F., KANEDA, M., O'CARROLL, D., HAJKOVA, P., BARTON, S. C., SUN, Y. A., LEE, C., TARAKHOVSKY, A., LAO, K. & SURANI, M. A. 2007a. Maternal microRNAs are essential for mouse zygotic development. *Genes Dev,* 21**,** 644-8.

TANG, R., DODD, A., LAI, D., MCNABB, W. C. & LOVE, D. R. 2007b. Validation of zebrafish (Danio rerio) reference genes for quantitative real-time RT-PCR normalization. *Acta Biochim Biophys Sin (Shanghai),* 39**,** 384-90.

TANSEY, M. G. & GOLDBERG, M. S. 2010. Neuroinflammation in Parkinson's disease: its role in neuronal death and implications for therapeutic intervention. *Neurobiol Dis,* 37**,** 510-8.

THIFFAULT, C., LANGSTON, J. W. & DI MONTE, D. A. 2000. Increased striatal dopamine turnover following acute administration of rotenone to mice. *Brain Res,* 885**,** 283-8.

THIRUCHELVAM, M., RICHFIELD, E. K., BAGGS, R. B., TANK, A. W. & CORY-SLECHTA, D. A. 2000. The nigrostriatal dopaminergic system as a preferential target of repeated exposures to combined paraquat and maneb: implications for Parkinson's disease. *J Neurosci,* 20**,** 9207-14.

TON, T. G., HECKBERT, S. R., LONGSTRETH, W. T., JR., ROSSING, M. A., KUKULL, W. A., FRANKLIN, G. M., SWANSON, P. D., SMITH-WELLER, T. & CHECKOWAY, H. 2007. Calcium channel blockers and beta-blockers in relation to Parkinson's disease. *Parkinsonism Relat Disord,* 13**,** 165-169.

VALKO, M., LEIBFRITZ, D., MONCOL, J., CRONIN, M. T., MAZUR, M. & TELSER, J. 2007. Free radicals and antioxidants in normal physiological functions and human disease. *Int J Biochem Cell Biol,* 39**,** 44-84.

VERSTRAETEN, B., VAN HENGEL, J. & HUYSSEUNE, A. 2016. Beta-Catenin and Plakoglobin Expression during Zebrafish Tooth Development and Replacement. *PLoS One,* 11**,** e0148114.

VINCOW, E. S., MERRIHEW, G., THOMAS, R. E., SHULMAN, N. J., BEYER, R. P., MACCOSS, M. J. & PALLANCK, L. J. 2013. The PINK1-Parkin pathway promotes both mitophagy and selective respiratory chain turnover in vivo. *Proc Natl Acad Sci U S A,* 110**,** 6400-5.

VIOTTI, M., NIU, L., SHI, S. H. & HADJANTONAKIS, A. K. 2012. Role of the gut endoderm in relaying left-right patterning in mice. *PLoS Biol,* 10**,** e1001276.

WANG, G., CADWALLADER, A. B., JANG, D. S., TSANG, M., YOST, H. J. & AMACK, J. D. 2011. The Rho kinase Rock2b establishes anteroposterior asymmetry of the ciliated Kupffer's vesicle in zebrafish. *Development,* 138**,** 45-54.

WANG, G., MANNING, M. L. & AMACK, J. D. 2012. Regional cell shape changes control form and function of Kupffer's vesicle in the zebrafish embryo. *Dev Biol,* 370**,** 52-62.

WARGA, R. M. & KIMMEL, C. B. 1990. Cell movements during epiboly and gastrulation in zebrafish. *Development,* 108**,** 569-80.

WATANABE, T., TOTOKI, Y., TOYODA, A., KANEDA, M., KURAMOCHI-MIYAGAWA, S., OBATA, Y., CHIBA, H., KOHARA, Y., KONO, T., NAKANO, T., SURANI, M. A., SAKAKI, Y. & SASAKI, H. 2008. Endogenous siRNAs from naturally formed dsRNAs regulate transcripts in mouse oocytes. *Nature,* 453**,** 539-43.

WEAVER, C. J., LEUNG, Y. F. & SUTER, D. M. 2016. Expression dynamics of NADPH oxidases during early zebrafish development. *J Comp Neurol,* 524**,** 2130-2141.

WEBB, J. L., RAVIKUMAR, B., ATKINS, J., SKEPPER, J. N. & RUBINSZTEIN, D. C. 2003. Alpha-Synuclein is degraded by both autophagy and the proteasome. *J Biol Chem,* 278**,** 25009-13.

WEINTRAUB, D., HAUSER, R. A., ELM, J. J., PAGAN, F., DAVIS, M. D., CHOUDHRY, A. & INVESTIGATORS, M. 2016. Rasagiline for mild cognitive impairment in Parkinson's disease: A placebo-controlled trial. *Mov Disord,* 31**,** 709-714.

WESTERFIELD, M. 2000. *The Zebrafish Book: A Guide for the Laboratory Use of Zebrafish, 4th ed.,* Eugene, Univ. of Oregon Press.

WHITMAN, M. & MERCOLA, M. 2001. TGF-beta superfamily signaling and left-right asymmetry. *Sci STKE,* 2001**,** re1.

WHITTON, P. S. 2007. Inflammation as a causative factor in the aetiology of Parkinson's disease. *Br J Pharmacol,* 150**,** 963-76.

WOJTERA, M., SIKORSKA, B., SOBOW, T. & LIBERSKI, P. P. 2005. Microglial cells in neurodegenerative disorders. *Folia Neuropathol,* 43**,** 311-21.

WU, D. C., JACKSON-LEWIS, V., VILA, M., TIEU, K., TEISMANN, P., VADSETH, C., CHOI, D. K., ISCHIROPOULOS, H. & PRZEDBORSKI, S. 2002. Blockade of microglial activation is neuroprotective in the 1-methyl-4-phenyl-1,2,3,6-tetrahydropyridine mouse model of Parkinson disease. *Journal of Neuroscience,* 22**,** 1763-1771.

XI, Y., RYAN, J., NOBLE, S., YU, M., YILBAS, A. E. & EKKER, M. 2010. Impaired dopaminergic neuron development and locomotor function in zebrafish with loss of pink1 function. *Eur J Neurosci,* 31**,** 623-33.

XU, C., FAN, Z. P., MULLER, P., FOGLEY, R., DIBIASE, A., TROMPOUKI, E., UNTERNAEHRER, J., XIONG, F., TORREGROZA, I., EVANS, T., MEGASON, S. G., DALEY, G. Q., SCHIER, A. F., YOUNG, R. A. & ZON, L. I. 2012. Nanog-like regulates endoderm formation through the Mxtx2-Nodal pathway. *Dev Cell,* 22**,** 625-38.

XU, J., WANG, T., WU, Y., JIN, W. & WEN, Z. 2016. Microglia Colonization of Developing Zebrafish Midbrain Is Promoted by Apoptotic Neuron and Lysophosphatidylcholine. *Dev Cell,* 38**,** 214-222.

YAMADA, T., PLACZEK, M., TANAKA, H., DODD, J. & JESSELL, T. M. 1991. Control of cell pattern in the developing nervous system: polarizing activity of the floor plate and notochord. *Cell,* 64**,** 635-47.

YANG, L. C., SUGAMA, S., CHIRICHIGNO, J. W., GREGORIO, J., LORENZL, S., SHIN, D. H., BROWNE, S. E., SHIMIZU, Y., JOH, T. H., BEAL, M. F. & ALBERS, D. S. 2003. Minocycline enhances MPTP toxicity to dopaminergic neurons. *Journal of Neuroscience Research,* 74**,** 278-285.

YOST, H. J. 1999. Diverse initiation in a conserved left-right pathway? *Curr Opin Genet Dev,* 9**,** 422-6.

YOUDIM, M. B., GROSS, A. & FINBERG, J. P. 2001. Rasagiline [N-propargyl-1R(+)-aminoindan], a selective and potent inhibitor of mitochondrial monoamine oxidase B. *Br J Pharmacol,* 132**,** 500-506.

YOUDIM, M. B. & WEINSTOCK, M. 2001. Molecular basis of neuroprotective activities of rasagiline and the anti-Alzheimer drug TV3326 [(N-propargyl-(3R)aminoindan-5-YL)-ethyl methyl carbamate]. *Cell Mol Neurobiol,* 21**,** 555-573.

YUAN, S., ZHAO, L., BRUECKNER, M. & SUN, Z. 2015. Intraciliary calcium oscillations initiate vertebrate left-right asymmetry. *Curr Biol,* 25**,** 556-67.

ZAMPONI, G. W. 2016. Targeting voltage-gated calcium channels in neurological and psychiatric diseases. *Nat Rev Drug Discov,* 15**,** 19-34.

ZENG, F. & SCHULTZ, R. M. 2005. RNA transcript profiling during zygotic gene activation in the preimplantation mouse embryo. *Dev Biol,* 283**,** 40-57.

ZHANG, C., LI, C., CHEN, S., LI, Z., JIA, X., WANG, K., BAO, J., LIANG, Y., WANG, X., CHEN, M., LI, P., SU, H., WAN, J. B., LEE, S. M., LIU, K. & HE, C. 2017. Berberine protects against 6-OHDA-induced neurotoxicity in PC12 cells and zebrafish through hormetic mechanisms involving PI3K/AKT/Bcl-2 and Nrf2/HO-1 pathways. *Redox Biol,* 11**,** 1-11.

ZHANG, L. Q., SA, F., CHONG, C. M., WANG, Y., ZHOU, Z. Y., CHANG, R. C., CHAN, S. W., HOI, P. M. & YUEN LEE, S. M. 2015. Schisantherin A protects against 6-OHDA-induced dopaminergic neuron damage in zebrafish and cytotoxicity in SH-SY5Y cells through the ROS/NO and AKT/GSK3beta pathways. *J Ethnopharmacol,* 170**,** 8-15.

ZHANG, Z. J., CHEANG, L. C., WANG, M. W. & LEE, S. M. 2011. Quercetin exerts a neuroprotective effect through inhibition of the iNOS/NO system and pro-inflammation gene expression in PC12 cells and in zebrafish. *Int J Mol Med,* 27**,** 195-203.

ZHU, J. & CHU, C. T. 2010. Mitochondrial dysfunction in Parkinson's disease. *J Alzheimers Dis,* 20 Suppl 2**,** S325-34.

ZHU, S., STAVROVSKAYA, I. G., DROZDA, M., KIM, B. Y. S., ONA, V., LI, M. W., SARANG, S., LIU, A. S., HARTLEY, D. M., DU, C. W., GULLANS, S., FERRANTE, R. J., PRZEDBORSKI, S., KRISTAL, B. S. & FRIEDLANDER, R. M. 2002. Minocycline inhibits cytochrome c release and delays progression of amyotrophic lateral sclerosis in mice. *Nature,* 417**,** 74-78.

ZIMPRICH, A., BENET-PAGES, A., STRUHAL, W., GRAF, E., ECK, S. H., OFFMAN, M. N., HAUBENBERGER, D., SPIELBERGER, S., SCHULTE, E. C., LICHTNER, P., ROSSLE, S. C., KLOPP, N., WOLF, E., SEPPI, K., PIRKER, W., PRESSLAUER, S., MOLLENHAUER, B., KATZENSCHLAGER, R., FOKI, T., HOTZY, C., REINTHALER, E., HARUTYUNYAN, A., KRALOVICS, R., PETERS, A., ZIMPRICH, F., BRUCKE, T., POEWE, W., AUFF, E., TRENKWALDER, C., ROST, B., RANSMAYR, G., WINKELMANN, J., MEITINGER, T. & STROM, T. M. 2011. A mutation in VPS35, encoding a subunit of the retromer complex, causes late-onset Parkinson disease. *Am J Hum Genet,* 89**,** 168-75.

Chapter 9: Website References

https://www.addgene.org/

https://blast.ncbi.nlm.nih.gov/Blast.cgi

http://www.d.umn.edu/~pschoff/documents/Gastrulation-chickfishmammal.pdf.

http://www.ensembl.org/index.html

https://expasy.org/

http://www.guidetopharmacology.org

https://hannahleaanimalkingdom.weebly.com/gastrulation.html

https://www.ncbi.nlm.nih.gov/genome/

https://www.predictprotein.org/

https://tale-nt.cac.cornell.edu/node/add/talen

https://uniprot.org/

https://www.wisc.edu/

Chapter 10: Appendix 1

Morphology scoring template used for all embryo and larval phenotypic scoring. 11 structures/systems were scored and total sores assigned each embryo and larva into normal development, mild, moderate or severely deformed as discussed in Section 2.2.4.

	Scoring date:		Age:			Group:			Tank:				
Unfertilized/Dead										total 44		Class I (normal):	37-44
6hpf	1dpf	2dpf	3dpf									Class II (mild):	25-36
												Class III (intermediate):	13-24
												Class IV (severe):	0-12
	Heart			Body		Brain			Yolk		Heart total	Class	Comm
Size	Oedema	pooling	Bloodflow	Tail	Somites	Brain oed	Brain struc	Eyes	Yolk sac	Yolk ext			
											0		
											0		
											0		
											0		
											0		
											0		
											0		
											0		
											0		
											0		
											0		
											0		
											0		
											0		
											0		
											0		
											0		
											0		
											0		
											0		

Peer Reviewed Manuscript:

Cronin A, Grealy M (2017), Neuroprotective and Neuro-restorative Effects of Minocycline and Rasagiline in a Zebrafish 6-Hydroxydopamine Model of Parkinson's Disease. Neuroscience 367:34-46.

NEUROSCIENCE
RESEARCH ARTICLE
A. Cronin, M. Grealy / Neuroscience 367 (2017) 34–46

Neuroprotective and Neuro-restorative Effects of Minocycline and Rasagiline in a Zebrafish 6-Hydroxydopamine Model of Parkinson's Disease

Aileen Cronin and Maura Grealy *

Pharmacology & Therapeutics, National University of Ireland, Galway, Ireland

Abstract—Parkinson's disease is a common, debilitating, neurodegenerative disorder for which the current gold standard treatment, levodopa (L-DOPA) is symptomatic. There is an urgent, unmet need for neuroprotective or, ideally, neuro-restorative drugs. We describe a 6-hydroxydopamine (6-OHDA) zebrafish model to screen drugs for neuroprotective and neuro-restorative capacity. Zebrafish larvae at two days post fertilization were exposed to 6-OHDA for three days, with co-administration of test drugs for neuroprotection experiments, or for 32 h, with subsequent treatment with test drugs for neuro-restoration experiments. Locomotor activity was assessed by automated tracking and dopaminergic neurons were visualized by tyrosine hydroxylase immunohistochemistry. Exposure to 6-OHDA for either 32 h or 3 days induced similar, significant locomotor deficits and neuronal loss in 5-day-old larvae. L-DOPA (1 mM) partially restored locomotor activity, but was neither neuroprotective nor neuro-restorative, mirroring the clinical situation. The calcium channel blocker, isradipine (1 μM) did not prevent or reverse 6-OHDA-induced locomotor deficit or neuronal loss. However, both the tetracycline analog, minocycline (10 μM), and the monoamine oxidase B inhibitor, rasagiline (1 μM), prevented the locomotor deficits and neuronal loss due to three-day 6-OHDA exposure. Importantly, they also reversed the locomotor deficit caused by prior exposure to 6-OHDA; rasagiline also reversed neuronal loss and minocycline partially restored neuronal loss due to prior 6-OHDA, making them candidates for investigation as neuro-restorative treatments for Parkinson's disease. Our findings in zebrafish reflect preliminary clinical findings for rasagiline and minocycline. Thus, we have developed a zebrafish model suitable for high-throughput screening of putative neuroprotective and neuro-restorative therapies for the treatment of Parkinson's disease.

Key words: zebrafish, Parkinsons's disease, 6-OHDA, locomotor activity, immunohistochemistry, neuro-restoration.

INTRODUCTION

Parkinson's disease is the second most common neurodegenerative disorder after Alzheimer's disease. It is characterized by loss of dopaminergic neurons from the nigrostriatal pathway and the formation of alpha-synuclein protein aggregates known as Lewy bodies. Although incompletely understood, the disease is thought to be due to a combination of environmental and genetic factors. Oxidative stress, mitochondrial dysfunction, and neuro-inflammation have all been linked to disease progression (Dauer and Przedborski (2003) for review). Early diagnosis of Parkinson's disease is rare as symptoms in patients only manifest after approximately 60% of nigral dopaminergic neurons have degenerated and 80% of striatal dopamine has been lost (Fearnley and Lees, 1991). In addition to the motor symptoms of tremor, rigidity and akinesia, many patients suffer from depression and slowed cognitive processes (Dauer and Przedborski, 2003) and can experience up to 84% decline in their cognitive function as the disease progresses (Jankovic, 1984).

Current treatment for the disease is symptomatic and does not slow or halt disease progression. The dopamine precursor, levodopa (L-DOPA) is still the best available treatment more than 50 years after it was first used in Parkinson's disease patients (Cotzias et al., 1969). It increases brain dopamine levels and decreases motor symptoms. Due to problems associated with fluctuating levels of L-DOPA, several drugs are approved as add-ons to prolong its effects by inhibiting the L-DOPA-degrading enzyme, DOPA-decarboxylase, for example carbidopa and opicapone, or by inhibiting the dopamine degrading enzyme, monoamine-oxidase B, for example selegiline, rasagiline and safinamide (reviewed by Oertel (2017)). Attempts to slow or stop disease progression

*Corresponding author.
E-mail address: maura.grealy@nuigalway.ie (M. Grealy).
Abbreviations: 6-OHDA, 6-hydroxydopamine; MAO, monoamine oxidase; MPTP, 1-methyl-4-phenyl-1,2,3,6-tetrahydropyridine.

https://doi.org/10.1016/j.neuroscience.2017.10.018
0306-4522/

have focussed on targeting alpha-synuclein aggregates, neuroprotection of mitochondria, or reduction of microglial activation and consequent neuro-inflammation (Singleton et al., 2003; Sadeghian et al., 2016; Kolahdouzan and Hamadeh, 2017).

There is an urgent, unmet need for neuroprotective and neuro-restorative treatments for Parkinson's disease, and to fill this need an animal model suitable for drug screening is required. The zebrafish has several advantages in this regard; it is vertebrate, produces hundreds of embryos per mating, embryos and larvae are transparent, allowing visualization of the developing larvae, chemicals can be applied in the swimming medium, and their small size allows for high-throughput assessment. In addition, zebrafish embryos and larvae may be used from 0 to 5 days post fertilization (dpf) without need for project authorization under Directive 2010/63/EU on the protection of animals used for scientific purposes, making them an ideal model for rapid high-throughput drug screens.

Although there is no structure analogous to the mammalian substantia nigra in zebrafish, there is evidence that the corresponding dopaminergic neurons are those of the posterior tuberculum of the ventral diencephalon which project to the subpallium (Rink and Wullimann, 2001, 2002a; Du et al., 2016). Development of the dopaminergic system in zebrafish begins at 15–18 h post fertilization (hpf), and most of the adult cell clusters are already present by 120 hpf (Rink and Wullimann, 2002b).

The catecholamine neurotoxin 6-hydroxydopamine (6-OHDA) is a hydroxylated analog of dopamine, which is widely used to produce animal models of idiopathic Parkinson's disease. It causes degeneration of both dopaminergic and noradrenergic nerve terminals and cell bodies by inhibiting mitochondrial respiratory enzymes, causing an increase in oxidative stress and inducing microglial activation. Most commonly used in rat Parkinson's disease models (Glinka et al., 1998; Zuch et al., 2000; Blandini et al., 2004), it has also been used to induce dopaminergic neuronal loss in zebrafish (Parng et al., 2007; Feng et al., 2014; Zhang et al., 2017). We tested three drugs; isradipine, minocycline and rasagiline, for neuroprotective and neuro-restorative effects in 6-OHDA-treated zebrafish larvae.

The calcium channel blocker, isradipine, is currently in clinical trials for treatment of Parkinson's disease (NCT02168842 on-going), based on observations that treatment of hypertension with calcium channel antagonists resulted in diminished risk of developing the disease (Becker et al., 2008). The proposed mechanism is that the pacemaking activity of neurons in the substantia nigra makes them vulnerable to excessive calcium influx, with increased risk with age, due to repetitive activation of calcium channels. This leads to increased calcium in the mitochondria and production of reactive oxygen species, ultimately causing neuronal death (reviewed by Zamponi (2016)). In mice, isradipine treatment restored juvenile pacemaking activity of neurons and protected neurons from degeneration *in vitro* and *in vivo* (Chan et al., 2007).

The tetracycline antibiotic, minocycline, protected against the loss of dopaminergic neurons by inhibition of microglial activation in 1-methyl-4-phenyl-1,2,3,6-tetrahydropyridine (MPTP)-treated mice, and it reduced iNOS and caspase-1 expression (Du et al., 2001). In contrast, Yang et al. (2003) and Diguet et al. (2004) reported that minocycline exacerbated the damage to dopaminergic neurons in MPTP-treated mice and primates. In clinical studies minocycline has been found to block microglial activation but so far has not shown any clinical improvement in motor function (Ravina et al., 2006; Kieburtz et al., 2008; Olson and Gendelman, 2016).

Rasagiline is an irreversible inhibitor of monoamine oxidase (MAO) B, and is thus used to prolong the effects of L-DOPA. However it also has anti-apoptotic properties unrelated to its MAO-B inhibition and these are thought to underlie neuroprotective effects seen in cell culture and animal experiments (Akao et al., 2002; Blandini et al., 2004). In clinical trials, rasagiline has been reported to have beneficial effects on patient symptoms in early Parkinson's disease (Olanow et al., 2009; Hauser et al., 2016).

In this study we demonstrate the merits of our zebrafish 6-OHDA model in drug screening for Parkinson's disease. We investigated whether three putative neuroprotective drugs, isradipine, rasagiline, and minocycline, could protect from or restore locomotor activity deficit and dopaminergic neuron loss due to 6-OHDA.

EXPERIMENTAL PROCEDURES

Adult zebrafish (wild-type AB strain) were housed in 20-L glass tanks maintained at 28 °C and kept on a 14-h light: 10-h dark cycle. When mating, spawning pairs were housed overnight in 1-L capacity spawning trays separated by a mesh grid. The following morning the pair were placed together to allow for controlled spawning. Embryos were collected, staged and cleared of debris to maintain water quality. They were maintained in an incubator at 28 °C for up to 5 dpf.

Reagents

All drugs and reagents were purchased from Sigma Aldrich, with the exception of the following; mouse anti-tyrosine hydroxylase primary antibody (MAB318) was supplied by Merck Millipore, Alexa Fluor 488 goat anti-mouse secondary antibody was purchased from Biosciences. Tissue-Tek® used for embedding was supplied by Sakura® Finetek, VWR.

Drug treatments

Embryos were manually dechorionated at 24 hpf, 10 embryos per well were placed in a 12-well plate and drugs were administered in the swimming medium beginning at 48 hpf (2 dpf). All solutions were rinsed out and replaced with a fresh solution daily during incubation periods (Fig. 1). Each experiment was repeated at least three times. All drug stock solutions (except L-DOPA) were stored in single-use aliquots

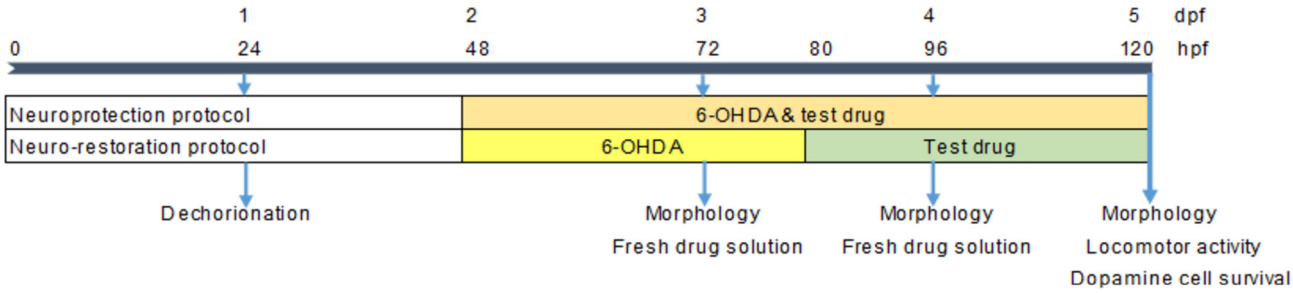

Fig. 1. Timeline of drug and toxin exposure and assessments for neuroprotection and neuro-restoration protocols.

(10× concentration) at −20 °C, thawed and applied to the swim water daily. L-DOPA is only slightly soluble in water, therefore, a 2× working stock was prepared fresh daily, and applied to the swim water. Control larvae were in a 0.01% DMSO solution in filter sterilized egg water (FSEW; Westerfield (2000)). Final concentrations of drugs in the swimming medium were: 6-OHDA, 250 μM, based on Parng et al. (2007); L-DOPA, 1 mM (Sheng et al., 2010); minocycline, 10 μM; and isradipine and rasagiline, 1 μM. Concentrations for isradipine, minocycline and rasagiline were selected following a dose-ranging toxicity study in which drugs were administered at 2, 3, and 4 dpf, with morphology scored each day from 3 dpf, and locomotor activity tested at 5 dpf.

When investigating neuroprotection, larvae were exposed to 6-OHDA alone or with co-administered test drugs from 2 to 5 dpf. In the neuro-restoration study, larvae were exposed to 6-OHDA from 48 hpf (2 dpf) up to 80 hpf, with test drugs introduced after washout of 6-OHDA, from 80 hpf to 120 hpf (5 dpf).

Morphological assessment

Body morphology was scored at 72, 96 and 120 hpf using a modified scale from Brannen et al. (2010). Thirty larvae were used per group and were categorized as normal, or having mild, moderate or severe defects. Subcategories further analyzed the drug effect on developing organs. Structures that were scored included the heart, brain, tail, eyes and yolk sac with yolk extension. Scores assigned were 4 for normal development of a structure, 3 for mild defects, 2 for moderate defects, 1 for severe defects and 0 if the organ was absent at time of scoring. A normally developing larva with no abnormalities was given a maximum score of 44. Any larva that was given an overall score between 40 and 44 was deemed to have normal development. An overall score of 25–40 was categorized as mild abnormalities, 13–24 had moderate abnormalities, 1–12 had severe abnormalities, and if a larva was dead at the time of scoring, it was given a score of 0.

Locomotor activity

Daniovision® (Noldus) was used as a tracking system to record individual locomotor activity over a 50 min time period between 9 and 11 am at 5 dpf. As switching from light to dark stimulates locomotor activity in zebrafish larvae, we used 10-min alternating light/dark cycles for all locomotor testing (Burgess and Granato, 2007). Larvae were transferred to 96-well plates (Uniplate®-Whatman square-well plates) with one larva per well on the evening before testing in a total volume of 250 μL. Test larvae were allocated to inner wells; larvae in the outer wells were excluded from analysis, as they have increased locomotor activity (data not shown). Water at 28 °C was circulated around the 96-well plate in the Daniovision® chamber. Larvae were acclimatized to the chamber for 30 min prior to the test. Data were exported to Excel and graphed using GraphPad Prism. Locomotor activity was recorded as mean distance moved per minute over 50 min, and the total distance moved (mm) over the duration of the test was used for statistical analysis. Data from the 10 larvae in each experiment were collapsed by reporting the mean group value for each experiment.

Immunohistochemistry

Larvae at 5 dpf were fixed in 4% paraformaldehyde and kept at 4 °C overnight. Following fixation, tissue was dehydrated in ethanol (50% for 5 min, 70% for 5 min), stored in 70% ethanol and later rehydrated by washing three times in phosphate-buffered saline (PBS) (3 × 5 min) followed by 20 min in 10% sucrose and at least 3 h in 30% sucrose solution in PBS. Larval tissue was then embedded in Tissue-Tek® (Sakura® Finetek, VWR) and rapidly frozen in iso-pentane, which had been cooled in liquid nitrogen. Tissue was cryosectioned in a rostral to caudal direction at 20-μm thickness mounted on positively charged glass slides.

Tissue sections were washed three times for 5, 10 and 15 min in PBS and blocked in 3% bovine serum albumin for 30 min followed by 3% normal goat serum for 30 min at room temperature. Sections were incubated with mouse anti-tyrosine hydroxylase primary antibody at a 1:300 dilution with 0.3% Triton X100 overnight at 4 °C. Sections were then washed three times (3 × 5 min) in PBS and incubated with secondary Alexa Fluor 488 Goat anti-mouse antibody at a 1:200 dilution with 0.3% Triton X100 for 1 h at room temperature before three final wash steps in PBS for 5, 10 and 15 min and slides were coverslipped. Images were examined by fluorescence microscopy (Nikon Eclipse E400 Epi-fluorescence microscope, 200× magnification – Olympus Cell Sens software). Dopaminergic cell numbers were quantified using Image J.

Statistical analyses

Morphological data was based on a scoring system and cell count data are discrete rather than continuous, therefore these were analyzed using Kruskal–Wallis non parametric ANOVA followed by Dunn's post hoc test with correction for multiple comparisons. Locomotor activity data were first tested for normality using the Shapiro–Wilks test and for homogeneity of variance using Levene's test and analyzed by one-way ANOVA followed by Tukey's post hoc test with correction for multiple comparisons to identify significant changes between groups. A P value less than 0.05 was deemed significant. In addition effect sizes were estimated using an online calculator (Lenhard and Lenhard, 2016; https://www.psychometrica.de/effect-size.html and power was estimated using G*power.

RESULTS

6-OHDA and L-DOPA effects

We first tested for acute toxicity of 6-OHDA (250 μM) and L-DOPA (1 mM) by assessing morphology in zebrafish larvae each day for three days post-treatment (3–5 dpf). Whereas L-DOPA did not cause any morphological defects, exposure to 6-OHDA caused mild morphological defects such as delayed development and cardiac edema and blood pooling at 3-, 4- and 5 dpf, with defects at 4 dpf (not shown) being similar to those at 3 dpf (Fig. 2A–D). No moderate or severe developmental effects were noted, and morphology scores were significantly different to controls only at 3 dpf (Fig. 2E; Kruskal–Wallis ANOVA ($\chi^2(2) = 11.2$; $P = 0.0037$; effect size $\boldsymbol{f} = 0.33$; power = 0.8; Dunn's post hoc test $P < 0.01$, 6-OHDA vs. control at 3 dpf). However, 13% of larvae in the 6-OHDA group died by 5 dpf (Fig. 2E).

Next we assessed dopaminergic cell survival and locomotor activity following 6-OHDA exposure for three days, as a basis for testing neuroprotective drugs, or for 32 h as a basis for testing neuro-restorative drugs (Fig. 1 for timeline). In addition, we examined the ability of L-DOPA to reverse the effects of 6-OHDA in both of these paradigms.

Either the 3-day or 32-h exposure to 6-OHDA caused a reduction in locomotor activity and a loss of dopaminergic neurons throughout the dopaminergic clusters of the brain. The retinal pigmented epithelium of the eye has intense tyrosine hydroxylase positive staining, because melanin is downstream of tyrosine hydroxylase in the catecholamine synthesis pathway; this was unaffected by 6-OHDA exposure (Fig. 3). In the control group dopaminergic neurons were clearly seen throughout the zebrafish brain with the expected clustered pattern of cell populations in the pretectum, ventral thalamus, posterior tuberculum and hypothalamus. In contrast, exposure to 6-OHDA caused a substantial loss of dopaminergic neurons, with few to no surviving cells (Fig. 3A–O). When assessed using 10-min light: dark cycles at 5 dpf, larvae moved more in the dark, with transition to the dark phase triggering movement. Exposure to 6-OHDA, for either 3 days or 32 h, resulted in a loss of locomotor activity (Fig. 3P). The reduction in locomotor activity caused by the three-day exposure to 6-OHDA (48–120 hpf) was statistically significant (Fig. 4H; one-way ANOVA $F_{(5,12)} = 6.251$, $P = 0.0045$; effect size $\boldsymbol{f} = 1.614$; power = 0.999; Tukey's post hoc test $P < 0.05$ 6-OHDA 3 days vs. control). Interestingly, the locomotor activity deficit caused by exposure to 6-OHDA for 32 h (48–80 hpf) was similar to that caused by the longer three-day exposure (Tukey's post hoc test $P < 0.05$ 6-OHDA 32 h vs. control), thus providing us with a paradigm for testing functional restoration potential of test drugs. L-DOPA partially restored locomotor activity (Fig. 4H;

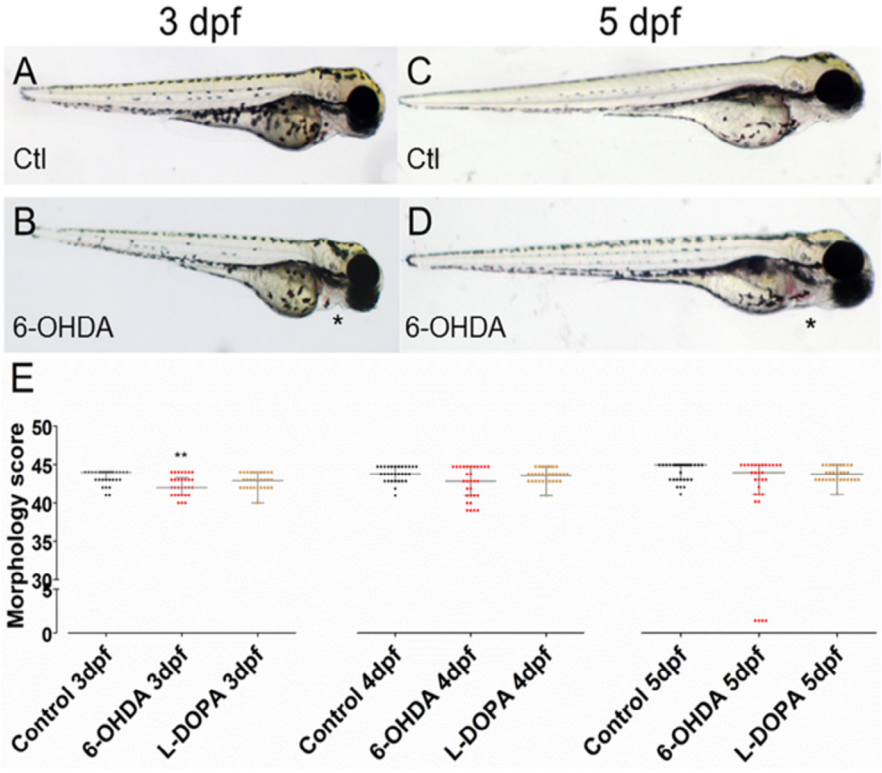

Fig. 2. Effects of 6-OHDA and L-DOPA on development, locomotor activity and dopaminergic cell number. When compared with controls (Ctl) at 3 dpf (A) heart edema and blood pooling (*) were seen in 6-OHDA (250 μM)-treated larvae (B). At 5 dpf larvae in the 6-OHDA-treated group (D) had delayed development such as slow development of the swim bladder along with cardiac edema and blood pooling (*) compared to 5 dpf control (C). (E) Morphology scores at 3 dpf, 4 dpf, and 5 dpf in control, 6-OHDA- and L-DOPA-treated groups. L-DOPA had no effect on development, however 6-OHDA groups had significantly lower body score at 3 dpf. Data are represented as median and interquartile range with $n = 30$ larvae per group; **$P < 0.01$ vs. control.

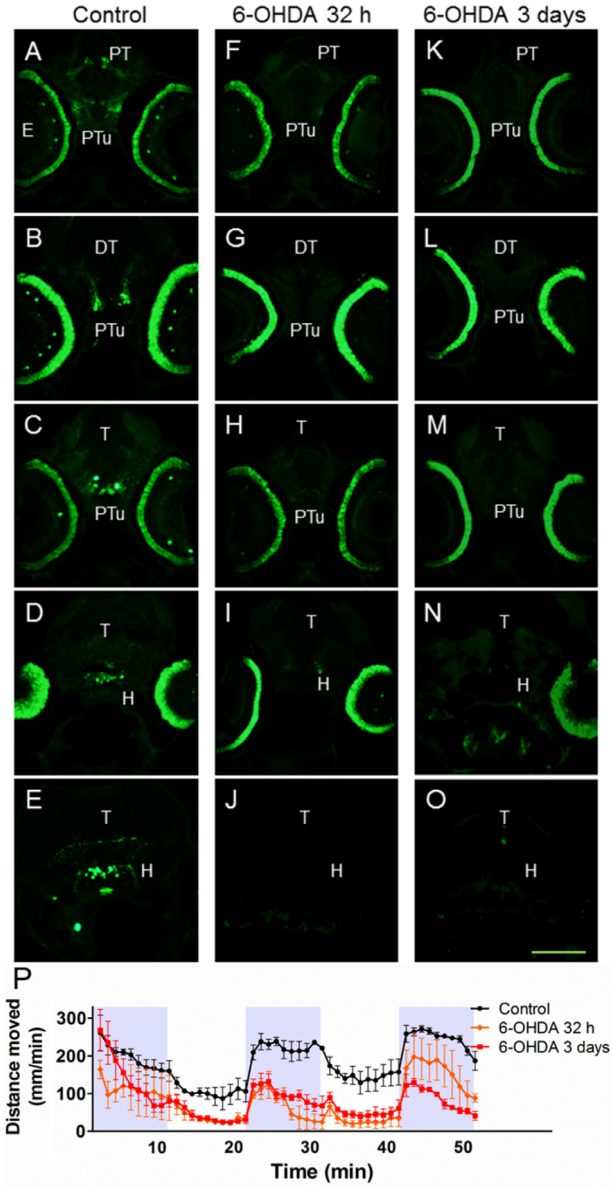

Fig. 3. Dopaminergic cell loss throughout the brain following 6-OHDA exposure for 32 h or 3 days. Control larvae at 5 dpf have expected dopamine cell populations in the pretectum (A), posterior tuberculum (A–C) and hypothalamus (D, E). Corresponding brain regions in 6-OHDA 32 h exposed larvae (F–J) or 3 day exposed larvae (K–O) have huge dopaminergic neuronal loss throughout the brain (DT, dorsal thalamus; H, hypothalamus; PT, pretectum; PTu, posterior tuberculum; T, tegmentum; Scale bar = 100 μm). (P) Distance moved over time in dark (shaded) and light conditions shows that larvae move more in the dark, with severe loss of movement in the dark phase in both 32-h and 3-day 6-OHDA-treated larvae; n = 3 separate experiments with 10 larvae per experiment. Data are represented as mean ± SEM.

6-OHDA + L-DOPA ns vs. any group), with movement intermediate between that of the control and the relevant 6-OHDA groups.

In contrast to the partial reversal by L-DOPA of the 6-OHDA-induced locomotor deficit, L-DOPA was unable to prevent or restore the loss of dopaminergic neurons caused by exposure to 6-OHDA (Fig. 4A–F) when tested at 5 dpf. The neuronal losses due to 6-OHDA were statistically significant (Fig. 4G; Kruskal–Wallis ANOVA ($\chi^2(4) = 13.5$; $P = 0.0091$; effect size $\boldsymbol{f} = 0.78$; power = 0.66; Dunn's post hoc test $P < 0.05$ 6-OHDA vs. control; L-DOPA groups ns vs. relevant 6-OHDA groups). This indicates that a 32-h exposure to 6-OHDA is sufficient to induce substantial neuronal loss with no recovery of neuronal cell numbers by 5 dpf, 40 h after withdrawal of the toxin. L-DOPA co-treatment did not prevent neuronal loss due to the three-day 6-OHDA exposure (Fig. 4E). Nor did post-treatment with L-DOPA following washout of 6-OHDA reverse the neuronal loss due to 32-h exposure to 6-OHDA (Fig. 4F). Thus, the effect of L-DOPA in our zebrafish model is similar to those observed clinically showing an improvement of locomotor function with no improvement in dopaminergic neuronal loss.

Drug toxicity study

Before testing the neuroprotective or neuro-restorative ability of our test drugs, we first assessed the toxicity of each test drug alone, when administered from 48 hpf to 120 hpf, by scoring morphology each day and assessing locomotor activity at 5 dpf.

No defects were recorded in minocycline (10 μM) or rasagiline (1 μM)-treated groups; morphology scores were similar to controls (Fig. 5G), and these drugs had no effect on locomotor activity (Fig. 5H). Whereas isradipine at 10 μM caused severe heart edema (Fig. 5C, F), the 1 μM concentration was much less toxic; it caused mild heart edema and mild blood pooling in approximately 20% of treated larvae (Fig. 5B, E). Morphology scores were only significantly different to controls at 5 dpf (Fig. 5G; Kruskal Wallis ANOVA $\chi^2(3) = 9.558$; $P = 0.0227$; effect size $\boldsymbol{f} = 0.24$; power = 0.55; Tykey's post hoc test $P < 0.05$ isradipine vs. control at 5 dpf). Therefore the 1 μM concentration of isradipine was chosen for further investigations. None of the drugs affected locomotor activity compared to controls (Fig. 5H; one-way ANOVA $F_{(3,31)} = 2.851$, $P = 0.0533$; effect size $\boldsymbol{f} = 0.52$; power = 0.68; Dunn's post hoc test all groups ns vs. control). Thus we tested these drugs for neuroprotection and neurorestoration.

Neuroprotective effect experiments

To test if isradipine, minocycline or rasagiline were neuroprotective, we co-administered these drugs with 6-OHDA for three days (2–5 dpf). Locomotor activity and dopaminergic cell counts were assessed at 5 dpf.

Co-treatment with isradipine did not prevent the 6-OHDA-induced loss of dopaminergic neurons (Fig. 6B, C, F; Kruskal–Wallis ANOVA ($\chi^2(4) = 21.18$; $P = 0.0003$; Effect size $\boldsymbol{f} = 0.98$; power = 0.99; Dunn's post hoc test $P < 0.05$ isradipine vs. control; ns vs. 6-OHDA), whereas pre-treatment with minocycline or rasagiline protected the dopaminergic neurons (Fig. 6D-F, Dunn's post hoc test $P < 0.05$ vs. 6-OHDA; ns vs. control), demonstrating that minocycline and rasagiline protect dopaminergic neurons, whereas isradipine does not.

Overall there were significant differences in distance moved between treatment groups (one-way ANOVA, $F_{(4,18)} = 6.435$, $P = 0.0021$; effect size $\boldsymbol{f} = 1.2$; power = 0.99). Isradipine co-treatment did not improve locomotor activity in 6-OHDA-treated larvae; distance moved was similar to the 6-OHDA-only group and significantly lower than controls (Tukey's post hoc test, $P < 0.05$ vs. controls). In contrast, larvae co-treated with minocycline moved as much as controls, and significantly more than the 6-OHDA-only group (Fig. 6G, H; Tukey's post hoc test $P < 0.05$ vs. 6-OHDA). Similarly, movement of larvae co-treated with 6-OHDA and rasagiline was similar to controls and was significantly higher than in the 6-OHDA-only group (Fig. 6G, H; Tukey's post hoc test $P < 0.05$ vs. 6-OHDA), demonstrating functional protection by minocycline and rasagiline in our 6-OHDA zebrafish model of Parkinson's disease and consistent with the dopaminergic cell imaging findings.

Neuro-restorative effect experiments

Having found that co-treatment with rasagiline or minocycline protected dopaminergic neurons from 6-OHDA effects, we wished to determine whether they could restore locomotor activity and dopaminergic cells in larvae pre-treated with 6-OHDA. Having established that exposure to 6-OHDA from 48 hpf to 80 hpf induced similar deficits in locomotor activity and dopaminergic neurons, at 5 dpf, to the longer, 3 day, exposure (Fig. 4), we then initiated treatment with isradipine, rasagiline, or minocycline at 80 hpf, just after withdrawal of the

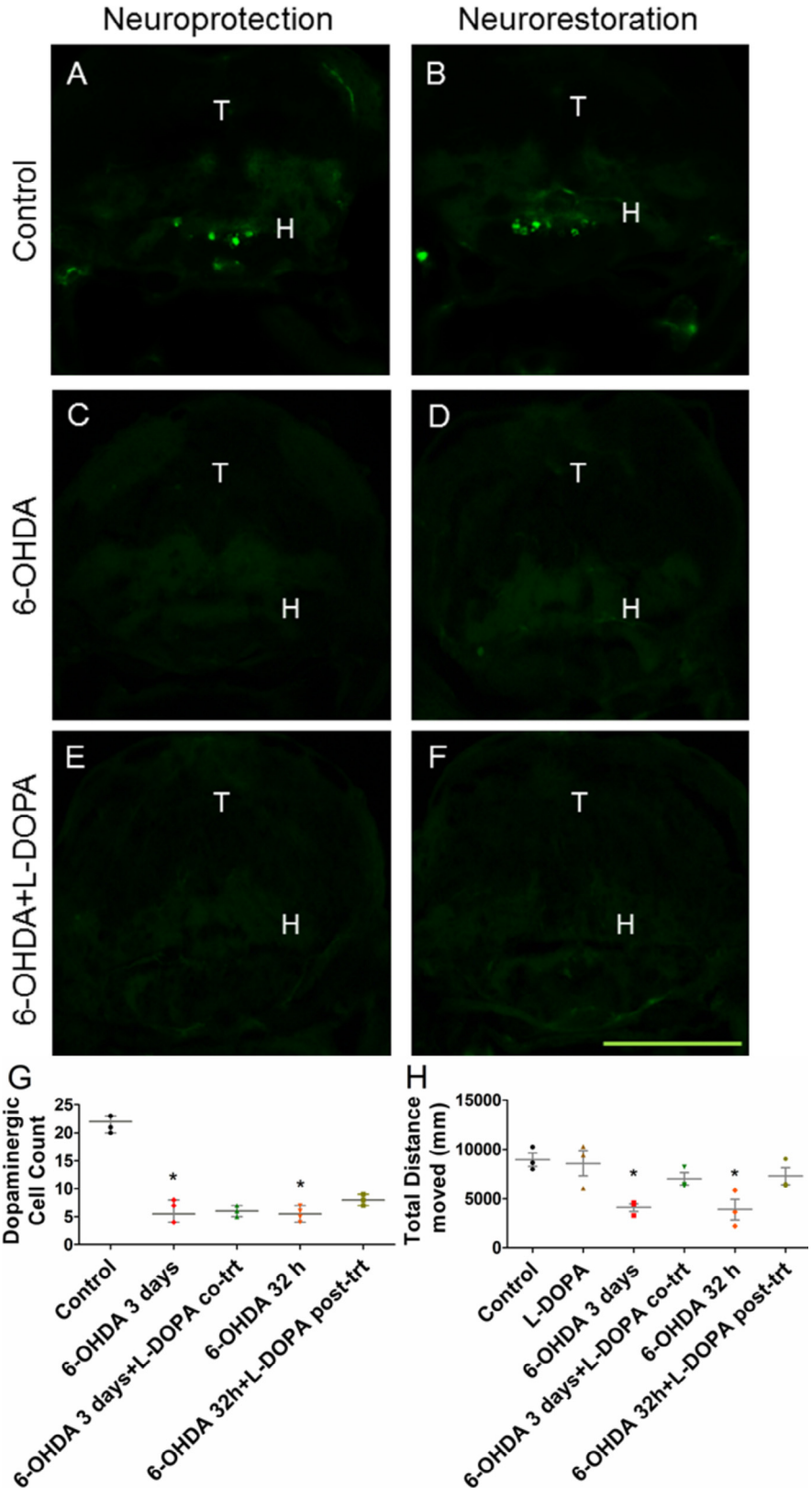

Fig. 4. Effect of L-DOPA on dopaminergic cell survival and locomotor activity in 6-OHDA treated larvae. Compared with their respective controls (A, B) 3-day (C) or 32-h (D) 6-OHDA treatment caused dopaminergic neuronal loss, L-DOPA co-treatment (E) or post-treatment (F) did not protect from or restore cell loss. (H, hypothalamus; T, tegmentum; Scale bar = 100 μm). (G) Dopaminergic cell count data are represented as median with range, $n = 4$ per group. (H) Locomotor testing at 5 dpf found decreased locomotor activity in both 6-OHDA groups when compared to controls. L-DOPA treatment in both co-treated (neuro-protective) and post-treated (neuro-restorative) groups had a partial rescue of locomotor activity; $n = 3$ separate experiments with 10 larvae per experiment. Data are represented as mean ± SEM; $^{*}P < 0.05$ vs. control.

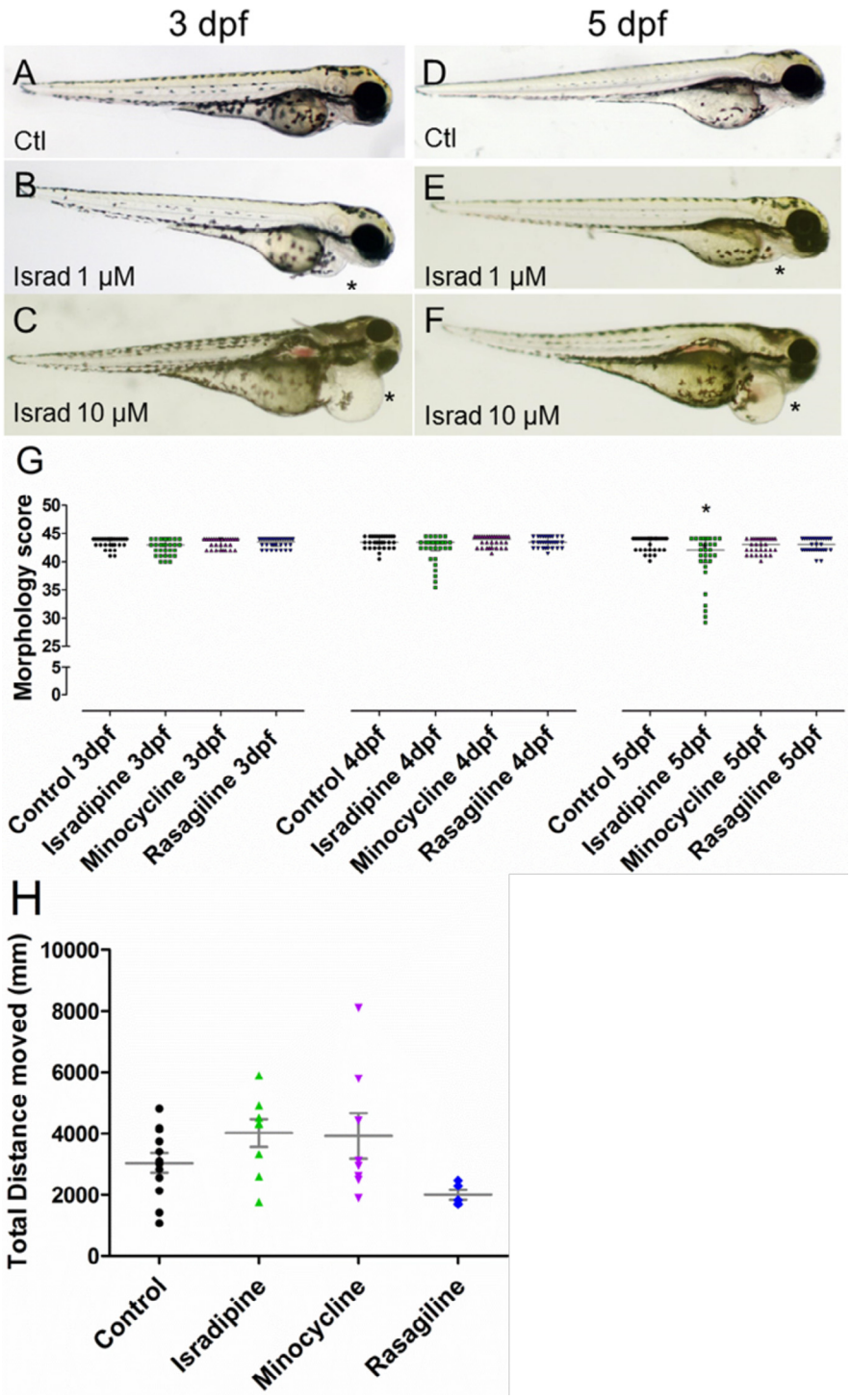

Fig. 5. Effects of test drugs alone. Compared with control larvae at 3 dpf (A) and 5 dpf (D) larvae treated with isradipine (10 μM) had severe cardiac edema at 3 dpf (C*) and 5 dpf (F*), whereas only some larvae in the 1 μM isradipine group had mild edema (*B and E). (G) Morphology was scored in isradipine, minocycline and rasagiline treated embryos at 3 dpf, 4 dpf, and 5 dpf. At 5 dpf isradipine-treated larvae had significantly lower morphology scores than controls. Data are represented as median and interquartile range with $n = 30$ larvae per group; *$P < 0.05$ vs. control. (H) Locomotor activity was assessed at 5 dpf. Total distance moved was similar in all groups. Data are represented as mean ± SEM, $n \geq 5$ separate experiments with 10 larvae per experiment.

6-OHDA. Treatment with these drugs continued until 120 hpf.

There was a significant effect of treatment on dopaminergic cell number (Fig. 7A–F; Kruskal–Wallis ANOVA ($\chi^2(4) = 23.72$; $P < 0.0001$; effect size $\boldsymbol{f} = 1.14$; power = 0.99). Rasagiline treatment from 80 hpf to 120 hpf rescued dopaminergic neurons by 5 dpf (Dunn's post hoc test $P = 0.0005$ vs. 6-OHDA, ns vs. control), whereas treatment with isradipine did not (Dunn's post hoc test $P < 0.05$ vs. control, ns vs. 6-OHDA). Although cell numbers in the minocycline group were similar to controls (Dunn's post hoc test $P > 0.999$) numbers were not significantly higher than in the 6-OHDA group (Dunn's post hoc test $P = 0.1097$), indicating a partial recovery of neuronal cell numbers.

Overall, there were significant differences in locomotor activity between treatment groups (Fig. 7G, H; one-way ANOVA $F_{(4,10)} = 8.267$, $P = 0.0033$; effect size $\boldsymbol{f} = 1.82$; power = 0.99). Treatment with isradipine from 80- to 120 hpf failed to improve the 6-OHDA-induced locomotor deficit (Fig. 7H; Tukey's post hoc test, $P < 0.05$ vs. control), whereas minocycline or rasagiline treatment restored movement to control levels (Fig. 7H; Tukey's post hoc test, $P < 0.05$ vs. 6-OHDA).

Together with the neuronal cell immunohistochemical findings, these results demonstrate that rasagiline restores both locomotor function and dopaminergic neurons in zebrafish larvae, whereas isradipine does not. Minocycline fully restores locomotor function but did not fully restore dopaminergic neurons to control levels.

DISCUSSION

In this study we demonstrate the value of zebrafish larvae for screening putative treatments for Parkinson's disease. For the first time we have shown that exposure of zebrafish larvae to 6-OHDA for 32 h can induce similar deficits to a 3-day exposure regimen. This allowed us to assess the

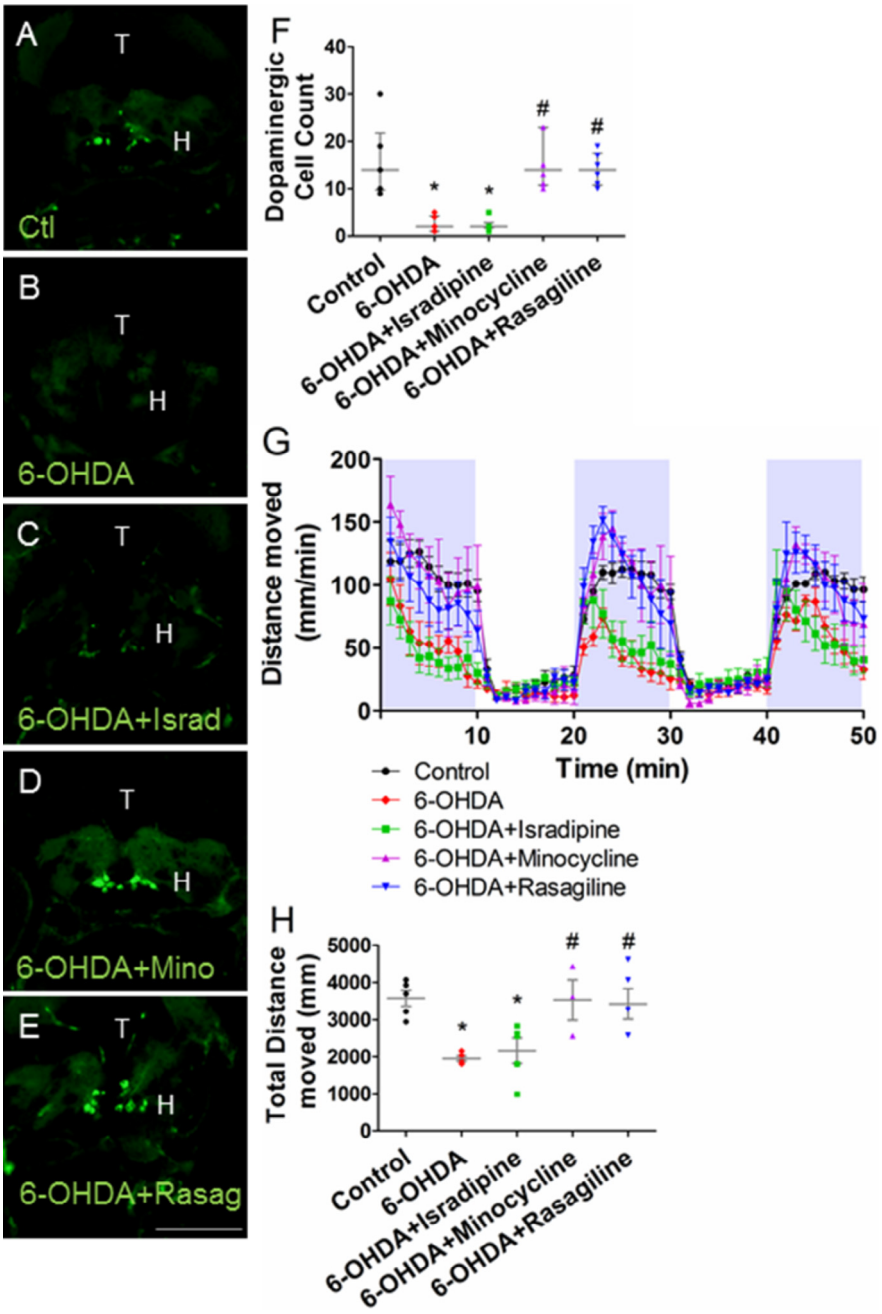

Fig. 6. Neuroprotective effects of test drugs. Compared to control (A) 6-OHDA treatment (B) caused dopaminergic neuron loss. Treatment with isradipine (C) did not prevent 6-OHDA-induced dopaminergic cell loss, whereas minocycline (D) or rasagiline (E) treatment was neuroprotective. Scale bar = 100 μm; H, hypothalamus; T, tegmentum. (F) Dopaminergic cell counts following immunohistochemical analysis. Data are represented as median with range, $n = 6$ larvae per group; $^{*}P < 0.05$ vs. control; $^{\#}P < 0.05$ vs. 6-OHDA. (G) Distance moved over time in dark (shaded) and light conditions shows that larvae move more in the dark, with severe loss of movement in the dark phase in 6-OHDA treated larvae, which was prevented by co-treatment with rasagiline or minocycline but not with isradipine. Total distance moved over the 50-min trial (H), shows overall effects of treatments. Data are represented as mean ± SEM, $n = 5$ separate experiments with 10 larvae per experiment, except minocycline group for which there were three separate experiments; $^{*}P < 0.05$ vs. control; $^{\#}P < 0.05$ vs. 6-OHDA.

neurorestorative as well as neuroprotective effects of drug treatments in 5-dpf zebrafish larvae, with the potential for high-throughput screening.

6-OHDA model and neurodegeneration

In agreement with published reports (Parng et al., 2007; Feng et al., 2014) we found that 6-OHDA, when administered for three days, beginning at 48 hpf, produced both robust deficits in locomotor activity and extensive dopaminergic neuronal loss in zebrafish larvae. Significantly, we were also able to demonstrate locomotor deficits and dopaminergic neuronal loss following a shorter, 32 h, exposure to 6-OHDA, thus allowing us to subsequently treat with putative neuro-restorative drugs and assess locomotor activity and dopaminergic neurons at 5 dpf. To our knowledge this is the first report of such studies in zebrafish larvae up to 5 dpf; previous studies have tested for neuroprotection at this early larval stage but not for neurorestoration (Zhang et al., 2011, 2015, 2017; Feng et al., 2014). (Chong et al., 2013) induced locomotor deficit following two days of 6-OHDA treatment; however they began exposure at 24 hpf. Feng et al. (2014) were unable to induce locomotor deficit in their system following two days of 6-OHDA exposure beginning at 48 hpf. The increased sensitivity of our system may be due to the use of 10-min dark phases to stimulate movement, coupled with the increased length of our locomotor testing.

L-DOPA

The finding that L-DOPA co-treatment could partially restore the 6-OHDA-induced locomotor activity deficit is similar to that of Feng et al. (2014). Despite this, L-DOPA could not prevent dopaminergic neuronal loss in 6-OHDA-treated larvae. This lack of protection of neurons is similar to findings in a Zebrafish LRRK2 morpholino knockdown model (Sheng et al., 2010). However, these authors were unable to monitor locomotor activity as the morphant phenotype was severe; in addition, morpholino effects are typically transient, lasting no more than three days because the antisense morpholino is diluted by new RNA in surviving larvae. Neither did we find that 1 mM L-DOPA itself caused neuronal loss, which was reported by Stednitz et al. (2015); in our study dopaminergic neuron numbers were similar in the

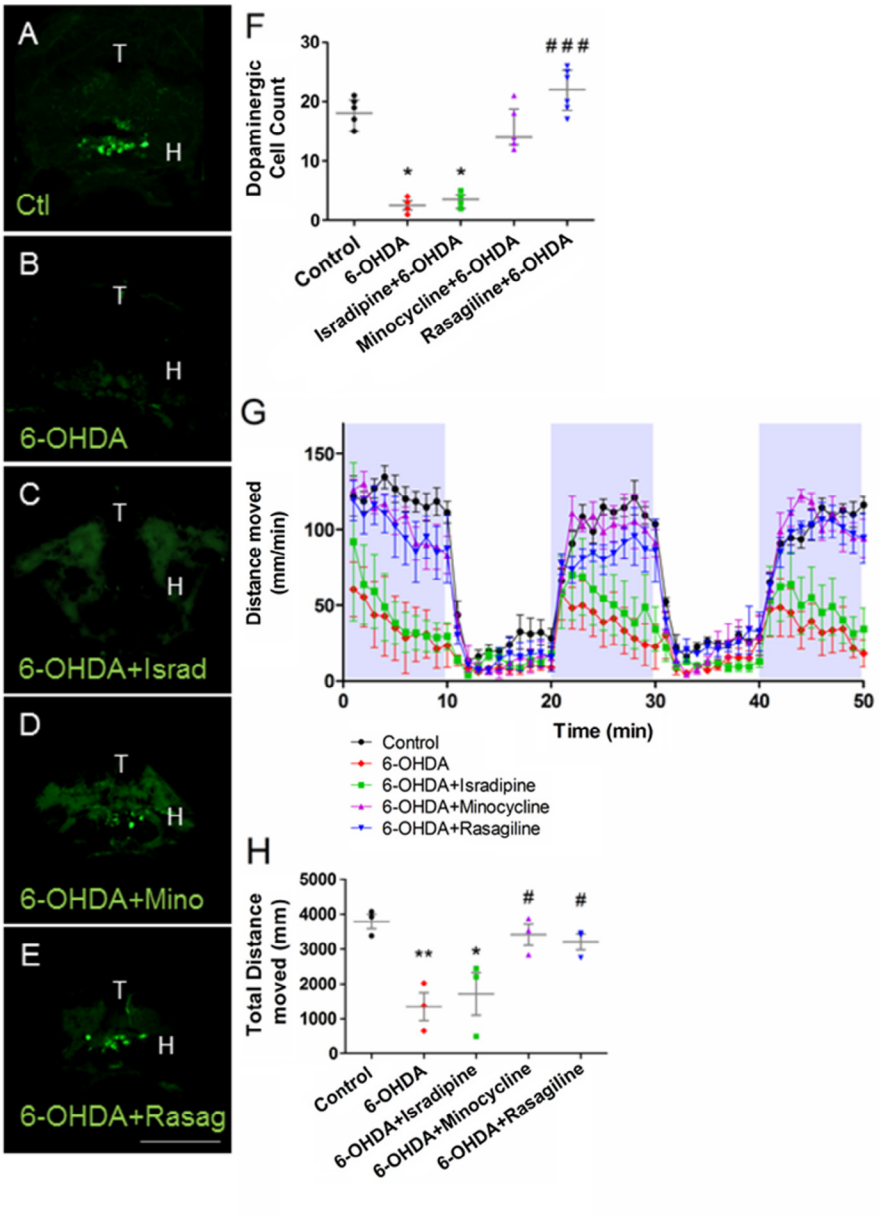

Fig. 7. Neuro-restorative effects of test drugs. Compared to control (A) 32-h 6-OHDA treatment (B) caused dopaminergic neuron loss. Subsequent treatment with isradipine (C) did not rescue 6-OHDA-induced dopaminergic cell loss, whereas minocycline partially restored dopaminergic neurons (D) and rasagiline (E) treatment was fully neuro-restorative. Scale bar = 100 μm; H, hypothalamus; T, tegmentum. (F) Dopaminergic cell count data are represented as median with range, $n = 6$ larvae per group; $^{*}P < 0.05$ vs. control; $^{\#\#\#}P < 0.0005$ vs. 6-OHDA. (G) Distance moved over time in dark (shaded) and light conditions shows that larvae move more in the dark, with severe loss of movement in the dark phase in 6-OHDA-treated larvae, which was rescued by post-treatment with rasagiline or minocycline but not with isradipine. Total distance moved per 50-min trial (H), shows overall effects of treatments. Data are represented as mean ± SEM, $n = 3$ separate experiments with 10 larvae per experiment; $^{*}P < 0.05$ vs. control; $^{**}P < 0.01$ vs. control; $^{\#}P < 0.05$ vs. 6-OHDA.

L-DOPA-treated and control groups, nor did we find that L-DOPA caused hyperactivity. The difference in findings may be due to different time of treatment; Stednitz and colleagues treated for one day starting at 5 dpf, whereas our treatments were from 2 to 5 dpf. Our findings correspond to clinical use of L-DOPA to improve movement without neuroprotection and are a further validation of a zebrafish 6-OHDA model for screening of novel symptomatic treatments for PD.

Isradipine

Isradipine was put forward for clinical trials for Parkinson's disease, based on the observation that patients treated for hypertension with calcium channel blockers had a lower risk of developing Parkinson's disease (Becker et al., 2008; Ritz et al., 2010; Pasternak et al., 2012). In addition, *in vitro* and *in vivo* animal studies on rodents and primates were promising (Kupsch et al., 1996; Chan et al., 2007; Ilijic et al., 2011). L-type calcium channels are essential for regulation of dopaminergic neuronal firing and are responsible for the majority of calcium currents entering dopaminergic neurons. As isradipine is specific to L-type calcium channels it was hypothesized that treatment would protect and rescue dopaminergic cell death through inhibition of calcium influx into the cell which would otherwise lead to neuronal vulnerability and subsequent cell death (Kruman and Mattson, 1999; Durante et al., 2004). Despite this, we failed to find any protective or restorative effect in our 6-OHDA zebrafish model, and isradipine itself caused mild heart edema. Although Ilijic et al. (2011) found that isradipine was neuroprotective in a 6-OHDA mouse model, a recent study by (Ortner et al., 2017) found that at therapeutic or even supra-therapeutic doses isradipine was not neuroprotective in their 6-OHDA mouse model of Parkinson's disease. They reason that this is because vascular calcium channels are more sensitive to isradipine than those in the substantia nigra. Our findings of mild edema in our zebrafish, without any neuroprotection would agree with this interpretation. Our results also correspond to preliminary results from a phase II study in patients which failed to show an effect of this drug as a treatment for Parkinson's disease at the maximum tolerated dose of 10 mg after 52 weeks (Parkinson Study G, 2013). In addition, there are several studies which did not find an association between calcium channel blocker use and protection from Parkinson's disease (Ton et al., 2007; Louis et al., 2009; Simon et al., 2010). Therefore this negative finding with

isradipine may be a better reflection of the clinical effects than previous animal studies.

Minocycline

There has been increasing evidence for the role of neuroinflammation in neurodegenerative diseases in recent years (De Virgilio et al., 2016 for review). Therefore, there has been an increased interest in the possible neuroprotective effects of anti-inflammatory drugs, with many reports of neuroprotection in genetic and neurotoxic animal models of neurodegenerative diseases through inhibition of microglial activation, anti-apoptotic properties and inhibition of reactive oxygen species production (Ramsey and Tansey, 2014 for review). Minocycline has been shown to be anti-inflammatory, anti-apoptotic, and anti-oxidant in cell culture and animal models (Garrido-Mesa et al., 2013 for review). It has been shown to inhibit the release of cytochrome C into the cytosol (Zhu et al., 2002) leading to inhibition of caspase-1 and caspase-3 as well as iNOS (Chen et al., 2000). It has also been shown to inhibit microglial activation following 6-OHDA in mice (He et al., 2001) and this effect may be due to inhibition of the generation of reactive oxygen species by NADPH oxidases (NOX), particularly NOX2 (Hernandes et al., 2013). During zebrafish development NOX2 is stably expressed in the brain by 24 hpf (Weaver et al., 2016), and microglia colonize zebrafish brain between 2.5 and 4.5 dpf, with increased apoptosis causing increased colonization (Casano et al., 2016; Xu et al., 2016). Therefore it is plausible that the neuroprotection and partial neurorestoration in our study was due to inhibition of NOX2 and microglia. Neuroprotective effects have also been shown in mouse MPTP model (Wu et al., 2002), and in a 6-OHDA zebrafish model (Feng et al., 2014); however these studies did not test for a neuro-restorative effect of minocycline. Our study is in agreement with Quintero et al. (2006) who found that treatment of rodents with minocycline before 6-OHDA-induced loss of dopaminergic neurons was neuroprotective, but although treatment with minocycline after 6-OHDA lesion reduced the loss of neurons, this effect was not statistically significant. However, in clinical studies minocycline did not improve motor symptoms after 12 or 18 months (Ravina et al., 2006; Kieburtz et al., 2008) in a small trial (66 to 67 patients in each treatment arm) although a longer trial period may be needed to assess the benefits of this drug in protection or symptomatic treatment of this disease. In patients with Parkinsonian related multiple system atrophy, it reduced microglial activation in the small subgroup tested but it did not improve motor function (n = 8; Dodel et al., 2010). Although the preclinical evidence is promising, further clinical evidence is needed to determine whether minocycline is beneficial in Parkinson's disease.

Rasagiline

The MAO B inhibitor, rasagiline, is effective at improving motor symptoms as monotherapy in early Parkinson's disease and as an adjunct to levodopa at more advanced stages (Olanow et al., 2009; Weintraub et al., 2016).

In contrast to humans, which have two MAO isoforms MAO A and MAO B, zebrafish have only one form of MAO which displays approximately 70% sequence identity to both MAO A and B in the human genome (Setini et al., 2005). Functionally, the zebrafish MAO is also intermediate between MAO A and MAO B (Arslan and Edmondson, 2010). In our study mean distance moved in the rasagiline (1 μM)-treated larvae was slightly lower than in the control group, although this decrease was not significant (Fig. 5H; $P = 0.53$ vs. control, Tukey's post hoc test). Hyperserotonergic effects have been reported in zebrafish using deprenyl with hypolocomotion and increased 5HT levels when deprenyl was given at high doses (> 10 μM) and for longer times (seven days rather than three in our study) than was rasagiline in our study (Sallinen et al., 2009). Although the IC_{50} for rasagiline in zebrafish has not been reported, in humans it is similar to deprenyl (Geha et al., 2001), therefore we would expect that the effects of the two drugs in zebrafish would be broadly equivalent. Given that we did not find a difference in locomotion, nor was there any cardiac edema or other morphological signs of toxicity, it is unlikely that it caused hyperserotonergic effects in our study. In addition, in humans rasagiline alone at therapeutic doses has not been reported to cause serotonin syndrome (Chen, 2011; Fernandes et al., 2011), and no correlation was found between rasagiline treatment, in combination with anti-depressants, and serotonin syndrome in 93 Parkinson's patients over a 36-week period in a clinical trial (Smith et al., 2015).

Rasagiline has been shown to be neuroprotective *in vitro* (Goggi et al., 2000) and was shown to protect SH-SY5Y neuroblastoma cells from apoptosis Maruyama et al. (2001). Neuroprotection has also been reported in primates and rodents (Kupsch et al., 2001; Blandini et al., 2004), and Sagi et al. (2007) have shown that rasagiline restores dopaminergic neurons when given subsequent to the neurotoxin MPTP. The S-isomer of rasagiline is 1000-fold less potent as an MAO-B inhibitor (Youdim and Weinstock, 2001), yet has been reported to protect dopaminergic cells *in vitro* and *in vivo* (Maruyama et al., 2001; Youdim et al., 2001).These findings led to the hypothesis that the neuroprotective effect is due to intrinsic anti-apoptotic properties and not due to its action on monoamine oxidase (Youdim et al., 2001; Akao et al., 2002).

Our findings that rasagiline both protects and restores neurons from the effects of 6-OHDA, and normalizes locomotor activity, agree with the findings in the cell culture and animal studies above. To our knowledge this is the first report of the neuroprotective and neurorestorative effects of rasagiline in zebrafish. In clinical studies rasagiline has been found to improve motor scores and activities of daily living (Siderowf et al., 2002; Olanow et al., 2009); however it did not improve mild cognitive impairment in Parkinson's patients in a small recent trial (Weintraub et al., 2016). Therefore it is not yet known whether the neuroprotective evidence from animal studies will be confirmed in the clinic.

CONCLUSION

Despite a clearer understanding of Parkinson's disease pathology, treatment to date is merely symptomatic; the ultimate goal is to protect against further degeneration and worsening of symptoms. The ability to screen drugs in a relatively high-throughput fashion is key to progress. This study aimed to further develop zebrafish as a model suitable for high-throughput drug screening for Parkinson's disease. Our findings for minocycline and rasagiline mirror those of studies in rodents and primates, and although, unlike studies in rodents, isradipine was not neuroprotective in zebrafish, this may better reflect the clinical situation. Thus we have shown that exposure of zebrafish larvae to 6-OHDA can be used to test for both neuroprotection and neurorestoration in a relatively high throughput manner, over a short time span of three days, making zebrafish an ideal model for high-throughput screening of novel therapies for Parkinson's disease.

Acknowledgments—This work was supported by a student stipend from the College of Medicine Nursing and Health Sciences, National University of Ireland, Galway. The advice of Dr. Eilis Dowd and the use of equipment in the Department of Anatomy, NUI Galway is gratefully acknowledged.

REFERENCES

Akao Y, Maruyama W, Yi H, Shamoto-Nagai M, Youdim MBH, Naoi M (2002) An anti-Parkinson's disease drug, N-propargyl-1(R)-aminoindan (rasagiline), enhances expression of anti-apoptotic Bcl-2 in human dopaminergic SH-SY5Y cells. Neurosci Lett 326:105–108.

Arslan BK, Edmondson DE (2010) Expression of zebrafish (Danio rerio) monoamine oxidase (MAO) in Pichia pastoris: purification and comparison with human MAO A and MAO B. Protein Expr Purif 70:290–297.

Becker C, Jick SS, Meier CR (2008) Use of antihypertensives and the risk of Parkinson disease. Neurology 70:1438–1444.

Blandini F, Armentero MT, Fancellu R, Blaugrund E, Nappi G (2004) Neuroprotective effect of rasagiline in a rodent model of Parkinson's disease. Exp Neurol 187:455–459.

Brannen KC, Panzica-Kelly JM, Danberry TL, Augustine-Rauch KA (2010) Development of a zebrafish embryo teratogenicity assay and quantitative prediction model. Birth Defects Res B 89:66–77.

Burgess HA, Granato M (2007) Modulation of locomotor activity in larval zebrafish during light adaptation. J Exp Biol 210:2526–2539.

Casano AM, Albert M, Peri F (2016) Developmental apoptosis mediates entry and positioning of microglia in the zebrafish brain. Cell Rep 16:897–906.

Chan CS, Guzman JN, Ilijic E, Mercer JN, Rick C, Tkatch T, Meredith GE, Surmeier DJ (2007) 'Rejuvenation' protects neurons in mouse models of Parkinson's disease. Nature 447:1081–1085.

Chen JJ (2011) Pharmacologic safety concerns in Parkinson's disease: facts and insights. Int J Neurosci 121(Suppl 2):45–52.

Chen M, Ona VO, Li M, Ferrante RJ, Fink KB, Zhu S, Bian J, Guo L, Farrell LA, Hersch SM, Hobbs W, Vonsattel JP, Cha JH, Friedlander RM (2000) Minocycline inhibits caspase-1 and caspase-3 expression and delays mortality in a transgenic mouse model of Huntington disease. Nat med 6:797–801.

Chong CM, Zhou ZY, Razmovski-Naumovski V, Cui GZ, Zhang LQ, Sa F, Hoi PM, Chan K, Lee SM (2013) Danshensu protects against 6-hydroxydopamine-induced damage of PC12 cells in vitro and dopaminergic neurons in zebrafish. Neurosci Lett 543:121–125.

Cotzias GC, Papavasi Ps, Gellene R (1969) Modification of Parkinsonism – chronic treatment with L-Dopa. New Engl J Med 280:337–338.

Dauer W, Przedborski S (2003) Parkinson's disease: mechanisms and models. Neuron 39:889–909.

De Virgilio A, Greco A, Fabbrini G, Inghilleri M, Rizzo MI, Gallo A, Conte M, Rosato C, Appiani MC, de Vincentiis M (2016) Parkinson's disease: autoimmunity and neuroinflammation. Autoimmun Rev 15:1005–1011.

Diguet E, Gross CE, Tison F, Bezard E (2004) Rise and fall of minocycline in neuroprotection: need to promote publication of negative results. Exp Neurol 189:1–4.

Dodel R, Spottke A, Gerhard A, Reuss A, Reinecker S, Schimke N, Trenkwalder C, Sixel-Doring F, Herting B, Kamm C, Gasser T, Sawires M, Geser F, Kollensperger M, Seppi K, Kloss M, Krause M, Daniels C, Deuschl G, Bottger S, Naumann M, Lipp A, Gruber D, Kupsch A, Du YS, Turkheimer F, Brooks DJ, Klockgether T, Poewe W, Wenning G, Schade-Brittinger C, Oertel WH, Eggert K (2010) Minocycline 1-year therapy in multiple-system-atrophy: effect on clinical symptoms and [C-11] (R)-PK11195 PET (MEMSA-Trial). Movement Disord 25:97–107.

Du YS, Ma ZZ, Lin SZ, Dodel RC, Gao F, Bales KR, Triarhou LC, Chernet E, Perry KW, Nelson DLG, Luecke S, Phebus LA, Bymaster FP, Paul SM (2001) Minocycline prevents nigrostriatal dopaminergic neurodegeneration in the MPTP model of Parkinson's disease. P Natl Acad Sci USA 98:14669–14674.

Du Y, Guo Q, Shan M, Wu Y, Huang S, Zhao H, Hong H, Yang M, Yang X, Ren L, Peng J, Sun J, Zhou H, Li S, Su B (2016) Spatial and temporal distribution of dopaminergic neurons during development in zebrafish. Front Neuroanat 10:115.

Durante P, Cardenas CG, Whittaker JA, Kitai ST, Scroggs RS (2004) Low-threshold L-type calcium channels in rat dopamine neurons. J Neurophysiol 91:1450–1454.

Fearnley JM, Lees AJ (1991) Aging and Parkinsons-disease – substantia-nigra regional selectivity. Brain 114:2283–2301.

Feng CW, Wen ZH, Huang SY, Hung HC, Chen CH, Yang SN, Chen NF, Wang HM, Hsiao CD, Chen WF (2014) Effects of 6-hydroxydopamine exposure on motor activity and biochemical expression in zebrafish (Danio rerio) larvae. Zebrafish 11:227–239.

Fernandes C, Reddy P, Kessel B (2011) Rasagiline-induced serotonin syndrome. Mov Disord 26:766–767.

Garrido-Mesa N, Zarzuelo A, Galvez J (2013) Minocycline: far beyond an antibiotic. Br J Pharmacol 169:337–352.

Geha RM, Rebrin I, Chen K, Shih JC (2001) Substrate and inhibitor specificities for human monoamine oxidase A and B are influenced by a single amino acid. J Biol Chem 276:9877–9882.

Glinka Y, Tipton KF, Youdim MB (1998) Mechanism of inhibition of mitochondrial respiratory complex I by 6-hydroxydopamine and its prevention by desferrioxamine. Eur J Pharmacol 351:121–129.

Goggi J, Theofilopoulos S, Riaz SS, Jauniaux E, Stern GM, Bradford HF (2000) The neuronal survival effects of rasagiline and deprenyl on fetal human and rat ventral mesencephalic neurones in culture. NeuroReport 11:3937–3941.

Hauser RA, Abler V, Eyal E, Eliaz RE (2016) Efficacy of rasagiline in early Parkinson's disease: a meta-analysis of data from the TEMPO and ADAGIO studies. Int J Neurosci 126:942–946.

He Y, Appel S, Le W (2001) Minocycline inhibits microglial activation and protects nigral cells after 6-hydroxydopamine injection into mouse striatum. Brain Res 909:187–193.

Hernandes MS, Santos GD, Cafe-Mendes CC, Lima LS, Scavone C, Munhoz CD, Britto LR (2013) Microglial cells are involved in the susceptibility of NADPH oxidase knockout mice to 6-hydroxydopamine-induced neurodegeneration. PLoS ONE 8:e75532.

Ilijic E, Guzman JN, Surmeier DJ (2011) The L-type channel antagonist isradipine is neuroprotective in a mouse model of Parkinson's disease. Neurobiol Dis 43:364–371.

Jankovic J (1984) Progressive supranuclear palsy – clinical and pharmacologic update. Neurol Clin 2:473–486.

Kieburtz K, Tilley B, Ravina B, Galpern W, Shannon K, Tanner C, Wooten GF, Investigators NN-P (2008) A pilot clinical trial of creatine and minocycline in early Parkinson disease: 18-month results. Clin Neuropharmacol 31:141–150.

Kolahdouzan M, Hamadeh MJ (2017) The neuroprotective effects of caffeine in neurodegenerative diseases. CNS Neurosci Ther 23:272–290.

Kruman II, Mattson MP (1999) Pivotal role of mitochondrial calcium uptake in neural cell apoptosis and necrosis. J Neurochem 72:529–540.

Kupsch A, Sautter J, Schwarz J, Riederer P, Gerlach M, Oertel WH (1996) 1-Methyl-4-phenyl-1,2,3,6-tetrahydropyridine-induced neurotoxicity in non-human primates is antagonized by pretreatment with nimodipine at the nigral, but not at the striatal level. Brain Res 741:185–196.

Kupsch A, Sautter J, Gotz ME, Breithaupt W, Schwarz J, Youdim MB, Riederer P, Gerlach M, Oertel WH (2001) Monoamine oxidase-inhibition and MPTP-induced neurotoxicity in the non-human primate: comparison of rasagiline (TVP 1012) with selegiline. J Neural Transm 108:985–1009.

Lenhard, W. and Lenhard, A. (2016) Calculation of Effect Sizes Dettelbach (Germany): Psychometrica. http://doi:10.13140/RG.2.1.3478.4245 available: https://www.psychometrica.de/effect_size.html.

Louis ED, Benito-Leon J, Bermejo-Pareja F, Neurological Disorders in Central Spain Study G (2009) Antihypertensive agents and risk of Parkinson's disease, essential tremor and dementia: a population-based prospective study (NEDICES). Neuroepidemiology 33:286–292.

Maruyama W, Youdim MB, Naoi M (2001) Antiapoptotic properties of rasagiline, N-propargylamine-1(R)-aminoindan, and its optical (S)-isomer, TV1022. Ann N Y Acad Sci 939:320–329.

Oertel WH (2017) Recent advances in treating Parkinson's disease. F1000Res 6:260.

Olanow CW, Rascol O, Hauser R, Feigin PD, Jankovic J, Lang A, Langston W, Melamed E, Poewe W, Stocchi F, Tolosa E, Investigators AS (2009) A double-blind, delayed-start trial of rasagiline in Parkinson's disease. New Engl J Med 361:1268–1278.

Olson KE, Gendelman HE (2016) Immunomodulation as a neuroprotective and therapeutic strategy for Parkinson's disease. Curr Opin Pharmacol 26:87–95.

Ortner NJ, Bock G, Dougalis A, Kharitonova M, Duda J, Hess S, Tuluc P, Pomberger T, Stefanova N, Pitterl F, Ciossek T, Oberacher H, Draheim HJ, Kloppenburg P, Liss B, Striessnig J (2017) Lower affinity of isradipine for L-Type Ca2+ channels during substantia nigra dopamine neuron-like activity: implications for neuroprotection in Parkinson's disease. J Neurosci 37:6761–6777.

Parkinson Study G (2013) Phase II safety, tolerability, and dose selection study of isradipine as a potential disease-modifying intervention in early Parkinson's disease (STEADY-PD). Mov Disord 28:1823–1831.

Parng C, Roy NM, Ton C, Lin Y, McGrath P (2007) Neurotoxicity assessment using zebrafish. J Pharmacol Tox Met 55:103–112.

Pasternak B, Svanstrom H, Nielsen NM, Fugger L, Melbye M, Hviid A (2012) Use of calcium channel blockers and Parkinson's disease. Am J Epidemiol 175:627–635.

Quintero EM, Willis L, Singleton R, Harris N, Huang P, Bhat N, Granholm AC (2006) Behavioral and morphological effects of minocycline in the 6-hydroxydopamine rat model of Parkinson's disease. Brain Res 1093:198–207.

Ramsey CP, Tansey MG (2014) A survey from 2012 of evidence for the role of neuroinflammation in neurotoxin animal models of Parkinson's disease and potential molecular targets. Exp Neurol 256:126–132.

Ravina B, Kieburtz K, Tilley B, Shannon K, Tanner C, Wooten F, Racette B, Deppen P, Dewey RB, Hayward B, Scott B, Field J, Carter J, Brodsky M, Andrews P, Manyam B, Whetteckey J, Rao J, Cook M, Aminoff MJ, Christine C, Roth J, Nance M, Parashos S, Peterson S, Shannon K, Jaglin J, Singer C, Perez MA, Blenke A, Hauser R, McClain T, Dawson T, Dunlop B, Pahwa R, Lyons K, Parsons A, Leehey M, Bainbridge J, Shulman L, Weiner W, Pabst K, Elble R, Young C, Sethi K, Dill B, Martin W, McInnes G, Calabrese VP, Roberge P, Hamill R, Homan C, Bodis-Wollner IG, Hayes E, Ross GW, Terashita S, Wooten GF, Trugman J, Keller MF, Sage JI, Caputo D, Fang J, Shearon D, Jennings D, Kelsey T, Jennings D, Kelsey T, Wojcieszek J, Feigin A, Watts RL, Stover N, McMurray R, Albin R, Wernette K, Siderowf A, Reichwein S, Simon D, Tarsy D, Tintner R, Hunter C, LeWitt P, Deangelis M, Burns RS, Shill H, Danielson J, Marlor L, Adler C, Lind M, Gorell J, Krstevska S, Flewellen M, Schneider J, Sendek S, Gollomp S, Vernon G, Coffey D, LeBlanc P, Lew MF, Wu A, Kawai C, Uitti R, Turk M, Bower J, Torgrimson S, Handler J, Greenbaum K, Sabbagh M, Obradov Z, Elm J, Guimaraes P, Huang P, Palesch Y, Kamp C, Shinaman A, Johnsen D, Brocht A, Bennett S, Weaver C, Goetz C, Fagan S, Investigators NN-P (2006) A randomized, double-blind, futility clinical trial of creatine and minocycline in early Parkinson disease. Neurology 66:664–671.

Rink E, Wullimann MF (2001) The teleostean (zebrafish) dopaminergic system ascending to the subpallium (striatum) is located in the basal diencephalon (posterior tuberculum). Brain Res 889:316–330.

Rink E, Wullimann MF (2002a) Connections of the ventral telencephalon and tyrosine hydroxylase distribution in the zebrafish brain (Danio rerio) lead to identification of an ascending dopaminergic system in a teleost. Brain Res Bull 57:385–387.

Rink E, Wullimann MF (2002b) Development of the catecholaminergic system in the early zebrafish brain: an immunohistochemical study. Brain Res Dev Brain Res 137:89–100.

Ritz B, Rhodes SL, Qian L, Schernhammer E, Olsen JH, Friis S (2010) L-type calcium channel blockers and Parkinson disease in Denmark. Ann Neurol 67:600–606.

Sadeghian M, Mullali G, Pocock JM, Piers T, Roach A, Smith KJ (2016) Neuroprotection by safinamide in the 6-hydroxydopamine model of Parkinson's disease. Neuropathol Appl Neurobiol 42:423–435.

Sagi Y, Mandel S, Amit T, Youdim MB (2007) Activation of tyrosine kinase receptor signaling pathway by rasagiline facilitates neurorescue and restoration of nigrostriatal dopamine neurons in post-MPTP-induced parkinsonism. Neurobiol Dis 25:35–44.

Sallinen V, Sundvik M, Reenila I, Peitsaro N, Khrustalyov D, Anichtchik O, Toleikyte G, Kaslin J, Panula P (2009) Hyperserotonergic phenotype after monoamine oxidase inhibition in larval zebrafish. J Neurochem 109:403–415.

Setini A, Pierucci F, Senatori O, Nicotra A (2005) Molecular characterization of monoamine oxidase in zebrafish (Danio rerio). Comp Biochem Physiol B 140:153–161.

Sheng DL, Qu DB, Kwok KHH, Ng SS, Lim AYM, Aw SS, Lee CWH, Sung WK, Tan EK, Lufkin T, Jesuthasan S, Sinnakaruppan M, Liu JJ (2010) Deletion of the WD40 domain of LRRK2 in zebrafish causes parkinsonism-like loss of neurons and locomotive defect. Plos Genet 6.

Siderowf A, Stern M, Shoulson I, Kieburtz K, Oakes D, Day D, Shinaman A, Plumb S, Fahn S, Blindauer K, Lew M, Hurtig H, Lloyd M, Hauser R, Gauger L, Golbe L, Wojcieszek J, Belden J, Feigin A, Klimek ML, Shannon B, Ondo W, Hunter C, Calabrese V, Allen C, Berry D, Gardiner I, Miyasaki J, Del Rizzo L, Mendis T, Mendis N, Gray P, Hubble J, Betcher K, Pahwa R, Molho E, Brown D, Shulman L, Rajput A, Ewanishin M, Stacy M, Williamson K, Bertoni J, Peterson C, Tuite P, Ebbitt B, Shannon K, Jaglin J, Tanner C, Marek K, Stavris K, Aminoff MJ, DiMinno M, Dowling G, Kang UJ, Richman J, Sethi K, Martin W, King P, McInnes G, Adler C, LeWitt P, DeAngelis M, Schear M, Gordon MF, Winnick R, Feldman R, Thomas CA, Conn K, Brocht A, Chadwick C, Connolly J, Daigneault S, Eberly S, Bausch M, Josephson L, Oliva R, Schwid S, Lang A, Cox C, Irvine C, Nutt J, White W, Oren S, Levy R, Eyal E, Ladkani D, Houck W, Grp PS (2002) A controlled trial of rasagiline in early Parkinson disease – The TEMPO study. Arch Neurol-Chicago 59:1937–1943.

Simon KC, Gao X, Chen H, Schwarzschild MA, Ascherio A (2010) Calcium channel blocker use and risk of Parkinson's disease. Mov Disord 25:1818–1822.

Singleton AB, Farrer M, Johnson J, Singleton A, Hague S, Kachergus J, Hulihan M, Peuralinna T, Dutra A, Nussbaum R, Lincoln S, Crawley A, Hanson M, Maraganore D, Adler C, Cookson MR, Muenter M, Baptista M, Miller D, Blancato J, Hardy J, Gwinn-Hardy K (2003) Alpha-synuclein locus triplication causes Parkinson's disease. Science 302:841.

Smith KM, Eyal E, Weintraub D, Investigators A (2015) Combined rasagiline and antidepressant use in Parkinson disease in the ADAGIO study: effects on nonmotor symptoms and tolerability. JAMA Neurol 72:88–95.

Stednitz SJ, Freshner B, Shelton S, Shen T, Black D, Gahtan E (2015) Selective toxicity of L-DOPA to dopamine transporter-expressing neurons and locomotor behavior in zebrafish larvae. Neurotoxicol Teratol 52:51–56.

Ton TG, Heckbert SR, Longstreth Jr WT, Rossing MA, Kukull WA, Franklin GM, Swanson PD, Smith-Weller T, Checkoway H (2007) Calcium channel blockers and beta-blockers in relation to Parkinson's disease. Parkinsonism Relat Disord 13:165–169.

Weaver CJ, Leung YF, Suter DM (2016) Expression dynamics of NADPH oxidases during early zebrafish development. J Comp Neurol 524:2130–2141.

Weintraub D, Hauser RA, Elm JJ, Pagan F, Davis MD, Choudhry A, Investigators M (2016) Rasagiline for mild cognitive impairment in Parkinson's disease: a placebo-controlled trial. Mov Disord 31:709–714.

Westerfield M (2000) The zebrafish book: a guide for the laboratory use of zebrafish. 4th ed. Eugene: Univ. of Oregon Press.

Wu DC, Jackson-Lewis V, Vila M, Tieu K, Teismann P, Vadseth C, Choi DK, Ischiropoulos H, Przedborski S (2002) Blockade of microglial activation is neuroprotective in the 1-methyl-4-phenyl-1,2,3,6-tetrahydropyridine mouse model of Parkinson disease. J Neurosci 22:1763–1771.

Xu J, Wang T, Wu Y, Jin W, Wen Z (2016) Microglia colonization of developing zebrafish midbrain is promoted by apoptotic neuron and lysophosphatidylcholine. Dev Cell 38:214–222.

Yang LC, Sugama S, Chirichigno JW, Gregorio J, Lorenzl S, Shin DH, Browne SE, Shimizu Y, Joh TH, Beal MF, Albers DS (2003) Minocycline enhances MPTP toxicity to dopaminergic neurons. J Neurosci Res 74:278–285.

Youdim MB, Weinstock M (2001) Molecular basis of neuroprotective activities of rasagiline and the anti-Alzheimer drug TV3326 [(N-propargyl-(3R)aminoindan-5-YL)-ethyl methyl carbamate]. Cell Mol Neurobiol 21:555–573.

Youdim MB, Wadia A, Tatton W, Weinstock M (2001) The anti-Parkinson drug rasagiline and its cholinesterase inhibitor derivatives exert neuroprotection unrelated to MAO inhibition in cell culture and in vivo. Ann N Y Acad Sci 939:450–458.

Zamponi GW (2016) Targeting voltage-gated calcium channels in neurological and psychiatric diseases. Nat Rev Drug Discov 15:19–34.

Zhang ZJ, Cheang LC, Wang MW, Lee SM (2011) Quercetin exerts a neuroprotective effect through inhibition of the iNOS/NO system and pro-inflammation gene expression in PC12 cells and in zebrafish. Int J Mol Med 27:195–203.

Zhang LQ, Sa F, Chong CM, Wang Y, Zhou ZY, Chang RC, Chan SW, Hoi PM, Yuen Lee SM (2015) Schisantherin A protects against 6-OHDA-induced dopaminergic neuron damage in zebrafish and cytotoxicity in SH-SY5Y cells through the ROS/NO and AKT/GSK3beta pathways. J Ethnopharmacol 170:8–15.

Zhang C, Li C, Chen S, Li Z, Jia X, Wang K, Bao J, Liang Y, Wang X, Chen M, Li P, Su H, Wan JB, Lee SM, Liu K, He C (2017) Berberine protects against 6-OHDA-induced neurotoxicity in PC12 cells and zebrafish through hormetic mechanisms involving PI3K/AKT/Bcl-2 and Nrf2/HO-1 pathways. Redox Biol 11:1–11.

Zhu S, Stavrovskaya IG, Drozda M, Kim BYS, Ona V, Li MW, Sarang S, Liu AS, Hartley DM, Du CW, Gullans S, Ferrante RJ, Przedborski S, Kristal BS, Friedlander RM (2002) Minocycline inhibits cytochrome c release and delays progression of amyotrophic lateral sclerosis in mice. Nature 417:74–78.

Zuch CL, Nordstroem VK, Briedrick LA, Hoernig GR, Granholm AC, Bickford PC (2000) Time course of degenerative alterations in nigral dopaminergic neurons following a 6-hydroxydopamine lesion. J Comp Neurol 427:440–454.

(Received 23 May 2017, Accepted 16 October 2017)
(Available online 24 October 2017)